VRIJE UNIVERSITEIT

Density functional theory with improved gradient and orbital dependent functionals

ACADEMISCH PROEFSCHRIFT

ter verkrijging van de graad van doctor aan
de Vrije Universiteit Amsterdam,
op gezag van de rector magnificus
prof.dr. T. Sminia,
in het openbaar te verdedigen
ten overstaan van de promotiecommissie
van de faculteit der Exacte Wetenschappen
op vrijdag 7 november 2003 om 15.45 uur
in het auditorium van de universiteit,
De Boelelaan 1105

door

Myrta Grüning

geboren te Macerata, Italië

promotor:	prof.dr. E.J. Baerends
copromotor:	dr. O.V. Gritsenko

Preface

This thesis collects the results of the research I carried out as PhD student at the department of theoretical chemistry of the Vrije Universiteit Amsterdam. Most of the results presented in this book have been already published.

List of publications

M. Grüning, O.V. Gritsenko, S.J.A. van Gisbergen and E.J. Baerends
"Shape corrections to exchange-correlation potentials by gradient-regulated seamless connection of model potentials for inner and outer region"
JOURNAL OF CHEMICAL PHYSICS, **114** (2001) 652-660, Chapter 7.

M. Grüning, O.V. Gritsenko, S.J.A. van Gisbergen and E.J. Baerends
"The failure of generalized gradient approximations (GGAs) and meta-GGAs for the two-center three-electron bonds in He_2^+, $(H_2O)_2^+$, and $(NH_3)_2^+$"
JOURNAL OF PHYSICAL CHEMISTRY A, **105** (2001) 9211-9218, Chapter 3.

M. Grüning, O.V. Gritsenko and E.J. Baerends
"Exchange potential from the common energy denominator approximation for the Kohn-Sham Green's function: Application to (hyper)polarizabilities of molecular chains"
JOURNAL OF CHEMICAL PHYSICS, **116** (2002) 6435-6442, Chapter 9.

M. Grüning, O.V. Gritsenko, S.J.A. van Gisbergen and E.J. Baerends
"On the required shape corrections to the local density and generalized gradient approximations to the Kohn-Sham potentials for molecular response calculations of (hyper)polarizabilities and excitation energies"
JOURNAL OF CHEMICAL PHYSICS, **116** (2002) 9591-9601, Chapter 8

M. Grüning, O.V. Gritsenko and E.J. Baerends
"Exchange-correlation energy and potential as approximate functionals of occupied

and virtual Kohn-Sham orbitals. Application to dissociating H_2"
JOURNAL OF CHEMICAL PHYSICS **118**, (2003) 7183-7191, Chapter 5.

M. Grüning, O.V. Gritsenko and E.J. Baerends
"Improved Description of Reaction Barriers with GGAs and meta-GGAs"
submitted, Chapter 4

Publications not included in this book:

A. Sergi, M. Grüning, M. Ferrario, F. Buda
"Density Functional study of the photoactive yellow protein's chromophore"
JOURNAL OF PHYSICAL CHEMISTRY B, **105** (2001) 4386-4391.

O.V. Gritsenko, M. Grüning and E.J. Baerends
"Kohn-Sham analogues of Koopmans theorem and the occupied-orbital-dependent Hartree-Fock exchange potential"
in REVIEWS OF MODERN QUANTUM CHEMISTRY (A Celebration of the Contribution of Robert Parr) Edited by K.D. Sen (World Scientific, Singapore) p.731-754 (2002).

D.P. Chong, M. Grüning and E.J. Baerends
"STO and GTO Field-Induced Polarization Functions for H to K"
JOURNAL OF COMPUTATIONAL CHEMISTRY **24**, (2003) 1582-1591.

Thanks

To Evert-Jan Baerends who gave me the opportunity to work at this project under his supervision and to benefit from his experience, broad knowledge and "sharp vision".
To Oleg Gritsenko who followed step by step my research work. With his ideas, his volcanic enthusiasm and his constant encouragement he gave an unquantifiable contribution to this thesis.
To Stan van Gisbergen who also contributed with code implementation, calculations, ideas and suggestions to most of the works in this thesis and followed with interest all the attempts to find better functionals.
To Franco Buda and Paolo Giannozzi who introduced me to scientific research.
To the members of the reading committee who took the time to study this thesis.
To all (ex-)members and guests of the Theoretical Chemistry group who – with their different experiences, cultural background and opinions – made the department a nice and interesting place to work at.
To Jeroen who helped me with all the practical and TeXnical aspects related to the preparation of this book.
To my family who supported and "followed" me in spite of 2000 km.
To the others, who know why.

Contents

Chapter 1

Introduction

The ultimate understanding of natural phenomena requires the study of processes at molecular and atomic scale. Density functional theory (DFT) [1] is a valuable tool to study the physics and the chemistry at this scale. The applications of this theory, that is exact, are based on the approximation for the electron-electron interaction energy. This approximation, that is the objective of this thesis, determines the accuracy of the results and therefore the possibility of making predictions.

In Sec. 1.1 it is shown how DFT transforms the original problem of solving the Schrödinger equation: starting from this equation for a many-electron wave function the Kohn-Sham [2] set of equations for a non-interacting system of electrons are derived and the approximations for the exchange and correlation (xc) energy functional and for the xc potential are introduced. Section 1.2 presents the main topics and the structure of this thesis.

1.1 From the Schrödinger equation to the Kohn-Sham set of equations

The result of an experimental measurement of a given physical quantity A of a quantum system in the stationary state Ψ can be predicted taking the expectation value of the associated (Hermitian) operator $\widehat{A}$

$$A[\Psi] = \langle \Psi | \widehat{A} | \Psi \rangle. \tag{1.1}$$

The time independent Schrödinger equation determines the stationary states Ψ and the corresponding energies E of N-particle systems (neglecting relativistic effects)

$$H(\mathbf{r}_1, \dots, \mathbf{r}_N)\Psi(\mathbf{r}_1\sigma_1, \dots, \mathbf{r}_N\sigma_1) = E\Psi(\mathbf{r}_1\sigma_1, \dots, \mathbf{r}_N\sigma_1). \tag{1.2}$$

H is the Hamiltonian of the system

$$H(\mathbf{r}_1, \dots, \mathbf{r}_N) = \sum_i^N -\frac{\nabla^2}{2} + v(\mathbf{r}_i) + \frac{1}{2} \sum_{j \neq i} w(\mathbf{r}_i, \mathbf{r}_j) \tag{1.3}$$

where $v(\mathbf{r}_i)$ is the external potential and $w(\mathbf{r}_i, \mathbf{r}_j)$ the internal particle interactions. The wave function Ψ is in fact a complicated function involving all the particles' space and spin coordinates $\mathbf{r}_i, \sigma_i$. Therefore the solution of the Schrödinger equation Eq. (1.2) cannot be found analytically except for very simple systems: the hydrogen atom and the harmonic oscillator. The application of approximate numerical techniques to solve Eq. (1.2) is in general not successful, if not combined with the physical/chemical knowledge of the system that allows a simplification of the original problem making assumptions and approximations.

For (most) atoms and molecules the first simplification comes by decoupling the electronic and nuclear degrees of freedom and reducing the problem to find the electronic wave function at fixed nuclear positions. The variational principle helps further to find an approximated ground state wave function: the exact electronic wave function minimizes in fact the energy E of the system.

In quantum chemistry the wave function (or *ab initio*) methods take advantage of this principle, starting from an *Ansatz* for the wave functions depending on a certain number of parameters. The minimization of the energy determines the parameters and thus the form of the wave functions. The simplest reasonable *Ansatz* for the N-electron wave function Ψ is the Hartree-Fock approximation considering the Slater determinant of N spin orbitals. In the Hartree-Fock wave function two electrons with the same spin are correlated: due to the property of the determinant, in fact, the probability that two electrons with the same spin occupy the same position in space is zero; while two electrons of unlike spin are not correlated. The description of (at least a part of) the remaining correlation due to the Coulomb interaction between electrons (both with parallel and opposite spin) requires a much more complicated *Ansatz* for the wave function and much more computational effort. This effort grows in particular with the number of degrees of freedom of the system.

Luckily, it is possible to describe a many-electron system uniquely through the density of Ψ

$$\rho(\mathbf{r}_1) = N \sum_{\sigma_1} \int |\Psi(\mathbf{r}_1\sigma_1, \mathbf{r}_2\sigma_2, \dots, \mathbf{r}_N\sigma_N)|^2 d\mathbf{r}_2 \dots d\mathbf{r}_N d\sigma_2 \dots d\sigma_N. \tag{1.4}$$

This possibility is attractive: the electronic density depends only on three space coordinates, whatever the size of the system.

The Hohenberg-Kohn theorem [1] states that the ground state expectation value A of an operator $\widehat{A}$ is a functional of the ground state density

$$A[\rho] = \langle \Psi[\rho] | \widehat{A} | \Psi[\rho] \rangle. \tag{1.5}$$

More precisely, for a many-electron system (ground state) with an interparticle interaction $w(\mathbf{r}_i, \mathbf{r}_j)$ there exists a one-to-one mapping (up to a trivial constant) between the density ρ and the external potential v. The density determines then uniquely the external potential and thus the Hamiltonian Eq. (1.3) that in its turn determines the (ground) wave function Ψ Eq. (1.2).

In particular the ground state energy E_0 of a system can be determined by its ground state density ρ_0. The total energy $E_v[\rho]$ is a functional of the density

$$E_v[\rho] = \langle \Psi[\rho] | \widehat{H} | \Psi[\rho] \rangle = \int v(r)\rho(r)dr + F_{\mathrm{HK}}[\rho] \tag{1.6}$$

where F_{HK} is a universal functional, not depending on the external potential v

$$F_{\mathrm{HK}}[\rho] = \langle \Psi[\rho] | \widehat{T} + \widehat{W} | \Psi[\rho] \rangle. \tag{1.7}$$

The variational principle can be also extended for the density: the exact ground state density ρ_0 minimizes the energy functional E_v. These are in principle all elements for a density functional method. In principle, given an *Ansatz* for the density that is flexible enough, minimizing the energy functional $E_v[\rho]$, one would find a very accurate approximation for the ground state density ρ_0 and the ground state energy E_0. In practice, the functional F_{HK} (1.7) cannot be calculated: the problem is then shifted from approximating the wave function to finding an approximation for the functional F_{HK}. A practical scheme to approximate F_{HK} has been proposed by Kohn and Sham (KS)[2]. A non-interacting system is considered: $\widehat{W}[\rho] = 0$ in Eq. (1.7) and F_{HK} reduces to the KS kinetic energy

$$T_s = \langle \Psi_s | \widehat{T} | \Psi_s \rangle. \tag{1.8}$$

$\Psi_s = |\psi_1 \cdots \psi_N|$ is the Slater determinant (N-electron system) of the ψ_i one-electron wave functions. For this system Eq. (1.6) can be rewritten as

$$E_{v_s}[\rho] = \int v_s(\mathbf{r})\rho(\mathbf{r})dr + T_s[\rho] \tag{1.9}$$

and we assume the existence of an external potential v_s that can reproduce the density of the corresponding interacting system in Eq. (1.4):

$$\rho(\mathbf{r}) = \rho_s(\mathbf{r})$$

$$\rho_s(\mathbf{r}) = \sum_i^N \|\psi_i(\mathbf{r})\|^2. \tag{1.10}$$

If v_s exists the one-to-one $v \leftrightarrow \rho$ mapping ensures its uniqueness.

The exchange and correlation (xc) energy is defined

$$E_{\mathrm{xc}}[\rho] = F_{\mathrm{HK}}[\rho] - T_s - \int \frac{\rho(\mathbf{r}_1)\rho(\mathbf{r}_2)}{|\mathbf{r}_1 - \mathbf{r}_2|} d\mathbf{r}_1 d\mathbf{r}_2 \tag{1.11}$$

where the latter is the classical Hartree electron-electron interaction energy, and the xc potential is obtained taking the functional derivative of the xc energy with respect to the density

$$v_{\mathrm{xc}}(\mathbf{r}) = \frac{\delta E_{\mathrm{xc}}[\rho]}{\delta \rho(\mathbf{r})}. \tag{1.12}$$

The form of v_s can be found by comparing the Euler-Lagrange equations for the two systems (whose solution should provide the same ground state density)

$$\begin{aligned} \frac{\delta}{\delta\rho}\left\{E_{v_s}[\rho] - \mu_s \int \rho\right\} &= 0 \\ \frac{\delta}{\delta\rho}\left\{E_{v}[\rho] - \mu \int \rho\right\} &= 0 \end{aligned}$$

and fixing asymptotic to zero so that $\mu = \mu_s$. The external potential of the non-interacting Kohn-Sham system v_s contains then the effect of the interaction between electrons

$$v_s(\mathbf{r}_1) = v(\mathbf{r}_1) + \int \frac{\rho(\mathbf{r}_2)}{|\mathbf{r}_1 - \mathbf{r}_2|} d\mathbf{r}_2 + v_{\mathrm{xc}}(\mathbf{r}_1). \tag{1.13}$$

Instead of $F_{\mathrm{HK}}[\rho]$ one needs to approximate thus only a smaller part of it: $E_{\mathrm{xc}}[\rho]$. Furthermore the computational scheme is quite simple requiring the self-consistent solution of the KS set of N one particle equations

$$\left(-\frac{\nabla_r^2}{2} + v_s(\mathbf{r})\right)\psi_i(\mathbf{r}) = \varepsilon_i \psi_i(\mathbf{r}) \tag{1.14}$$

The eigenvalues and eigenvectors of this set of equations are respectively the one electron KS orbital functions $\{\psi_i\}$ and the KS orbital energies $\{\varepsilon_i\}$. The density is calculated from the occupied KS orbital functions through Eq. (1.10).

1.2 This thesis

The fact that the xc energy $E_{\mathrm{xc}}[\rho]$ is a minor part of the total electronic energy does not imply that the effect of the xc approximation is not important. An immediate example in chemistry is the theoretical prediction of reaction barriers requiring the reliable estimate of energy differences of the order of 1-10 kcal/mol. Another example comes from the calculation of molecular response properties using time dependent density functional perturbation theory demanding the KS orbital functions $\{\psi_i\}$ and their energies $\{\varepsilon_i\}$; the shape of the approximated xc potential is therefore crucial for the quality of the results.

This thesis tackles the central problem in KS density functional theory of finding an approximation for the xc energy and potential that should be reliable and accurate enough to describe the physical and chemical properties of an electronic system. The existing approximations are in general based on the uniform electron gas model (local density approximations) [3] and on the slowly varying electron gas expansion (generalized gradient approximations) [4, 5, 6, 7]. These approximations are successful, despite their simplicity, for some properties and systems, while in other cases they are clearly inadequate. This thesis analyses some of the problematic cases for the existing KS DFT approximated methods and investigates alternatives to the standard approximations. In particular, besides approximations depending on the density and its gradient, it considers functionals explicitly dependent on KS orbitals.

The book is divided in two parts. The first regards the approximation of the xc energy functional and is related to the problem of calculating the energy barriers and dissociation energies of molecules. The second is dedicated to the xc potential and concerns molecular response properties.

In part one, the first chapter introduces the concept of exchange and correlation hole, discusses some well-known pathological cases for standard approximations and gives a brief overview of improved approximations both gradient and orbital dependent. Finally it describes the optimized effective potential method providing the xc potential from orbital-dependent energy functionals. The following chapters present prototypes of problematic cases that are studied in more detail: the dissociation energy of molecules with a three-electron two-center bond, the transition states of S_N2 and hydrogen abstraction reactions, the dissociation curve of the H_2 molecule.

The first chapter of part two describes, after building some rudiments of time dependent density functional perturbation theory, the features of the xc potential that are crucial for the quality of the results in molecular response property calculations. Examples of approximations where these features are modeled properly, are given in the following two chapters and their performance is tested quite successfully for excitation spectra, (hyper)polarizability and related properties of light prototype molecules. The last chapter deals with the problem of the description of the variation of the xc potential in a perturbed system, that is another necessary ingredient to calculate response properties. In particular, it treats the critical case of the (hyper)polarizability of hydrogen chains.

Part I

Reaction barriers and molecular dissociation: approximations of the exchange and correlation energy

Chapter

2

The exchange and correlation energy functional

The generalized gradient approximations (GGAs) for the xc energy functional are widely used in density functional calculation of dissociation energies and reaction barriers. In spite of their success, their performance is not always satisfactory. For example in the case of the bimolecular nucleophilic substitution (S_N2) reactions and hydrogen abstraction reactions for which the standard GGAs underestimate the reaction barriers.

It is an actual problem in the development of approximations for the xc energy to model functionals that can work also for these systems. The improved functionals in particular should grasp the orbital nature of chemical bonds. Functionals that explicitly depend on KS orbitals can thus provide a solution. Alternatively one can try to improve GGAs still remaining within the gradient corrected functionals. The next chapters explore both these alternatives.

In this chapter, after introducing the exchange and correlation hole function, the problematic types of bond for the standard GGA functionals are discussed in Sec. 2.2 while in Sec. 2.3 are presented some of the orbital-dependent functionals proposed in the literature.

2.1 The exchange and correlation hole function

This section introduces the xc hole function that is employed in the analysis of the approximated energy functionals in the following sections and chapters.

The part of the xc energy coming from the electron repulsion,

$$W_{\mathrm{xc}} = W - \frac{1}{2}\int \frac{\rho(\mathbf{r}_1)\rho(\mathbf{r}_2)}{\mathbf{r}_{12}} d\mathbf{r}_1 d\mathbf{r}_2. \tag{2.1}$$

the difference between the total interaction energy and the classical Coulomb energy, can be written

$$W_{\mathrm{xc}} = \frac{1}{2} \sum_{\sigma_1\sigma_2} \int \rho_{\sigma_1}(\mathbf{r}_1) \frac{\rho^{\mathrm{xc}}_{\sigma_1\sigma_2}(\mathbf{r}_1,\mathbf{r}_2)}{|\mathbf{r}_1 - \mathbf{r}_2|} d\mathbf{r}_1 d\mathbf{r}_2 \tag{2.2}$$

as the interaction of an electron in $\mathbf{r}_1$ (taken as reference) with its own xc hole function. The xc hole function

$$P_{\sigma_1\sigma_2}(\mathbf{r}_2|\mathbf{r}_1) = \frac{\Gamma_{\sigma_1\sigma_2}(\mathbf{r}_1,\mathbf{r}_2)}{\rho_{\sigma_1}(\mathbf{r}_1)} = \rho_{\sigma_2}(\mathbf{r}_2) + \rho^{\mathrm{xc}}_{\sigma_1\sigma_2}(\mathbf{r}_1,\mathbf{r}_2) \tag{2.3}$$

describes the effects of the exchange and correlation on the probability $P_{\sigma_1\sigma_2}(\mathbf{r}_2|\mathbf{r}_1)$ of finding an electron in $\mathbf{r}_2$ with spin σ_2 when the reference electron is in $\mathbf{r}_1$ with spin σ_1. This probability in its turn is defined by the ratio of the diagonal two electron density matrix

$$\Gamma_{\sigma_1\sigma_2}(\mathbf{r}_1,\mathbf{r}_2) = N(N-1) \int |\Psi(\mathbf{r}_1\sigma_1, \mathbf{r}_2\sigma_2, x_3, \ldots, x_N)|^2 dx_3 \ldots dx_N. \tag{2.4}$$

with the spin density $\rho_{\sigma_2}(\mathbf{r}_2)$. The xc hole contains one electron

$$\int \rho^{\mathrm{xc}}_{\sigma_1\sigma_2}(\mathbf{r}_1,\mathbf{r}_2) d\mathbf{r}_2 = -\delta_{\sigma_1\sigma_2} \tag{2.5}$$

and reduces the probability of finding an electron near the reference electron in $\mathbf{r}_1$.

The part due to the effects of the Fermi statistics, the exchange or Fermi hole, and the part due to the Coulomb repulsion, the correlation or Coulomb hole, are (often) treated separately. The exchange part of the xc hole function can be written explicitly as a function of the KS spin-orbitals $\psi_{i\sigma}$

$$\begin{aligned} \rho^{x}_{\sigma_1\sigma_2}(\mathbf{r}_1,\mathbf{r}_2) &= -\frac{|\sum_i^N \psi_{i\sigma_1}(\mathbf{r}_1)\psi^*_{i\sigma_1}(\mathbf{r}_2)|^2}{\rho_{\sigma_1}(\mathbf{r}_1)} \delta_{\sigma_1\sigma_2} \\ &= -\left| \sum_i^N \frac{\psi_{i\sigma_1}(\mathbf{r}_1)}{\sqrt{\rho_{\sigma_1}(\mathbf{r}_1)}} \psi_{i\sigma_1}(\mathbf{r}_2) \right|^2 \delta_{\sigma_1\sigma_2}. \end{aligned} \tag{2.6}$$

In the lower expression the exchange hole is rewritten as the square of the linear combination of the occupied orbitals with coefficients depending on the value of the orbital in the reference position $\mathbf{r}_1$. As long as the reference electron stays in the region where one orbital is localized and "dominate" the density, the hole does not change markedly remaining almost equal to the square of that orbital, while, if the reference electron crosses the overlap region between orbitals, the exchange hole varies very rapidly. From the definition (2.6) is clear that the exchange hole is negative for all $\mathbf{r}_1, \mathbf{r}_2$ and it can be easily verified that it integrates to -1.

The correlation hole instead integrates to zero. In fact the correlation hole reduces the probability of finding electrons close to the reference electron and increases the probability of finding an electron far from it. In general in molecules one distinguishes a dynamical atomic-like contribution to the correlation, from the core regions, and nondynamical left-right contribution due to the instantaneous localization of electrons on different fragments. The effect of the latter contribution is clear in molecular dissociation processes. For example, in the dissociation of an homo-atomic molecule, the exchange reduces the probability $P(\mathbf{r}_1, \mathbf{r}_2)$ equally around both fragments and alone it cannot yield the correct dissociation limit. The correct dissociation limit can be obtained considering the nondynamical correlation contribution that reduces the probability $P(\mathbf{r}_1, \mathbf{r}_2)$ on the site where the reference electron is located and increases it on the other site. The resulting total xc hole is then localized on the site where the reference electron is located.

Finally, it is important to notice that in the expression of W_{xc} is needed the knowledge of only the spherical averaged part of the xc hole function ρ_{xc}. This simplifies the developing of approximations of the xc energy functional: the approximated xc hole has to grasp only the features of the spherical averaged part of ρ_{xc}.

2.2 Generalized gradient approximations

The GGAs modify the local density approximation [3] (LDA) adding the dependence on the gradient of the density that measures how fast the density itself changes. This approximation may be put in the general form

$$E_{\mathrm{xc}}^{\mathrm{GGA}} = \int \rho^{4/3}(\mathbf{r}) F_{\mathrm{xc}}(r_s(\mathbf{r}), s(\mathbf{r})) d\mathbf{r}. \tag{2.7}$$

The enhancement factor over the local exchange F_{xc} is a function of the reduced density gradient

$$s(\mathbf{r}) = \frac{1}{2(3\pi^2)^{1/3}} \frac{\nabla\rho(\mathbf{r})}{\rho^{4/3}(\mathbf{r})} \tag{2.8}$$

and of the local Wigner-Seitz radius

$$r_s(\mathbf{r}) = \left(\frac{4\pi}{3}\rho(\mathbf{r})\right)^{-1/3}.$$

The form of the factor F_{xc} depends on the specific approximation, it is usually modeled for slowly varying density systems, considering key properties of the exact xc functional. It can eventually contain empirical parameters optimized by fitting a set of chemical data.

Looking at the form of factor $F_{\mathrm{xc}}(s, r_s = 0)$ the exchange part of the GGAs can be "classified" into two groups that will be addressed in this book as "standard" [4, 5, 6, 7] and "modified" GGAs [8, 9, 10]. While "standard" GGAs exchange reduce to the LDA one

$$E_x^{\mathrm{LDA}} = \frac{3}{4}\left(\frac{3}{\pi}\right)^{1/3} \int \rho^{4/3}(\mathbf{r}) d\mathbf{r} \tag{2.9}$$

the "modified" GGAs reduce to the Xα exchange with α that scaled the LDA exchange by a factor ~ 1.05. In fact in the construction of the former functionals F_{xc}^0 (F_{xc} at

$s = 0$) is fixed by the uniform gas limit, in the construction of the latter, F^0_{xc} is considered as a parameter and optimized.

A second difference is the dominant s^4 dependence of the “modified” GGAs in the region of $0 \leq s \leq 1$ instead of the dominant quadratic behavior s^2 of the “standard” GGAs.

Therefore in the bonding region of molecules, characterized just by value of s between 0 and 1, the “modified” exchange functionals are less sensitive to density variations than the “standard” ones and they are more closer to the Xα exchange functional. In the next chapter, from the analysis of s^2_σ in the bonding region of prototype molecular bonds, it is shown how the different behavior in this region of the “modified” GGAs improves the performance of these functionals for problematic types of bond.

2.2.1 Problematic cases for the standard GGAs: the n/m rule

This section is dedicated to the discussion of the molecular bonds which are problematic for the application of DFT at the standard GGA level.

The standard GGA functionals substantially overestimate the stability of the bifragmental radical cations A_2^+ with a two-center one-electron and two-center three-electron bond A–A [11, 12, 13], they also overestimate the stability of the transition states of radical abstraction reactions and S_N2 reactions and as a consequence they tend to underestimate the reaction barriers [14, 15, 16, 17, 18]. Furthermore they fail to properly describe the dissociation of an electron pair bond, yielding large errors at long bond distances.

To understand why the GGAs do not provide satisfactory results for these systems one has to analyze why do they work. Both LDA and GGA xc holes are substantially localized around the reference electron. As a consequence the GGA can provide satisfactory results only for systems with a substantially localized xc hole.

This is the case for atoms where both the exchange and the correlation holes are localized. The GGAs improve greatly on LDA reducing the error by an order of magnitude. This is also the case of systems with covalent bond. As discussed in Sec. 2.1 the xc hole is substantially localized around the site where the reference electron is located. As a matter of fact the GGA functionals are not a good approximation for the molecular exchange and correlation considered separately. The (negative) exchange contribution is not negative enough because the GGA exchange hole is localized. On the other hand the localized GGA correlation hole causes the overestimation of the correlation contribution. These two errors cancel each other and in general the GGAs predict correctly the xc energy for covalent bond systems. As explained in Ref. [19] on the ground of accurate KS calculations on Li_2, N_2 and F_2 molecules, the localized GGA exchange hole takes into account effectively the exchange and nondynamical correlation contributions, while the GGA correlation covers only dynamical correlation effects.

This mechanism clearly does not work in the case of the H_2^+ molecule (two-center one-electron bond). In fact this one-electron molecule has no Coulomb correlation and the exchange is just the self-interaction. The latter cancels exactly with the Hartree energy. The GGAs cannot reproduce the exchange hole delocalized on the two centers and because of the artificial localization they overestimate badly the stability of the molecule with respect to the H atom and H^+ cation. Because of the incomplete cancellation of the self-interaction contributions of the exchange and the Hartree part the error of the exchange part of the GGA is addressed as “self-interaction error”.

In the case of He_2^+ and the other bifragmental cation dimers with two-center three-electron bond, the exchange hole is delocalized on the atomic centers as in the case of covalent bond, but, as discussed in [20], the “unfavorable electron count” hampers the nondynamical correlation contribution. The GGA hole is more localized than the true xc hole. In particular the error of the GGA correlation functionals cancels only partially the error of the GGA exchange and the spurious nondynamical correlation produced by the latter yields the overestimation of the stability of these systems. This is shown in Chapt. 3 for the molecule of He_2^+ on the basis of accurate KS results.

The underestimation of the reaction barrier for the S_N2 reaction due to the overstabilization of the transition state has the same source. These problematic cases can be recognized on the basis of the ratio n/m between the number n of the electrons participating to the bond and the number m of centers on which the bond is delocalized [20]. If the ratio n/m is an integer as in the case of covalent bond molecules ($n = 2$, $m = 2$) the GGAs give reasonable results. If n/m is a fractional number, as for the H_2^+ molecule ($n = 1$, $m = 2$), the two-center three-electron bond ($n = 3$, $m = 2$) and the transition state of the symmetrical S_N2 reaction ($n = 4$, $m = 3$) the GGAs might overestimate the stability of the systems because of the “spurious” nondynamical correlation produced by the GGA exchange functionals.

In the case of the overestimation of the stability of the transition state of the radical abstraction reactions the error of the GGA is not due to the exchange part. In fact following the n/m rule this system with $n = 3$ electron and $m = 3$ centers involved in the bond does not belong to “problematic cases”. It has been recognized [21] from accurate KS calculations on the prototype $H \cdots H \cdots H$ system that in this case the approximated exchange covers correctly the exchange and nondynamical correlation contributions and the overestimation is produced by the approximated correlation. The origin of this overestimation has been attributed to the dependence of the GGA correlation on the spin polarized density

$$\zeta(\mathbf{r}) = \frac{\rho^{\uparrow}(\mathbf{r}) - \rho^{\downarrow}(\mathbf{r})}{\rho^{\uparrow}(\mathbf{r}) + \rho^{\downarrow}(\mathbf{r})}.$$

Finally, in its spin restricted version, the GGA fails to describe the dissociation of the electron-pair. As discussed above the GGAs describe qualitatively and quantitatively the electron-pair bond at equilibrium distance: the GGA exchange hole is localized and simulates the combined effects of the exchange and nondynamical correlation. In the infinite separation limit, the true xc hole is of course completely localized on the site where the reference electron is located and contains one electron. The GGA exchange hole is well localized, but it is not “deep” enough. This problem is explained in more detail on the basis of quantitative and qualitative arguments in Chapt. 5.

2.3 Orbital-dependent functionals

A promising way to improve on GGAs is to use explicitly orbital-dependent functionals.

In the meta-GGAs the orbitals are introduced through the KS kinetic energy spin-density τ_σ

$$\tau_\sigma(\mathbf{r}) = \frac{1}{2}\sum_{i=1}^{N_\sigma} |\nabla\psi_{i\sigma}(\mathbf{r})|^2 \tag{2.10}$$

This variable gives a measure of the “localization” of the electron [22, 23, 24] and it can be used to determine whether or not the localized model of the xc hole is a good approximation for the true xc hole function. Several meta-GGAs are tested in the following chapters for the problematic cases discussed above and their performances analyzed looking at the behavior of τ along the different types of bond. The meta-GGAs are rather simple functionals depending only on the density and the KS orbitals at the position $\mathbf{r}_1$ and in a infinitesimal interval around it.

The functionals that follow instead are “nonlocal” depending on the orbitals (or orbital densities) not only at the position $\mathbf{r}_1$, but also at every finite distance $|\mathbf{r}_1 - \mathbf{r}_2|$. In Ref. [25] the orbital densities

$$\rho_{i\sigma} = |\psi_{i\sigma}(\mathbf{r})|^2$$

are used to correct the self-interaction error in existing GGAs

$$E_{\text{xc}}^{\text{SIC-GGA}}[\rho_\uparrow, \rho_\downarrow] = E_{\text{xc}}^{\text{GGA}}[\rho_\uparrow, \rho_\downarrow] - \left\{ \frac{1}{2}\sum_{i\sigma}^{N_\sigma} \int\int \frac{\rho_{i\sigma}(\mathbf{r})\rho_{i\sigma}(\mathbf{r}_2)}{|\mathbf{r}_1 - \mathbf{r}_2|} d\mathbf{r}_1 d\mathbf{r}_2 + E_{\text{xc}}^{\text{GGA}}[\rho_{i\sigma}, 0] \right\}$$

The self-interaction-corrected (SIC) GGAs have been applied quite successfully in Ref. [26] to calculate reaction barriers.

The exact orbital expression for the exchange energy can be employed instead of the GGA exchange functionals

$$E_x = -\frac{1}{2}\sum_{ij\sigma}^{N_\sigma} \int\int \frac{\psi_{i\sigma}(\mathbf{r}_1)\psi_{i\sigma}^*(\mathbf{r}_2)\psi_{j\sigma}(\mathbf{r}_2)\psi_{j\sigma}^*(\mathbf{r})}{|\mathbf{r}_1 - \mathbf{r}_2|} d\mathbf{r}_1 d\mathbf{r}_2. \tag{2.11}$$

Nevertheless the correlation cannot be described anymore with GGA functionals that, as discussed in Ref. [19] and mentioned above, cover only the dynamical part of the correlation. A functional has to be found to cover the remaining nondynamical part.

A solution is to mix the exact exchange with a GGA exchange [27, 28] that takes into account also the nondynamical correlation

$$E_{\text{xc}}^{\text{exact-GGA}} = E_x + a_x(E_x^{\text{GGA}} - E_x) + E_c^{\text{GGA}}$$

The nondynamical effects are then given by the difference in energy of the GGA and exact exchange energy weighted with a mixing factor a_x. The mixing factor a_x is not “universal”: the effects of nondynamical correlation depend on the type of bond and vary strongly with the bond distance. In Ref. [29] a variable mixing factor a_x has been proposed

$$a_x = (1 - \tau_W/\tau)$$

involving the KS kinetic energy density τ and the von Weiszäcker kinetic energy density $\tau_W = |\nabla\rho|^2/8\rho$. This functional corrects the self-interaction error for the H_2^+ molecule yielding the correct dissociation limit, in fact for a one-electron system $\tau = \tau_W$ and (providing that the approximation for the correlation part gives also no contribution for a one-electron system) $E_{\mathrm{xc}}^{\text{exact-GGA}} = E_x$. Further this hybrid functional has been employed successfully to calculate the bifragmental cation dimers with two-center three-electron bond and the prototype hydrogen exchange between the hydrogen molecule and hydrogen atom. Note however that this nondynamical correlation functional is still not “universal”, it worsens the results for the atomization energy of the small G2 set and fails to describe the dissociation of the H_2 molecule at large distances.

In Ref. [30] an orbital-dependent functional has been proposed that, including both occupied and virtual orbitals, describes properly the building-up of nondynamical correlation for the dissociating molecular hydrogen and gives the correct result in the infinite separation limit. Chapter 5 discusses the implementation of this functional in a self-consistent scheme and the results obtained for the dissociation curve of the hydrogen molecule.

2.3.1 Optimized effective potential

A problem to be solved when employing orbital-dependent functionals is the derivation of the corresponding potential. The xc potential in fact is the functional derivative of the xc energy with respect to the density.

Orbital functions are implicitly functional of the density and the xc potential can be found by solving the integral equation

$$v_{\mathrm{xc}}(\mathbf{r}_1) = \sum_i^N \int \frac{\delta E_{\mathrm{xc}}[\{\psi_j\}]}{\delta\psi_i(\mathbf{r}_2)} G_i(\mathbf{r}_2, \mathbf{r}_3)\psi_i(\mathbf{r}_3)\chi_s^{-1}(\mathbf{r}_3, \mathbf{r}_1) d\mathbf{r}_2 d\mathbf{r}_3 + \text{c.c.} \tag{2.12}$$

where G_i is the Green function of the KS system

$$G_i(\mathbf{r}_2, \mathbf{r}_3) = \sum_{j \neq i} \frac{\psi_j(\mathbf{r}_3)\psi_j^*(\mathbf{r}_2)}{\varepsilon_j - \varepsilon_i}, \tag{2.13}$$

and χ_s^{-1} the inverse of the KS response function

$$\chi_s(\mathbf{r}_1, \mathbf{r}_2) = \frac{\delta\rho(\mathbf{r}_1)}{\delta v_s(\mathbf{r}_2)} = -\sum_i^N \psi_i^*(\mathbf{r}_1) G_i(\mathbf{r}_1, \mathbf{r}_2)\psi_i(\mathbf{r}_2) + \text{c.c.} \tag{2.14}$$

defined by

$$\int \chi_s(\mathbf{r}_1,\mathbf{r}_3)\chi_s^{-1}(\mathbf{r}_3,\mathbf{r}_2)d\mathbf{r}_3 = \delta(\mathbf{r}_1-\mathbf{r}_2).$$

The inverse function χ_s^{-1} of the KS density response is defined up to a constant that can be determined fixing the gauge for the KS potential v_s.

To find the xc potential it is then required to solve the non-trivial problem of inverting the KS density response function (2.14). In the case of spherical atomic systems the inversion can be performed numerically on a grid (Optimized Potential Method [31]). For molecular systems this problem has been solved either using an auxiliary basis set to expand the equation for the potential (plane wave, Gaussian type of orbital) [32, 33, 34, 35] or introducing the exchange charge density defined as the charge distribution whose electrostatic potential is the exchange potential [36]. Further, in Ref. [37] the xc potential is found through an iterative scheme avoiding the direct solution of the integral equation (2.12) and thus the inversion of the KS response.

Alternatively one can approximate the inverse function χ_s^{-1} of the KS density response. In Ref. [38] the following approximation for the Green function (2.13) has been proposed

$$G_i^{\mathrm{KLI}}(\mathbf{r}_1,\mathbf{r}_2) = \frac{1}{\Delta\varepsilon}\Big(\delta(\mathbf{r}_1-\mathbf{r}_2) - \psi_i(\mathbf{r}_1)\psi_i^*(\mathbf{r}_2)\Big). \tag{2.15}$$

Substituting this approximated Green function in Eq. (2.14) one obtains an approximated expression for the KS density response function:

$$\chi_s^{\mathrm{KLI}}(\mathbf{r}_1,\mathbf{r}_2) = -\frac{1}{\Delta\varepsilon}\Big(\sum_i^N\sum_j \psi_i^*(\mathbf{r}_1)\psi_j(\mathbf{r})\psi_j^*(\mathbf{r}_2)\psi_i(\mathbf{r}_2) - \sum_i^N |\psi_i(\mathbf{r}_1)|^2|\psi_i(\mathbf{r}_2)|^2 + \mathrm{c.c.}\Big) \tag{2.16}$$

that can be “analytically” inverted as shown in Ref. [39]. Nevertheless it should be noticed that in the sum of the approximated expression (2.16) only the diagonal occupied orbital products are excluded while in the exact expression

$$\chi_s(\mathbf{r}_1,\mathbf{r}_2) = -\sum_i^N\sum_{a>N}\frac{\psi_i^*(\mathbf{r}_1)\psi_a(\mathbf{r})\psi_a^*(\mathbf{r}_2)\psi_i(\mathbf{r}_2)}{\varepsilon_a-\varepsilon_i} + \mathrm{c.c.} \tag{2.17}$$

all occupied-occupied products are excluded as an effect of the cancellation due to the energy denominator $\varepsilon_j - \varepsilon_i = -(\varepsilon_i - \varepsilon_j)$. To avoid this drawback the following approximation as been proposed [40] for the KS Green function (2.13)

$$\begin{aligned} G_i^{\mathrm{CEDA}}(\mathbf{r}_1,\mathbf{r}_2) &= \frac{1}{\Delta\varepsilon}\Big(\sum_{j\neq i}\Delta\varepsilon\frac{\psi_j(\mathbf{r}_1)\psi_j^*(\mathbf{r}_2)}{\varepsilon_j-\varepsilon_i} + \sum_{a>N}\psi_a(\mathbf{r}_1)\psi_a^*(\mathbf{r}_2)\Big) \\ &= \frac{1}{\Delta\varepsilon}\Big(\delta(\mathbf{r}_1-\mathbf{r}_2) + \sum_{j\neq i}\Delta\varepsilon\frac{\psi_j(\mathbf{r}_1)\psi_j^*(\mathbf{r}_2)}{\varepsilon_j-\varepsilon_i} - \sum_j^N\psi_j(\mathbf{r}_1)\psi_j^*(\mathbf{r}_2)\Big) \end{aligned} \tag{2.18}$$

where the common energy denominator approximation has been made only for the unoccupied KS orbitals. This leads to the common energy denominator approximation (CEDA) for the KS response function (2.17):

$$\chi_s^{\mathrm{CEDA}}(\mathbf{r}_1,\mathbf{r}_2) = -\frac{1}{\Delta\varepsilon}\Big(\sum_i^N \sum_{a>N} \psi_i^*(\mathbf{r}_1)\psi_a(\mathbf{r}_1)\psi_a^*(\mathbf{r}_2)\psi_i(\mathbf{r}_2) + \mathrm{c.c.}\Big). \tag{2.19}$$

In this case, in fact, all the occupied-occupied orbital products are correctly excluded from the summation. Also, the approximated expression (2.19) has an analytical expression for the inverse [40].

The CEDA for the KS response function has been applied in Chapts. 5 and 9 to derive the potential corresponding respectively to the orbital-dependent functional proposed in [30] and the exact exchange functional (2.11). In those chapters (2.12) is solved with the approximation (2.18) for the Green function leading to an analytical expression for the xc potential.

Chapter

3

GGAs and meta-GGAs for the two-center three-electron bond

The radical cations He_2^+, $(H_2O)_2^+$, $(NH_3)_2^+$ with two-center three-electron A–A bonds are investigated at the configuration interaction, accurate Kohn-Sham, generalized gradient approximation, and meta-GGA levels. Assessment of seven different GGA and six meta-GGA methods shows, that the A_2^+ systems remain a difficult case for DFT. All methods that have been tested, consistently overestimate the stability of A_2^+, the corresponding D_e errors decrease for more diffuse valence densities in the series $He_2^+ > (H_2O)_2^+ > (NH_3)_2^+$. By comparison to the energy terms of the accurate Kohn-Sham solutions, the approximate exchange functionals are found to be responsible for the errors of GGA-type methods, which characteristically overestimate exchange in A_2^+. These so-called exchange functionals implicitly use localized holes. Such localized holes do occur if there is left-right correlation, i.e. the exchange functionals then also describe nondynamical correlation. However, in the hemibonded A_2^+ systems the typical molecular (left-right, nondynamical) correlation of the two-electron pair bond is absent. The nondynamical correlation built into the exchange functionals is then spurious and yields too low energies.

3.1 Introduction

The most comprehensive way to analyze the performance of the LDA, GGAs and meta-GGAs of DFT[41] in molecular calculations is to compare the approximate exchange and correlation energies and energy densities with those calculated for the essentially accurate KS solution. The latter can be obtained from an accurate *ab initio* electron density $\rho(\mathbf{r})$. Benchmark KS solutions have been obtained previously for a number of atoms [42, 43, 44, 45], molecules [46, 47, 48, 49, 50, 51], prototype hydrogen abstraction and hydrogen exchange reactions [21] and the bimolecular nucleophilic substitution (S_N2) reaction [20]. The comparison with the accurate KS quantities is of special importance in problematic cases, where standard DFT GGAs [4, 5, 6, 7] produce relatively large errors. Such cases [11, 12, 13, 14, 15, 16, 17, 18, 21, 52, 53, 54, 55, 56, 57] and the qualitative rule put forward in Ref. [20] to predict success or failure of GGAs have been discussed in Chapt. 2.

This chapter in particular investigates the prototype difficult case of bifragmental radical cations A_2^+ with a two-center three-electron bond A–A, the stability of which is substantially overestimated by GGAs. This has been established in [11, 12, 13] by comparison of the GGA results with those of the *ab initio* Møller-Plesset perturbation (MP2 and MP4) and coupled-cluster CCSD(T) methods. Still, to our knowledge, no accurate KS solution has been reported for A_2^+. Furthermore, it is also desirable to assess the performance for A_2^+ of the recently developed meta-GGAs [58, 59, 60, 61] in which, in addition to the density gradient $\nabla\rho$, the KS kinetic energy density $\tau(\mathbf{r})$ and/or the density Laplacian $\nabla^2\rho(\mathbf{r})$ have been employed.

In this chapter the Kohn-Sham solutions are constructed for the hemibonded systems He_2^+, $(H_2O)_2^+$ and $(NH_3)_2^+$ from *ab initio* densities obtained with configuration interaction (CI) calculations. In Sec. 3.2 the results of CI calculations are discussed. The correlation contribution to the A–A hemibond is analyzed. It is stressed that the typical left-right (nondynamical, molecular) correlation of a bonding electron pair is absent in the hemibonded systems. This shows up in the structure of the CI wavefunctions. High quality of the CI solution has been achieved for the lightest system, He_2^+, while for the heavier $(H_2O)_2^+$ and $(NH_3)_2^+$ a size-consistency correction is required. In Sec. 3.3 the KS solutions are constructed from the correlated CI densities and the components of the total energy E^{KS} of the KS determinant are compared with those of the total energy E^{HF} of the Hartree-Fock (HF) determinant. The E^{KS} and E^{HF} values appear to be close to each other for A_2^+, as well as the exchange energies E_x^{KS}, E_x^{HF} and the correlation energies with respect to HF, $E_c^{\mathrm{HF}} = E - E^{\mathrm{HF}}$ and with respect to the KS determinantal energy, $E_c^{\mathrm{KS}} = E - E^{\mathrm{KS}}$.

In Sec. 3.4 a comparative assessment of seven different GGA and six meta-GGA methods is made. GGA-type methods overestimate the stability of A_2^+. On average, GGAs and meta-GGAs show a similar quality of the results and even the best methods yield relatively large errors (in the range 25–40%) of the dissociation energy in the difficult case of A_2^+. Comparison to the accurate KS quantities shows that this is due to overestimation of the molecular exchange energy by the approximate exchange energy functionals. Following the analysis given in Refs. [19, 20, 21], this is interpreted as inclusion of left-right correlation by the approximate exchange functionals, which is spurious in these systems. In Sec. 3.5 the conclusions are drawn.

3.2 CI calculations of A_2^+

The *ab initio* ground state calculations of the radical cations A_2^+ (A=He, H_2O, NH_3) and the corresponding fragments A and A^+ have been performed with the CI method with inclusion of all single and double excitations (CISD) of the reference Hartree-Fock (HF) configuration Ψ^{HF} by means of the ATMOL package [62]. The effect of size-extensivity on the CI energy has been estimated with the correction of Ref. [63]. The restricted HF and the subsequent CI calculations have been performed in the large correlation-consistent polarized valence quintuple zeta (cc-pV5Z) basis for He [64] and in the smaller core-valence (cc-pCVTZ) basis sets for N and O [65], while for H the triple zeta (TZ) basis [66] augmented with polarization functions has been used. The experimental equilibrium bond distance R(He–He)=1.081 Å [67] has been taken for He_2^+, and the hemibonded structures of $(H_2O)_2^+$ and $(NH_3)_2^+$ with the direct bonds O–O and N–N (with R(O–O)=2.023 Å and R(N–N)=2.151 Å) have been taken from Ref. [68], where they were optimized at the MP2 level.

The two-center three-electron bond $(A\text{–}A)^+$ is at the HF level represented by double occupancy of the $\psi_+ = (a+b)/\sqrt{2+2S}$ orbital between the A lone-pair orbitals ($1s$ for He, $2p_\pi$ for H_2O and sp^3 for NH_3), and single occupancy of the antibonding combination $\psi_- = (a-b)/\sqrt{2-2S}$. There is a remarkable difference between the simple MO wavefunction for an electron pair bond $\Psi_{\text{pairbond}} = \left|\psi_+^2\right|$ and the hemibond wavefunction $\Psi_{\text{hemibond}} = \left|\psi_+^2\psi_-\alpha\right|$ as far as the electron correlation is concerned. The electron pair bond, in particular at long distance, suffers from the well-known unwarranted inclusion of ionic configurations,

$$\Psi_{\text{pairbond}} = (1/2)\{|a^2| + |b^2| + |a\bar{b}| - |\bar{a}b|\} = (1/\sqrt{2})\{\Psi^{\text{ionic}} + \Psi^{\text{HL}}\}.$$

In particular at long distances the 50% inclusion of ionic configurations deteriorates the quality of the wavefunction since the covalent Heitler-London wavefunction then becomes the exact solution. Combining with the doubly excited configuration

$$\Psi_{\text{exc}} = \left|\psi_-^2\right| = (1/\sqrt{2})\left|\Psi^{\text{ionic}} - \Psi^{\text{HL}}\right|$$

is able to remove the ionic contributions. In terms of exchange-correlation holes: if we consider a reference electron close to nucleus b, say, the HF wavefunction has equal probability for the second electron to be at either nucleus, i.e. the hole is delocalized over both nuclei (Ref. [13]) (it represents only exchange, which is just self-interaction correction in this case). On the other hand, the full exchange-correlation hole of Ψ^{HL} is localized at the site where the reference electron is located [69]. GGA exchange approximations work implicitly with localized holes and therefore incorporate the left-right correlation in a KS calculation on an electron pair bond, actually to a surprisingly quantitative accuracy [19, 20, 48]. The HF wavefunction of the hemibonded systems does not suffer from the left-right correlation error. When expanding $\Psi_{\text{hemibond}} = \left|\psi_+^2\psi_-\alpha\right|$ for He_2^+ at long bond distance one obtains

$$\Psi_{\text{hemibond}} = (1/\sqrt{2})\left\{\left|a\alpha b^2\right| - \left|a^2 b\alpha\right|\right\}.$$

At long distance the exact wavefunction approaches

$$\Psi_{\text{hemibond}} = (1/\sqrt{2})\hat{N}\hat{A}\Psi(\text{He}_a^+)\Psi(\text{He}_b) - \hat{N}\hat{A}\Psi(\text{He}_a)\cdot\Psi(\text{He}_b^+),$$

where $\hat{N}\hat{A}$ are the normalization and antisymmetrization operators respectively. In fact, completely different from H_2, the He_2^+ system at equilibrium distance can be

		single excitations		double excitations	
Molecule	HF	coeff	exc. type	coeff.	exc. type
He_2^+	0.991	0.058	$1\sigma_g \rightarrow 3\sigma_g$	0.034	$1\sigma_g^2 \rightarrow 1\sigma_u 2\sigma_u$
$(H_2O)_2^+$	0.953	0.036	$4a_g \rightarrow 9a_g$	0.034	$3a_g 4a_g \rightarrow 4b_u 7b_u$
$(NH_3)_2^+$	0.949	0.054	$3a_{1g} \rightarrow 7a_{1g}$	0.037	$1e_u 3a_{1g} \rightarrow 3a_{2u} 2e_g$

Table 3.1: CI coefficients of the HF configuration and the leading coefficients among the singly and doubly excited configurations in the CISD wavefunctions of A_2^+.ψ_+ is $1\sigma_g$, $4a_g$, $3a_{1g}$ in He_2^+, $(H_2O)_2^+$ and $(NH_3)_2^+$ respectively, ψ_- $1\sigma_u$, $4b_u$, $3a_{2u}$.

considered to be aproaching the long distance limit. For H_2 at the bonding distance of R_e=0.7 Å the $\langle a|b\rangle$ overlap is 0.8, whereas for He_2^+ at the R_e of 1.1 Å the overlap is only 0.23 [68] (the He 1s is much more contracted), which is only reached in H_2 at a distance of 1.95 Å. So the MO wavefunction for He_2^+ does not exhibit a left-right correlation error, but it does have two obvious errors. First, lack of intra-atomic correlation on the non-ionized He atom, i.e. the configurations a^2 and b^2 should be correlated He wavefunctions. Second, the symmetrical effective field in the one-electron equations has a charge +1/2 at each He fragment, which is different from the charges 0 and +1 in the correlated wavefunction. This a rather large difference, in particular in view of the low nuclear charge charge $Z = 2$, so in a term like $\left|a\alpha b^2\right|$ the a orbital is too diffuse, and the b orbital is too contracted. We thus expect the CI calculations to correct first of all for the He atom dynamical correlation, which is known to have in He little effect on the one-electron energy terms, but also for the wrong orbital expansion and contraction, which will also affect the one-electron energies. Similar considerations hold for the other hemibonded systems.

We have carried out CISD calculations for all systems. These are capable of fully correlating the lone pairs in the A–A$^+$ systems, but except for He_2^+ there will be size-inconsistency effects in these CISD wavefunctions we will have to correct for. The CISD wavefunctions Ψ^{CI} show the same pattern of configuration interaction for all three systems and Table 3.1 presents the CI coefficient of the HF configuration Ψ^{HF} $\left[\psi_+^2\psi_-^1\right]$ and the largest contributions among all singly and doubly excited configurations. The HF configuration completely dominates Ψ^{CI}, indicating there is no strong nondynamical correlation, the next largest (though much smaller) contribution comes from the configuration with a single excitation from ψ_+ which, by virtue of Brillouin's theorem, does not interact directly with Ψ^{HF}. These single excitations cannot be $\psi_+ \rightarrow \psi_-$ for symmetry reasons, they are all excitations out of ψ_+ to higher-lying orbitals of the same symmetry whose primary function is to correct the one-electron density. Among doubly excited configurations the largest contribution comes from the configuration, which includes single excitation $\psi_+ \rightarrow \psi_-$, while another electron is excited to some unoccupied orbital of the proper symmetry from ψ_+ (in the case of He_2^+) or from another doubly occupied orbital. The corresponding CI coefficients are small and the values around 0.035 are remarkably similar for all three systems (see Table 3.1). This can be contrasted with the simple pattern of nondy-

method	He^+	He	He_2^+	D_e
HF	−1.9999	−2.8616	−4.9228	38.47
CI		−2.9032	−4.9934	56.66
CI(corrected)		−2.9032	−4.9939	56.98
MP4a				55.3
CCSD(T)[a]				56.0
exp[b]/exact[c]	−2.0000	−2.9037		56.9

---

[a] Ref. [12]
[b] Ref. [67]
[c] Ref. [70]

Table 3.2: Total energies of He_2^+, He, and He^+ (Hartrees) and dissociation energies of He_2^+ (kcal/mol) calculated with *ab initio* methods.

method	$(H_2O)^+$	H_2O	$(H_2O)_2^+$	D_e
HF	−75.6499	−76.0540	−151.7248	13.13
CI	−75.9141	−76.3598	−152.3003	16.57
CI(corrected)	−75.9245	−76.3742	−152.3570	36.58
MP4[a]				43.1
CCSD(T)[b]				39.2

---

[a] Ref. [12]
[b] Ref. [13]

Table 3.3: Total energies of $(H_2O)_2^+$, H_2O, and H_2O^+ (Hartrees) and dissociation energies of $(H_2O)_2^+$ (kcal/mol) calculated with *ab initio* methods.

namical left-right correlation in an ordinary covalent bond with a strong interaction between Ψ^{HF} and the doubly excited configuration with two electrons excited from ψ_+ to ψ_-. Evidently, this latter pattern cannot be realized in our A_2^+ case, since ψ_- is (singly) occupied in $\Psi^{\mathrm{HF}}(A_2^+)$, and it is not required since the left-right correlation error that such excitations correct for, is absent. The energetics of the bonding and the CI effects can be seen from Tables 3.2, 3.3, 3.4, which present the total energies E of the systems A_2^+, A, A^+ and the dissociation energies D_e of A_2^+ calculated with the HF and CI methods (in the last case the energies obtained with and without size-consistency correction [63] are presented). The D_e values are compared with those calculated with the MP4 [12], CCSD(T) [12, 13] and with the experimental data [67]. Note that, due to the larger basis set used, the HF total energies in Tables 3.2, 3.3 and 3.4 are consistently lower than the corresponding energies reported in Ref. [68], while our CI total energies are lower than the best MP2 energies obtained in Ref. [68].

We would like to stress, in particular, the high quality of the CISD calculation for the lightest He_2^+ system (see Table 3.2). The CISD D_e=56.66 kcal/mol of He_2^+ is closer to the experimental value D_e^{exp}=56.9 kcal/mol (corrected for the zero-point vi-

method	$(NH_3)^+$	NH_3	$(NH_3)_2^+$	D_e
HF	−55.8952	−56.2152	−112.1370	16.69
CI	−56.1370	−56.4952	−112.6560	14.93
CI(corrected)	−56.1476	−56.5103	−112.7116	33.70
MP4[a]				37.9

---

[a] Ref. [12]

Table 3.4: Total energies of $(NH_3)_2^+$, NH_3, and $(NH_3)^+$ (Hartrees) and dissociation energies of $(NH_3)_2^+$ (kcal/mol) calculated with *ab initio* methods.

brational energy [12]) than the MP4 D_e=55.3 kcal/mol and even than the CCSD(T) D_e=56.0 kcal/mol of Ref. [12], as a consequence of our larger basis set. The size-consistency correction for He_2^+ is small since, as pointed out above, there is only one electron pair that has to be correlated and we do not need quadruple excitations to correlate two electron-pairs simultaneously. Still, the size-consistency correction works in the right direction and the resulting corrected value D_e=56.98 kcal/mol nearly coincides with D_e^{exp}. We note that correlation effects add 18.2 kcal/mol (18.5 after size-consistency correction) to the calculated D_e, which is 38.5 kcal/mol at HF level. For the simple He_2^+ system the origin of the correlation contribution to D_e is easy to trace. Since He^+ is a one-electron system, the only correlation contribution for the individual fragments He and He^+ comes from dynamical correlation of the 1s electron-pair of the He atom. The CISD correlation energy for the He atom $E_c^{\text{HF}}(\text{He}) = E^{\text{CI}}(\text{He}) - E^{\text{HF}}(\text{He}) = -0.0416$ Hartree (see Table 3.2) is very close to the conventional empirical correlation energy $E_c^{\text{HF(emp)}}(\text{He}) = -0.0420$ Hartree [70]. The total correlation energy of He_2^+ (−0.071 H) contains apart from this expected −0.042 Hartree dynamical correlation of a single He, see above, an additional −0.029 Hartree = −18.2 kcal/mol. This is much smaller than the ca. 58 kcal/mol correlation correction to the H_2 bond energy at R=1.95 Å (corresponding to $\langle a|b\rangle = 0.23$) in agreement with the lack of nondynamical correlation in the He_2^+ bond. The 18.2 kcal/mol correlation contribution is to be attributed to both dynamical correlation corrections to the electron-electron repulsion energy and to orbital and density shape corrections affecting one-electron energy terms (kinetic energy, electron-nuclear energy), see below. As was shown above, the CISD wavefunctions of the heavier systems $(H_2O)_2^+$ and $(NH_3)_2^+$ exhibit the same configuration interaction pattern as the one for He_2^+. However, CISD substantially underestimates the stability of $(H_2O)_2^+$ and $(NH_3)_2^+$ as compared to CCSD(T) of Ref. [13] and MP4 of Ref. [12] (see Tables 3.3 and 3.4). This is clearly the effect of size inconsistency of the restricted CI [71] for these systems with many electron pairs. The relatively large size-consistency corrections for $(H_2O)_2^+$ and $(NH_3)_2^+$, compared to that for He_2^+, bring the CISD dissociation energies of $(H_2O)_2^+$ and $(NH_3)_2^+$ much closer to those of CCSD(T) and MP4 (see Tables 3.3 and 3.4). In fact, the corrected CISD D_e=36.6 kcal/mol for $(H_2O)_2^+$ is slightly closer to the CCSD(T) D_e=39.2 kcal/mol [13] (which, we believe, is the most accurate

	He_2^+	$(H_2O)_2^+$	$(NH_3)_2^+$
T^s	4.926	151.663	112.179
$\Delta T^{s,\mathrm{HF}}$	0.021	0.214	0.247
T_c^s	0.060	0.461	0.330
T_c^{HF}	0.082	0.674	0.577
V^s	−13.901	−439.421	−349.923
$\Delta V^{s,\mathrm{HF}}$	−0.021	−0.402	−0.397
W_H^s	3.657	111.115	94.835
$\Delta W_H^{s,\mathrm{HF}}$	−0.001	0.107	0.164
W_c^s	−0.132	−1.045	−0.858
W_c^{HF}	−0.131	−0.970	−0.868
E_x	−1.561	−17.460	−15.020
$\Delta E_x^{s,\mathrm{HF}}$	0.002	0.016	0.005
E_c	−0.072	−0.584	−0.527
E_c^{HF}	−0.0706	−0.575	−0.519
$\Delta E_c^{s,\mathrm{HF}}$	−0.002	0.065	−0.019

Table 3.5: Comparison of the KS and HF energy components (Hartrees) for A_2^+

calculated value) than the MP4 D_e=43.1 kcal/mol [12]. Thus, we expect that also for $(NH_3)_2^+$ the true dissociation energy is in between the corrected CISD D_e=33.7 kcal/mol and the MP4 D_e=37.9 kcal/mol. For good correlated densities we should do MRCI calculations to get close to the present size-consistency corrected energies.

3.3 Comparison of the KS and HF one-electron solutions for A_2^+

The correlated electron densities $\rho^{\mathrm{CI}}(\mathbf{r})$ of the CISD wavefunctions of He_2^+, $(H_2O)_2^+$ and $(NH_3)_2^+$ have been used to generate the Kohn-Sham orbitals $\psi_i^s(\mathbf{r})$ and potential $v_s(\mathbf{r})$ for these systems. The KS solution has been obtained with the iterative procedure of Ref. [72], which is based on the theory of linear response of the KS orbitals to a potential change Δv_s. The accuracy of this solution can be characterized by the absolute integral error

$$\Delta\rho = \int |\rho^s(\mathbf{r}) - \rho^{\mathrm{CI}}(\mathbf{r})| d\mathbf{r}$$

of the density $\rho^s(\mathbf{r})$ obtained from the generated KS orbitals $\psi_i^s(\mathbf{r})$. A rather accurate KS solution has been constructed for He_2^+ with $\Delta\rho$ of only 0.0003 E, while the KS solutions for $(H_2O)_2^+$ and $(NH_3)_2^+$ have larger errors of 0.007 and 0.0045 E. For the energy terms displayed in Tables 3.5–3.7 the difference between ρ^s and ρ^{CI} is insignificant.

Using $\rho^s(\mathbf{r})$ and $\{\psi_i^s(\mathbf{r})\}$, the KS energy functionals have been calculated and, in order to assess the effect of electron correlation on the KS solution, they are compared in Table 3.5 with the HF ones. The total energies E^{KS} and E^{HF} of the KS and HF determinants are expressed in the same way through the corresponding densities $\rho^{s/\mathrm{HF}}(\mathbf{r})$, spin-densities $\rho_\sigma^{s/\mathrm{HF}}(\mathbf{r})$ and orbitals $\{\psi_\sigma^{s/\mathrm{HF}}(\mathbf{r})\}$

$$E^{\mathrm{KS/HF}} = T_{s/\mathrm{HF}} + V^{s/\mathrm{HF}} + W_H^{s/\mathrm{HF}} + E_x^{s/\mathrm{HF}} \tag{3.1}$$

In (3.1) $T_{s/\mathrm{HF}}$ is the kinetic energy

$$T_{s/\mathrm{HF}} = \sum_\sigma \sum_{i=1}^{N_\sigma} \int d\mathbf{r} \psi_{i\sigma}^{s/\mathrm{HF}*}(\mathbf{r}) \left(-\frac{1}{2}\nabla^2\right) \psi_{i\sigma}^{s/\mathrm{HF}}(\mathbf{r})$$

$V^{s/\mathrm{HF}}$ is the electron-nuclear attraction energy

$$V^{s/\mathrm{HF}} = -\sum_j \int d\mathbf{r} \frac{Z_j \rho^{s/\mathrm{HF}}(\mathbf{r})}{|\mathbf{r} - \mathbf{R}_j|}$$

$W_H^{s/\mathrm{HF}}$ is the Hartree energy of the electron-electron electrostatic repulsion

$$W_H^{s/\mathrm{HF}} = \frac{1}{2} \int d\mathbf{r}_1 d\mathbf{r}_2 \frac{\rho^{s/\mathrm{HF}}(\mathbf{r}_1)\rho^{s/\mathrm{HF}}(\mathbf{r}_2)}{|\mathbf{r}_1 - \mathbf{r}_2|}$$

and $W_x^{s/\mathrm{HF}}$ is the exchange energy

$$W_x^{s/\mathrm{HF}} = \frac{1}{2} \sum_\sigma \int d\mathbf{r}_1 d\mathbf{r}_2 \frac{\rho_\sigma^{s/\mathrm{HF}}(\mathbf{r}_1)\rho_{x\sigma}^{s/\mathrm{HF}}(\mathbf{r}_2|\mathbf{r}_1)}{|\mathbf{r}_1 - \mathbf{r}_2|} \tag{3.2}$$

expressed via the exchange (Fermi) hole function $\rho_{x\sigma}^{s/\mathrm{HF}}(\mathbf{r}_2|\mathbf{r}_1)$, the latter being determined from $\rho_\sigma^{s/\mathrm{HF}}(\mathbf{r})$ and $\{\psi_\sigma^{s/\mathrm{HF}}(\mathbf{r})\}$

$$\begin{aligned} \rho_{x\sigma}^{s/\mathrm{HF}}(\mathbf{r}_2|\mathbf{r}_1) = &- \frac{1}{\rho_\sigma^{s/\mathrm{HF}}(\mathbf{r}_1)} \\ &\times \sum_{i=1}^{N_\sigma} \sum_{j=1}^{N_\sigma} \psi_{i\sigma}^{s/HF*}(\mathbf{r}_1) \psi_{j\sigma}^{s/\mathrm{HF}}(\mathbf{r}_1) \psi_{j\sigma}^{s/HF*}(\mathbf{r}_2) \psi_{i\sigma}^{s/\mathrm{HF}}(\mathbf{r}_2). \end{aligned} \tag{3.3}$$

The correlation correction W_c to the electron-electron interaction energy is defined as the difference between the exact W, as approximated here by the CI calculation, and the Hartree and exchange contributions,

$$W_c^{s/\mathrm{HF}} = W - W_H^{s/\mathrm{HF}} - W_x^{s/\mathrm{HF}}$$

Just as the exchange energy can be obtained by integrating the density with the exchange hole potential, the correlation correction W_c can be obtained by integrating the density against the Coulomb hole potential [73]. Note that the total correlation energy in the KS case has only components T_c^s and V_c^s since the KS density is equal to the CI one, whereas the HF correlation energy also contains electron-nuclear and electron-electron Hartree energy corrections:

$$E_c^s = T_c^s + W_c^s \tag{3.4}$$

$$E_c^{\mathrm{HF}} = T_c^{\mathrm{HF}} + V_c^{\mathrm{HF}} + W_{H,c}^{\mathrm{HF}} + W_c^{\mathrm{HF}}.$$

Both KS and HF solutions for the open-shell systems A_2^+ are of the restricted type, in the sense that the orbitals $\psi_\sigma^{s/\mathrm{HF}}(\mathbf{r})$ are the same for different spins σ. Table 3.5 presents the KS quantities T_s, V^s, W_H^s, E_x^s, as well as the differences $\Delta T_{s,\mathrm{HF}}$, $\Delta V^{s,\mathrm{HF}}$, $\Delta W_H^{s,\mathrm{HF}}$, $\Delta E_x^{s/\mathrm{HF}}$ between the KS and HF energies. We refer to Refs. [48, 73, 74] for explanation and other applications of this type of energy decomposition.

One can conclude from the He_2^+ column of Table 3.5, by comparing to similar results for He atom (see Refs. [46, 69]) that the correlation effects in He_2^+ have atomic and molecular contributions of the same order of magnitude. For instance, the correlation correction to the electron-electron repulsion energy has a negligible contribution from the effect of the density change $\rho^{\mathrm{HF}} \rightarrow \rho^s$ on the Hartree term, W_H, and is almost completely a Coulomb hole contribution W_c^{HF} of -0.131 H. In the He atom this is -0.077 H, so the dynamical correlation between the three electrons of He_+^2 is indeed larger, but not nearly in the proportion of three pairwise interactions in He_2^+ to one pair interaction in He. This confirms our expectation on the basis of the wavefunctions, see Sec. 3.2. There are more significant changes in the one-electron energies of He_2^+ than of He atom, for instance T_c^{HF} is $+0.082$ H, compared to $+0.04$ H in He. This indicates a net contraction effect of the correlation on the density, which is in agreement with the negative V_c^{HF} of -0.021 H, compared to only -0.004 H in He. These results confirm the expectation that He_2^+ has in addition to the dynamical correlation of the He electron pair relatively small additional dynamical correlation effects with the third electron, and somewhat larger one-electron energy effects due to the different charges of the symmetrical density distribution in the HF wavefunction and the unsymmetrical charges in the VB structures. The typical large nondynamical correlation effects of the electron pair bond (cf. H_2 at R=1.95 Å) are absent. We note that, as always [48, 74] the "errors" of the KS determinant and the HF determinant with respect to the correlated wavefunction are not so different and to the extent they are, as showing up in $\Delta T^{s,\mathrm{HF}} = 0.021$ H and $\Delta V^{s,\mathrm{HF}} = -0.021$ H, they largely cancel. As a result, the correlation energies E_c and E_c^{HF} are very close.

In the case of $(H_2O)_2^+$ and $(NH_3)_2^+$ correlation appears to produce an appreciable contraction of the correlated density around the nuclei compared to the HF one. These numbers are however dominated by the correlation effects in the two fragments, where the correlation in the A–H bonds will already produce this effect, and it is much harder to draw conclusions about the correlation effects in the three-electron bond. Note (cf. Table 3.4) that the correlation energies in NH_3^+ and NH_3 are -0.252 Hartree and -0.295 Hartree respectively, summing up to -0.547 Hartree. The correlation energy of $(NH_3)_2^+$ is with -0.575 H only little larger. Because of the contraction (in monomers as well as dimers), the differences of the electron-nuclear attraction energies $\Delta V^{s,\mathrm{HF}}$ are negative, while those of the kinetic $\Delta T^{s,\mathrm{HF}}$ and Hartree $\Delta W_H^{s,\mathrm{HF}}$ energies are positive. Again, as in the case of He_2^+, compensation of differences of opposite sign occurs, and moreover $\Delta E_x^{s,\mathrm{HF}}$ are small, so that the total energies E^{KS} and E^{HF} of the KS and HF determinants are close to each other. As a matter of fact the KS and conventional (with the HF reference) correlation energies $E_c^{s/\mathrm{HF}}$

$$E_c^{s/\mathrm{HF}} = E^{\mathrm{CI}} - E^{\mathrm{KS/HF}}$$

are very close and their difference $\Delta E_c^{s/\mathrm{HF}} = E_c^s - E_c^{\mathrm{HF}} = E^{\mathrm{HF}} - E^{\mathrm{KS}}$, is very small (certainly percentage wise). Note, that the HF determinant is, by definition, the one with the lowest possible energy, so that $\Delta E_c^{s/\mathrm{HF}}$ should be negative. This is true for He_2^+ and $(\mathrm{NH}_3)_2^+$, while for $(\mathrm{H}_2\mathrm{O})_2^+$ a positive $\Delta E_c^{s/\mathrm{HF}}$ value has been obtained, which indicates that the KS solution in this case has not been obtained to sufficient accuracy to obtain a meaningful $\Delta E_c^{s/\mathrm{HF}}$.

Just as the HF orbitals discussed in Sec. 3.2, the KS orbitals of the two-center three-electron bond are well represented with the doubly occupied bonding orbital

$$\psi_+ = (a+b)\,/\sqrt{(2+2S)}$$

and the singly occupied antibonding orbital

$$\psi_- = (a-b)\,/\sqrt{(2-2S)}.$$

Inserting these orbitals in (3.3) and neglecting the two-center overlap $a(\mathbf{r})b(\mathbf{r})$, one can obtain an estimate of the exchange hole functions $\rho_{x\alpha}^s(\mathbf{r}_2|\mathbf{r}_1)$ for the major-spin α and $\rho_{x\beta}^s(\mathbf{r}_2|\mathbf{r}_1)$ for the minor-spin β of He_2^+

$$\begin{aligned}
\rho_{x\alpha}^s(\mathbf{r}_2|\mathbf{r}_1) &= -\frac{1}{\rho_\alpha(\mathbf{r}_1)} \times [\psi_{+\alpha}(\mathbf{r}_1)^2\psi_{+\alpha}(\mathbf{r}_2)^2 \\
&+ \psi_{-\alpha}(\mathbf{r}_1)^2\psi_{-\alpha}(\mathbf{r}_2)^2 + 2\psi_{+\alpha}(\mathbf{r}_1)\psi_{-\alpha}(\mathbf{r}_1)\psi_{+\alpha}(\mathbf{r}_2)\psi_{-\alpha}(\mathbf{r}_2)] \\
&\approx -\frac{a^2(\mathbf{r}_1)a^2(\mathbf{r}_2) + b^2(\mathbf{r}_1)b^2(\mathbf{r}_2)}{a^2(\mathbf{r}_1) + b^2(\mathbf{r}_1)}
\end{aligned}$$

$$\rho_{x\beta}^s(\mathbf{r}_2|\mathbf{r}_1) = -\psi_{+\beta}(\mathbf{r}_1)^2 \approx -\frac{1}{2}[a^2(\mathbf{r}_1) + b^2(\mathbf{r}_1)]$$

It follows from (3.4), that for an α spin electron the exchange hole is localized around the reference electron $(\mathbf{r}_1\alpha)$. Indeed, if the reference electron is on the atom He_A with the orbital a$(\mathbf{r})$, $\mathbf{r}_1 \in \Omega_A$, the exchange hole (3.4) in the distribution of α spin electrons is, essentially, $-a^2(\mathbf{r}_2)$, while if $\mathbf{r}_1 \in \Omega_B$, it is $-b^2(\mathbf{r}_2)$. Such a localized hole is what the GGA functionals implicitly employ. They are therefore expected to perform well for α spin.

In contrast, for the single β electron the exchange hole is just the delocalized self-interaction hole $-\psi_+^2(\mathbf{r}_2)$. The exchange GGA functionals make a large error here, since they employ a localized hole and are therefore much too stabilizing, cf. the case of H_2^+. Since He_2^+ is rather far to the elongated bond side when comparing to H_2^+, the error will be as large as it is in H_2^+ at long bond length [11].

Turning now to the correlation holes, we note that when an α reference electron is close to atom He_A say, the other α electron will be at He_B, but the β electron will be equally likely at He_A and He_B. So there is no left-right correlation hole in the β electron density around an α reference electron. Similarly, there will be no left-right corrrelation hole in the α electron density around the β electron. There will of course be some dynamical correlation between the α and β electrons. The lack of left-right Coulomb correlation in He_2^+ is actually a crucial difference between He_2^+ and H_2. In H_2 at long bond distance the α electron is in a when the β electron is in b. Therefore, the localized exchange hole of GGA's in the α spin electron distribution, which is in fact erroneous, may be said to mimick Coulomb correlation between α and β electrons and the GGAs are actually performing reasonably in H_2. In He_2^+, however, as in H_2^+, this left-right correlation between the α and β electrons is absent and the localized hole around the β electron of the GGA exchange functionals is mimicking a spurious left-right correlation between electrons of different spin.

Considering the GGA correlation functionals, we note that they usually reproduce well the dynamical correlation in atomic systems. Thus, they are expected to perform reasonably also for He_2^+, with its dynamical correlation effects as discussed in Sec. 3.2. In the next section we investigate whether these considerations provide a basis for understanding the performance of GGAs and meta-GGAs.

3.4 Assessment of GGAs and meta-GGAs

In this section the CI results of Sec. 3.2 and the KS solution of Sec. 3.3 are employed to analyze the performance of DFT generalized gradient approximations (GGAs) and meta-GGAs for A_2^+. GGA models the exchange-correlation (xc) energy functional $E_{\mathrm{xc}}[\rho]$

$$E_{\mathrm{xc}}^{\mathrm{GGA}}[\rho] = \int e_{\mathrm{xc}}^{\mathrm{GGA}}\left(\rho(r), \nabla\rho(r)\right) d\mathbf{r}$$

with the xc energy density $E_{\mathrm{xc}}^{\mathrm{GGA}}(\rho(\mathbf{r}),\nabla\ \rho(\mathbf{r}))$, which is an explicit function of the density $\rho(\mathbf{r})$ and its gradient $\nabla\ \rho(\mathbf{r})$, while meta-GGAs employ also the kinetic energy density $\tau(\mathbf{r})$

$$\tau_\sigma(r) = \frac{1}{2}\sum_{i=1}^{N_\sigma}\left|\nabla\psi_{i\sigma}(r)\right|^2$$

and/or the Laplacian $\nabla^2\rho(\mathbf{r})$

$$E_{\mathrm{xc}}^{\mathrm{meta\text{-}GGA}}[\rho] = \int e_{\mathrm{xc}}^{\mathrm{meta\text{-}GGA}}\left(\rho(r), \nabla\rho(r), \tau(r), \nabla^2\rho(r)\right) d\mathbf{r}$$

Table 3.6 compares the CI total and dissociation energies for He_2^+ with those cal-

method	He^+	He	He_2^+	D_e	error[a]
CI	-1.9999[b]	-2.9032	-4.9934	56.66	-0.30
BP	-1.9921	-2.9068	-5.0307	82.66	26.36
BLYP	-1.9999	-2.9069	-5.0322	78.63	22.33
PW	-1.9960	-2.9002	-5.0203	77.87	21.57

---

[a] Error of D_e (kcal/mol) compared to the experimental value of 56.9 kcal/mol [67]

[b] The HF energy

Table 3.6: Comparison of the total energies of He_2^+, He, and He^+ (Hartrees) and dissociation energies of He_2^+ (kcal/mol) calculated with the CI and self-consistent GGA methods.

	KS	BP	BLYP	PW
D_e^x	-55.47	$-25.32(30.15)$	$-25.32(30.15)$	$-24.79(30.68)$
D_e^c	19.11	$13.55(-5.56)$	$12.65(-6.46)$	$8.25(-10.86)$
D_e^{xc}	-36.36	$-11.77(24.69)$	$-12.67(23.79)$	$-16.54(19.82)$

Table 3.7: Comparison of the KS and GGA exchange and correlation contributions to the dissociation energy of He_2^+ (kcal/mol). The GGA contributions are calculated non-self-consistently, (i.e. not with ρ^{GGA} but with the KS density $\rho^s = \rho^{\mathrm{CI}}$) in $E_{\mathrm{xc}}^{\mathrm{GGA}}[\rho]$. The differences with respect to KS are indicated between parentheses.

culated self-consistently with three standard GGA functionals, namely, with the xc functional of Perdew and Wang (PW91) [5, 75, 76], the combination BP of the exchange functional of Becke (B88) [4] and the correlation functional of Perdew (P86) [6] and the combination BLYP of the same exchange functional B88 with the correlation functional of Lee, Yang, and Parr (LYP) [7]. The self-consistent GGA calculations have been performed in the same basis as was used in the CI calculations by means of a Gaussian orbital density functional code [21, 46, 77] based on the ATMOL package. The GGAs of Table 3.6 reproduce rather accurately the total energies of the atomic systems He and He^+, but they consistently overestimate the energy of He_2^+. This leads to the overestimation of the dissociation energy of He_2^+ to He and He^+. The corresponding errors are, with ca. 25 kcal/mol (ca. 40%), large. In order to trace their origin, one can compare the GGA and the accurate KS quantities. The accurate KS quantities are given in the second column of Table 3.7. The exchange energies that enter D_e^x are calculated from the HF expression (Eqs. (3.2), (3.3)) but using the KS orbitals. The KS corrrelation contributions use the difference between the exact (CI) total energy and the energy of the KS determinant, E^{KS}, as the correlation energies for the various systems. So if we add to D_e^{xc} the rest of the energy terms ($T_s[\rho^s]$, $V^s[\rho^s]$, $W_H^s[\rho^s]$), we obtain the CI D_e. In the other columns the GGA numbers are given. These are all calculated with the same KS density ρ^s substituted in the various $E_{\mathrm{xc}}^{\mathrm{GGA}}[\rho]$ rather than with the different self-consistent GGA densities ρ^{GGA}. However, the densities ρ^s and ρ^{GGA} do not differ much and the $E_{\mathrm{xc}}^{\mathrm{GGA}}[\rho^s]$ are rather close to the $E_{\mathrm{xc}}^{\mathrm{GGA}}[\rho^{\mathrm{GGA}}]$. When one compares the self-consistent GGA values for the other energy terms ($T_s[\rho^s]$, $V^s[\rho^s]$, $W_H^s[\rho^s]$) with the KS values, the terms may individually differ between KS and GGA, but their sum is always close. Therefore, the errors in the GGA exchange-correlation terms D_e^{xc} in Table 3.7 are actually close to the total errors in the GGA dissociation energies in Table 3.6. So we may use the errors in Table 3.7 to analyze the cause of the GGA errors.

The KS exchange contribution D_e^x is quite negative (−55.5 kcal/mol) because the exchange energy of the fragments is more stabilizing than of the He_2^+ molecule. This is the case because for both He and He^+ the exchange energy is just self-interaction correction for localized $1s$ electrons, three in total, while for He_2^+ we have seen that this the case for the two α spin electrons but the exchange hole for the β electron (also just self-interaction correction) is delocalized and therefore the exchange energy much less stabilizing. The GGA exchange functionals do not faithfully describe this delocalized hole for the β electron, they have implicitly a too localized hole around the β electron and a too stabilizing exchange energy in He_2^+. This implies that they will increase the dissociation energy relative to the KS exchange energy. The error is large, ca. 30 kcal/mol.

The KS correlation contribution D_e^c increases the dissociation energy, i.e. the correlation energy is more stabilizing for He_2^+ than for He and He^+. The GGA correlation functionals do exhibit this effect, but they tend to underestimate correlation in He_2^+. A possible explanation is that, though reproducing properly the short-range dynamical correlation of the electron pair of He, the GGA correlation functionals cannot fully grasp the relatively long-range dynamical correlation of this electron pair with the unpaired electron. The result is that the GGA correlation functionals decrease the dissociation energy relative to the KS correlation energy, i.e. they make errors of opposite sign compared to the GGA exchange functionals, but the errors are much smaller, see Table 3.7.

In conclusion then the GGA errors in Table 3.6 are caused by the large errors in the GGA exchange energies, which are actually somewhat compensated (but not completely) by smaller errors of opposite sign for the GGA correlation errors. The large exchange error arises from the unduly localized GGA exchange hole for the β electron.

The functionals BP, BLYP and PW considered in Tables 3.6,3.7 were developed in the period 1986–1992 and they have become standard DFT tools. In order to test more recent GGAs as well as meta-GGAs, some post-local-density-approximation (LDA) of He_2^+, $(H_2O)_2^+$, and $(NH_3)_2^+$ have been performed with the Amsterdam Density Functional (ADF2000) package [78]. Besides BP, BLYP and PW, the GGAs tested are the xc functional of Perdew, Burke, and Ernzerhof (PBE) [79] as well as its revised version (revPBE) [80], the xc functional of Filatov and Thiel (FT97) [81], the xc functionals of Hamprecht, Cohen, Tozer, and Handy (HCTH/93 and HCTH/402) [9, 82] parametrized for test sets of 93 and 402 molecules, respectively, and the combination (BOP) of the exchange functional B88 [4] with the one-parameter progressive (OP) approximation of Tsuneda, Suzumura, and Hirao [83] to the correlation functional of Colle and Salvetti [84]. Meta-GGAs are the combinations (BLAP3 and Bmτ1) of the exchange functional B88 with the correlation functional of Proynov, Sirois, and Salahub (LAP3) [58] and with the recent extension of LAP3 by Proynov, Cher-

Molecule	LDA	BP	BLYP	BOP	FT97
He_2^+	86.0(29.1)	83.5(26.6)	82.9(26.0)	83.9(27.0)	82.2(25.3)
$(H_2O)_2^+$	66.7(27.5)	55.9(16.7)	55.8(16.6)	54.0(14.8)	54.0(14.8)
$(NH_3)_2^+$	56.2(22.4)	46.0(12.2)	45.7(11.9)	44.4(10.6)	45.6(11.8)
	PW	PBE	revPBE	HCTH/93	HCTH/402
He_2^+	78.5(21.6)	77.6(20.7)	77.4(20.5)	79.1(22.2)	78.5(21.6)
$(H_2O)_2^+$	57.7(18.5)	59.8(20.6)	56.8(17.6)	52.4(13.2)	54.0(14.8)
$(NH_3)_2^+$	47.8(14.0)	49.7(15.9)	46.9(13.1)	43.0(9.2)	44.2(10.4)

Table 3.8: Dissociation energies (kcal/mol) obtained with the GGA (post-LDA calculations, the errors with respect to the reference data are given in parentheses).

Molecule	FT98	BLAP3	Bmτ1	PKZB	PKZB-KCIS	VS98
He_2^++	85.2(28.3)	78.6(21.7)	78.3(21.4)	78.0(21.1)	78.3(21.4)	75.8(18.9)
$(H_2O)_2^+$	55.2(16.0)	53.0(13.8)	52.6(13.4)	51.1(11.9)	52.5(13.3)	53.0(13.8)
$(NH_3)_2^+$	45.0(11.2)	43.6(9.8)	43.3(9.5)	41.4(7.6)	42.7(8.9)	43.8(10.0)

Table 3.9: Dissociation energies (kcal/mol) obtained with the meta-GGA (post-LDA calculations, the errors with respect to the reference data are given in parentheses).

mette, and Salahub (mτ1) [85], the xc functional of Filatov and Thiel (FT98) [61], the xc functional of Van Voorhis and Scuseria (VS98) [59], the xc functional of Perdew, Kurth, Zupan, and Blaha (PKZB) [60], and the combination (PKZB-KCIS) of the exchange functional PKZB [60] with the correlation functional of Krieger, Chen, Iafrate, and Savin (KCIS) [86]. All calculations have been performed in basis sets of Slater-type orbitals (STOs) ($6s3p2d$ for H and He and $8s6p3d2f$ for O and N) with the geometry optimized at the LDA level. Tables 3.8 and 3.9 present the dissociation energies of He_2^+, $(H_2O)_2^+$, and $(NH_3)_2^+$ calculated with GGAs and meta-GGAs as well as the corresponding errors with respect to the experimental D_e=56.9 kcal/mol for He_2^+ [67], CCSD(T) D_e=39.2 kcal/mol for $(H_2O)_2^+$ [13] and the corrected CISD D_e=33.8 kcal/mol for $(NH_3)_2^+$. All GGAs and meta-GGAs consistently overestimate the stability of A_2^+ resulting in significant errors, so that the analysis given above is also valid in this case. The standard LDA yields the largest errors and the gradient as well as higher-order corrections incorporated in GGAs and meta-GGAs produce, as a rule, a definite improvement.

Meta-GGAs (with the exception of FT98) appear to produce slightly better dissociation energies (see Table 3.9) compared to GGAs (see Table 3.8), still both groups of methods show a similar quality of the results. For He_2^+ revPBE yields the least error ΔD_e=20.5 kcal/mol among GGAs, while VS98 does this among meta-GGAs with ΔD_e=18.9 kcal/mol. For $(H_2O)_2^+$ and $(NH_3)_2^+$ HCTH/93 is the best among GGAs with errors of 13.2 and 9.2 kcal/mol, respectively, while PKZB yields the least meta-GGA errors of 11.9 and 7.6 kcal/mol. Note, that in all cases the errors decrease for a system with a more diffuse valence density in the series He_2^+>$(H_2O)_2{}^+$>$(NH_3)_2^+$. A possible interpretation of this trend is that GGA/meta-GGA xc functionals depend solely on the local density $\rho(\mathbf{r})$ and the related semi-local quantities $\nabla\rho(\mathbf{r})$, $\nabla^2\rho(\mathbf{r})$, and $\tau(\mathbf{r})$, so that for more diffuse densities the effective size of the corresponding localized xc hole becomes relatively larger and closer to that of the delocalized KS hole, which results in smaller GGA/meta-GGA errors. To conclude, Tables 3.8 and 3.9 show that, in spite of a definite improvement, neither recent GGAs, nor meta-GGAs have achieved a definite breakthrough in accuracy in this difficult case and the corresponding errors are still relatively large compared to the desired chemical accuracy.

3.5 Conclusions

In this chapter the difficult case, for DFT methods, of the radical cations He_2^+, $(H_2O)_2^+$, $(NH_3)_2^+$ with two-center three-electron A–A bonds has been investigated at the CI, accurate KS, GGA, and meta-GGA levels. The correlation of the three electrons of the A–A bond has been analyzed. It is predominantly dynamical correlation of two electrons in a He closed shell plus some dynamical electron correlation of these electrons with the third electron on He^+, plus correlation corrections to the one-electron energy terms. This correlation shows up in a characteristic CI pattern. The CISD calculation of He_2^+ yields a calculated value of the dissociation energy D_e which is very close to experiment. CISD calculations of $(H_2O)_2^+$ and $(NH_3)_2^+$ suffer from the size-inconsistency effect, the size-extensivity correction repairs this effect for the calculated energies, so that the corrected CISD D_e value for $(H_2O)_2^+$ becomes close to the benchmark CCSD(T) value of Ref. [13].

The Kohn-Sham solutions of He_2^+, $(H_2O)_2^+$, $(NH_3)_2^+$ have been constructed from the CI densities and the components of the total energies E^{KS} and E^{HF} of the KS and HF determinants are compared. In all cases the E^{KS} and E^{HF} values are close to each other, and so are the corresponding exchange energies E_x^{KS}, E_x^{HF} and correlation energies E_c^{HF} and E_c^{KS}.

Assessment of seven different GGA and six meta-GGA methods has shown that, in spite of the recent intensive methodical development, the radical cations A_2^+ remain a difficult case for DFT. All methods tha thave been tested, consistently overestimate the stability of A_2^+, the corresponding D_e errors decrease for more diffuse valence densities in the series He_2^+>$(H_2O)_2^+$>$(NH_3)_2^+$. On average, meta-GGAs appear to perform slightly better than GGAs and both groups of methods provide a definite improvement over LDA. Still, even the best performers, like PKZB or HCTH/93, produce large errors comparable to those of the other functionals.

Comparison of the BP, BLYP, and PW exchange-correlation energies with the corresponding KS benchmark quantities for He_2^+ has indicated that the approximate exchange functionals are responsible for the errors of GGA-type methods. They characteristically overestimate exchange in A_2^+, so that the combined xc contribution to D_e is overestimated by about 25 kcal/mol. The cause for this overestimation of the exchange has been traced to the automatic inclusion of left-right correlation by the functionals, by virtue of their localized holes, while in the present systems this left-right correlation is absent. So there is a typical difference between a two-center two-electron bond, with left-right correlation present and therefore correctly included by the exchange functional, and a two-center three-electron bond where left-right correlation is absent so inclusion by the GGA functionals becomes spurious. We note that for the two-center ($m = 2$) three-electron ($n = 3$) A–A bond we have a fractional ratio $n/m = 3/2$. This supports the qualitative rule of Ref. [20] which predicts a possible failure of GGAs for a chemical bond with fractional ratio n/m.

Chapter 4

Improved Description of Reaction Barriers with GGAs and meta-GGAs

The performance of 17 xc functionals of the GGA type and of the meta-GGA type is assessed for 15 hydrogen abstraction reactions and 3 symmetrical $\mathrm{S_N2}$ reactions. Topological features of the electron density as well as features of the functionals which determine their performance, are analyzed. Systems that are problematic for standard GGAs characteristically have enhanced values of the dimensionless gradient argument s_σ with local maxima in the bonding region. Due to this local enhancement of s_σ^2, spurious correlation is built into standard GGAs for the transition state of the $\mathrm{S_N2}$ reaction, which leads to the reduced calculated reaction barriers. Barriers are improved with the recent GGA xc functionals which have a modified dependence on s_σ^2 for the exchange component, such as the optimal exchange functional (OPTX) of Ref. [8]. Standard GGAs also underestimate the barriers for the hydrogen abstraction reactions. In this case the barriers are improved by correlation functionals, such as the Laplacian-dependent (LAP3) functional of Ref. [58], which have a modified dependence on the Coulomb correlation of the opposite- and like-spin electrons. The best overall performance is established for the combination OLAP3 of OPTX and LAP3.

4.1 Introduction

The development of novel xc functionals of DFT is to be accompanied with an assessment of their performance for the cases which are problematic for DFT functionals. Such cases [11, 12, 13, 14, 15, 16, 17, 18, 21, 52, 53, 54, 55, 56, 57, 87] have been discussed in Chapt. 2 together with the qualitative rule put forward in Ref. [20] to predict the success or the failure of standard GGA [4, 5, 6, 7]. Problematic molecular systems and transition states (TSs) of chemical reactions with a particular chemical bond have been identified in [20] by a non-integer ratio n/m of the number n of electrons involved in the bond to the number m of relevant fragment orbitals.

The prototype cases discussed in the literature are radical abstraction reaction

$$\mathrm{X + R{-}Y \rightarrow X{-}R + Y} \tag{4.1}$$

and the $\mathrm{S_N2}$ reaction

$$\mathrm{X^- + ZY \rightarrow XZ + Y^-}. \tag{4.2}$$

Standard GGA methods tend to underestimate barriers of both reactions (4.1) and (4.2) due to the overestimated stability of their TSs (Refs. [14, 15, 16, 17, 18] and Tables 4.1- 4.8 below). However, as also explained in Chapt. 2, according to the rule of Ref. [20] the cases of (4.1) and (4.2) belong to different types. In the radical abstraction reaction (4.1) a three-center (m=3) three-electron (n=3) bond is formed in its open-shell TS, so that with the integer ratio n/m=1 the TS belongs to "normal" systems. Improved description of such systems does not require alteration of the dominant GGA exchange energy functional $E_x^{\mathrm{GGA}}[\rho]$, instead, the modification of the relatively small GGA correlation energy functional $E_c^{\mathrm{GGA}}[\rho]$, more precisely, the dependence of E_c^{GGA} on the local spin polarization $\zeta(\mathbf{r})$ [21]. On the other hand, in the closed-shell TS of the $\mathrm{S_N2}$ reaction (4.2) a three-center (m=3) four-electron (n=4) bond is formed. With the non-integer ratio n/m=4/3 this TS belongs to truly "problematic" systems, the proper description of which requires improvement of E_x^{GGA}. Then the question is, could this improvement be achieved by a natural modification and extension of the standard GGA methods without resorting to rather different approaches like hybrid [27, 28] or self-interaction-corrected (SIC) [25, 26] methods.

In this chapter, the performance of 17 exchange-correlation functionals is assessed for 15 reactions of hydrogen abstraction and 3 symmetrical $\mathrm{S_N2}$ reactions. One group of functionals considered are the standard GGAs and their recent modifications, in which the LDA or Xα approximations are corrected with functions containing the dimensionless argument s_σ of the spin-density gradient $\nabla\rho_\sigma$

$$s_\sigma(\mathbf{r}) = \frac{1}{2(6\pi^2)^{1/3}} \frac{\nabla\rho_\sigma(\mathbf{r})}{\rho_\sigma^{4/3}(\mathbf{r})} \tag{4.3}$$

Another group of functionals are the meta-GGAs, which depend also on the KS kinetic energy spin-density τ_σ

$$\tau_\sigma = \frac{1}{2}\sum_i^{N_\sigma} |\nabla\psi_{i\sigma}(\mathbf{r})|^2 \tag{4.4}$$

and/or on the Laplacian of the spin-density $\nabla^2\rho_\sigma$.

In Sec. 4.2 of this chapter the behavior of the basic GGA argument $s_\sigma^2(z)$ along the bond axis z is analyzed for $\mathrm{N_2}$, a prototype molecule with covalent bonds, $\mathrm{He_2^+}$, a prototype "problematic" molecule with the two-center three-electron bond (n/m=3/2), the TS $\mathrm{H\cdots Cl\cdots H}$ of the hydrogen abstraction reaction, and the TS $\mathrm{[F\cdots CH_3\cdots F]^-}$ of the $\mathrm{S_N2}$ reaction. A topological pattern of the density in "problematic" cases is established with a local maximum/maxima of s_σ^2 in the bonding region. This allows us to rationalize the failure in the "problematic" cases of the standard GGAs, for which terms with s_σ^2 dominate the gradient correction for the exchange functional. It also provides an explanation of the improved performance for the $\mathrm{S_N2}$ reactions (described in Sec. 4.4) of modified GGA exchange functionals, for which the terms with the fourth power s_σ^4 of the argument s_σ actually dominate the gradient correction. In Sec. 4.3 the behavior along the bond axis of the meta-GGA correction factor f_σ, which is a function of τ_σ, is analyzed for the above-mentioned prototype systems. This analysis rationalizes the improved performance of meta-GGAs for the $\mathrm{S_N2}$ reactions. In Sec. 4.4 the results of calculations of the symmetrical $\mathrm{S_N2}$ reactions are presented. In agreement with the analysis of Ref. [20], alteration of the exchange functionals produces the most substantial improvement of the calculated central and overall reaction barriers. In Sec. 4.5 the results of the GGA and meta-GGA calculations of the hydrogen abstraction reactions are presented. In this case, modified correlation energy functionals produce substantial improvement of the calculated forward and reverse reaction barriers. An original combination OLAP3 of the modified GGA exchange OPTX functional [8] and the correlation τ_σ dependent functional LAP3 [58] shows the best overall performance for both hydrogen abstraction and symmetrical $\mathrm{S_N2}$ reactions. In Sec. 4.6 the conclusions are drawn.

4.2 Behavior of s_σ^2 and its relation to the orbital nature of the chemical bond

In order to understand the above-mentioned uneven performance of the GGA exchange functionals for various types of systems, we analyze the behavior of their basic argument s_σ^2 for prototype systems. This approach is justified, since standard GGA exchange functionals can be considered as extensions of the gradient expansion approximation (GEA) [88], with the latter being the LDA exchange functional corrected just with $-\beta s_\sigma^2$ (β is a positive coefficient). In this chapter standard GGA exchange functionals are represented by either the one of Becke (B88) [4], or of Perdew and Wang (PW91) [5, 75, 76], or Perdew, Burke, and Ernzerhof (PBE) [79].

A typical behavior of s_σ^2 for a strong covalent bond is presented in Fig. 4.1, where it is plotted along the bond axis z of the N_2 molecule. Distinguished features of the plot are the divergence of $s_\sigma^2(z)$ at the asymptotics $|z| \to \infty$, and in the bulk region local maxima in the atomic regions and nearly complete vanishing of $s_\sigma^2(z)$ in the bonding region. Due to these features of s_σ^2, as was discussed in Ref. [89], GGAs correct the overbinding produced with LDA for covalent bonds. As was argued in Refs. [20, 21], the GGA exchange functionals with their localized model exchange holes represent effectively not only exchange, but also nondynamical (left-right in the case of N_2) Coulomb correlation.

A typical behavior of s_α^2 (α is the major spin) for a "problematic" molecule is presented in Fig. 4.2, where it is plotted for He_2^+. In this case, unlike for N_2, $s_\alpha^2(z)$ is clearly non-zero in the bonding region and, before going to the required zero value

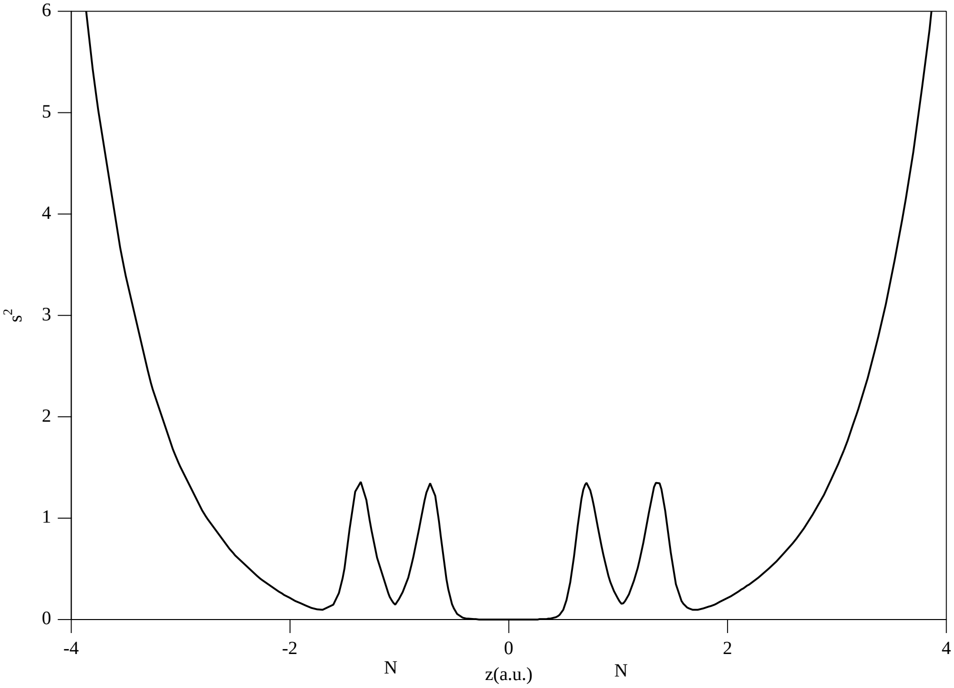

Figure 4.1: s^2 (4.3) is plotted along the bond axis of the N_2 molecule

at the bond midpoint, s_α^2 increases with the increasing distance from the nearest He nucleus, so that it displays two symmetrical local maxima of the height ~0.9 at $z \approx \pm 0.25$ a.u. In order to understand this topological feature of the density, we recall that the two-center three-electron bond $[\mathrm{He}_A\text{-}\mathrm{He}_B]^+$ is represented, essentially, by double occupancy of the $\psi_g = (a+b)/\sqrt{(2+2S)}$ bonding KS molecular orbital (MO) between $1s$ atomic orbitals (AOs) a and b on He_A and He_B, and single occupancy of the antibonding combination $\psi_u = (a-b)/\sqrt{(2-2S)}$ (S is the overlap integral between a and b). In this case, a straightforward calculation of the corresponding $s_\alpha^2(z)$ for a point z on the axis between He_A and He_B shows, that it is proportional to the following combination of the orbital densities $\psi_{g\alpha}^2$ and $\psi_{u\alpha}^2$

$$s_\alpha^2(z) \simeq \frac{1}{[\psi_{g\alpha}^{4/3}]} \frac{x(z)}{[x(z)+1]^{8/3}} \tag{4.5}$$

where $x = \psi_{u\alpha}^2/\psi_{g\alpha}^2$ is the ratio of these densities. The non-monotonic part of (4.5) is its second, x-dependent fraction, which attains its maximum at x=3/5. Note, that x decreases steadily from its infinite (due to the more diffuse nature of $\psi_{u\alpha}$) value at the asymptotics $z \to \infty$ to $x = 0$ at the bond midpoint, where $\psi_{u\alpha}$ has the node, so that $x = 3/5$ is well in the bonding region. Then, the first fraction of (4.5), which increases

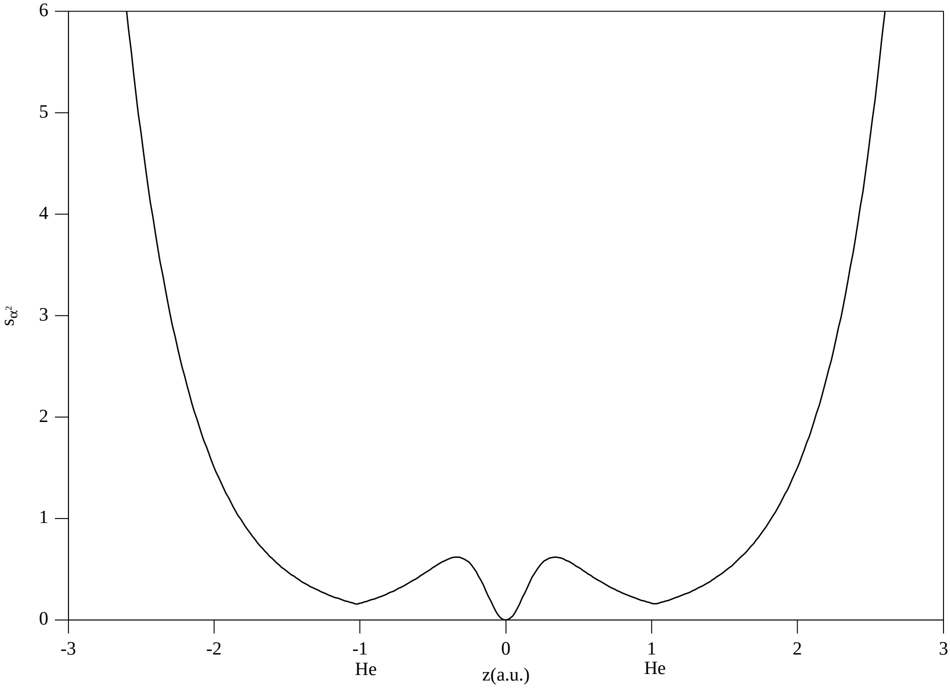

Figure 4.2: s_α^2 (4.3) is plotted along the bond axis of the He_2^+cation dimer.

when going from the nuclei to the bond midpoint, should shift the local maxima of $s_\alpha^2(z)$ further towards the bond midpoint. Thus, the expression (4.5) explains the appearance of the local maxima of $s_\alpha^2(z)$ in the bonding region of He_2^+ as the result of occupation of the antibonding orbital $\psi_{u\alpha}$.

To see, whether this topological feature appears also for the considered "problematic" case of TS of S_N2 reaction, we plot $s_\sigma^2(z)$ for the TS $[F\cdots CH_3\cdots F]^-$ in Fig. 4.3. Indeed, besides pronounced atomic shell structure for the two terminal F atoms and one central C atom, Fig. 4.3 displays also distinct local maxima of the height ~0.5 at $z \approx \pm\ 2.1$ a.u. in the regions between the F nuclei and the nodes of s_σ^2. These maxima correlate with the orbital structure of the three-center four-electron bond. In this case the relation between the s_σ^2 local maxima in the bonding region and the orbital structure is more involved than for He_2^+ [20].

In Fig. 4.4 $s_\alpha^2(z)$ is plotted for a prototype hydrogen exchange TS $[H\cdots Cl\cdots H]$ which, according to the rule of Ref. [20], is another example of "normal" systems besides the N_2 molecule considered in Fig. 4.1. Again in agreement with this rule, the behavior of s_α^2 in the regions of the $H\cdots Cl$ bonds beyond the Cl atomic shell structure is closer to the vanishing pattern of s_σ^2 in the N_2 bonding region (see Fig. 4.1) than the behavior of s_σ^2 in the corresponding regions of He_2^+ (Fig. 4.2) and $[F\cdots CH_3\cdots F]^-$

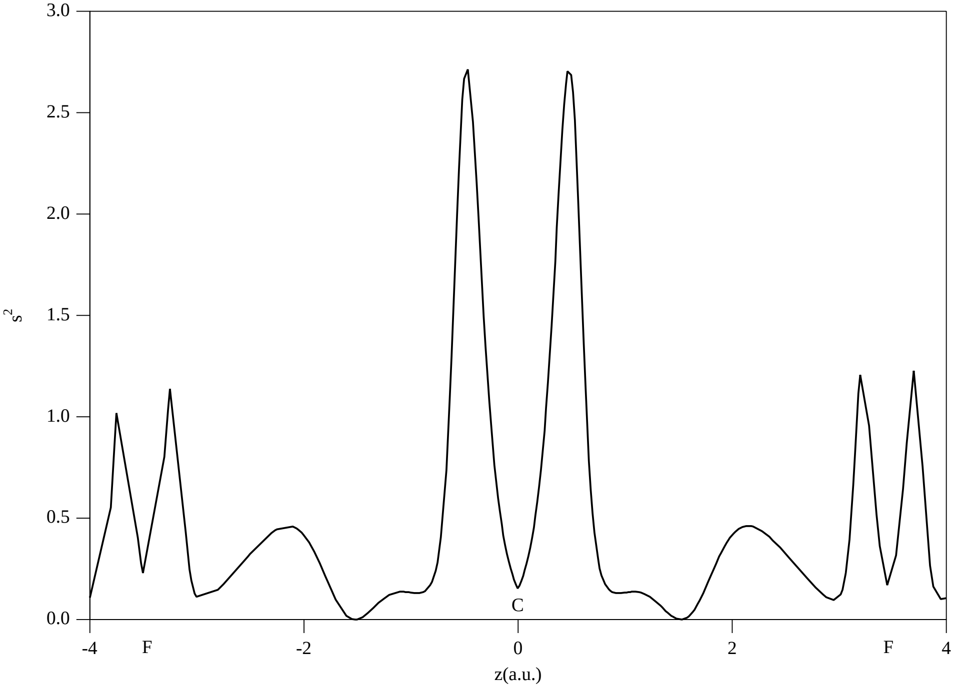

Figure 4.3: s^2 (4.3) is plotted along the bond axis of the TS of the S_N2 reaction $[F\cdots CH_3\cdots F]^-$.

(Fig. 4.3). Indeed, as one can see from Fig. 4.4, s^2_α in the H$\cdots$Cl bonding regions is rather flat, it does not display pronounced maxima, and its values in these regions are much smaller compared to those in the bonding regions of the "problematic" systems considered above.

A characteristic topological feature of the density of "problematic" systems, which emerges from this comparative analysis, is the enhanced values of s^2_σ with local maxima in the bonding regions. The origin of this enhancement for the He_2^+ molecule is the occupation of valence orbitals with an antibonding character. In reality, as was argued in Refs. [20, 87], occupation of antibonding orbitals hampers nondynamical correlation. In fact, the accompanying s^2_σ enhancement builds in spurious correlation through the increased contributions of GGA gradient corrections from the bonding regions. This causes the above-mentioned overestimation by standard GGAs of the stability of "problematic" systems. More enhanced values and higher maxima of s^2_σ in the bonding region of He_2^+ compared to those for $[F\cdots CH_3\cdots F]^-$ (compare Figs. 4.2 and 4.3) correlate with larger GGA errors for the former system [12, 87].

The analysis performed in this section helps to understand the possibility of the improvement for "problematic" cases offered by the recent modified GGA exchange functionals (see also Chapter 6), namely, the functional of the optimal exchange

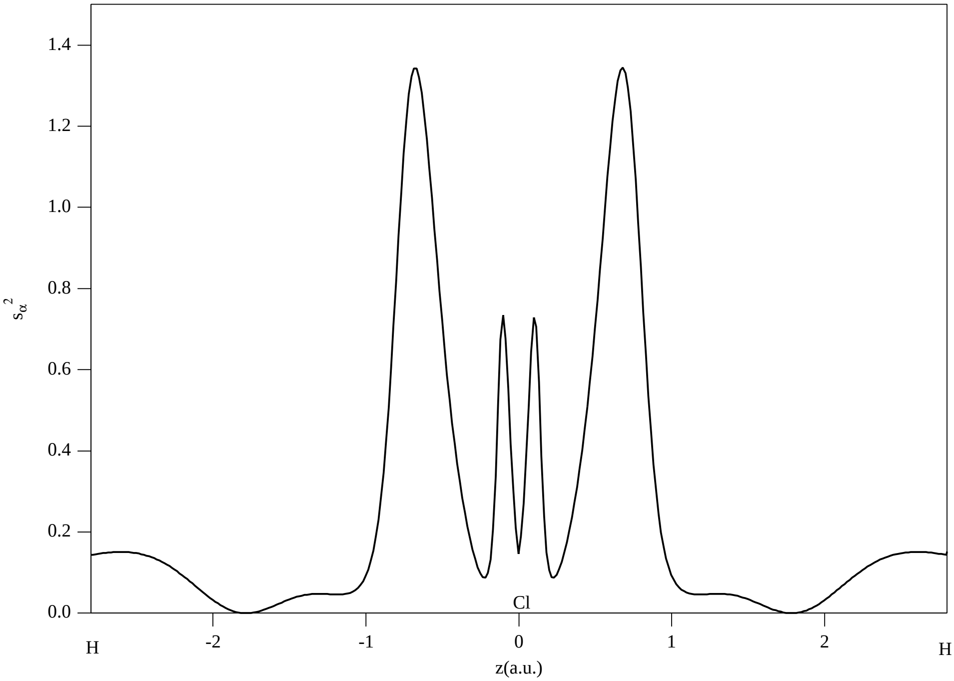

Figure 4.4: s_α^2 (4.3) is plotted along the bond axis of the prototype hydrogen abstraction TS [H$\cdots$Cl$\cdots$H].

method (OPTX) of Cohen and Handy [8], and that of the method of Hamprecht, Cohen, Tozer, and Handy (HCTH) [9]. Unlike standard GGAs, both OPTX and HCTH have as their zero-gradient limit the Xα exchange functional, in which the parameter α by ca. 1.05 enhanced compared to its standard LDA value. Another difference is that both functionals have effectively the fourth power s_σ^4 as the leading power of their gradient corrections in the bulk region. Since the values of s_σ in the bonding regions are less than 1 for all prototype systems considered, while in other regions their can be rather high (see Figs. 4.1–4.4), the contributions from the gradient corrections are reduced in OPTX and HCTH, which might substantially correct the overstability of standard GGAs for "problematic" systems.

In Secs. 4.4 and 4.5 the performance of GGAs will be assessed for the S_N2 and hydrogen abstraction reactions. In this assessment, the above-mentioned exchange functional B88 is taken in standard combinations BLYP and BP with the GGA correlation energy functionals of Lee, Yang, and Parr (LYP) [7], and Perdew (P86) [6]. Also, the combination OLYP of the exchange functional OPTX and the correlation functional LYP is considered. GGA exchange functionals PW91, PBE, and HCTH mentioned in this section are taken with "their own" correlation functionals, so that their abbreviations in the subsequent tables are extended to the corresponding exchange-correlation (xc) combinations.

An alternative way of improvement is offered by meta-GGAs with their dependence on τ_σ of (4.4). This will be analyzed in the next section.

4.3 Behavior of τ_σ and the performance of meta-GGAs

The KS kinetic energy density τ_σ is usually employed in meta-GGAs as the denominator of the ratio t_σ

$$t_\sigma(\mathbf{r}) = \frac{\tau_\sigma^{\mathrm{LSDA}}(\mathbf{r})}{\tau_\sigma(\mathbf{r})} \tag{4.6}$$

where $\tau_\sigma^{\mathrm{LSDA}}$

$$\tau_\sigma^{\mathrm{LSDA}}(\mathbf{r}) = \frac{3}{10}(6\pi^2)^{2/3}\rho_\sigma^{5/3}(\mathbf{r})$$

is the local spin-density approximation (LSDA) for the kinetic energy density. The basic point of our further analysis is that the meta-GGA argument t_σ is, actually, closely related to the GGA argument s_σ. Indeed, the KS τ_σ of (4.4) can be expressed as the sum

$$\tau_\sigma(\mathbf{r}) = \tau_\sigma^W(\mathbf{r}) + \tau_\sigma^P(\mathbf{r})$$

of the von Weiszäcker τ_σ^W

$$\tau_\sigma^W(\mathbf{r}) = \frac{1}{8}\frac{|\nabla\rho_\sigma(\mathbf{r})|^2}{\rho_\sigma(\mathbf{r})} \tag{4.7}$$

and Pauli $\tau_\sigma^P(\mathbf{r})$

$$\tau_\sigma^P(\mathbf{r}) = \frac{\rho_\sigma(\mathbf{r})}{2}\sum_i^{N_\sigma}\left|\nabla\frac{\psi_{i\sigma}(\mathbf{r})}{\rho_\sigma^{1/2}(\mathbf{r})}\right|^2 \tag{4.8}$$

terms. In the region of localization of a certain occupied KS orbital $\psi_{i\sigma}$, where it dominates ρ_σ, the Pauli term (4.8) vanishes and τ_σ turns to (4.7)

$$\tau_\sigma^W(\mathbf{r}) \approx \frac{1}{8}\frac{|\nabla\rho_\sigma(\mathbf{r})|^2}{\rho_\sigma(\mathbf{r})} \tag{4.9}$$

With (4.9), the meta-GGA argument t_σ becomes just proportional to the inverse of s_σ^2

$$t_\sigma(\mathbf{r}) \approx \left[\frac{3}{10}\rho_\sigma^{5/3}(\mathbf{r})\right]\left[\frac{1}{8}\frac{|\nabla\rho_\sigma(\mathbf{r})|^2}{\rho_\sigma(\mathbf{r})}\right]^{-1} = \frac{3}{5s_\sigma^2(\mathbf{r})} \tag{4.10}$$

When other orbitals $\psi_{j\neq i\sigma}(\mathbf{r})$ have appreciable local contributions to $\rho_\sigma(\mathbf{r})$, the argument t_σ of (4.6) could be substantially smaller than its estimate $3/5s_\sigma^{-2}$ from (4.10). Still, the expression (4.10) provides a rough idea of the relation between t_σ and s_σ^2 and of how t_σ could be employed in meta-GGAs.

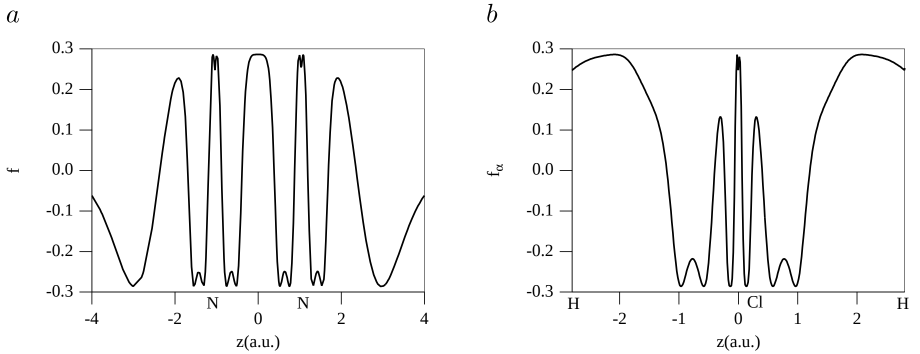

Figure 4.5: *a.* f (4.12) is plotted along the bond axis of the N_2 molecule. *b.* f_α (4.12) is plotted along the bond axis of the prototype hydrogen abstraction TS [H$\cdots$Cl$\cdots$H].

The use of t_σ in meta-GGAs can be illustrated with the t_σ-dependent function $f_\sigma(t_\sigma)$, which is employed in the meta-GGA exchange functional of Becke (B00) [22] as a correction factor

$$E_{x\sigma}^{\mathrm{B00}} = \int \{1 + a f_\sigma[t_\sigma(\mathbf{r})]\} e_{x\sigma}^{\mathrm{BR89}}(\mathbf{r}) dr \tag{4.11}$$

In (4.11) $e_{x\sigma}^{\mathrm{BR89}}$ is the energy density of the exchange functional of Becke and Roussel (BR89) obtained from a model localized Fermi hole [90] and a is an empirical parameter, which in B00 is a=0.14. The correction factor f_σ is defined as follows

$$f_\sigma = w_\sigma - 2w_\sigma^3 + w_\sigma^5 \tag{4.12}$$

where the auxiliary argument w_σ is the following function of t_σ

$$w_\sigma(\mathbf{r}) = \frac{t_\sigma(\mathbf{r}) - 1}{t_\sigma(\mathbf{r}) + 1} \tag{4.13}$$

By the construction (4.11), positive values of $f_\sigma(\mathbf{r})$ make the energy $E_{x\sigma}^{\mathrm{B00}}$ lower, while negative $f_\sigma(\mathbf{r})$ makes $E_{x\sigma}^{\mathrm{B00}}$ higher.

In Figs. 4.5,4.6 the correction factor f_σ is plotted for the prototype systems considered in the previous section. By its design, the function $f_\sigma(z)$ oscillates in the molecular regions, while it vanishes at the long-range asymptotics. Such an oscillatory behavior is required in order to maintain the overall energy balance achieved with the uncorrected functional BR89. However, the oscillation patterns are different for "normal" systems N_2 and [H$\cdots$Cl$\cdots$H], on the one hand, and for "problematic" systems He_2^+ and [F$\cdots$CH$_3\cdots$F]$^-$, on the other hand. Indeed, while $f_\sigma(z)$ is, generally, positive in the bonding regions of "normal" systems (see Fig. 4.5 a,b), it is negative in the bonding regions of "problematic" systems (see Fig. 4.6 a,b). With this, the correction factor f_σ should reduce the energy contributions from the bonding regions,

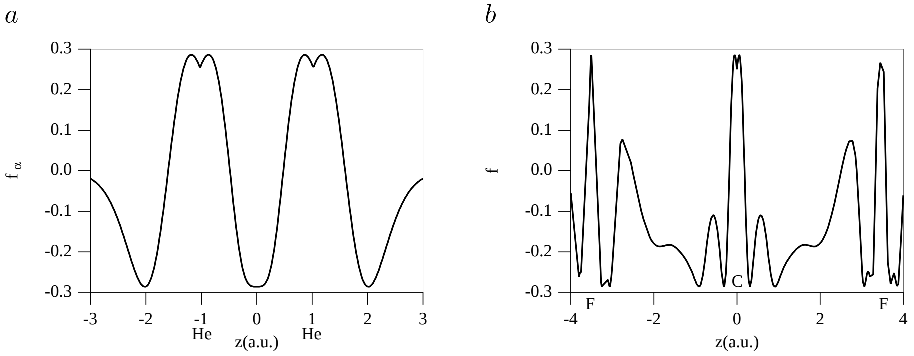

Figure 4.6: *a*. f (4.12) is plotted along the bond axis of the He_2^+ cation dimer. *b*. f_α (4.12) is plotted along the bond axis of the TS of the S_N2 reaction $[F\cdots CH_3\cdots F]^-$.

which are overestimated for "problematic" systems by the uncorrected functionals. As follows from the construction (4.11)–(4.13), the approximate relation (4.10) between t_σ and s_σ, and from the analysis of s_σ presented in the previous section, the above-mentioned characteristic pattern of f_σ with negative values in the bonding regions can be traced to the orbital structure of the bond in the "problematic" cases.

In the next sections the performance of meta-GGAs will be assessed for the S_N2 and hydrogen abstraction reactions. In this assessment, the above-mentioned exchange functionals B00 and BR89 are taken in combinations B00c and BR89c with the correlation functional of Becke (Bc88) [91, 92]. Among other meta-GGAs considered are the xc functionals of Van Voorhis and Scuseria (VS98) [59], and of Perdew, Kurt, Zupan, and Blaha (PKZB) [60], the exchange part of PKZB is also combined with the meta-GGA correlation functional of Krieger, Chen, Iafrate, and Savin (KCIS) [86]. Other meta-GGA correlation functionals considered are the LAP3 of Proynov, Sirois, and Salahub [58], and its modified version $\tau 1$ of Proynov, Chermette, and Salahub [85]. They are taken in combinations Bmτ1, BLAP3 with the exchange functional B88, and LAP3 is also combined in this chapter with the above-mentioned GGA exchange functional OPTX to form the xc combination OLAP3.

4.4 Assessment of GGAs and meta-GGAs for S_N2 reactions

The prototype S_N2 reaction considered in this chapter is the following symmetrical substitution of the halide anion X^-

$$X^- + CH_3X \rightarrow XCH_3 + X^- \tag{4.14}$$

where X=F, Cl, Br. The reaction goes through the formation of unsymmetrical ion-dipole intermediate complex (IC) $X^-\cdots CH_3X$ and symmetrical TS $[X\cdots CH_3\cdots X]^-$,

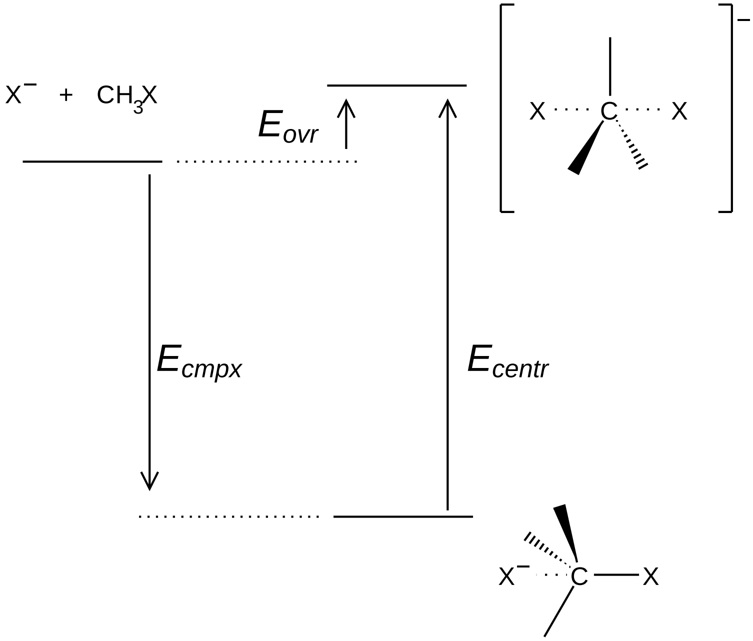

Figure 4.7: Schematic representation of the intermediates IC and TS, the barriers and E_{cmpx} for the S_N2 reaction (4.14)

the special case of which with X=F was considered in the previous sections. These intermediates determine the key parameters of the reaction (4.14), the complexation energy E_{cmpx}, which is the energy difference between IC and free reagents, the central barrier E_{centr}, which is the energy difference between TS and IC, and the overall barrier E_{ovr}, the energy difference between TS and free reagents. The intermediates IC and TS, the barriers and E_{cmpx} are schematically shown in Fig. 4.7.

All GGA and meta-GGA calculations have been performed with the Amsterdam Density Functional (ADF) program [93, 94, 95]. Geometries for reagents, IC and TS were taken from [96]. All self-consistent calculations have been performed with the BLYP xc potential, so that for other functionals the energies E_{cmpx}, E_{centr}, and E_{ovr} have been calculated in the post-BLYP manner. The reference data for these energies are the results of the *ab initio* coupled-cluster CCSD(T) calculations for X=F [97], and the experimental data for X=Cl, Br [98, 99, 100, 101, 102]. The calculations have been carried out in the triple-zeta basis plus two correlation functions TZ2P of Slater-type orbitals (STOs). For X=F and for X=Cl respectively the quadruple-zeta (for valence orbitals) and double zeta (for core orbitals) even-tempered basis augmented with 5 polarization functions (ETQZ+5P) and the similar basis ETQZ3P has been used for the halide.

Absolute values of the calculated energies E_{cmpx}, E_{centr}, and E_{ovr} for X=F, Cl,

	X = F			X = Cl			X = Br		
	E_{cmpx}	E_{ovr}	E_{centr}	E_{cmpx}	E_{ovr}	E_{centr}	E_{cmpx}	E_{ovr}	E_{centr}
LDA	−15.97	−9.53	6.43	−13.83	−8.39	5.44	−13.25	−9.74	3.51
PW91	−13.72	−6.65	7.07	−12.23	−6.68	5.55	−11.54	−7.79	3.75
BLYP	−12.63	−5.58	7.05	−10.85	−6.26	4.60	−10.07	−6.89	3.18
BP	−12.35	−5.21	7.14	−10.71	−5.43	5.28	−10.20	−6.59	3.61
PBE	−13.27	−5.88	7.40	−12.00	−6.06	5.95	−11.27	−7.14	4.13
revPBE	−11.34	−3.20	8.14	−10.42	−3.93	6.57	−9.76	−5.05	4.72
OLYP	−9.16	0.76	9.92	−9.11	−0.25	8.86	−8.03	−1.33	6.70
HCTH/93	−9.23	1.13	10.36	−8.84	−0.07	8.77	−8.02	−1.52	6.50
HCTH/402	−11.27	−0.48	10.78	−10.48	−0.72	9.77	−9.57	−2.48	7.09
KCIS	−11.18	−1.67	9.52	−9.70	−1.02	8.68	−9.25	−2.93	6.32
PKZB	−10.97	−1.50	9.47	−9.52	−1.13	8.39	−9.11	−2.89	6.22
VS98	−17.58	−5.84	11.74	−14.83	−5.25	9.58	−14.24	−7.11	7.13
Bmτ 1	−11.80	−1.94	9.86	−10.80	−3.25	7.55	−11.00	−5.29	5.71
BLAP3	−11.65	−1.73	9.92	−10.62	−2.86	7.76	−10.80	−4.93	5.87
OLAP3	−8.18	4.61	12.80	−8.88	3.15	12.02	−8.76	0.63	9.39
B00c	−11.89	−1.46	10.43	−10.20	−1.89	8.31	−9.52	−3.31	6.21
BR89c	−12.82	−4.36	8.46	−10.42	−4.88	5.63	−10.27	−6.40	3.87
Reference data	−13.7 ± 0.5	−0.8	13.0 ± 1.5	−12.2 ± 2.0	1.0±1.0	13.2 ± 2.2	−9.2 ± 0.5	1.3	11.2

Table 4.1: Calculated energies E_{cmpx}, E_{ovr}, E_{centr} for the $\mathrm{S_N2}$ reactions (X = F, Cl, Br).

	X = F			X = Cl			X = Br		
	ΔE_{cmpx}	ΔE_{ovr}	$\Delta E_{\mathrm{centr}}$	ΔE_{cmpx}	ΔE_{ovr}	$\Delta E_{\mathrm{centr}}$	ΔE_{cmpx}	ΔE_{ovr}	$\Delta E_{\mathrm{centr}}$
LDA	−2.27	−8.73	−6.57	−1.63	−9.39	−7.76	−4.05	−11.04	−7.69
PW91	−0.02	−5.85	−5.93	−0.03	−7.68	−7.65	−2.34	−9.09	−7.45
BLYP	1.07	−4.78	−5.95	1.35	−7.26	−8.60	−0.87	−8.19	−8.02
BP	1.35	−4.41	−5.86	1.49	−6.43	−7.92	−1.00	−7.89	−7.59
PBE	0.43	−5.08	−5.60	0.20	−7.06	−7.25	−2.07	−8.44	−7.07
revPBE	2.36	−2.40	−4.86	1.70	−4.93	−6.63	−0.56	−6.35	−6.48
OLYP	4.54	1.56	−3.08	3.09	−1.25	−4.34	1.17	−2.63	−4.50
HCTH/93	4.47	1.93	−2.64	3.36	−1.07	−4.43	1.18	−2.82	−4.70
HCTH/402	2.43	0.32	−2.22	1.72	−1.72	−3.43	−0.37	−3.78	−4.11
KCIS	2.52	−0.87	−3.48	2.50	−2.02	−4.52	−0.05	−4.23	−4.88
PKZB	2.73	−0.70	−3.53	2.68	−2.13	−4.81	0.09	−4.19	−4.98
VS98	−3.88	−5.04	−1.26	−2.63	−6.25	−3.62	−5.04	−8.41	−4.07
Bmτ1	1.90	−1.14	−3.14	1.40	−4.25	−5.65	−1.80	−6.59	−5.49
BLAP3	2.05	−0.93	−3.08	1.58	−3.86	−5.44	−1.60	−6.23	−5.33
OLAP3	5.52	5.41	−0.20	3.32	2.15	−1.18	0.44	−0.67	−1.81
B00c	1.81	−0.66	−2.57	2.00	−2.89	−4.89	−0.32	−4.61	−4.99
BR89c	0.88	−3.56	−4.54	1.69	−5.88	−7.57	−1.07	−7.70	−7.33

Table 4.2: Errors ΔE_{cmpx}, ΔE_{ovr}, $\Delta E_{\mathrm{centr}}$ of the calculated energies with respect to the reference data for the S_N2 reactions (X= F, Cl, Br).

functional	ΔE_{cmpx}	ΔE_{ovr}	ΔE_{centr}
LDA	2.65	9.72	7.34
BLYP	1.10	6.74	7.52
BP	1.28	6.24	7.12
PW91	0.80	7.54	7.01
PBE	0.90	6.86	6.84
revPBE	1.54	4.56	5.99
OLYP	2.93	1.81	3.97
HCTH/93	3.00	1.94	3.92
HCTH/402	1.51	1.94	3.25
KCIS	1.69	2.37	4.29
PKZB	1.83	2.34	4.44
VS98	3.85	6.57	2.98
Bmτ 1	1.70	3.99	4.76
BLAP3	1.74	3.67	4.62
OLAP3	3.09	2.74	1.06
B00c	1.38	2.72	4.15
BR89c	1.21	5.71	6.48

Table 4.3: Mean absolute error for the $\text{S}_\text{N}2$ reactions (X = F, Cl, Br).

and Br are compared with the reference data in Table 4.1, in Table 4.2 the corresponding errors of LDA, GGAs and meta-GGAs are shown, while Table 4.3 presents the mean average error for the 3 reactions considered. One can see from these Tables the important difference between LDA and standard GGAs, on the one hand, and modified GGAs and meta-GGAs, on the other hand. LDA reproduces satisfactorily the reference complexation energies E_{cmpx}, more precisely, it slightly overestimates the relative stability of the IC with the average error $\Delta E^{\text{LDA}}_{\text{cmpx}} = -2.65$ kcal/mol (see Table 4.3). However, the above-mentioned typical LDA tendency to overbind is much more pronounced for TS. According to the reference data, the TS is slightly more stable than reagents for X=F and it is slightly less stable for X=Cl, Br (see Table 4.1). Unlike this, LDA greatly overestimates the stability of TS, which leads to the large negative values of -8 to -10 kcal/mol of $E^{\text{LDA}}_{\text{ovr}}$ and small positive values of 3.5–6.5 kcal/mol for the central barrier $E^{\text{LDA}}_{\text{centr}}$.

Standard GGAs reduce further the already not very significant LDA error for the complexation energy. Actually, PW91 and PBE yield the best E_{cmpx} values among all functionals with an absolute average errors of only 0.8 and 0.9 kcal/mol, respectively. However, standard GGAs fail to reduce significantly the large LDA errors for the barriers. Indeed, the LDA average error of 9.72 kcal/mol for the overall barriers is reduced to 6.2–9.7 kcal/mol with BLYP, BP, PW91, and PBE, and only revPBE reduces it to somewhat smaller 4.56 kcal/mol. Moreover, standard GGAs fail to reduce appreciably the LDA average error of 7.34 kcal/mol for the central barriers, in particular, the BLYP error of 7.52 kcal/mol is even slightly larger than the LDA one (see Table 4.3).

An improved description of the barriers is achieved with the modified GGAs and meta-GGAs (see Tables 4.1–4.3). Since the functional B00 has been analyzed in the previous section as an example of the meta-GGA correction (in this particular case the functional BR89 is corrected), it is instructive to compare the performance of the corresponding combinations B00c and BR89c. Due to the destabilizing effect of the correction factor f_σ of (4.11), (4.12) on the TS, B00c yields improved higher central and overall barriers in all cases considered (see Tables 4.1, 4.2). As a result, the average BR89c barrier errors $\Delta E_{\text{ovr}}^{\text{BR89c}}$=5.71 kcal/mol and $\Delta E_{\text{ovr}}^{\text{BR89c}}$=6.48 kcal/mol are reduced in B00c to $\Delta E_{\text{ovr}}^{\text{B00c}}$=2.72 kcal/mol and $\Delta E_{\text{centr}}^{\text{B00c}}$=4.15 kcal/mol, respectively.

Combinations with the modified GGA exchange functional OPTX show the best performance. Indeed, the best overall barriers are produced with OLYP with the average error of only 1.81 kcal/mol (see Table 4.3). It is clear, that this improvement is solely due to OPTX, since the combination BLYP with the same standard correlation functional LYP produces much larger average error $\Delta E_{\text{centr}}^{\text{BLYP}}$=6.74 kcal/mol. Note that another modified GGA functional HCTH taken in combinations HCTH/93 and HCTH/402 produces nearly as good overall barriers as OLYP with the average error of 1.94 kcal/mol.

In turn, the combination OLAP3 yields the best central barriers, which are the key parameters for the kinetics of the S_N2 reaction. The corresponding average OLAP3 error of only 1.06 kcal/mol is definitely lower than the errors of other functionals (see Table 4.3). This improvement is due to both OPTX and the meta-GGA correlation functional LAP3. Indeed, change of the exchange functional from BLYP to OLYP reduce the average error for central barriers by 3.55 kcal/mol (from 7.52 to 3.97 kcal/mol). The subsequent change of the correlation functional from OLYP to OLAP3 reduce the error further by 2.91 kcal/mol. For the overall barriers the OLAP3 error of 2.74 kcal/mol is somewhat larger than the above-mentioned smallest error of 1.81 kcal/mol of OLYP. However, OLAP3 is the only method in which, in agreement with the experiment, the overall barriers are present for X=Cl and Br, while in other methods they are absent, so that in the latter cases TSs are made artificially more stable than reagents (see Table 4.1). Somewhat larger OLAP3 errors for the overall barrier and the complexation energy in the case X=F is due to the apparent overestimation of the electron correlation in the F^- anion by LAP3.

Considering the successful performance of OLAP3 for the reaction barriers, it is interesting to note that neither OPTX, nor LAP3 were parameterized specially for "problematic" systems. Indeed, the simple form of the OPTX functional

$$E_{x\sigma}^{\text{OPTX}} = -\int [1.05151 c_x + 1.43169 u_\sigma^2] \rho_\sigma^{4/3}(\mathbf{r}) dr \tag{4.15}$$

$$u_\sigma(\mathbf{r}) = \frac{\gamma x_\sigma^2(\mathbf{r})}{1+\gamma x_\sigma^2(\mathbf{r})} \tag{4.16}$$

where $x_\sigma = 2(6\pi^2)^{1/3} s_\sigma$, $c_x = (3/4)(6/\pi)^{1/3}$ is the Dirac coefficient, and γ=0.006, has been chosen in Ref. [8] to reproduce the Hartree-Fock atomic exchange energies.

In turn, the LAP3 functional contains the logarithmic and polynomial dependence on the argument $(t'_\sigma)^{1/2}\rho^{1/3}$, where $t'_\sigma = \tau_\sigma^{\mathrm{LSDA}}/\tau'_\sigma$ and τ'_σ is the alternative to (4.6), the Laplacian-dependent form of the kinetic energy density

$$\tau'_\sigma(\mathbf{r}) = -\frac{1}{2}\sum_i^{N_\sigma} \psi^*_{i\sigma}(\mathbf{r})\nabla^2\psi_{i\sigma}(\mathbf{r}). \tag{4.17}$$

The dependence on $(t'_\sigma)^{1/2}\rho^{1/3}$ has been parameterized in Ref. [58] to reproduce the energies of (dynamical) Coulomb correlation in atoms and molecules with "normal" covalent bonds. In this sense, the successful performance of OLAP3 for the $\mathrm{S_N2}$ reactions seems to be accidental. However, with the analysis of the previous sections in mind, one can understand that the true reason for the success of OLAP3 is the effective s_σ^4 dependence of OPTX and the proper dependence of LAP3 on τ'_σ. This factor leads to the corrected lower stability of TSs and, as a result, to the improved description of the reaction barriers with OLAP3.

To conclude, the results of this section confirm the above-mentioned rule of Ref. [20] according to which $\mathrm{S_N2}$ reactions with the three-center four-electron bonds in their TSs were attributed to truly "problematic" cases for standard GGAs. In agreement with the conclusions of Ref. [20], better description of $\mathrm{S_N2}$ reactions requires improvement of the GGA exchange functionals.

4.5 Assessment of GGAs and meta-GGAs for hydrogen abstraction reactions

The prototype hydrogen abstraction reactions considered in this chapter are listed in Table 4.4. The reference data for the energies of reactions E, and the barriers of the forward E_{for} and reverse E_{rev} reactions of the first 14 reactions in Table 4.4 has been taken from the database of reactions in [103]. The geometries of the reagents and products are obtained at the quadratic single and double configuration interaction (QCISD) level of *ab initio* theory [103]. The barrier of the last reaction (also calculated with QCISD) has been taken from Ref. [104]. All GGA and meta-GGA calculations have been performed with the ADF program [93, 94, 95]. The energies E, E_{for}, and E_{rev} have been calculated in the post-LDA manner in the TZ2P basis of STOs.

A pure assessment of GGAs and meta-GGAs for the three-center three-electron bond can be provided with the simplest symmetrical hydrogen abstraction reaction

$$\mathrm{H} + \mathrm{H_2} \rightarrow \mathrm{H_2} + \mathrm{H}, \tag{4.18}$$

the symmetrical TS $\mathrm{H}\cdots\mathrm{H}\cdots\mathrm{H}$ of which consists just of this bond. Table 4.5 presents the calculated values of the barrier height E_{barr} (the reference value is 9.6 kcal/mol) for the reaction (4.18) together with the corresponding errors ΔE_{barr}. At first glance, the pattern of the performance of various functionals is similar to that established for the $\mathrm{S_N2}$ reactions in the previous section. Again, LDA overbinds the TS with the

Reaction	E_{for}	E_{rev}	E
$HCl+H\rightarrow Cl+H_2$	5.6	8.7	−3.1
$OH+H_2\rightarrow H+H_2O$	5.7	22.0	−16.3
$CH_3+H_2\rightarrow H+CH4$	12.1	15.0	−2.9
$OH+CH_4\rightarrow CH_3+H_2O$	6.7	20.2	−13.5
$H+H_2\rightarrow H_2+H$	9.6	9.6	0.0
$OH+NH_3H_2\rightarrow O+NH_2$	3.2	13.2	−10.0
$HCl+CH_3\rightarrow Cl+CH_4$	1.8	7.8	−6.0
$F+H_2\rightarrow H+HF$	1.8	33.2	−31.4
$OH+CH_3\rightarrow O+CH_4$	7.8	13.7	−5.9
$H+PH_3\rightarrow PH_2+H_2$	3.2	25.5	−22.3
$H+ClH'\rightarrow HCl+H'$	18.0	18.0	0.0
$OH+H\rightarrow H_2+O$	10.1	13.1	−3.0
$H+H_2S\rightarrow H_2+HS$	3.6	17.4	−13.8
$O+HCl\rightarrow OH+Cl$	9.8	9.9	−0.1
$H_2O+OH\rightarrow OH+H_2O$	10.1	10.1	0.0

Table 4.4: Reference data for the prototype hydrogen abstraction reactions.

large error ΔE_{barr}=−12.49 kcal/mol, i.e. the TS is by 2.89 kcal/mol more stable than the reactants. Standard GGAs reduce substantially this error, though the remaining GGA errors are close to their typical errors for the S_N2 reactions (compare Tables 4.3 and 4.5). Modified GGAs and meta-GGAs reduce further the barrier error.

However, there is a qualitative difference between these two types of reactions in the importance of the exchange-correlation functionals for the observed improvement of the calculated barriers. While for the S_N2 reactions the major improvement comes from modification of the exchange functionals, this is not the case for the reaction (4.18). For example, as was mentioned in the previous section, modification of the exchange functional BR89 to the functional B00 with the t_σ-dependent correction factor f_σ of (4.12) reduces significantly the errors of the combination B00c for the S_N2 reaction barriers compared to those of BR89c (see Table 4.3). Contrary to this, in the case of (4.18) the same correction leads, actually, to a larger error of B00c for E_{barr} compared to BR89c (see Table 4.5). Note, as another example, that a change of the exchange functional from BLYP to OLYP reduces ΔE_{barr} by only 0.5 kcal/mol. This correlates with the established in Secs. 4.2, 4.3 “normal” behavior of the GGA argument s_σ^2 and of the meta-GGA factor f_σ for the TS of the hydrogen abstraction reaction.

Unlike for the S_N2 reactions, the major improvement for the reaction (4.18) comes from modification of the correlation functional. Indeed, independently of whether B88 or OPTX is employed in the xc combination, a change of the correlation functional from LYP to LAP3 reduces ΔE_{barr} by 4.1 kcal/mol for BLAP3 or OLAP3 compared to the corresponding combination BLYP or OLYP. This reduction produces the smallest error among all functionals ΔE_{barr}=−1.94 kcal/mol for OLAP3 (see Table 4.5). A

XC functional	E_{barr}	ΔE_{barr}
LDA	−2.89	−12.49
PW91	3.33	−6.27
BLYP	3.06	−6.54
BP	0.85	−8.75
PBE	3.71	−5.89
revPBE	4.90	−4.70
OLYP	3.56	−6.04
HCTH/93	7.10	−2.50
HCTH/402	7.36	−2.24
KCIS	5.09	−4.51
PKZB	5.46	−4.28
VS98	5.56	−4.04
Bmτ 1	7.47	−2.13
BLAP3	7.16	−2.44
OLAP3	7.66	−1.94
B00c	4.42	−5.18
BR89c	6.22	−3.38

Table 4.5: Calculated values E_{barr} and errors ΔE_{barr} with respect to reference data, (see Table 4.4) of the barrier height for the reaction (4.18).

slightly larger error (in absolute value) of −2.13 kcal/mol is produced with the combination Bmτ1 with the correlation functional τ1 which, as was mentioned above, is a modified version of LAP3. In Tables 4.6, 4.7 the calculated reaction energy E and the barriers E_{for} and E_{rev} are presented with the corresponding errors for two unsymmetrical hydrogen abstraction reactions, and Table 4.8 presents the average errors of the functionals for all 15 reactions. In general case, because of the more complex nature of the reactants, the pattern of improvement due to the exchange-correlation functionals is more complicated than for the reaction (4.18), though the general trend is the same. Standard GGAs reduce the large LDA average absolute error for barriers from ca. 18.5 kcal/mol to 8.5–10.5 kcal/mol, with revPBE producing somewhat smaller errors of 6.75 and 7.46 kcal/mol for E_{for} and E_{rev}, respectively (see Table 4.8). They also reduce the substantial LDA reaction energy error of 6.33 kcal/mol, in particular, the corresponding revPBE error is only 1.16 kcal/mol.

Further significant improvement of the calculated barriers is achieved with the use of the correlation functionals LAP3 and τ1. Indeed, a change of the exchange functional from B88 to OPTX reduces $\Delta E^{\mathrm{av}}_{\mathrm{for}}$ by 2.1 kcal/mol from 8.5 kcal/mol for BLYP to 6.4 kcal/mol for OLYP which is, actually, close to the above-mentioned value of 6.75 kcal/mol for revPBE. In turn, a subsequent change of the correlation functional from LYP to LAP3 produces further error reduction by 3.73 kcal/mol and the resultant smallest error among all functionals $\Delta E^{\mathrm{av}}_{\mathrm{for}}$=2.67 kcal/mol of OLAP3 (see Table 4.8). The combination OLAP3 also produces the best reverse barriers

XC functional	$E_{\rm for}$	$\Delta E_{\rm for}$	$E_{\rm rev}$	$\Delta E_{\rm rev}$	E	ΔE
LDA	−3.08	−8.68	−10.70	−19.40	7.61	10.71
PW91	0.01	−5.59	−1.55	−10.25	1.56	4.66
BLYP	−2.29	−7.89	2.68	−6.02	−4.97	−1.87
BP	−2.82	−8.42	0.20	−8.50	−3.01	0.09
PBE	0.73	−4.87	−1.15	−9.85	1.88	4.98
revPBE	1.09	−4.51	2.53	−6.17	−1.44	1.66
OLYP	−0.11	−5.71	3.96	−4.74	−4.07	−0.97
HCTH/93	1.80	−3.80	5.14	−3.56	−3.34	−0.24
HCTH/402	2.29	−3.31	3.84	−4.86	−1.54	1.56
KCIS	2.51	−3.09	2.88	−5.82	−0.37	2.73
PKZB	0.01	−5.59	5.75	−2.95	−5.74	−2.64
VS98	4.18	−1.42	3.14	−5.56	1.03	4.13
Bmτ 1	1.94	−3.66	7.11	−1.59	−5.17	−2.07
BLAP3	1.92	−3.68	6.60	−2.10	−4.68	−1.58
OLAP3	4.10	−1.50	7.88	−0.82	−3.79	−0.69
B00c	0.79	−4.81	4.20	−4.50	−3.41	−0.31
BR89c	0.75	−4.85	3.11	−5.59	−2.35	0.75

Table 4.6: Calculated values $E_{\rm for}$, $E_{\rm rev}$, E and errors $\Delta E_{\rm for}$, $\Delta E_{\rm rev}$, ΔE with respect to reference data, (see Table 4.4) of the barrier height for the reaction HCl+H→Cl+H_2.

with the average error $\Delta E^{\rm av}_{\rm rev}$=3.48 kcal/mol. The second best barriers are produced with Bmτ1 with the average errors $\Delta E^{\rm av}_{\rm for}$=4.18 kcal/mol and $\Delta E^{\rm av}_{\rm rev}$=4.64 kcal/mol. Note, that OLAP3 yields also reasonable reaction energies with an average error of 1.6 kcal/mol.

Thus, just as in the case of the S_N2 reactions considered in the previous section, the original combination OLAP3 shows the best overall performance also for the hydrogen abstraction reactions. However, unlike for the S_N2 reactions, the major improvement in the latter case is achieved with a change of the correlation functionals. This is in agreement with the analysis of Ref. [21], according to which the improvement in this particular "normal" case could be gained with the modification of the local density polarization dependence of standard GGA correlation functionals. Apparently, such a modification has been effectively undertaken in Ref. [58], where the correlation energy functional LAP3 was constructed with the explicit account of the Coulomb correlation of the opposite- and like-spin electrons.

4.6 Conclusions

The goal of this chapter has been three-fold. First, to assess the quality of GGA and meta-GGA exchange-correlation functionals for the prototype S_N2 and hydrogen abstraction reactions. Second, to establish the specific topological features of the electron density of "problematic" (for standard GGAs) systems and to relate them to the

XC functional	E_{for}	ΔE_{for}	E_{rev}	ΔE_{rev}	E	ΔE
LDA	−9.41	−17.21	−9.63	−23.33	0.23	6.13
PW91	−0.83	−8.63	−0.18	−13.88	−0.65	5.25
BLYP	1.77	−6.03	2.23	−11.47	−0.45	5.45
BP	0.56	−7.24	1.29	−12.41	−0.73	5.17
PBE	−0.65	−8.45	0.23	−13.47	−0.87	5.03
revPBE	2.39	−5.41	4.11	−9.59	−1.73	4.17
OLYP	3.04	−4.76	6.61	−7.09	−3.58	2.32
HCTH/93	2.74	−5.06	7.11	−6.59	−4.38	1.52
HCTH/402	1.80	−6.00	6.21	−7.49	−4.41	1.49
KCIS	3.32	−4.48	7.07	−6.63	−3.75	2.15
PKZB	4.40	−3.40	8.80	−4.90	−4.40	1.50
VS98	3.14	−4.66	7.94	−5.76	−4.80	1.10
Bmτ 1	5.53	−2.27	6.44	−7.26	−0.90	5.00
BLAP3	5.18	−2.62	6.05	−7.65	−0.87	5.03
OLAP3	6.45	−1.35	10.44	−3.26	−3.99	1.91
B00	3.31	−4.49	7.52	−6.18	−4.21	1.69
BR89c	1.81	−5.99	5.95	−7.75	−4.14	1.76

Table 4.7: Calculated values E_{for}, E_{rev}, E, and errors ΔE_{for}, ΔE_{rev}, ΔE with respect to reference data (see Table 4.4), of the barrier height for the reaction OH + CH_3 → O + CH_4.

orbital structure of the chemical bonds involved. Third, to try new xc combinations like OLAP3 for the reactions.

A characteristic topological feature of the density of "problematic" systems has been established, which is the enhanced values of the basic gradient argument s_σ^2 with local maxima in the bonding region. With the direct evaluation of s_σ^2 for the simple [He-He]$^+$ bond, the origin of this topological feature has been traced to the occupation of valence orbitals with an antibonding character. Due to this local enhancement of s_σ^2, spurious correlation is built in with standard GGAs, which leads to their overestimation of the stability of "problematic" systems.

The performance of 17 GGA and meta-GGA functionals has been assessed for the prototype "problematic" cases, the symmetrical S_N2 reactions. Standard GGAs reduce substantially the reaction barriers calculated by LDA, and further reduction is gained with the "modified" GGAs and meta-GGAs. The best overall performance has been observed for the combination OLAP3. The basis of this success is the modified dependence of the exchange OPTX functional, with respect to "standard" GGA exchange functionals, with the effective leading s_σ^4 term of its gradient correction. Another factor appears to be the proper dependence of the correlation LAP3 functional on the meta-GGA argument.

The performance of GGA and meta-GGA functionals has also been assessed for 15 hydrogen abstraction reactions. Here, again, standard GGAs reduce substantially the reaction barriers calculated by LDA. However, further reduction is obtained, mainly,

XC functional	ΔE_{for}	ΔE_{rev}	ΔE
LDA	18.62	18.49	6.33
PW91	9.90	10.52	2.66
BLYP	8.50	8.68	1.85
BP	9.91	10.27	1.57
PBE	9.53	10.20	2.72
RevPBE	6.75	7.46	1.16
OLYP	6.40	6.54	1.35
HCTH/93	5.09	5.09	1.09
HCTH/402	5.65	5.64	1.09
KCIS	5.44	6.61	1.34
PKZB	4.45	6.21	3.38
VS98	4.60	5.16	1.63
Bmτ 1	4.18	4.64	1.87
BLAP3	4.50	4.77	1.74
OLAP3	2.67	3.48	1.60
B00c	5.26	5.83	1.24
BR89c	6.58	6.61	0.85

Table 4.8: Mean absolute error for the prototype hydrogen abstraction reactions.

due to the modified correlation functionals. Again, the best overall performance has been observed for OLAP3. For the considered systems with the non-zero spin-density polarization the basis of the success of OLAP3 appears to be the modified structure of the correlation LAP3 functional with the explicit account of the Coulomb correlation of the opposite- and like-spin electrons.

The analysis of the behavior of s_σ^2 and the meta-GGA correction factor f_σ confirms the qualitative rule of Ref. [20]. Indeed, for the "normal" system H+ClH with the three-center three-electron (n/m=1) bond s_σ^2 and f_σ behave like for the molecule N_2. On the other hand, for the "problematic" system $[F\cdots CH_3\cdots F]^+$ with the three-center four-electron (n/m=4/3) bond s_σ^2 and f_σ behave like for the prototype "problematic" system He_2^+ with the two-center three-electron (n/m=3/2) bond. The results of the GGA and meta-GGA calculations also confirm the conclusions of Ref. [20] in the sense, that for the "problematic" case of the S_N2 reactions the improvement of the results has been achieved with the modified exchange energy functionals, while for the "normal" case of the hydrogen abstraction reactions the improvement has been achieved with the modified correlation energy functionals.

Based on the assessment performed in this chapter, we can recommend the original combination OLAP3 for calculations of chemical reactions. For the considered prototype reactions OLAP3 produces the best overall reaction barriers, and it also reproduces well the energies of the hydrogen abstraction reactions. On the other hand, OLAP3 is certainly not the best functional for thermochemical calculations. Our calculations for the standard thermochemical G2 set of molecules show that the quality of OLAP3 for these calculations is superior to that of BP, but it is somewhat inferior to that of BLYP, and it is definitely worse than the quality of the meta-GGA functional VS98. With this, OLAP3 can only be considered as yet another approach to the universally good xc functional. Then, the challenge is to develop a functional which would combine the quality of OLAP3 for chemical reactions and that of VS98 for thermochemistry.

Chapter

5

Approximate functionals of occupied and virtual Kohn-Sham orbitals

The standard LDA and GGA fail to properly describe the dissociation of an electron pair bond, yielding large errors (in the order of 50 kcal/mol) at long bond distances. To remedy this failure, a self-consistent KS method is proposed with the xc energy and potential depending on both occupied and virtual KS orbitals. The xc energy functional of Buijse and Baerends [30, 105] is employed which, based on an *Ansatz* for the xc hole amplitude, is able to reproduce the important dynamical and nondynamical effects of Coulomb correlation through the efficient use of virtual orbitals. Self-consistent calculations require the corresponding xc potential to be obtained, to which end the optimized effective potential (OEP) method is used within the common energy denominator approximation (CEDA) for the static orbital Green's function, The problem of the asymptotic divergence of the xc potential of the OEP when a finite number of virtual orbitals is used, is addressed. The self-consistent calculations reproduce very well the entire H_2 potential curve, describing correctly the gradual build-up of strong left-right correlation in stretched H_2.

5.1 Introduction

The development of the Kohn-Sham density functional theory can be viewed as going upstairs the "Jacob's ladder" [106] of xc functionals. From LDA [3] to the direct gradient expansion approximation (GEA) [107, 108] and GGAs [4, 5, 6, 7]. Then, up to the functionals depending on the occupied KS orbitals, such as meta-GGA xc-energy functionals [55, 58, 59, 60] and occupied-orbital-dependent exchange [38, 40, 109, 110] and xc [87, 111] potentials. Recently, DFT has arrived at the level of xc functionals depending on both occupied and virtual KS orbitals [30, 112]. Far from being "art for art's sake", this new development is aimed at yet unsolved DFT problems. In particular, in Fig. 5.1 it is demonstrated that the widely employed LDA

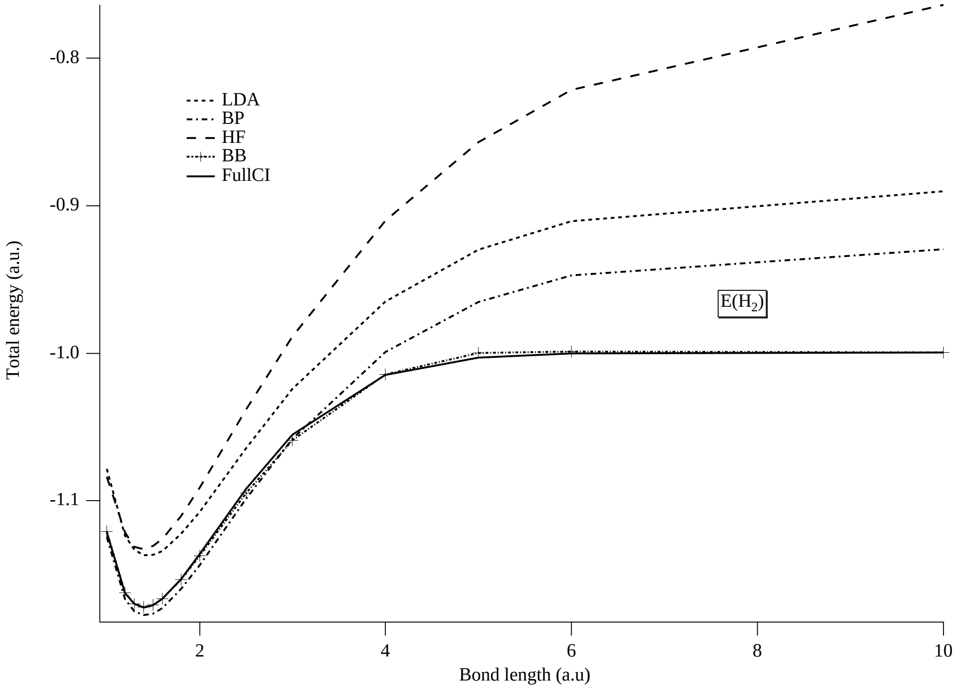

Figure 5.1: Total energy of H_2 as a function of internuclear distance for the Hartree-Fock approximation (HF), the local-density approximation (LDA), the Becke88-Perdew86 generalized gradient approximation (BP), a full CI calculation, and the exchange-correlation functional of Refs. [30, 105].

and GGA approximations (taking Becke88-Perdew86 as an example) fail rather badly in the description of the full potential energy curve for dissociating H_2. The LDA curve exhibits the well-known underestimation of the bond energy close to equilibrium geometry, but it is making a much larger error (ca. 70 kcal/mol!) at large distances, although not as large as the restricted Hartree-Fock method, (the DFT calculations are also spin and symmetry restricted, since the true Kohn-Sham solutions of this closed shell system are of that nature, and in fact exist at all bond distances [113]). The BP GGA gives the well-known nice correction around the equilibrium geometry. However, while it reduces the error at the dissociation limit compared to LDA, it still yields a very large error in that case (ca. 45 kcal/mol). The error of the current DFT approximations in the case of electron pair bond dissociation has received less attention than the well-known failure for odd electron systems like H_2^+ [11, 12, 13], but is hardly less dramatic.

It can easily be seen in Figs. 5.2 and 5.3 (to be discussed more extensively in Sec. 5.5) that the GGA error arises since the GGA correlation energy is far too small (not negative enough), an error which is only partly, but by no means sufficiently, compensated by a more negative GGA exchange energy than the exact exchange

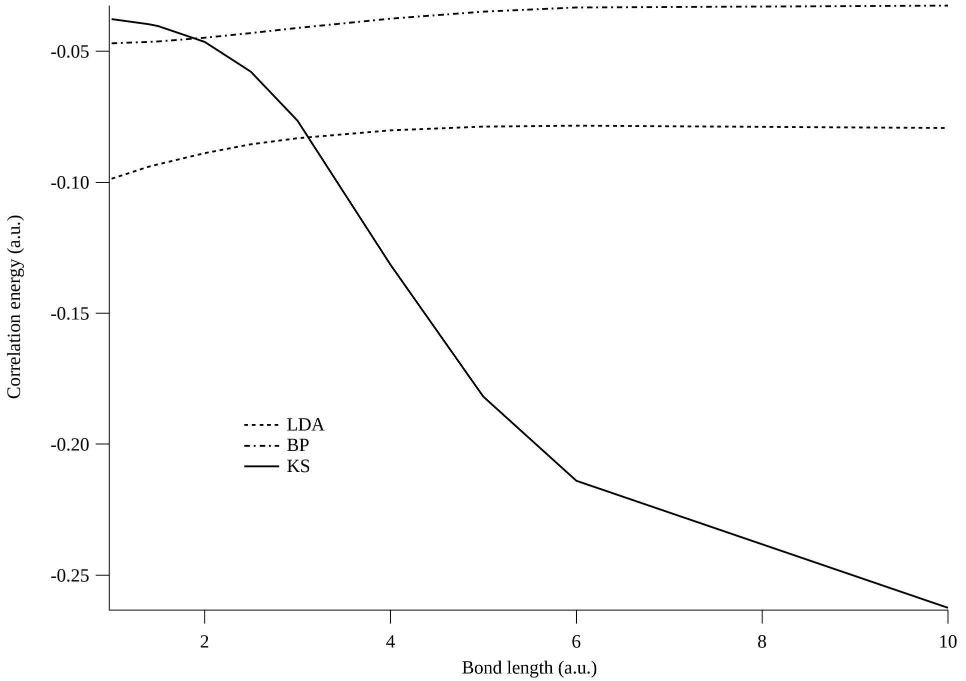

Figure 5.2: Correlation energy of H_2 as a function of internuclear distance. See caption of Fig. 5.1.

energy E_x^{KS}. The well-known "compensation of errors" between exchange and correlation, or rather "the exclusion of nondynamical correlation in the GGA correlation but inclusion into GGA exchange" [48] breaks down for the extreme nondynamical correlation in the dissociating electron pair bond. It is to be noted that hybrid functionals would not provide a remedy; they would deteriorate the dissociation curve by shifting it towards Hartree-Fock. As was stressed in Ref. [30], orbital-dependent functionals with inclusion of virtual orbitals seems to be a natural way to describe properly within DFT dissociation of molecular electron pair bonds. It would seem, at first glance, that functional dependence on virtual orbitals does not present any principal problem. Both occupied and virtual KS orbitals are density functionals $\psi_j(\mathbf{r};[\rho])$, $j \leq N/2$; $\psi_a(\mathbf{r};[\rho])$ $a < N/2$ (we consider a closed-shell N electron system), so that the xc energy $E_{\mathrm{xc}}[\rho]$ can be, in principle, considered within the KS energy expression as an orbital-dependent functional

$$E\left[\rho\right] = T_s\left(\{\psi_j[\rho]\}\right) + E_{ne}\left[\rho\right] + E_H\left[\rho\right] + E_{\mathrm{xc}}\left[\{\psi_j\left[\rho\right]\},\{\psi_a\left[\rho\right]\}\right] \tag{5.1}$$

Other functionals in (5.1) are the KS kinetic energy T_s, an explicit functional of the occupied orbitals $\{\psi_j\}$, the electron-nuclear attraction energy E_{ne} and the Hartree energy of the electrostatic electron repulsion E_H, which are both explicit density

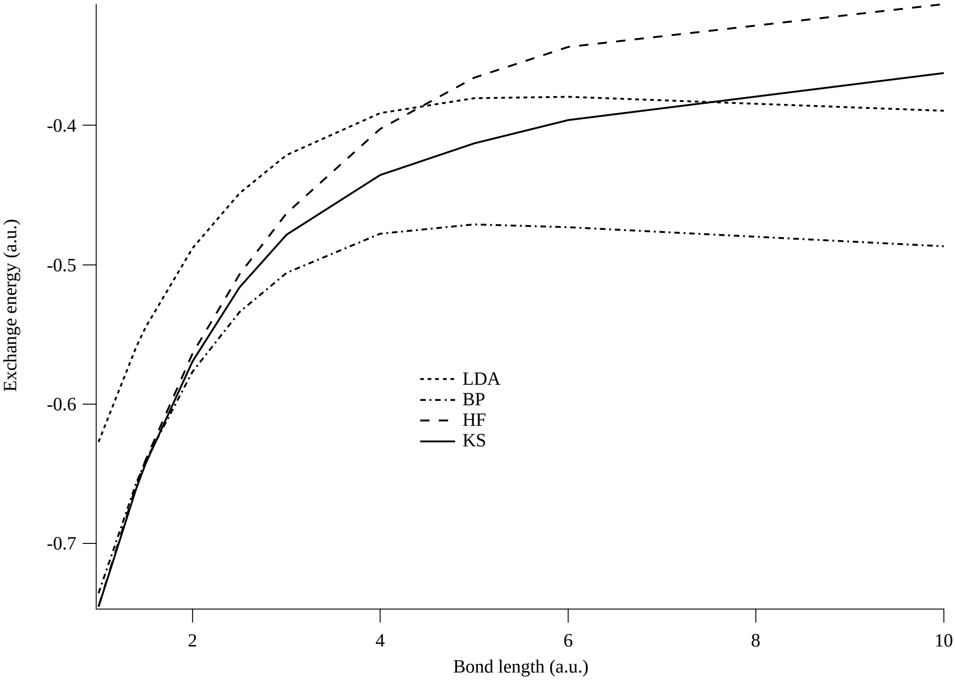

Figure 5.3: Exchange energy of H_2 as a function of internuclear distance. See caption of Fig. 5.1.

functionals of the electron density ρ

$$\rho(\mathbf{r}_1) = \sum_i n_i \left|\psi_i(\mathbf{r}_1)\right|^2;\ n_i = 2,\ i \leq N/2;\ n_i = 0,\ i > N/2 \tag{5.2}$$

Within the self-consistent KS theory, the orbitals are determined from the KS one-electron equations

$$\left\{-\frac{1}{2}\nabla^2 + v_s(\mathbf{r}_1)\right\}\psi_i(\mathbf{r}_1) = \varepsilon_i\psi_i(\mathbf{r}_1) \tag{5.3}$$

$$v_s(\mathbf{r}_1) = v_{ne}(\mathbf{r}_1) + v_H(\mathbf{r}_1) + v_{\mathrm{xc}}(\mathbf{r}_1) \tag{5.4}$$

where the index i refers to both occupied and virtual orbitals. The local xc potential v_{xc} in (5.4) can be obtained according to the optimized potential method (OPM) [31] via the chain differentiation rule

$$v_{\mathrm{xc}}(\mathbf{r}_1) = \sum_i \int \frac{\delta E_{\mathrm{xc}}\left[\{\psi_j\},\{\psi_a\}\right]}{\delta\psi_i(\mathbf{r}_2)} \frac{\delta\psi_i(\mathbf{r}_2)}{\delta v_s(\mathbf{r}_3)} \frac{\delta v_s(\mathbf{r}_3)}{\delta\rho(\mathbf{r}_1)} d\mathbf{r}_2 d\mathbf{r}_3 + \text{c.c.} \tag{5.5}$$

from the orbital derivatives of the functional $E_{\mathrm{xc}}[\{\psi_j\},\{\psi_a\}]$[1]. Since the exact functional form of E_{xc} is not known, restricted approximate functionals with a finite number M of orbitals are to be taken, so that (5.5) turns to a finite sum

$$v_{\mathrm{xc}}\left(\mathbf{r}_1\right)=\sum_{i}^{M}\int\frac{\delta E_{\mathrm{xc}}\left[\{\psi_j\},\{\psi_a\}\right]}{\delta\psi_i\left(\mathbf{r}_2\right)}\frac{\delta\psi_i\left(\mathbf{r}_2\right)}{\delta v_s\left(\mathbf{r}_3\right)}\frac{\delta v_s\left(\mathbf{r}_3\right)}{\delta\rho\left(\mathbf{r}_1\right)}d\mathbf{r}_2 d\mathbf{r}_3+\text{c.c.}\tag{5.6}$$

In Ref. [112] a perturbation theoretic approach, yielding the Kohn-Sham analogue of the second order Møller-Plesset (MP2) energy correction has been used. In Ref. [30] a simple *Ansatz* for $E_{\mathrm{xc}}[\{\psi_j\},\{\psi_a\}]$ [77, 105] that can describe strong correlation effects, has been applied to the dissociating H_2 molecule. However, as was recognized in [30, 112], the OPM potential v_{xc} of (5.6) may diverge in the asymptotic region (at long distance) when virtual Kohn-Sham orbitals are included in the xc energy (i.e. $M > N/2$ in Eq. (5.6)), although the Coulombic asymptotics $v_{\mathrm{xc}}\left(\mathbf{r}_1\right)\rightarrow -1/\left|\mathbf{r}_1\right|$ was established for the exact xc potential [114]. In this chapter an approximate self-consistent KS scheme based on an orbital-dependent xc functional [77, 105] is presented. In Sec. 5.2 this functional $E_{\mathrm{xc}}[\{\psi_j\},\{\psi_a\}]$ is characterized. The required "weights" with which the occupied and virtual orbitals enter, which in the original density-matrix functional formulation were obtained as the square roots of natural orbital occupation numbers, are here written as the square roots of "fictitious occupations" $\tilde{n}_i$ that are estimated with a Fermi-type distribution as functions of the orbital energies ε_j. In Sec. 5.3 the problem of divergence of the OEP potential (5.6) alluded to above, is considered. It is a consequence of the necessary restriction, in practice, that the number M of the KS orbitals in the functional $E_{\mathrm{xc}}[\{\psi_j\},\{\psi_a\}]$ be finite. In that case the requirement of correct asymptotics of the xc potential should be imposed as a constraint in the optimization of the potential. An appropriate modification of the OEP equations is introduced to achieve correct asymptotics of the constructed v_{xc}. In Sec. 5.4 the OEP equations for the local potential v_{xc} are approximately but accurately and efficiently solved with the recent common energy denominator approximation (CEDA) to the static orbital Green's function [40, 110]. In Sec. 5.5 an application is made to the prototype electron pair bond, the ground-state potential energy curve of the H_2 molecule. Contrary to the standard LDA and GGA methods, the present method is able to reproduce the whole potential curve of H_2, including the dissociation region. A comparative analysis of individual energy components is made to interpret the obtained results. In Sec. 5.6 implications of the present work for DFT are discussed and the conclusions are drawn.

We note that very recently the problem of dissociation of an electron pair bond, exemplified by the H_2 case, has been approached by many-body perturbation theory based methods, where use of the random phase approximation is an essential ingredient [115, 116, 117]. Encouraging results are obtained for the strong nondynamical correlation at long distance, but improvement is still required for the energy at geometries around equilibrium bond length (i.e. atomization energies).

---

[1] Sometimes the denotation OPM is used for the exact exchange-only functional, and optimized effective potential (OEP) method for more general orbital-dependent xc functionals.

5.2 A (virtual) orbital-dependent xc energy functional

The orbital-dependent functional we will use is obtained with a simple *Ansatz* [77, 105] for the density of the xc hole $\bar{\rho}_{\mathrm{xc}}^{\mathrm{hole}}$ which through its potential $\bar{v}_{\mathrm{xc}}^{\mathrm{hole}}$ determines the xc energy

$$E_{\mathrm{xc}}\left[\{\psi_j\},\{\psi_a\}\right]=\frac{1}{2}\int\rho\left(\mathbf{r}_1\right)\bar{v}_{\mathrm{xc}}^{\mathrm{hole}}\left(\mathbf{r}_1\right)d\mathbf{r}_1=\frac{1}{2}\int d\mathbf{r}_1\rho\left(\mathbf{r}_1\right)\int d\mathbf{r}_2\frac{\bar{\rho}_{\mathrm{xc}}^{\mathrm{hole}}\left(\mathbf{r}_2|\mathbf{r}_1\right)}{\mathbf{r}_{12}}$$

where the density ρ is the exact density, which can be obtained from the occupied $(n_i=2)$ KS orbitals

$$\rho\left(\mathbf{r}_1\right)=\sum_i^{N/2}n_i\left|\psi_i\left(\mathbf{r}_1\right)\right|^2.$$

The over bar in $\bar{\rho}_{\mathrm{xc}}^{\mathrm{hole}}$ and $\bar{v}_{\mathrm{xc}}^{\mathrm{hole}}$ indicates that we are dealing with the coupling-constant integrated xc hole and potential, i.e. the kinetic correlation energy $T-T_s$ is incorporated. In the case of the xc contribution of the electron-electron interaction energy,

$$W_{\mathrm{xc}}=(1/2)\int\rho\left(\mathbf{r}_1\right)v_{\mathrm{xc}}^{\mathrm{hole}}\left(\mathbf{r}_1\right)d\mathbf{r}_1=(1/2)\int d\mathbf{r}_1\rho\left(\mathbf{r}_1\right)\int d\mathbf{r}_2\rho_{\mathrm{xc}}^{\mathrm{hole}}\left(\mathbf{r}_2|\mathbf{r}_1\right)/\mathbf{r}_{12}$$

($\rho_{\mathrm{xc}}^{\mathrm{hole}}$ not coupling constant integrated), it has been shown that a very good approximation for the xc hole can be obtained from the *Ansatz* that it is the square of an amplitude $\varphi_{\mathrm{xc}}^{\mathrm{hole}}(\mathbf{r}_2|\mathbf{r}_1)$,

$$-|\varphi_{\mathrm{xc}}^{\mathrm{hole}}(\mathbf{r}_2|\mathbf{r}_1)|^2=\rho_{\mathrm{xc}}^{\mathrm{hole}}.$$

When the amplitude is expanded in the natural orbitals, the coefficients can be shown, from symmetry properties of the two-electron density matrix, to depend on the square roots of the NO occupation numbers [77, 105]. The expansion of the hole amplitude into natural orbitals implies that one is approximating the two-electron density matrix in terms of tensor products of the one-electron density matrix. It has been shown by Csanyi and Arias [118] that there is only a limited number of possibilities for such approximate forms, because of the symmetry requirements. A further restriction to one term in the tensor expansion of the two-matrix, leads to an approximation which is equivalent to our approximation of the hole as minus the square of an amplitude. These authors indeed also obtain the $\sqrt{n}$ dependence of the coefficients upon expansion in the natural orbitals (cf. Ref. [119] for an earlier argument leading to the same $\sqrt{n}$ dependence). Following Refs. [30, 105], we propose a similar expression for the amplitude of the coupling constant integrated xc hole, the KS orbitals being used instead of the NOs,

$$\bar{\varphi}_{\mathrm{xc}}^{\mathrm{hole}}\left(\mathbf{r}_2|\mathbf{r}_1\right)=\sum_i^M\sqrt{\frac{\tilde{n}_i}{\rho\left(\mathbf{r}_1\right)}}\psi_i^*\left(\mathbf{r}_1\right)\psi_i\left(\mathbf{r}_2\right),\qquad(5.7)$$

$$\bar{\rho}_{\mathrm{xc}}^{\mathrm{hole}}\left(\mathbf{r}_2|\mathbf{r}_1\right)=-\sum_{ij}^{M}\frac{\sqrt{\tilde{n}_i\tilde{n}_j}}{\rho\left(\mathbf{r}_1\right)}\psi_i^*\left(\mathbf{r}_1\right)\psi_i\left(\mathbf{r}_2\right)\psi_j\left(\mathbf{r}_1\right)\psi_j^*\left(\mathbf{r}_2\right) \tag{5.8}$$

which yields the orbital-dependent potential of the xc hole $v_{\mathrm{xc}}^{\mathrm{hole}}$

$$\bar{v}_{\mathrm{xc}}^{\mathrm{hole}}\left(\mathbf{r}_1\right)=-\sum_{ij}^{M}\frac{\sqrt{\tilde{n}_i\tilde{n}_j}}{\rho\left(\mathbf{r}_1\right)}\psi_i^*\left(\mathbf{r}_1\right)\psi_j\left(\mathbf{r}_1\right)\int\frac{\psi_i\left(\mathbf{r}_2\right)\psi_j^*\left(\mathbf{r}_2\right)}{\mathbf{r}_{12}}d\mathbf{r}_2 \tag{5.9}$$

and the xc energy functional E_{xc}

$$E_{\mathrm{xc}}\left[\left\{\psi_j\right\},\left\{\psi_a\right\}\right]=-\frac{1}{2}\sum_{ij}^{M}\sqrt{\tilde{n}_i\tilde{n}_j}\int d\mathbf{r}_1 d\mathbf{r}_2\frac{\psi_i^*\left(\mathbf{r}_1\right)\psi_i\left(\mathbf{r}_2\right)\psi_j\left(\mathbf{r}_1\right)\psi_j^*\left(\mathbf{r}_2\right)}{\mathbf{r}_{12}} \tag{5.10}$$

Here the $\tilde{n}_i$ no longer refer to NO occupation numbers, but they are the parameters that govern the involvement of the occupied and virtual KS orbitals in the functional. They have to absorb the change from "pure" xc hole to coupling constant integrated hole, and ultimately the success or failure of this functional will depend on our ability to construct a suitable algorithm for the determination of the $\tilde{n}_i$. It should be emphasized that the $\tilde{n}_i$ are *not* the true occupation numbers of the Kohn-Sham orbitals. We continue to use the standard Kohn-Sham prescription of $N/2$ occupied orbitals, i.e. in a closed shell system we have Kohn-Sham occupation numbers n_i of either 2.0 or 0.0.

Having been derived in Refs. [77, 105] as a generalization of the exchange (Fermi) hole amplitude [120, 121], the *Ansatz* (5.8) describes correlation remarkably well for cases of dynamical correlation, such as the He atom (becoming exact in the high-Z two-electron ions with configuration $(1s)^2$) and also for cases of near degeneracy or nondynamical correlation, such as dissociating H_2. In the latter case the Fermi hole ρ_x^{hole} is just minus the density of the σ_g MO,

$$\rho_x^{\mathrm{hole}}(\mathbf{r}_2|\mathbf{r}_1)=-|\sigma_g(\mathbf{r}_2)|^2\approx\frac{1}{2}[|a(\mathbf{r}_2)|^2+|b(\mathbf{r}_2)|^2]$$

(a and b are the atomic orbitals, AOs), so that it does not depend on $\mathbf{r}_1$ and is delocalized over both H atoms. Such delocalization produces the well-known failure of the Hartree-Fock (HF) method for dissociating H_2 (see also Sec. 5.5). Contrary to this, the hole (5.8), which in this case can be fairly represented as

$$\begin{aligned}\rho_{\mathrm{xc}}^{\mathrm{hole}}(\mathbf{r}_2|\mathbf{r}_1)\approx&-\frac{1}{\rho(\mathbf{r}_1)}\{|\sigma_g(\mathbf{r}_1)|^2|\sigma_g(\mathbf{r}_2)|^2\\&+[\sigma_g^*(\mathbf{r}_1)\sigma_u(\mathbf{r}_1)\sigma_g(\mathbf{r}_2)\sigma_u^*(\mathbf{r}_2)+\mathrm{c.c.}]+|\sigma_u(\mathbf{r}_1)|^2|\sigma_u(\mathbf{r}_2)|^2\}\end{aligned} \tag{5.11}$$

is correctly localized around the reference electron at $\mathbf{r}_1$, i.e. when $\mathbf{r}_1$ is in the neighborhood of atom H_A, $\rho_{\mathrm{xc}}^{\mathrm{hole}}\left(\mathbf{r}_2|\mathbf{r}_1\in\Omega_A\right)\approx-\left|a\left(\mathbf{r}_2\right)\right|^2$([2]). This correct form

---

[2] In this particular case the coupling constant integration has no effect and $\rho_{\mathrm{xc}}^{\mathrm{hole}}$ and $\bar{\rho}_{\mathrm{xc}}^{\mathrm{hole}}$ are identical, see [30] and [74].

of $\rho_{\mathrm{xc}}^{\mathrm{hole}}$ is the result of the inclusion of the lowest unoccupied MO (LUMO) σ_u in (5.7),(5.8),(5.11), in particular, through the cross-products $\sigma_g^* \sigma_u$ in (5.8),(5.11). Within the KS scheme (5.1)–(5.4), we consider the fictitious occupations $\tilde{n}_i$ as density functionals and we approximate their functional dependence with the Fermi-type distribution,

$$\tilde{n}_i = \frac{2}{1 + \exp\left[f\left(\varepsilon_i - \varepsilon_F\right)\right]} \tag{5.12}$$

where ε_i are the KS orbital energies in (1.3) and the actual form of the model function $f(\varepsilon_i - \varepsilon_F)$ will be considered in Sec. 5.5.

5.3 OEP derivation of the xc potential, with a constraint to ensure proper asymptotic decay.

The chain differentiation rule (5.6) for v_{xc} takes into account that all KS orbitals are solutions in the same local KS potential v_s, which is in one-to-one correspondence with the density ρ. It can be easily transformed into the optimized effective potential (OEP) equations, which have originally been formulated explicitly as a variational problem for the energy minimization under variation of the local potential [31]. The second derivative in the r.h.s. of (5.6) is expressed through the static orbital Green's function G_i

$$\frac{\delta \psi_i\left(\mathbf{r}_2\right)}{\delta v_s\left(\mathbf{r}_3\right)} = -G_i\left(\mathbf{r}_2, \mathbf{r}_3\right) \psi_i\left(\mathbf{r}_3\right), \tag{5.13}$$

$$G_i\left(\mathbf{r}_1, \mathbf{r}_2\right) = \sum_{j \neq i} \frac{\psi_j\left(\mathbf{r}_1\right) \psi_j^*\left(\mathbf{r}_2\right)}{\varepsilon_j - \varepsilon_i} \tag{5.14}$$

and the third derivative is the inverse

$$\frac{\delta v_s\left(\mathbf{r}_3\right)}{\delta \rho\left(\mathbf{r}_1\right)} = \chi_s^{-1}\left(\mathbf{r}_3, \mathbf{r}_1\right) \tag{5.15}$$

of the static KS linear response function χ_s

$$\chi_s\left(\mathbf{r}_1, \mathbf{r}_3\right) = \frac{\delta \rho\left(\mathbf{r}_1\right)}{\delta v_s\left(\mathbf{r}_3\right)} = -\sum_i^{N/2} n_i \psi_i^*\left(\mathbf{r}_1\right) G_i\left(\mathbf{r}_1, \mathbf{r}_3\right) \psi_i\left(\mathbf{r}_3\right) + \text{c.c.}, \;\; n_i = 2.$$

Inserting (5.13) and (5.15) in (5.6), multiplying both its sides by $\chi_s(\mathbf{r}_1, \mathbf{r}_3)$, integrating over $\mathbf{r}_1$ and relabeling the indices, we obtain the OEP equation

$$\begin{aligned} &\sum_i^{N/2} n_i \psi_i^*\left(\mathbf{r}_1\right) \int v_{\mathrm{xc}}\left(\mathbf{r}_2\right) G_i\left(\mathbf{r}_1, \mathbf{r}_2\right) \psi_i\left(\mathbf{r}_2\right) d\mathbf{r}_2 + \text{c.c.} \\ &= \sum_i^{M} \psi_i^*\left(\mathbf{r}_1\right) \int v_{\mathrm{xc}}^i\left(\mathbf{r}_2\right) G_i\left(\mathbf{r}_1, \mathbf{r}_2\right) \psi_i\left(\mathbf{r}_2\right) d\mathbf{r}_2 + \text{c.c.} \end{aligned} \tag{5.16}$$

where the nonlocal potentials v_{xc}^{k} are defined as

$$v_{\mathrm{xc}}^{k}\left(\mathbf{r}_{2}\right)=\left[\frac{1}{\psi_{k}\left(\mathbf{r}_{2}\right)} \frac{\delta E_{\mathrm{xc}}\left[\left\{\phi_{i}\right\}\right]}{\delta \psi_{k}^{*}\left(\mathbf{r}_{2}\right)}\right]$$

According to the analysis of Refs. [112, 122], it appears that the l.h.s. and r.h.s. of (5.16) have (as functions of $\mathbf{r}_1$) different asymptotics at $|\mathbf{r}_1| \rightarrow \infty$. Indeed, since the Green's function G_i has the asymptotics [112, 122, 123] $G_i(\mathbf{r}_1, \mathbf{r}_2) \rightarrow \psi_i(\mathbf{r}_1)$ at $|\mathbf{r}_1| \gg |\mathbf{r}_2|$ the l.h.s. sum over occupied orbitals decays as the density $|\psi_{N/2}(\mathbf{r})|^2$ of the highest occupied molecular orbital (HOMO) $\psi_{N/2}$. On the other hand, the extended (but still finite) r.h.s. sum decays as the density $|\psi_a(\mathbf{r})|^2$ of the most diffuse virtual orbital ψ_a included in the summation, i.e. it decays more slowly than the l.h.s. This produces the divergence of the solution of the OEP equations, the potential v_{xc} in the l.h.s. of (5.16) [112, 122]. It is to be noted [123] that this divergence is not a necessary consequence of the use of virtual orbitals. If the complete (infinite) set is used, the asymptotic behavior is not necessarily governed by the most diffuse function of the set (which would not be defined anyway in the complete set of KS orbitals which comprises unbound states). The divergence can be considered as the result of the restriction to a finite summation over virtual orbitals in (5.6) and in the r.h.s. of (5.16). From a theoretical point of view it is, of course, desirable to operate with a more physically reasonable, non-divergent approximation to v_{xc}. In practice, as was recognized in Refs. [30, 112], this divergence prevents approximate solution of the OEP equations (5.16) with virtual KS orbitals with the method of Krieger-Li-Iafrate (KLI) [38] or with the common energy denominator approximation (CEDA) [40, 110]. Bearing this in mind, we propose a modification of the OEP equations (5.5), (5.16), so as to impose correct asymptotic behavior of the xc potential. It has been made clear in Ref. [112] that in the KLI approximation the origin of the divergence can be identified as arising from terms in the potential of the form $\psi_i(\mathbf{r}_1)\psi_j(\mathbf{r}_1)/\rho(\mathbf{r}_1)$. When $\psi_i(\mathbf{r}_1)$ and/or $\psi_j(\mathbf{r}_1)$ are virtual orbitals, the numerator may decay more slowly than the denominator, which asymptotically decays as the highest occupied Kohn-Sham orbital. In the CEDA the same type of terms lead to divergence. As a pragmatic solution we change the asymptotic behavior of the denominator from $\rho(\mathrm{r})$ to

$$\tilde{\rho}(r)=\sum\nolimits_{i}^{M} \tilde{n}_{i} \psi_{i}(r) * \psi_{i}(r),$$

i.e. we interpret the fictitious occupation numbers $\tilde{n}_i$ in the xc functional as effective occupation numbers in an effective density $\tilde{\rho}(r)$, which is only used in the denominator of expressions we derive according to the KLI or CEDA approximations for the potential (see below). It is to be expected that $\tilde{\rho}(r)$ is actually a close approximation to $\rho(\mathbf{r})$, except for the crucial difference in how these two densities tend asymptotically to zero. That this is the case can be easily verified in the case of dissociating H_2, which wil be discussed in Sec. 5.5.

5.4 Explicit expression for v_{xc} using the CEDA to the OEP method

We now proceed to the derivation of v_{xc} corresponding to the (virtual) orbital-dependent xc functional of Sec. 5.2 by the common energy denominator approximation (CEDA) [40, 110]. The CEDA approximation uses for the static orbital Green's function G_i,

$$\begin{aligned} G_i^{\mathrm{CEDA}}(\mathbf{r}_1,\mathbf{r}_2) \approx & \frac{\delta(\mathbf{r}_1-\mathbf{r}_2)}{\Delta\varepsilon} - \frac{1}{\Delta\varepsilon}\sum_j^M \psi_j(\mathbf{r}_1)\psi_j^*(\mathbf{r}_2) + \sum_{j\neq i}^M \frac{\psi_j(\mathbf{r}_1)\psi_j^*(\mathbf{r}_2)}{\varepsilon_j-\varepsilon_i} \\ = & \frac{\delta(\mathbf{r}_1-\mathbf{r}_2)}{\Delta\varepsilon} - \frac{1}{\Delta\varepsilon}\sum_j^M d_{ij}\psi_j(\mathbf{r}_1)\psi_j^*(\mathbf{r}_2) \end{aligned} \tag{5.17}$$

where $d_{ij} = [\varepsilon_j - \varepsilon_i - \Delta\varepsilon(1-\delta_{ij})]/(\varepsilon_j-\varepsilon_i)$, i.e. d_{ij}=1 when $i=j$, and $d_{ij} = 1-\Delta\varepsilon/(\varepsilon_j-\varepsilon_i)$ when $i\neq j$. This Green's function includes all occupied KS orbitals ψ_i, $i \leq N/2$, and some unoccupied ones ψ_a, $N/2 < a \leq M$, in finite summations. The third term in the first line of Eq. (5.17) is the rigorous expression for G_i truncated to M orbitals, while the first and the second terms with a common energy denominator $\Delta\varepsilon$ produce an estimate of the remaining terms.

To get the explicit expression for the potential v_{xc} in terms of the occupied and virtual orbitals, we insert the CEDA Green's function (5.17) in the OEP equations (5.16), thus obtaining the equation for the v_{xc} potential

$$\begin{aligned} & \frac{1}{\Delta\varepsilon}\sum_i^{N/2} n_i v_{\mathrm{xc}}^{\mathrm{CEDA}}(\mathbf{r}_1)\left|\psi_i(\mathbf{r}_1)\right|^2 - \frac{1}{\Delta\varepsilon}\sum_i^M v_{\mathrm{xc}}^i(\mathbf{r}_1)\left|\psi_i(\mathbf{r}_1)\right|^2 \\ & - \frac{1}{\Delta\varepsilon}\sum_i^{N/2}\sum_j^M d_{ij} n_i v_{\mathrm{xc},ji}^{\mathrm{CEDA}}\psi_i^*(\mathbf{r}_1)\psi_j(\mathbf{r}_1) \\ & + \frac{1}{\Delta\varepsilon}\sum_i^M\sum_j^M d_{ij} v_{\mathrm{xc},ji}^i \psi_i^*(\mathbf{r}_1)\psi_j(\mathbf{r}_1) + \mathrm{c.c.} = 0 \end{aligned} \tag{5.18}$$

where v_{xc}^i is the orbital derivative of the xc energy functional (5.10)

$$v_{\mathrm{xc}}^i(\mathbf{r}_1) = \frac{1}{\psi_i(\mathbf{r}_1)}\frac{\delta E_{\mathrm{xc}}}{\delta\psi_i^*(\mathbf{r}_1)} = -\sum_j^M \sqrt{\tilde{n}_i\tilde{n}_j}\frac{\psi_j(\mathbf{r}_1)}{\psi_i(\mathbf{r}_1)}\int\frac{\psi_i(\mathbf{r}_2)\psi_j^*(\mathbf{r}_2)}{\mathbf{r}_{12}}d\mathbf{r}_2$$

and $v_{\mathrm{xc},ji}^{\mathrm{CEDA}}$, $v_{\mathrm{xc},ji}^i$ are the matrix elements of the potentials $v_{\mathrm{xc}}^{\mathrm{CEDA}}$ and v_{xc}^i for the orbitals ψ_j^* and ψ_i:

$$v_{\mathrm{xc},ji}^{\mathrm{CEDA}} = \int \psi_j^*(\mathbf{r}_2)\, v_{\mathrm{xc}}^{\mathrm{CEDA}}(\mathbf{r}_2)\,\psi_i(\mathbf{r}_2)\, d\mathbf{r}_2,$$

$$v^{i}_{\mathrm{xc},ji} = \int \psi^{*}_{j}\left(\mathbf{r}_2\right) v^{i}_{\mathrm{xc}}\left(\mathbf{r}_2\right) \psi_i\left(\mathbf{r}_2\right) d\mathbf{r}_2 .$$

From Eq. (5.18) it follows that

$$\begin{aligned} v^{\mathrm{CEDA}}_{\mathrm{xc}}\left(\mathbf{r}_1\right) =& \bar{v}^{\mathrm{hole}}_{\mathrm{xc}}\left(\mathbf{r}_1\right) + \sum_{i}^{N/2} \sum_{j}^{M} d_{ij} n_i \mathrm{Re}\left[v^{\mathrm{CEDA}}_{\mathrm{xc},ji} \psi^{*}_{i}\left(\mathbf{r}_1\right) \psi_j\left(\mathbf{r}_1\right)\right] \frac{1}{\rho\left(\mathbf{r}_1\right)} \\ & - \sum_{i}^{M} \sum_{j}^{M} d_{ij} \mathrm{Re}\left[v^{i}_{\mathrm{xc},ji} \psi^{*}_{i}\left(\mathbf{r}_1\right) \psi_j\left(\mathbf{r}_1\right)\right] \frac{1}{\rho\left(\mathbf{r}_1\right)} \end{aligned} \tag{5.19}$$

where $\bar{v}^{\mathrm{hole}}_{\mathrm{xc}}\left(\mathbf{r}_1\right)$ is the xc-hole potential (5.9)

$$\bar{v}^{\mathrm{hole}}_{\mathrm{xc}}\left(\mathbf{r}_1\right) = \sum_{i}^{M} \frac{\left|\psi_i\left(\mathbf{r}_1\right)\right|^2 \mathrm{Re}\left[v^{i}_{\mathrm{xc}}\left(\mathbf{r}_1\right)\right]}{\rho\left(\mathbf{r}_1\right)} . \tag{5.20}$$

Note that divergence of the potentials (5.19) and (5.20) is avoided by replacing the asymptotic behavior of $\rho(\mathbf{r})$ in terms with diffuse orbital products in the numerator with that of $\tilde{\rho}(r)$, which is, as discussed earlier, the way in which we introduce the constraint that the potential should not diverge. This comment is also applicable to subsequent equations and will not be repeated.

In the following we will, for simplicity of notation, specialize to real orbitals, which is the case at hand. Equation (5.19) can be solved in the same way as the corresponding equations for the potential of Krieger-Li-Iafrate (KLI) [38] or the occupied-orbital-dependent CEDA potential [39, 40, 110]

$$\begin{aligned} v^{\mathrm{CEDA}}_{\mathrm{xc}}\left(\mathbf{r}_1\right) =& \bar{v}^{\mathrm{hole}}_{\mathrm{xc}}\left(\mathbf{r}_1\right) + \sum_{i}^{N/2} \sum_{j}^{M} d_{ij} n_i v^{\mathrm{CEDA}}_{\mathrm{xc},ij} \frac{\psi_i\left(\mathbf{r}_1\right) \psi_j\left(\mathbf{r}_1\right)}{\rho\left(\mathbf{r}_1\right)} \\ & - \sum_{i}^{N/2} \sum_{j}^{M} d_{ij} v^{i}_{\mathrm{xc},ij} \frac{\psi_i\left(\mathbf{r}_1\right) \psi_j\left(\mathbf{r}_1\right)}{\rho\left(\mathbf{r}_1\right)} \end{aligned} \tag{5.21}$$

Multiplying both sides of (5.21) by $\psi_k(\mathbf{r}_1)\psi_l(\mathbf{r}_1)$ ($k \leq N/2$, $l \leq M$) and integrating over $\mathbf{r}_1$, one obtains the equations for the matrix elements $v^{\mathrm{CEDA}}_{\mathrm{xc},ij}$

$$\sum_{i}^{N/2} \sum_{j}^{M} \left(\delta_{ki}\delta_{lj} - M_{kl,ij}\right) v^{\mathrm{CEDA}}_{\mathrm{xc},ij} = \bar{v}^{\mathrm{hole}}_{\mathrm{xc},kl} - \sum_{i}^{M} \sum_{j}^{M} N_{kl,ij} v^{i}_{\mathrm{xc},ij} , \tag{5.22}$$

where $M_{kl,ij}$ and $N_{kl,ij}$ are the weighted overlap integrals between the orbital products $\psi_k\psi_l$ and $\psi_i\psi_j$

$$M_{kl,ij} = n_i d_{ij} \int \frac{\psi_k\left(\mathbf{r}_1\right) \psi_l\left(\mathbf{r}_1\right) \psi_i\left(\mathbf{r}_1\right) \psi_j\left(\mathbf{r}_1\right)}{\rho\left(\mathbf{r}_1\right)} d\mathbf{r}_1 ,\ N_{kl,ij} = M_{kl,ij}/n_i$$

and $\bar{v}^{\text{hole}}_{\text{xc},kl}$ is the matrix element of the xc-hole potential (5.20)

$$\bar{v}^{\text{hole}}_{\text{xc},kl} = \sum_{i}^{M} \int \frac{\psi_k\left(\mathbf{r}_1\right)\psi_l\left(\mathbf{r}_1\right)\psi_i^2\left(\mathbf{r}_1\right)v^i_{\text{xc}}\left(\mathbf{r}_1\right)}{\rho\left(\mathbf{r}_1\right)} d\mathbf{r}_1 .$$

The equations (5.22) for the constants $v^{\text{CEDA}}_{\text{xc},ij}$ are, like the KLI equations are for the KLI constants, a dependent set of linear equations. In fact it is easily verified that the $N/2$ rows with $k = l$ are linearly dependent (multiplying these rows with n_k and summing them leads to a row of zeros, and the right hand side becomes zero as well). We therefore can only solve for $M \cdot N/2 - 1$ unknowns, and have chosen $v^{\text{CEDA}}_{\text{xc},\,N/2\,N/2}$ as the undetermined constant that can be chosen freely. It has been conveniently put to zero. So Eq. (5.22) is solved by inversion of the square subblock $(\mathbf{I}-\mathbf{M})'$ of the matrix $(\mathbf{I}-\mathbf{M})$, where $1 \leq i,k \leq N/2$ and $1 \leq j,l \leq M$, but with $i = j = N/2$ and $k = l = N/2$ excluded (rows are indexed with kl and columns with ij). Defining the $M \cdot N/2 - 1$ by $M \cdot N/2 - 1$ matrix ξ and the $M \cdot N/2 - 1$ by $M \cdot N/2$ matrix η

$$\xi_{mn,kl} = \left[(\mathbf{I}-\mathbf{M})'\right]^{-1}_{mn,kl}$$

with rows $\xi_{N/2\,N/2\,,\,mn}$ and columns $\xi_{mn,N/2\,N/2}$ nonexistent;

$$\eta_{mn,ij} = \sum_{k}^{N/2}{}' \sum_{l}^{M}{}' \xi_{mn,kl} N_{kl,ij},$$

where the primes on the summations mean omission of the $k = l = N/2$ term, we obtain upon multiplying Eq. (5.22) with $\xi_{mn,kl}$ and summing over kl

$$v^{\text{CEDA}}_{\text{xc},mn} = \sum_{k}^{N/2}{}' \sum_{l}^{M}{}' \xi_{mn,kl}\bar{v}^{\text{hole}}_{\text{xc},kl} - \sum_{i}^{M}\sum_{j}^{M} \eta_{mn,ij} v^{i}_{\text{xc},ij}. \tag{5.23}$$

Finally, inserting Eq. (5.23) in Eq. (5.21), we obtain for $v^{\text{CEDA}}_{\text{xc}}$ the following expression

$$v^{\text{CEDA}}_{\text{xc}}(\mathbf{r}_1) = \bar{v}^{\text{hole}}_{\text{xc}}(\mathbf{r}_1) + v^{\text{CEDA}}_{\text{resp}}(\mathbf{r}_1) \tag{5.24}$$

where $v^{\text{CEDA}}_{\text{resp}}$ is the response potential

$$v^{\text{CEDA}}_{\text{resp}}\left(\mathbf{r}_1\right) = \sum_{i,j}^{M} w_{ij} \frac{\psi_i\left(\mathbf{r}_1\right)\psi_j\left(\mathbf{r}_1\right)}{\tilde{\rho}\left(\mathbf{r}_1\right)} \tag{5.25}$$

where for $\theta(k) = 1$ for $k \geq 0$ and $\theta(k) = 0$ for $k < 0$

$$w_{ij} = \theta\left(\frac{N}{2} - i\right) d_{ij} n_i v^{\text{CEDA}}_{\text{xc},ij} - d_{ij}\, v^{i}_{\text{xc},ij} v^{\text{CEDA}}_{\text{xc},N/2\,N/2} = 0). \tag{5.26}$$

With our choice of $v_{\mathrm{xc},N/2\,N/2}^{\mathrm{CEDA}}=0$, the potential does not asymptotically go to zero but to a constant. However, we have found that the inversion of $(\mathbf{I}-\mathbf{M})'$ may become numerically less stable when a $v_{\mathrm{xc},ia}^{\mathrm{CEDA}}$ related to a diffuse orbital ψ_a with low effective occupation $\tilde{n}_a$ is chosen as free constant. The constant asymptotic behavior has no consequences, if desired a shift can be applied to the total potential to make it asymptotically tend to zero. Equations (5.20), (5.24)–(5.26) define the Kohn-Sham xc potential $v_{\mathrm{xc}}^{\mathrm{CEDA}}$ corresponding within the modified OPM-CEDA to the orbital-dependent xc energy functional (5.10). $v_{\mathrm{xc}}^{\mathrm{CEDA}}$ is subdivided naturally into an attractive xc-hole potential $\bar{v}_{\mathrm{xc}}^{\mathrm{hole}}(\mathbf{r}_1)$ and a repulsive response potential $v_{\mathrm{resp}}^{\mathrm{CEDA}}(\mathbf{r}_1)$. The former potential represents the main exchange-correlation effect, namely, interaction of the reference electron with the xc hole in the distribution of other electrons. In particular, due to the inclusion of virtual KS orbitals, the present $\bar{v}_{\mathrm{xc}}^{\mathrm{hole}}(\mathbf{r}_1)$ represents the important effects of Coulomb correlation discussed in Sec. 5.2. By construction, the present $\bar{v}_{\mathrm{xc}}^{\mathrm{hole}}(\mathbf{r}_1)$ has Coulombic long-range asymptotics $\bar{v}_{\mathrm{xc}}^{\mathrm{hole}}(\mathbf{r}_1)\rightarrow 1/|\mathbf{r}_1|$ at $|\mathbf{r}_1|\rightarrow\infty$. In turn, the response potential $v_{\mathrm{resp}}^{\mathrm{CEDA}}$ of Eq. (5.25) has the characteristic orbital step structure with the step heights w_{ij} of (5.26) corresponding to the individual orbital products $\psi_i\psi_j$ in (5.25). The orbital structure follows from the fact that in the region, where a particular orbital density ψ_i^2 brings a dominant contribution to the effective density $\tilde{\rho}$, the potential $v_{\mathrm{resp}}^{\mathrm{CEDA}}$ is close to the corresponding weight w_{ii}. The form of the present response part of the xc potential, $v_{\mathrm{resp}}^{\mathrm{CEDA}}$ of Eq.(5.25), is similar to that of the KLI [38] or CEDA [40, 110] exchange-only response potentials and correlation manifests itself in the presence of “steps” with products ψ_a^2 and $\psi_a\psi_j$ of virtual orbitals ψ_a.

5.5 Calculation of the H$_2$ potential curve

Based on the theory presented in the previous sections, we propose a self-consistent KS scheme with our occupied and virtual orbital-dependent xc energy functional. In this scheme the total energy is,

$$E=T_s\left[\{n_i\},\{\psi_i\}\right]+E_{ne}\left[\rho\left(r\right)\right]+E_H\left[\rho\right]+E_{\mathrm{xc}}\left[\{\tilde{n}_i\},\{\psi_i\}\right] \tag{5.27}$$

where E_{xc} is defined with (5.10). The orbitals ψ_i in (5.27) are obtained from the KS one-electron equations,

$$\left\{-\frac{1}{2}\nabla^2+v_{ne}\left(\mathbf{r}_1\right)+v_H\left(\mathbf{r}_1\right)+v_{\mathrm{xc}}^{\mathrm{CEDA}}\left(\mathbf{r}_1\right)\right\}\psi_i\left(\mathbf{r}_1\right)=\varepsilon_i\psi_i\left(\mathbf{r}_1\right) \tag{5.28}$$

where $v_{\mathrm{xc}}^{\mathrm{CEDA}}$ is defined with with (5.20),(5.24)–(5.26). The functionals T_s, E_{ne}, E_H in (5.27) and the potential v_H in (5.28) are calculated with the conventional KS density (5.2), i.e. with the occupations n_i of the orbitals ψ_i, while the expressions for E_{xc} and $v_{\mathrm{xc}}^{\mathrm{CEDA}}$ contain the fictitious occupations $\tilde{n}_i$. The latter are calculated within the self-consistent procedure as explicit functions (5.12) of the orbital energies. In this chapter we use the Fermi type distribution

$$\tilde{n}_i = \frac{2}{1+\exp\left[(\varepsilon_i - \varepsilon_F)\Big/\sqrt{a\left(\varepsilon_{(N/2+1)} - \varepsilon_{N/2}\right) + b\left(\varepsilon_{(N/2+1)} - \varepsilon_{N/2}\right)^2}\right]}. \tag{5.29}$$

with the parameters a and b, which appears to be flexible enough for our purpose. In (5.29) $\varepsilon_{N/2}$ and $\varepsilon_{(N/2+1)}$ are the HOMO and LUMO energies. The parameter ε_F is determined to satisfy the normalization condition $\sum_i^M \tilde{n}_i = N$, which yields a value close to $(\varepsilon_{LUMO} + \varepsilon_{HOMO})/2$ for ε_F. Alternatively one can fix ε_F at the average of HOMO and LUMO energies and scale the $\tilde{n}_i$ so that $\sum_i^M \tilde{n}_i = N$ is satisfied. These procedures both work wel. We apply the self-consistent method of Eqs. (5.27)–(5.29) to the calculation of the potential curve of the H_2 molecule. The nine lowest virtual orbitals have been included in the summations in the xc energy (5.10) and the xc potential v_{xc}^{CEDA}. Figure 5.1 compares the total energy curve obtained with the xc energy functional (5.10) (denoted BB) with those calculated with the Hartree-Fock (HF) and full configuration interaction (FCI) methods as well as with the local density approximation (LDA) and with a generalized gradient approximation (GGA) consisting of a combination (BP) of Becke's exchange (B88) [4] and Perdew's (P86) correlation [6] functionals. The correlation-consistent triple-zeta basis cc-pVTZ [65] of Gaussian type orbitals (GTO) has been used. All calculations have been performed within the spin-restricted approach by means of a Gaussian orbital density functional code [46, 77] based on the ATMOL package [62]. Figure 5.1 clearly displays the failures of HF, LDA, and GGA-BP for the H_2 potential curve. The most dramatic is the well-known HF failure due to the neglect of the Coulomb correlation in the HF method. The HF curve goes higher than other curves at nearly all the H–H distances and at R(H–H)=10 Bohr the error of the HF total energy, $E^{HF} - E^{FCI}$=148 kcal/mol, and the error of the dissociation energy (estimated at R(H–H)=10 Bohr and comparing to $E(R_e\ ))$, $D_e^{HF} - D_e^{FCI}$=123 kcal/mol. The displayed failure of LDA and standard GGA is, perhaps, less well known than their poor performance for the dissociating cation H_2^+ [11, 12, 13], the total energy of which the GGAs greatly underestimate (ca. 60 kcal/mol too negative). In contrast, spin-restricted LDA and GGA-BP greatly overestimate the energy of the dissociating H_2 (see Fig. 5.1), although not as much as HF. In particular, near the equilibrium distance R(H–H)=1.401 Bohr the LDA curve is close to the HF one, while at large R(H–H) it goes in between the HF and FCI curves. At R(H–H)=10 Bohr the LDA total energy error $E^{LDA} - E^{FCI}$=69 kcal/mol, and the LDA dissociation energy error $D_e^{LDA} - D_e^{FCI}$=46 kcal/mol. The gradient correction lowers the GGA-BP energy compared to the LDA one and the BP curve goes below and almost in parallel to the LDA curve. Near the equilibrium the BP curve is close to FCI one, however, BP still considerably overestimates the energy at long distance. The BP total energy error at R(H–H)=10 Bohr is $E^{BP} - E^{FCI}$=44 kcal/mol, and the BP dissociation energy error $D_e^{BP} - D_e^{FCI}$=47 kcal/mol is even slightly larger than the LDA one.

The errors in the DFT dissociation energies seem to contradict the notion that

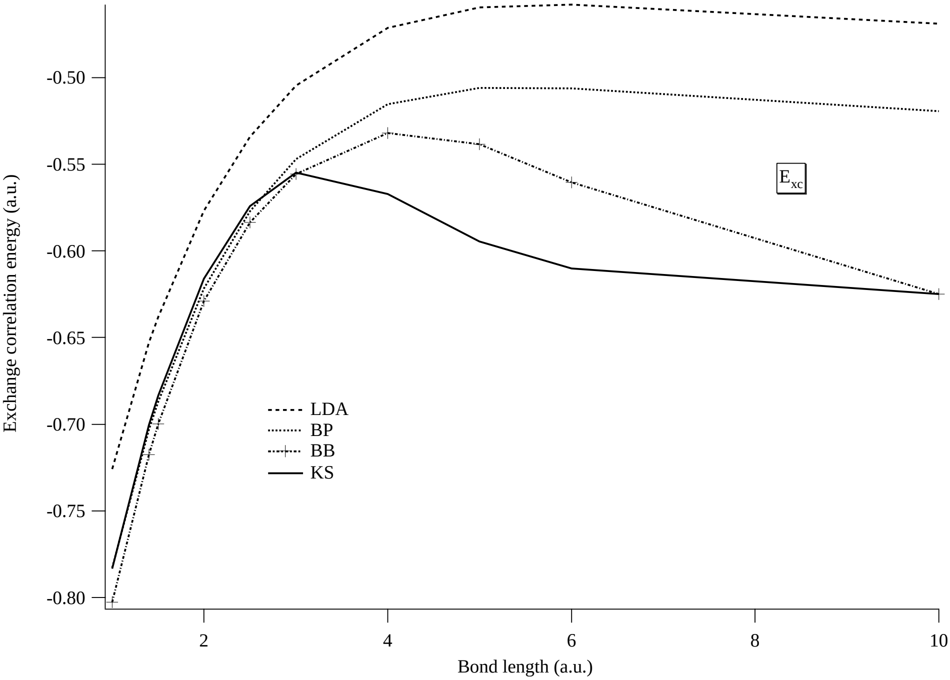

Figure 5.4: Total exchange-correlation energy of H_2 as a function of internuclear distance. See caption of Fig. 5.1.

the LDA and GGA approximations by the very fact that they work with model holes that are local, do not exhibit the typical Hartree-Fock error due to the completely delocalized exchange hole. Apparently the local nature of the holes of the LDA and GGA approximations is not sufficient to ensure proper behavior at long distance, a point to which we will return below. In contrast to the LDA and GGA curves, the potential curve of the self-consistent BB method (5.27)–(5.29) excellently reproduces the FCI curve, both curves practically coincide at all H–H distances (see Fig. 5.1). The best agreement is achieved for the parameters a=0.008 and b=0.045 in the distribution (5.29) with a total energy average error (for various H–H distances) of only -0.07 kcal/mol, an average absolute error of 0.72 kcal/mol, and a maximal error of -2.4 kcal/mol at R(H–H)=3 Bohr. The important feature of the functional (5.10) is its correct behavior for dissociating H_2 (see Sec. 5.2). Due to this, the dissociation energy error is only -0.20 kcal/mol. The above-mentioned energy differences of LDA, GGA and BB, which share the same functionals T_s, E_{ne} and E_H, originate from the different xc functionals of these methods. Figure 5.4 compares their $E_{\text{xc}}(R)$ curves with the benchmark curve $E_{\text{xc}}^{\text{KS}}(R)$ for the accurate KS solution obtained from the FCI density ρ^{FCI} with the iterative scheme of van Leeuwen and Baerends [89]. One can see from Fig. 5.4, that the LDA and GGA-BP xc energies as functions of the

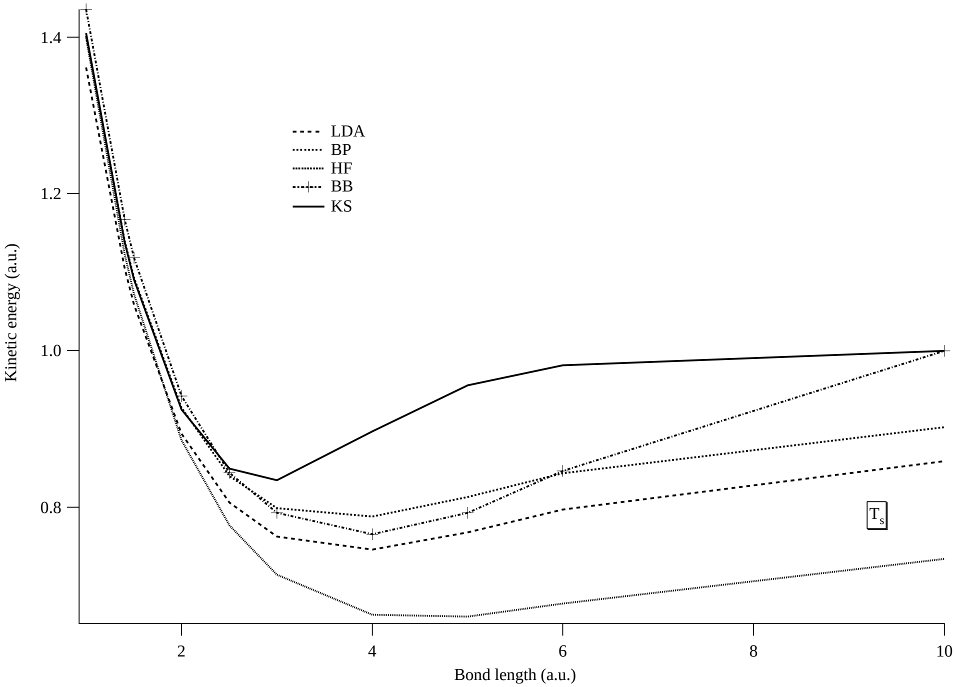

Figure 5.5: HF kinetic energy and KS kinetic energy of H_2 as a function of internuclear distance. See caption of Fig. 5.1.

internuclear distance have a qualitatively different behavior compared to the accurate E_{xc}^{KS}. Both LDA and BP xc energies increase monotonically with R(H–H), with the latter being consistently lower than the former. In its turn, $E_{xc}^{KS}[R(\text{H–H})]$ passes through a maximum at R(H–H)=3 Bohr and at larger R(H–H) it decreases monotonically. For the distances R(H–H)$\leq$3 Bohr the GGA energy E_{xc}^{BP} is close to E_{xc}^{KS}, however both LDA and BP greatly overestimate the xc energy of dissociating H_2 (i.e. do not have it negative enough). The corresponding errors at R(H–H)=10 Bohr of 98 and 66 kcal/mol are, in fact, larger than the above-mentioned LDA/GGA total energy errors. Thus, the latter errors originate from the errors of the LDA/GGA xc functionals, which are partly compensated with the errors of opposite sign in other energy components. Contrary to LDA/GGA, the BB xc functional (5.10) reproduces qualitatively the benchmark dependence $E_{xc}^{KS}(R)$ (see Fig. 5.4). E_{xc}^{BB} is close to E_{xc}^{KS} for R(H–H)$\leq$3 Bohr and it again coincides with E_{xc}^{KS} at large R(H–H). Note, however, that the maximum of the BB curve is somewhat displaced from that of $E_{xc}^{KS}(R)$ and E_{xc}^{BB} differs appreciably from E_{xc}^{KS} in the region 3.5$\leq R$(H–H)$\leq$8 Bohr. This indicates that the very good BB total energies in this region (see Fig. 5.1) are the result of compensation of errors of opposite signs in various energy components. This compensation can be clearly seen when one compares Fig. 5.4 with Fig. 5.5, the latter figure presents the dependence of the LDA, BP, BB, KS kinetic energies T_s and the HF kinetic energy T^{HF} on R(H–H). While the $E_{\mathrm{xc}}^{\mathrm{BB}}$ energy is higher than $E_{\mathrm{xc}}^{\mathrm{KS}}$ in the region $3.5 \leq R(\mathrm{H{-}H}) \leq 8$ Bohr (see Fig. 5.4), the BB kinetic energy T_s^{BB} is lower than T_s^{KS} in the same region (see Fig. 5.5). Note, that in the case of H_2 only the lowest MO σ_g contributes to T_s and T^{HF}, so that the comparison of the kinetic energies reveals the relative size of the σ_g MO in various methods: the more diffuse σ_g is in a particular method, the lower is T_s. Thus, Fig. 5.5 indicates the well-known feature of HF, a too diffuse character of the HF σ_g MO for dissociating H_2. Indeed, for larger R(H–H) the HF kinetic curve goes much lower than other curves. Judging from this criterion, LDA yields a more contracted (towards the nuclei) σ_g than HF, GGA-BP further increases this contraction and in BB the size of σ_g gradually changes with R(H–H) from that of BP to that of σ_g of the accurate KS solution. Further analysis shows, that the above-mentioned underestimation of the xc energy of dissociating H_2 (in the sense of being not negative enough) by LDA/GGA is due to the inability of these methods to grasp nondynamical left-right electron correlation in the stretched H_2 molecule. Figure 5.2 displays the totally different dependence on R(H–H) of the LDA/GGA correlation energy functionals and the benchmark correlation energy E_c^{KS} corresponding to the accurate KS solution. The S-shaped $E_c^{\mathrm{KS}}(R)$ curve represents a rather sharp transition from dynamical-like correlation in the region R(H–H)=1.4–2.5 Bohr to strong nondynamical correlation for $R(\mathrm{H{-}H}) < 7$ Bohr. Indeed, near equilibrium E_c^{KS} is close to the typical energy -0.045 Hartree of dynamical correlation of an electron pair in atomic systems. On the other hand, due to the strong left-right correlation at larger R(H–H), E_c^{KS} exceeds -0.25 Hartree at R(H–H)=10 Bohr, i.e. it experiences 4.5-fold increase in its absolute value. In its turn, the LDA/GGA correlation energy remains nearly constant for all R(H–H), with E_c^{LDA} being about twice as low as the GGA E_c^P (see Fig. 5.2). This happens, because the LDA functional represents Coulomb correlation in a model system, the homogeneous electron gas [3], for which the correlation energy per particle $\varepsilon_c(\rho)$ at typical atomic electron densities ρ is about twice that of dynamical electron correlation in atoms. The gradient correction of GGA-P86 removes this discrepancy and near the equilibrium E_c^P is close to E_c^{KS}. Still, both LDA and P86 share the basic shallow logarithmic dependence of $\varepsilon_c[\rho(\mathbf{r}_1)]$ on the local density $\rho(\mathbf{r}_1)$, to which a dependence on the local density gradient $\nabla\rho(\mathbf{r}_1)$ is added in P86. With this local $\rho(\mathbf{r}_1)$ dependence, LDA and GGA have no way to describe, from the H atom densities with which a zero correlation energy corresponds in the isolated atoms, the above-mentioned build-up of the strong left-right nondynamical correlation, which is a characteristic feature of dissociating H_2. Indeed, according to the interpretation of the GGA performance given in Refs. [19, 20, 48], in typical cases of covalent bonds nondynamical correlation should be effectively taken into account not by the GGA correlation functionals, but by the GGA exchange functionals. This proved to be almost quantitatively the case for the molecules N_2, Li_2 and F_2, at their equilibrium geometries, as discussed in Ref. [48]. We therefore expect GGA exchange energies that are more negative than the HF or KS exchange energy by the nondynamical correlation energy. Figure 5.3 compares, along the H_2 dissociation coordinate, the B88 exchange energy with the HF one as well as with the energy E_x^{KS}

corresponding to the accurate KS solution. Let us first comment on the difference between HF and KS exchange energies. We note that around R_e the HF and KS exchange energies are very similar. For long H–H distances, however, the KS exchange energy becomes clearly lower than the HF exchange energy. Usually the KS and HF exchange energies are quite close [48], being little affected by the small differences between HF and KS orbitals. In the present case, however, the HF density and the HF σ_g orbital are significantly too diffuse [73], and the KS exchange energy, which is based on the more contracted true density (the exchange hole is $-(1/2)\rho$) becomes clearly more negative. Let us next compare the DFT exchange energies (LDA and GGA-BP) to the "true" exchange energy E_x^{KS}. At long distance the LDA and in particular the GGA exchange energy indeed become significantly more negative than E_x^{KS}, in agreement with the notion that it incorporates nondynamical correlation, i.e. has effectively a more localized hole than the true, delocalized, exchange hole. However, the GGA exchange energy at 10 Bohr is only ca. 80 kcal/mol more negative than E_x^{KS}, but from Fig. 5.2 it is clear that it should have been some 146 kcal/mol more negative in order to cover the very large error in the GGA correlation energy with respect to the full correlation energy. As a consequence, the total GGA exchange-correlation energy of Fig. 5.4 is not nearly negative enough. So the observation that the GGA exchange energy incorporates the nondynamical correlation energy almost quantitatively at equilibrium geometry[48], does not extend to the more extreme case of nondynamical correlation in the dissociating electron pair bond.

It appears that the general notion that LDA and GGA are superior for dissociating H_2, and for weak electron-pair bonds in general, due to the inherent locality of the "exchange" hole which mimics the full, local, exchange-correlation hole, is not wrong (the dissociation curves in Fig. 5.1 are indeed much better for LDA and GGA than for HF), but is not quantitatively reliable. This can be easily understood from the fact that the DFT exchange holes are not deep and localized enough. Let us consider the full exchange-correlation hole $\rho_{\mathrm{xc}}^{\mathrm{hole}}(\mathbf{r}_2|\mathbf{r}_1)$, which is a function of position coordinate $\mathbf{r}_2$ and surrounds a reference position $\mathbf{r}_1$ that is in the neighborhood of one H nucleus. It has a depth $\rho_{\mathrm{xc}}^{\mathrm{hole}}(\mathbf{r}_1|\mathbf{r}_1)= -\rho(\mathbf{r}_1)$ at $\mathbf{r}_1$ and in fact its shape is $-\rho(\mathbf{r}_2)$ at the H atom where the reference position $\mathbf{r}_1$ is located (and zero at the other H atom), cf [30, 73]. The exchange-correlation hole integrates to -1 electron, and so does the exchange hole. The exchange hole, however, has a depth of only $-(1/2)\rho(\mathbf{r}_1)$ since it is only in the electronic density of either spin α or spin β electrons. We can roughly estimate the effect of the difference in depth between the complete exchange-correlation hole and the exchange-only hole. When one uses the simple Slater model that the hole has uniform depth (either $-\rho(\mathbf{r}_1)$ for $\rho_{\mathrm{xc}}^{\mathrm{hole}}(\mathbf{r}_2|\mathbf{r}_1)$ or $-(1/2)\rho(\mathbf{r}_1)$ for $\rho_x^{\mathrm{hole}}(\mathbf{r}_2|\mathbf{r}_1)$) and radius R such that it integrates to -1 electron, then one obtains for the xc energy

$$E_{\mathrm{xc}}^{\mathrm{model}} = -\frac{1}{2}\int d\mathbf{r}_1 \rho(\mathbf{r}_1) \int d\mathbf{r}_2 \frac{\rho_{\mathrm{xc}}^{\mathrm{hole}}(\mathbf{r}_2|\mathbf{r}_1)}{\mathbf{r}_{12}} \approx -\frac{4\pi}{2}\int d\mathbf{r}_1 \rho^2(\mathbf{r}_1) \int_0^R \mathbf{r}_{12} d\mathbf{r}_{12}.$$

the simple estimate

$$E_{\mathrm{xc}}^{\mathrm{model}} \approx -\left(\frac{9\pi}{16}\right)^{1/3} \int \rho^{4/3}\left(\mathbf{r}_1\right) d\mathbf{r}_1 .$$

The radius $R = \{3/[4\pi\rho(\mathbf{r}_1)]\}^{1/3}$ is here taken from the unit sum rule. This is 1.27 times as large in absolute magnitude as the exchange energy obtained with a uniform hole of depth $-(1/2)\rho(\mathbf{r}_1)$,

$$E_{x}^{\mathrm{model}} \approx -\left(\frac{9\pi}{32}\right)^{1/3} \int \rho^{4/3}\left(\mathbf{r}_1\right) d\mathbf{r}_1$$

This is roughly comparable to the ratio of $E_{\mathrm{xc}}^{\mathrm{KS}}$ (see Fig. 5.4) and E_{x}^{BP} (see Fig. 5.3) $E_{\mathrm{xc}}^{\mathrm{KS}}/E_{x}^{\mathrm{BP}}$=1.21 at R(H–H)=10 Bohr. This supports the view that the breakdown of the DFT exchange hole models for the description of the nondynamical correlation in this case is a simple consequence of their shallowness. The large difference with a hole that is not only "localized" (on one H-atom site) but also of sufficient depth can be compensated neither with the B88 exchange gradient correction, nor with the addition of relatively small LDA/GGA correlation energies (see Fig. 5.2), so that a dramatic underestimation results of the xc (see Fig. 5.4) and total (see Fig. 5.1) energy of dissociating H_2 with LDA and GGA-BP. It is to be noted that hybrid functionals, which introduce a more delocalized hole than LDA or GGA, would do worse than the pure density functionals at long distance. Note that, based on the concept of the xc hole, the functional of Eq. (5.10) treats exchange and correlation in a unified way, so that the $E_{\mathrm{xc}}^{\mathrm{BB}}$ curve (Fig. 5.4) cannot be separated in exchange (Fig. 5.3) and correlation (Fig. 5.2) curves, as can be done for LDA and GGA approximations. Still, comparison of the total BB and FCI energies (see Fig. 5.1) and the xc BB and KS energies (see Fig. 5.4) shows, that due to the proper modelling of the xc hole with inclusion of virtual orbitals, the BB functional reproduces successfully the build-up of strong nondynamical left-right correlation in dissociating H_2.

5.6 Conclusions

In this chapter the functional dependence on virtual Kohn-Sham orbitals has been incorporated into the self-consistent KS method. To accomplish this, several methodological questions had to be addressed and solved. Foremost among them is the choice of an exchange-correlation energy functional, which would efficiently utilize both occupied and virtual orbitals. In this chapter the functional proposed by Buijse and Baerends [77, 105] has been employed. With its simple orbital dependence (5.10) derived from an *Ansatz* for the xc-hole amplitude, $E_{\mathrm{xc}}^{\mathrm{BB}}$ is able to reproduce the important dynamical and nondynamical effects of Coulomb correlation through the efficient use of virtual orbitals.

The next question to be addressed is the construction of the Kohn-Sham potential, which now also depends on both occupied and virtual orbitals. The problem here is the asymptotical divergence of the xc potential, since it depends on a finite number of the KS orbitals. The problem is evident from the construction of the potential by functional differentiation, or equivalently by the OEP scheme. In order to build in the desirable constraint of correct (finite) asymptotic behavior, a modification of the OEP equations has been proposed, which leads to a finite xc potential. With a generalization of the common energy denominator approximation (CEDA) for the static orbital Green's function, the explicit expression in terms of occupied and virtual orbitals has been derived for the xc potential $v_{\text{xc}}^{\text{CEDA-BB}}$ corresponding to the $E_{\text{xc}}^{\text{BB}}$ functional.

The present method requires an algorithm for the involvement ("weight") of the virtual KS orbitals in the xc functional. In this chapter this has been realized by using the analogy with the development of an one-electron density matrix dependent xc part of the two-electron density matrix, which leads to $\sqrt{n_i}$ dependence (where n_i are the natural orbital occupation numbers) in the coefficients for the expansion of the xc hole in terms of natural orbitals [77, 105, 118, 119, 124]. We have used weights in the form of $\sqrt{\tilde{n}_i}$, where $\tilde{n}_i$ are fictitious "occupation numbers" which were approximated with a Fermi-type distribution dependence on the orbital energies.

The resulting self-consistent method has been applied to calculation of the H_2 potential curve and a detailed comparison has been made with HF, FCI, LDA, GGA-BP methods as well as with the energy components corresponding to the accurate KS solution for H_2. The failure of spin-restricted LDA and GGA-BP has been stressed: LDA/GGA greatly underestimate the bond energy and the xc energy of dissociating H_2, due to their inability to grasp the strong left-right electron correlation at large H–H distances.

In its turn, the present method reproduces very well the entire H_2 potential curve and it reproduces qualitatively (but not quantitatively) the dependence of the xc energy on the H–H distance. With the proper inclusion of virtual KS orbitals in its orbital structure the functional (5.10) correctly describes the transition from a dynamical-like correlation near the equilibrium to the strong left-right correlation in stretched H_2. Of particular importance is the correct asymptotic behavior of the functional at large R(H–H). In this region the localized xc hole that is implicit in this functional [30] correctly describes the combined effect of exchange and left-right correlation, so that the total energy and its components coincide with the corresponding FCI and accurate KS quantities.

These results demonstrate, in principle, the ability of a functional like $E_{\text{xc}}^{\text{BB}}$ with virtual orbital dependence to describe properly dissociation of molecular electron pair bonds. This is especially encouraging, since the observed failure of LDA and BP-GGA demonstrates the virtual impossibility of functionals that use only local information (local density and derivatives of the density) to represent the gradual build-up of the strong nondynamical correlation which accompanies bond dissociation. Such nonlocal information is built into the $E_{\text{xc}}^{\text{BB}}$ functional through its orbital dependence, which makes it a full fledged (not only perturbatively defined) exchange *plus* correlation functional.

Nevertheless, important problems remain to be solved. Further development of functionals along these lines will depend on finding a successful scheme to determine the effective weights of the occupied and virtual orbitals, or equivalently the fictitious "occupations" $\tilde{n}_i$. The present Fermi-type distribution (5.12),(5.29) can be considered as only a provisional answer. In the second place the problem of the asymptotic divergence of the Kohn-Sham potential arising from the use of a finite set of virtual orbitals has only been addressed in an *ad hoc* manner in this chapter.

Part II

Calculations of molecular response properties: approximations of the exchange and correlation potential

Chapter 6

The exchange and correlation potential

The xc potentials obtained by differentiation of the LDA/GGA energy functionals are not a good approximation for the KS xc potential. In this chapter the main shortcomings of the LDA/GGAs for the xc potential are analyzed and discussed in relation to the accuracy of the results for molecular response properties, in particular for excitation energies and polarizabilities. The calculations of linear (and non-linear) properties in time dependent density functional response theory (TDDFRT) require in fact two approximations: the approximation for the ground state static xc potential and the approximation of the xc kernels, describing the change of the xc potential in response to an external perturbation. Section 6.1 shows how the two approximations enter in the calculation of excitation energies and polarizability. The relative weights of these two approximations are evaluated in Sec. 6.2. The relevant features of the xc KS potential are analyzed in Sec. 6.3. On the basis of this analysis the shortcomings of the LDA/GGA potentials are discussed in Sec. 6.4.1: they are both too repulsive in the bulk region and decay too rapidly in the asymptotic region. These distortions of the approximated potentials can be recognized in the distortions of the excitation spectra calculated at this level of approximation. Section 6.4.2 presents two alternatives to correct these shortcomings: either model potentials depending on KS orbitals or "asymptotically corrected" LDA/GGA xc potentials.

6.1 The calculation of linear response properties

In Sec. 1.1 the advantages of the density functional approach have been illustrated for the stationary state. The basic theorem that states the one-to-one mapping between the density and the external potential can be extended for time dependent densities $\rho(t)$ and time dependent external potentials $v(t)$ [125] and therefore the KS-DFT formalism can be extended to time dependent systems [126, 127, 128, 129].

The calculation of polarizabilities and excitation energies requires only the linear response of the density that can be obtained by a perturbative solution of the time-dependent KS equations. The linear response $\delta\rho$ of the density of a quantum system to an external perturbation δv_{ext}

$$\delta\rho_{\sigma_1}(\mathbf{r}_1,t) = \int d\mathbf{r}_2 \int\limits_{-\infty}^{t} dt' \chi(\mathbf{r}_1,\mathbf{r}_2;t-t')\delta v_{\text{ext}}(\mathbf{r}_2,t') \tag{6.1}$$

is described by the linear density response function $\chi(\mathbf{r}_1,\mathbf{r}_2;t-t')$ of the system that contains information on the ground state wave functions Ψ_0 and energy E_0, on all the excitation energies $\omega_\alpha = E_\alpha - E_0$ and excited wave functions Ψ_α of the system.

For the noninteracting KS system the linear density response function takes the simple form (in the frequency, Fourier transform)

$$\chi_s(\mathbf{r}_1,\mathbf{r}_2;\omega) = \lim_{\eta\to 0^+}\sum_{k,j}(f_k - f_j)\frac{\psi_j(\mathbf{r}_1)\psi_k^*(\mathbf{r}_1)\psi_j^*(\mathbf{r}_2)\psi_k(\mathbf{r}_2)}{\omega-(\varepsilon_j-\varepsilon_k)+i\eta} \tag{6.2}$$

depending only on the solutions of ground state KS set of equations $\{\varepsilon_i,\psi_i\}$.

The change in the density of the KS noninteracting system causes a change in the Coulomb and xc part of the KS potential, depending on the density, that in turn causes a change in the density itself. The changes in the density $\delta\rho$ and in the KS potential δv_s have therefore to be solved self-consistently

$$\begin{aligned}
\delta\rho(\mathbf{r}_1,t) &= \int d\mathbf{r}_2 \int\limits_{-\infty}^{t} dt' \chi_s(\mathbf{r}_1,\mathbf{r}_2;t-t')\delta v_s(\mathbf{r}_2,t') &(6.3)\\
\delta v_s(\mathbf{r}_1,t) &= \delta v_{\text{ext}}(\mathbf{r}_1,t) + \int d\mathbf{r}_2 \frac{\delta\rho(\mathbf{r}_2,t)}{|\mathbf{r}_1-\mathbf{r}_2|}\\
&+ \int d\mathbf{r}_2 \int\limits_{-\infty}^{t} dt' f_{\text{xc}}(\mathbf{r}_1,\mathbf{r}_2;t-t')\delta\rho(\mathbf{r}_2,t'). &(6.4)
\end{aligned}$$

Equations (6.3) and (6.4) can be condensed (after a Fourier transform) into the expression for the frequency dependent density change:

$$\begin{aligned}
\delta\rho(\mathbf{r}_1,\omega) = \int d\mathbf{r}_2\chi_s(\mathbf{r}_1,\mathbf{r}_2;\omega)\delta v_{\text{ext}}(\mathbf{r}_2,\omega)+\\
\int d\mathbf{r}_2\chi_s(\mathbf{r}_1,\mathbf{r}_2;\omega)\int d\mathbf{r}_3\Big(\frac{1}{|\mathbf{r}_2-\mathbf{r}_3|}+f_{\text{xc}}(\mathbf{r}_2,\mathbf{r}_3;\omega)\Big)\delta\rho(\mathbf{r}_3,\omega).
\end{aligned} \tag{6.5}$$

The change in the xc potential in Eq. (6.3) is described by the xc kernel $f_{\text{xc}}(\mathbf{r}_1,\mathbf{r}_2;t-t')$

$$f_{\text{xc}}(\mathbf{r}_1,\mathbf{r}_2;t-t') = \frac{\delta v_{\text{xc}}(\mathbf{r}_1,t)}{\delta\rho(\mathbf{r}_2,t')}. \tag{6.6}$$

This object is quite complicated being not local both in space and in time (frequency dependent). It relates the linear response density functions $\chi_s(\mathbf{r}_1,\mathbf{r}_2;t-t')$ in Eq. (6.2) and $\chi(\mathbf{r}_1,\mathbf{r}_2;t-t')$ of respectively the KS and the interacting systems:

$$f_{\mathrm{xc}}(\mathbf{r}_1,\mathbf{r}_2;t-t') = \chi_s^{-1}(\mathbf{r}_1,\mathbf{r}_2;t-t') - \chi^{-1}(\mathbf{r}_1,\mathbf{r}_2;t-t') - \frac{\delta(t-t')}{|\mathbf{r}_1-\mathbf{r}_2|}.$$

For the calculation of the polarizabilities and excitation energies (6.5) can be conveniently rewritten as a set of equations for the first order density matrix $\delta P_{ia}^{\sigma_1}$ in the KS eigenfunction basis. For a real perturbation, the real part of the first-order density matrix $\mathrm{Re}\,\delta P$ is given by solving [130]

$$[\Delta - 2K](\mathrm{Re}\,\delta P) = \delta v_{\mathrm{ext}}, \tag{6.7}$$

where Δ is a diagonal matrix containing only the eigenvalues of the ground state KS equations

$$\Delta_{ia\sigma_1,jb\sigma_2} = \delta_{\sigma_1\sigma_2}\delta_{ij}\delta_{ab}\left[(\varepsilon_a-\varepsilon_i) - \frac{\omega^2}{(\varepsilon_a-\varepsilon_i)}\right], \tag{6.8}$$

while K contains the changes in the Coulomb (K^{Coul}) and xc part (K^{xc}) of the potential and is responsible for the coupling between different transitions of the non-interacting system

$$\begin{aligned} K_{ia\sigma_1,jb\sigma_2} &= K^{\mathrm{Coul}}_{ia\sigma_1,jb\sigma_2} + K^{\mathrm{xc}}_{ia\sigma_1,jb\sigma_2} = \\ &= \int d\mathbf{r}_1 \int d\mathbf{r}_2 \psi_{i\sigma_1}(\mathbf{r}_1)\psi_{a\sigma_1}(\mathbf{r}_1)\frac{1}{|\mathbf{r}_1-\mathbf{r}_2|}\psi_{j\sigma_2}(\mathbf{r}_2)\psi_{b\sigma_2}(\mathbf{r}_2) \\ &+ \int d\mathbf{r}_1 \int d\mathbf{r}_2 \psi_{i\sigma_1}(\mathbf{r}_1)\psi_{a\sigma_1}(\mathbf{r}_1) f_{\mathrm{xc}}^{\sigma_1\sigma_2}(r,\mathbf{r}_2,\omega)\psi_{j\sigma_2}(\mathbf{r}_2)\psi_{b\sigma_2}(\mathbf{r}_2). \end{aligned} \tag{6.9}$$

The (Fourier transform of the) real part of the first-order density matrix $\mathrm{Re}\,\delta P$ multiplied by the dipole moment in the x direction $x_{ia}^{\sigma_1} = \langle\psi_{i,\sigma_1}|\hat{x}|\psi_{a,\sigma_1}\rangle$ gives the frequency dependent polarizability $\alpha_{x,z}$ in response to an external perturbation $F_z = \mathcal{E}_z\hat{z}$

$$\alpha_{x,z}(\omega) = -2\sum_{i,a,\sigma_1} x_{ia}^{\sigma_1}\frac{(\mathrm{Re}\,\delta P_{ia}^{\sigma_1})(\omega)}{\mathcal{E}_z(\omega)}. \tag{6.10}$$

The excitation energies ω and oscillator strengths f are the poles and the residues of the frequency dependent polarizability and are determined by the (pseudo) eigenvalues and eigenvectors of [128]

$$\Omega\vec{F}_\alpha = \omega_\alpha^2\vec{F}_\alpha \tag{6.11}$$

where the Ω-matrix is

$$\Omega_{ia\sigma_1,jb\sigma_2} = \delta_{\sigma_1\sigma_2}\delta_{ij}\delta_{ab}(\varepsilon_a-\varepsilon_i)^2 + 2\sqrt{(\varepsilon_a-\varepsilon_i)}K_{ia\sigma_1,jb\sigma_2}\sqrt{(\varepsilon_b-\varepsilon_j)}. \tag{6.12}$$

In the spin-restricted case, the Ω-matrix is split in a singlet part Ω^S (spin unchanged processes) and triplet part Ω^T (spin-flip processes):

$$\begin{aligned}\Omega^S_{ia,jb} &= \delta_{ij}\delta_{ab}(\varepsilon_a-\varepsilon_i)^2+2\sqrt{(\varepsilon_a-\varepsilon_i)}\times\\ &\quad 2\Big[K^{\text{Coul}}_{ia,jb}+\frac{1}{4}(K^{\text{xc},\uparrow\uparrow}_{ia,jb}+K^{\text{xc},\downarrow\downarrow}_{ia,jb}+K^{\text{xc},\uparrow\downarrow}_{ia,jb}+K^{\text{xc},\downarrow\uparrow}_{ia,jb})\Big]2\sqrt{(\varepsilon_b-\varepsilon_j)}\\ \Omega^T_{ia,jb} &= \delta_{ij}\delta_{ab}(\varepsilon_a-\varepsilon_i)^2+2\sqrt{(\varepsilon_a-\varepsilon_i)}\times\\ &\quad 2\Big[\frac{1}{4}(K^{\text{xc},\uparrow\uparrow}_{ia,jb}+K^{\text{xc},\downarrow\downarrow}_{ia,jb}-K^{\text{xc},\uparrow\downarrow}_{ia,jb}-K^{\text{xc},\downarrow\uparrow}_{ia,jb})\Big]2\sqrt{(\varepsilon_b-\varepsilon_j)}.\end{aligned} \tag{6.13}$$

The oscillator strengths f can be calculated from the eigenvectors $\vec{F}_\alpha$ [128]

$$f_\alpha=\frac{2}{3}\left(|\vec{x}^\dagger\mathbf{S}^{-1/2}\vec{F}_\alpha|^2+|\vec{y}^\dagger\mathbf{S}^{-1/2}\vec{F}_\alpha|^2+|\vec{z}^\dagger\mathbf{S}^{-1/2}\vec{F}_\alpha|^2\right), \tag{6.14}$$

where $x^{\sigma_1}_{ia}$ are the components of $\vec{x}$, while

$$S_{ia\sigma_1,jb\sigma_2}=\frac{\delta_{\sigma_1,\sigma_2}\delta_{i,j}\delta_{a,b}}{\varepsilon_{b\sigma_2}-\varepsilon_{j\sigma_2}}.$$

In summary the polarizability, the excitation energies and oscillator strengths are determined by Eqs. (6.10–6.14). The basic ingredients are on one hand the transition energies and oscillator strengths of the noninteracting KS system

$$\omega^s_q=\varepsilon_a-\varepsilon_i$$

$$f^s_q=\frac{2}{3}\omega^s_q|\langle\psi_a|\hat{\mu}|\psi_i\rangle|^2$$

that are obtained by the KS ground state calculation ($q\equiv ia$, superscript s indicates just that these are relative to the KS system). These quantities are determined by the KS potential and therefore by the choice of the approximation for the xc potential.

On the other hand in the TDDFRT calculation the coupling matrix $\mathbf{K}$ (6.9) relates the excitation energies ω^s_q and oscillator strengths f^s_q of the KS system to the corresponding quantities ω_α, f_α of the interacting system. The coupling matrix involves the approximation for the xc kernel (6.6). In the next section these two approximations are weighed against each other.

6.2 Dr. Potential and Mr. Kernel

The relative weights of the approximation for the potential and for the kernel have been studied [131, 132, 133, 134, 135, 136, 137] by calculating the response properties of atoms and small molecules with accurate xc potentials constructed from *ab initio* densities. From these studies emerge that in general the KS transitions are already quite a good approximation for the excitation energies, especially for highlying excitations. The approximation of the ground state xc potential has therefore, at least for these systems, the largest effect on the calculated spectra and polarizabilities. The standard LDA and GGA xc potentials do not provide a good approximation for KS transitions and as consequence they do not yield good results for excitations and the other related response properties (see also Sec. 6.4.1). On the contrary, the approximation of the xc kernel plays for these small, compact system a secondary role and in general already the simple adiabatic local density approximation (ALDA)

$$f_{\mathrm{xc}}^{\mathrm{ALDA}}(\mathbf{r}_1,t) = \frac{\delta v_{\mathrm{xc}}^{\mathrm{LDA}}(\mathbf{r}_1,t)}{\delta\rho(\mathbf{r}_2,t')}\Big|_{\rho_0}, \tag{6.15}$$

that neglects the nonlocality both in space and in time (the frequency dependence), provides together with an accurate approximation for the potential good results.

This trend has been analyzed and rationalized in several studies. In Ref. [138] the Görling-Levy perturbation theory [139] has been applied to excitation states and as a result the difference of KS eigenvalues has been found to be an approximation to the excitation energy of the zeroth order in the electron-electron interaction. In Ref. [137, 140] the matrix Ω in the eigenvalue equations (6.11) has been expanded [141]

$$\Omega = \Omega_q^{\mathrm{SMA}} + \sum_{r\neq q}\frac{4\omega_q\omega_r|K_{qr}|^2}{\Omega_q^{\mathrm{SMA}}-\Omega_r^{\mathrm{SMA}}} + \cdots \tag{6.16}$$

where the diagonal terms in Eq. (6.12) are collected in

$$\Omega_q^{\mathrm{SMA}} = \Omega_q^s + 2\omega_q^s K_{qq}$$

(small matrix approximation, SMA). At the “zero order” the excitation energies are again approximated by the KS transition frequencies. The “first order correction” is a shift from Ω_q^s due to the diagonal elements of the coupling matrix, while the next term of the expansion involves the second order in the off-diagonal elements K_{qr} and thus the coupling between different KS transitions. The oscillator strength is then expanded as

$$f = \frac{2}{3}\Big\{\omega_q^s(\mu_q^s)^2 + \sum_{r\neq q}\frac{4K_{qr}\omega_q^s\omega_r^s\mu_q^s\mu_r^s}{\Omega_q^{\mathrm{SMA}}-\Omega_r^{\mathrm{SMA}}} + \cdots\Big\}.$$

The first term is the KS oscillator strength and there are no corrections coming from the diagonal elements of the coupling matrix, in fact if the off-diagonal elements in Eq. (6.11) are neglected the eigenvectors, that enter the expression for the oscillator strengths (6.14), remain unit vectors. The first order correction involves the off-diagonal elements of the coupling matrix and mixes various KS oscillator strengths. The idea behind this expansion is just that the off-diagonal elements decay rapidly with the distance from the diagonal [137]. In particular one has to compare the off-diagonal elements of the coupling matrix K_{qr} with the separation between q and r transition frequencies. If they are small on this scale then the oscillator strengths are well approximated by the KS value, and the excitation energies are well represented by the transition frequency from the small matrix approximation.

In Ref. [142] the relative importance of the xc potential and kernel has been studied looking at the single pole approximation[1] for the singlet and triplet excitations (6.13). In this approximation the average $\bar{\omega}$ of ω^S and ω^T is

$$\bar{\omega} = \frac{(\omega^S + \omega^T)}{2} = \omega^s_q + K^{\mathrm{Coul}}_{qq} + K^{x\uparrow\uparrow}_{qq} + K^{c\uparrow\uparrow}_{qq}$$

and depends on the KS transition frequency corrected by the Coulomb and the parallel xc parts of the coupling matrix. This correction is expected to be in general small: in fact the Coulomb and the exchange part of the matrix partially cancel (exact cancellation in the two electrons case), and the effects of parallel correlation are in most of cases weak because electrons with the same spin are already taken apart by the exchange. The singlet-triplet splitting on the other hand

$$(\omega^S - \omega^T) = 2(K^{\mathrm{Coul}}_{qq} + K^{c\uparrow\downarrow}_{qq})$$

is determined uniquely by the coupling matrix, in particular by the Coulomb and the antiparallel correlation parts, in general larger than the correction to ω^s_q discussed above. This ensures in most of the cases that the shift $\bar{\omega} - \omega^s_q$ away from the KS transition frequency is smaller than the singlet-triplet splitting $\omega^S - \omega^T$.

Nevertheless there are cases for which the kernel has to “correct” substantially the KS transition frequencies. The most illustrative example is the dissociating H_2 molecule for which the separation ω^s_q between the highest occupied and the lowest unoccupied KS orbitals approaches zero for large separation. The lowest triplet excitation approaches zero as well for large separation, while the singlet excitation approaches the atomic energy difference between $1s$ and $2s$ or $2p_\sigma$ [143]. The ALDA kernel (6.15) fails to reproduce the differential curves for the lowest singlet [143, 144] (and triplet [145, 146]) excitations for dissociating H_2: in particular it cannot bring the ω^s_q, going to zero, to the singlet excitation energy that remains finite. The locality in space in this case is a severe restriction, both the exchange and the antiparallel correlation part of the kernel are as a matter of fact strongly nonlocal.

The ALDA kernel is clearly inadequate also for conjugated molecular chains for which it leads up to a huge overestimation of the polarizability [147, 148]. In this case the response of the exchange-correlation should contain an “ultra-nonlocal” term counteracting the external field and thus reducing the polarizability [148, 149]. Further in solid state physics better approximations are needed to reproduce properly the optical absorption spectra of solids [150, 151, 152]. In this case it has been shown [153, 154, 155] that, at least the qualitative features of the spectra, can be recovered with a long-range Coulombic tail which is absent in the ALDA kernel.

---

[1] This approximation can be derived from the small matrix approximation above with the additional requirement that $K_{qq} \ll \omega_q$ [137].

Attempts to go beyond the ALDA for the xc kernel have been made in both directions of including the frequency dependence or the spatial nonlocality. Nevertheless it is not possible to retain the local approximation for a frequency dependent kernel [156] without violating fundamental physical theorems [157, 158]. The way to construct a kernel that is still "local"[2], but frequency dependent, is to consider not only the density, but also the density current as fundamental quantity in the theory (current-density functional theory) [158, 159]. Recently the frequency dependent kernel proposed in Ref. [158] has been applied quite successfully (in the zero frequency limit) to current-density functional calculations of response properties of the (hyper)polarizability of conjugated molecular chains [160, 161] and to the absorption spectra of infinite systems [162].

The nonlocality can be introduced through the orbital dependence as in the exchange kernel proposed in [163] derived by differentiation of the Slater hole potential [164]

$$f_x(\mathbf{r}_1, \mathbf{r}_2) = -\frac{|\sum_k \psi_k(\mathbf{r}_1)\psi_k^*(\mathbf{r}_2)|^2}{\rho(\mathbf{r}_1)|\mathbf{r}_1 - \mathbf{r}_2|\rho(\mathbf{r}_2)}. \tag{6.17}$$

This exchange functional has been combined [142] with the ALDA for the antiparallel correlation part of the kernel and this "hybrid" kernel has been applied to the helium and the beryllium excitation energy spectra. The exchange part, that in the two-electrons case cancels exactly the Coulomb part, provides a good estimate of the singlet-triplet average frequency, while the ALDA is accurate enough to provide good singlet-triplet splittings.

In Ref. [40] a kernel is derived from the CEDA (common energy denominator approximation, see later) exchange potential. In addition to the kernel in Eq. (6.17) coming from the Slater hole, it has also a part corresponding to the response of the exchange potential (see next section) that is considered essential to estimate correctly the polarizability of molecular chains [148, 149].

Recently a number of kernels have been proposed to improve the optical absorption spectra of solids; apart the current-density functional calculations already cited [162], in Ref. [155, 165, 166] the exchange part of the kernel has been calculated exactly, in Ref. [153, 167] an xc kernel has been derived starting from the Bethe-Salpeter equation and in Ref. [154] an effective kernel has been developed. These kernels, all including the correct long-range behavior, reproduce quite successfully the features of the optical absorption spectra of solids.

To summarize, the differences between KS orbital energies represent approximately the one electron excitations of the interacting system, and in many cases, this approximation is already quite good, i.e. the shift of the excitation energies from difference between KS orbital energies is quite small. For these systems in particular the approximation for the xc potential is very important in order to reproduce correctly the spacing of occupied and unoccupied KS orbitals, while for the kernel the simple ALDA

---

[2] In the sense that it depends only on quantities calculated at r and in a infinitesimal interval around it

is accurate enough. The next sections analyze the properties of the xc potential and its approximations.

6.3 Holes, steps and peaks: the morphology of v_{xc}

6.3.1 A physically meaningful decomposition of v_{xc}

In this section the potential is decomposed in physically meaningful parts with the aim to analyze its properties [73, 168].

The xc potential is obtained by differentiation with respect to the density of the xc energy functional E_{xc}, the sum of a kinetic part $T_c = (T - T_s)$ and interaction part $W_{\mathrm{xc}} = (W - W_H)$:

$$v_{\mathrm{xc}}(\mathbf{r}_1) = \frac{\delta E_{\mathrm{xc}}}{\delta \rho(\mathbf{r}_1)} = \frac{\delta T_c}{\delta \rho(\mathbf{r}_1)} + \frac{\delta W_{\mathrm{xc}}}{\delta \rho(\mathbf{r}_1)}.$$

From Eq. (2.2), W_{xc} can be rewritten

$$W_{\mathrm{xc}} = \frac{1}{2} \sum_{\sigma_1} \int \rho_{\sigma_1}(\mathbf{r}_1) v_{\mathrm{xc,hole}}(\mathbf{r}_1) d\mathbf{r}_1 \tag{6.18}$$

in term of the local potential $v_{\mathrm{xc,hole}}$

$$v_{\mathrm{xc,hole}}(\mathbf{r}_1) = \sum_{\sigma_2} \int \frac{\rho^{\mathrm{xc}}_{\sigma_1\sigma_2}(\mathbf{r}_1, \mathbf{r}_2)}{|\mathbf{r}_1 - \mathbf{r}_2|} d\mathbf{r}_2 \tag{6.19}$$

of the exchange and correlation hole function $\rho^{\mathrm{xc}}_{\sigma_1\sigma_2}(\mathbf{r}_1, \mathbf{r}_2)$. The kinetic part

$$T_c = \int d\mathbf{r}_1 \rho(\mathbf{r}_1) v_{\mathrm{c,kin}}(\mathbf{r}_1) \tag{6.20}$$

can be also rewritten in term of the local potential $v_{\mathrm{c,kin}}$ [46]

$$v_{\mathrm{c,kin}}(\mathbf{r}_1) = \frac{1}{2} \int |\nabla_1 \Phi|^2 ds_1 d\mathbf{x}_2 \dots d\mathbf{x}_N - \frac{1}{2} \sum_{i=1}^{N} \left| \nabla \frac{\psi_i(\mathbf{r}_1)}{\sqrt{\rho(\mathbf{r}_1)}} \right|^2, \tag{6.21}$$

where Φ is conditional amplitude probability [169] ($\mathbf{x}_i = \mathbf{r}_i, s_i$, s_i spin variable)

$$\Phi(s_1, \mathbf{x}_2 \dots \mathbf{x}_N | \mathbf{r}_1) = \frac{\Psi(\mathbf{x}_1 \cdots \mathbf{x}_N)}{\sqrt{\rho(\mathbf{r}_1)/N}} \tag{6.22}$$

The differentiation with respect to the density of W_{xc} (6.18) and T_c (6.20) leads to the expression

$$v_{\mathrm{xc}}(\mathbf{r}_1) = v_{\mathrm{xc,hole}}(\mathbf{r}_1) + v_{\mathrm{c,kin}}(\mathbf{r}_1) + v_{\mathrm{xc,resp}}(\mathbf{r}_1) \tag{6.23}$$

where the potential is decomposed into a xc hole part $v_{\text{xc,hole}}$ (6.19), a kinetic part $v_{\text{c,kin}}$ (6.21) and a response part $v_{\text{xc,resp}}$ that collects the response from the hole and the kinetic part:

$$v_{\text{xc,resp}}(\mathbf{r}_1) = \iint d\mathbf{r}_2 d\mathbf{r}_3 \frac{\rho(\mathbf{r}_2)\rho(\mathbf{r}_3)}{|\mathbf{r}_2 - \mathbf{r}_3|} \frac{\delta g(\mathbf{r}_2, \mathbf{r}_3)}{\delta\rho(\mathbf{r}_1)} + \int d\mathbf{r}_2 \rho(\mathbf{r}_2) \frac{\delta v_{\text{c,kin}}(\mathbf{r}_2)}{\delta\rho(\mathbf{r}_1)}. \tag{6.24}$$

$g(\mathbf{r}_1, \mathbf{r}_2) = \Gamma(\mathbf{r}_1, \mathbf{r}_2)/\rho(\mathbf{r}_1)\rho(\mathbf{r}_2)$ is the pair correlation function. An alternative expression for the response potential (6.24) has been derived in Ref. [46]:

$$v_{\text{xc,resp}}(\mathbf{r}_1) = v^{N-1}(\mathbf{r}_1) - v_s^{N-1}(\mathbf{r}_1). \tag{6.25}$$

The response part is given by the difference between the potentials v^{N-1} and v_s^{N-1} that are defined through the $(N-1)$ Hamiltonians H^{N-1} and H_s^{N-1} and the conditional amplitude probabilities (6.22) Φ and Φ_s of the interacting and KS systems:

$$v_{(s)}^{N-1}(\mathbf{r}_1) = \int d\mathbf{x}_2 \dots d\mathbf{x}_N \Phi^*_{(s)}(\mathbf{x}_2 \dots \mathbf{x}_N|\mathbf{r}_1) H_{(s)}^{N-1} \Phi_{(s)}(\mathbf{x}_2 \dots \mathbf{x}_N|\mathbf{r}_1) - E_{(s,)0}^{N-1}$$

In particular v^{N-1} and v_s^{N-1} are defined, respectively for the interacting and the noninteracting KS system, as the difference between the expectation value of the $(N-1)$ Hamiltonian with respect the conditional amplitudes and the ground state energy of the $(N-1)$ system E_0^{N-1} $(E_{s,0}^{N-1})$.

Both v^{N-1} and v_s^{N-1} are positively defined because of the variational principle for the energy and tend to zero at infinity because

$$\Phi(s, \mathbf{x}_2 \dots \mathbf{x}_N|r) \overset{r\to\infty}{\to} \Psi_0^{N-1}(\mathbf{x}_2 \dots \mathbf{x}_N).$$

The one electron nature of H_s^{N-1} and the one determinantal nature of Φ_s allow to rewrite v_s^{N-1} in terms of KS orbitals and orbital energies:

$$v_s^{N-1}(\mathbf{r}_1) = \varepsilon_N - \sum_{i=1}^{N} \varepsilon_i \frac{|\psi_i(\mathbf{r}_1)|^2}{\rho(\mathbf{r}_1)}. \tag{6.26}$$

For v^{N-1} an analogous expression can be found [46]

$$v^{N-1}(\mathbf{r}_1) = \sum_{i=1} E_i^{N-1} \frac{|g_i(\mathbf{r}_1)|^2}{\rho(\mathbf{r}_1)} - E_0^{N-1} \tag{6.27}$$

in terms of the eigenvalues of the H^{N-1} Hamiltonian, E_i^{N-1}, and of the Dyson orbitals, or quasiparticle amplitudes, $g_i(\mathbf{r}_1)$. The latter are defined from the expansion of the ground state N-electron wave function Ψ_0^N in the eigenfunctions Ψ_i^{N-1} of the H^{N-1} Hamiltonian:

$$\Psi_0^N(\mathbf{r}_1 \dots \mathbf{r}_N) = \frac{1}{\sqrt{N}} \sum_i g_i(\mathbf{r}_1) \Psi_i^{N-1}(\mathbf{r}_2 \dots \mathbf{r}_N).$$

6.3.2 Properties of the xc hole and response part

This discussion will concentrate on the asymptotic properties of the potential determined by the exchange hole part, and on the structure of the response part: in the next section different approximations for the xc potential are analyzed on the basis of these two features that strongly influence the quality of the solutions of the KS equation. The properties of the kinetic part $v_{\mathrm{c,kin}}$ of the xc potential instead are not relevant for the response calculations. $v_{\mathrm{c,kin}}$ produces noticeably effect in dissociating molecules, in particular for the H_2 molecule $v_{c,\mathrm{kin}} = v_{\mathrm{kin}}$, being $v_{s,\mathrm{kin}} = 0$, contributes at the bond midpoint with a peculiar peak structure[170].

The xc hole potential $v_{\mathrm{xc,hole}}$ (6.19) describes the screening effect on the classical Coulomb potential due to xc hole $\rho_{\mathrm{xc}}(\mathbf{r}_1, \mathbf{r}_2)$ surrounding the reference electron in $\mathbf{r}_1$.

The exchange hole (2.6), as also discussed in Chapt. 2 integrates to -1 electron, it follows that the exchange hole potentials $v_{x,\mathrm{hole}}$ behaves for finite systems like $-1/r$ at the asymptotics. The other parts of the potential decays more rapidly[114] and the asymptotic behavior of the xc potential is determined by the asymptotic decay of the $v_{x,\mathrm{hole}}$.

The response potential $v_{\mathrm{xc,resp}}$ (6.24) describes the "response" of the xc hole function (6.19) and the kinetic potentials (6.21) to a density variation.

The form of $v_{\mathrm{xc,resp}}$ can be studied from Eqs. (6.25), (6.26) and (6.27):

$$v_{\mathrm{xc,resp}}(\mathbf{r}_1) = \sum_{i=1} (E_i^{N-1} - E_0^{N-1}) \frac{|g_i(\mathbf{r}_1)|^2}{\rho(\mathbf{r}_1)} - \sum_{i=1}^{N} (\varepsilon_N - \varepsilon_i) \frac{|\psi_i(\mathbf{r}_1)|^2}{\rho(\mathbf{r}_1)}. \tag{6.28}$$

The two parts of Eq. (6.28), have an analogous structure: in the region where only one Dyson or KS orbital (or more orbitals of the same form) mainly contributes to the density, for example within an atomic shell, they both give almost a constant contribution, respectively $(E_i^{N-1} - E_0^{N-1})$ and $(\varepsilon_N - \varepsilon_i)$; where two or more orbitals strongly overlap, e.g. inter-shell regions, the potentials in Eqs. (6.26) and (6.27) vary rapidly. As a result they both have a stepped structure, descending in atoms (both potentials are positively defined) from the core region to the valence region where the steps become smaller. In the region where the density is dominated by the Dyson orbital corresponding to the first ionization energy $I_0 = E_0^{N-1} - E_0^N$, in the case of v^{N-1}, or by the KS highest occupied orbital, in case of v_s^{N-1}, the potentials decay rapidly to zero.

The resulting potential shows also in general a stepped repulsive structure, with higher steps in the core region becoming smaller in the valence region. The KS highest occupied orbital have the same asymptotic behavior of the Dyson orbital corresponding to the first ionization energy I_0: in fact at the asymptotic the KS highest occupied orbital determines the density, that is the same in the interacting and noninteracting system. Therefore response potential goes to zero and moreover the relation $\varepsilon_N = -I_0$ should be satisfied.

The response part has a crucial role, even if it does not enter explicitly into the expression for the xc energy. The accurate modeling of this structure is important in the construction of approximations for the ground state potential in order to obtain reliable estimate of the first vertical ionization potential from the highest occupied molecular orbital and of the energy differences of KS orbitals. Moreover, it has been shown that the step structure of the response part is "needed" to describe the dissociation of heteronuclear molecules AB into the neutral atoms A and B [73, 74], and to calculate the polarizability of extended systems [148, 149] (see also Chapt. 9).

6.4 Approximations for the $v_{\mathbf{xc}}$

6.4.1 LDA and GGAs

The LDA and GGAs for the xc potential are derived by differentiation with respect to the density of the corresponding xc energy functional. The success of the approximation for the energy does not imply that the derived xc potential would be a good approximation for calculating molecular response properties. The energy is in fact mainly determined by the quality of the approximation for the hole in the regions where the density is not negligible. The behavior of the xc hole potential at the asymptotic is, in general, not energetically important because in this region the density is very small. On the other hand calculation of the excitation energies and oscillator strengths, for example, requires a good approximation for KS orbital energies and eigenfunctions of unoccupied highlying orbitals localized mainly in the region of the potential tail. The following discussion concentrates on the asymptotic behavior and response part of the LDA and GGA xc potentials.

The LDA exchange hole potential is, following the definition in Eq. (6.19),

$$v_{x,\mathrm{hole}}^{\mathrm{LDA}}(\mathbf{r}_1) = -\frac{3}{2}\left(\frac{3}{\pi}\right)^{1/3} \rho^{1/3}(\mathbf{r}_1).$$

At the asymptotic the density behaves like $\exp\left(-2\sqrt{-2\mu} r\right)$ (μ is the chemical potential), it follows that the LDA potential also decay exponentially, too rapidly compared with the correct Coulombic decay.

Going to the gradient corrected exchange functionals described by the general form

$$E_x[\rho] = \int \rho^{4/3} f(x(\mathbf{r}_1)) dr \tag{6.29}$$

one can choose $f(x)$, function of the dimensionless argument $x = |\nabla\rho|\rho^{-4/3}$, in order to fix the correct asymptotic behavior for the exchange hole potential:

$$f(x) \sim -\frac{1}{6}\frac{x}{\log x}, r \to \infty, x \to \infty.$$

Nevertheless the total exchange potential obtained by differentiation of a exchange functional of this form behaves like $1/r^2$ [89, 171]. Then is not possible to derive a potential with the correct asymptotic behavior from energy expression of the form Eq. (6.29).

Both LDA and GGAs are too repulsive in the asymptotic region and as a consequence highlying energy orbitals, localized in this region, are too destabilized and mostly unbound.

Regarding the response part of the LDA exchange energy

$$v_{\mathrm{x,resp}}^{\mathrm{LDA}} = \frac{1}{2}\left(\frac{3}{\pi}\right)^{1/3} \rho^{1/3}(\mathbf{r}_1),$$

notice that in the region of the highest occupied molecular orbital it gives an important contribution to the total potential, reducing the attractive hole by one third, while, as discussed in the previous section, it should almost vanish so that in this region $v_x \sim v_{x,\mathrm{hole}}$.

This fact has heavy consequences for the KS orbital energies obtained with the LDA xc potential: the HOMO energy ε_N and in general all outer valence orbital energies are overestimated (not negative enough) by approximately one third. This implies in particular that the relation $\varepsilon_N = -I_0$ required by the rigorous exact theory (for a xc potential going to zero at infinity) does not hold[3]. The gradient corrections cannot solve this deficiency and the response of the GGA xc potentials are affected by the same plague.

As a consequence LDA and GGA potentials are too repulsive also in the region of the valence orbitals and being not deep enough, do not support enough virtual levels. In particular the Rydberg levels with energies close to the energy zero have a much too small gap with respect to the HOMO, while the distortion is usually less severe for lowlying virtuals, which are located in roughly the same region of space as the HOMO. So LDA and GGA underestimate vertical excitation energies, given at the zero order by the difference of KS orbital energies, for the higher-lying excitations, i.e. to one-electron levels which approach the energy zero. The wrong spectral structure influences also the polarizability and hyperpolarizability: for molecules that have relatively large HOMO-LUMO gaps and thus low polarizabilities arising from highlying excitations LDA and GGA usually overestimate (hyper)polarizabilities and their frequency dependence.

For the excitation energies the effect of the error on the HOMO energy (almost one third of its value) is more severe than the destabilization of the higher-lying energy levels coming from the wrong asymptotic behavior. On the other hand the wrong asymptotic behavior affects the form of the virtual orbital functions and thus the zero order for the oscillator strengths.

In conclusion two basic shortcomings have been individuated in the shape of the approximated xc potentials derived from LDA and GGA xc functionals: in the "outer"

---

[3] It was an old notion of the $X\alpha$ theory [172], that reasonable ε_N values can be obtained with the Xα potential with α=1.0, which is 1.5 times as attractive as the LDA exchange potential v_x^{LDA}, the dominant part of $v_{\mathrm{xc}}^{\mathrm{LDA}}$: $v_{x\alpha}(\alpha{=}1.0) = 1.5 v_x^{\mathrm{LDA}}$. The potential $1.5 v_x^{\mathrm{LDA}}$ is in fact the electron gas approximation to the exchange hole potential $v_{x,\mathrm{hole}}$. In the variation procedure to obtain one-electron equations a factor 2/3 is introduced to give $v_{x\alpha}(\alpha{=}0.667) = v_x^{\mathrm{LDA}}$ as exchange potential in the one-electron equations.

region they do not have the correct Coulombic behavior and decaying too rapidly, in the "inner" region they are too repulsive. These shortcomings dramatically affects the results for the highlying excitation energies.

6.4.2 Model xc potentials

The latter arguments demonstrate the substantial inadequacy of the xc potentials derived from LDA and GGA energy functionals. The alternative is to model directly an approximated xc potential "that more closely resembles the exact KS potential", in particular to incorporate the structure of the response part and the correct asymptotic behavior. Modeling the xc potential has the additional advantage that the potential is uniquely determined by the exact density. It is then possible to compare the model potentials with the potential constructed from accurate densities [89]. The main drawback is that the corresponding energy functional is missing: in a way model potentials are specialized for molecular response properties.

In principle, an improved model can be developed either by correction of the standard LDA or GGA potentials, or one can consider an entirely different model of the response potential and, in general, of v_{xc}. The latter option has been followed in the construction of the nonlocal correction to the LDA potential proposed by van Leeuwen and Baerends (LB) in Ref. [89]:

$$v_{\mathrm{xc}}^{\mathrm{LB}} = -\beta\rho_\sigma^{1/3}\frac{x_\sigma^2}{1+3\beta x_\sigma \sinh^{-1} x_\sigma} \tag{6.30}$$

that reproduces the correct long-range asymptotics of the potential. The parameter β has been parameterized to reproduce the difference between the LDA and the accurate xc potential of beryllium atom. In this way $v_{\mathrm{xc}}^{\mathrm{LB}}$ not only adds to the LDA the good asymptotic behavior, but it also deepens it, correcting in this way the spacing between the HOMO and the highlying orbitals.

The potential proposed in Ref. [173] by Gritsenko, van Leeuwen, van Lenthe and Baerends (GLLB) is modeled as the sum of a xc hole part, approximated by the xc hole potential of Becke and Perdew [4, 5, 75, 76] and an orbital-dependent response part, having the same form of the weighted sum of orbital densities of the response part in Ref. [38], but with the weights w_i that have a simple dependence on the square root of the difference of orbital energies:

$$w_i = K\sqrt{\varepsilon_i - \varepsilon_N}.$$

K=0.38 is a parameter derived for the homogeneous electron gas. The GLLB response potential reproduces then the stepped structure of the exact response potential and vanishes in the region where $\rho \sim |\psi_N|^2$.

The two model potentials LB (6.30), and GLLB, one having a good asymptotic behavior, the other reproducing the atomic shell structure have been combined in Ref. [111, 174, 175] in a potential that has the form of a statistical average of (model) potentials (SAOP)

$$v_{\text{xc}}^{\text{SAOP}} = \sum_{i}^{N} v_i^{\text{xc,mod}} \frac{|\psi(\mathbf{r}_1)|^2}{\rho(\mathbf{r}_1)}.$$

The model potentials $v_i^{\text{xc,mod}}$ are obtained from an exponential interpolation of the LB and GLLB potentials, so that the resulting potential $v_{\text{xc}}^{\text{SAOP}}$ is therefore close to $v_{\text{xc}}^{\text{GLLB}}$ in the inner region and close to $v_{\text{xc}}^{\text{LB}}$ in the outer region.

The asymptotic corrected LDA and GGA potentials, proposed in Refs. [176, 177] and in the Chapt. 7, correct instead the existing LDA and GGA xc potential. The trick used in these approaches is to shift the original GGA and LDA in order to satisfy the exact relation $\varepsilon_N = -I_0$ (NB: potential to zero) and to connect it to a potential having the correct asymptotic. The differences between the various schemes concern mainly how and where the connection between the GGA/LDA and the asymptotic corrected potential is made and are illustrated in Chapt. 7. Notice that the even if these potentials have been dubbed "asymptotic corrected potential" the major correction comes in fact from the shift that adjusts the spacing between the valence occupied orbitals and the highlying unoccupied orbitals.

Finally the exchange potential of Krieger Li and Iafrate [38] and the one obtained with the CEDA[4], are also "good" model potentials in the sense that they both possess the stepped response structure and the correct asymptotic behavior. Nevertheless the highest occupied molecular orbital obtained with only exchange potential is too stabilized and as a consequence the orbital energy differences are uniformly shifted to larger values.

---

[4] The same potential has been obtained with a different approach in Ref. [109].

Chapter

7

A density functional scheme to correct GGA potentials

Shape corrections to the standard approximate KS xc potentials are considered with the aim to improve the excitation energies (especially for higher excitations) calculated with TDDFRT. A scheme of gradient-regulated connection (GRAC) of inner to outer parts of a model potential is developed. Asymptotic corrections based either on the potential of Fermi and Amaldi (FA) or van Leeuwen and Baerends (LB) are seamlessly connected to the (shifted) xc potential of Becke and Perdew (BP) with the GRAC procedure, and are employed to calculate the vertical excitation energies of the prototype molecules N_2, CO, CH_2O, C_2H_4, C_5NH_5, C_6H_6, Li_2, Na_2, K_2. The results are compared with those of the alternative interpolation scheme of Tozer and Handy as well as with the results of the potential obtained with the SAOP (Chapt. 6. Various asymptotically corrected potentials produce high quality excitation energies, which in quite a few cases approach the benchmark accuracy of 0.1 eV for the electronic spectra. Based on these results, the potential BP-GRAC-LB is proposed for molecular response calculations, which is a smooth potential and a genuine "local" density functional with an analytical representation.

7.1 Introduction

In spite of the success of TDDFRT, the problem remains to provide a uniform high quality for both lowest and higher-lying excitations with model potentials v_{xc}. Here, the traditional LDA and GGAs for v_{xc} have met with limited success. Even though LDA produces reasonable lowest excitation energies [178, 179], it consistently underestimates the zero-order excitation energy $\Delta\varepsilon_{ia}$ for higher excitations. The LDA xc potential $v_{\mathrm{xc}}^{\mathrm{LDA}}$ in fact is not attractive enough in the molecular bulk region where the occupied and lowest unoccupied orbitals are localized, so that the corresponding orbital energies are too high (not negative enough). In particular, the LDA energy

$\varepsilon_N^{\mathrm{LDA}}$ of the highest occupied molecular orbital (HOMO) is much higher (less negative) than the value $\varepsilon_N = -I_p$ (I_p is the ionization potential) required by the rigorous KS theory.

Thus, accurate modeling of v_{xc} becomes an actual problem of TDDFRT. As it has been also noted in Chapt. 6 not only a correction is required in the far asymptotic region, to the effect that the exponential decay of the LDA potential in the outer density tail has to be replaced by a $-1/r$ behavior, but a more general shape correction is needed to adjust in particular the spacing between the occupied orbitals and the highlying virtuals. In the "asymptotic corrected" potentials of Refs. [177] and [176] this adjustment occur simply shifting the unmodified LDA or GGA potential in the bulk by an amount of $(\varepsilon_N^{\mathrm{LDA/GGA}} + I_p)$. The Coulombic asymptotic is provided by "replacing" in the outer region the LDA/GGA with a potential with the correct decay.

In this chapter the connection schemes of Refs. [177] and [176] are improved by introducing a density gradient-regulated connection method between bulk and asymptotic potentials, which is presented in Sec. 7.2. This scheme allows to construct smooth asymptotically corrected potentials, which are genuine density functionals with an analytical representation. In Sec. 7.3 GRAC together with the GGA bulk potential of Becke [4] and Perdew [6], and with the Fermi and Amaldi or van Leeuwen and Baerends asymptotic potentials [89] is applied to the TDDFRT calculations of the vertical excitation energies of the prototype molecules N_2, CO, CH_2O, C_2H_4, C_5NH_5, C_6H_6, Li_2, Na_2, K_2. The results are compared with those obtained with the linear interpolation function of Ref. [176] as well as with SAOP. In Sec. 7.4 the conclusions are drawn.

7.2 Connection between bulk and asymptotic potentials

In general, an asymptotically corrected xc potential $v_{\mathrm{xc}}^{b\text{-AC}}$ can be written in the following form

$$v_{\mathrm{xc}}^{b\text{-AC}}(\mathbf{r}) = [1 - f(\mathbf{r})]\, v_{\mathrm{xc}}^{b}(\mathbf{r}) + f(\mathbf{r}) v_{\mathrm{xc}}^{a}(\mathbf{r}) \tag{7.1}$$

where v_{xc}^{b} is a potential in the bulk region, which is to be corrected, v_{xc}^{a} is an asymptotic correction in the region of atomic and molecular density tails, and f is an interpolation or switching function, which is close to 1 in the asymptotic region and vanishes in the bulk region. It is desirable that, with a proper choice of $f(\mathbf{r})$, the corrected potential $v_{\mathrm{xc}}^{b\text{-AC}}$ be a smooth potential and also a genuine density functional, which has an analytical representation and which possesses usual scaling and invariance properties.

In Ref. [177] the LDA potential $v_{\mathrm{xc}}^{\mathrm{LDA}}$ has been shifted in the bulk region downward by $(I_p+\varepsilon_N^{\mathrm{LDA}})$, where I_p and $\varepsilon_N^{\mathrm{LDA}}$ have been pre-calculated with additional self-consistent field (ΔSCF) calculations of the neutral molecule and its cation. In the asymptotic region (ca. 4–5 a.u. from the nearest nucleus) $v_{\mathrm{xc}}^{\mathrm{LDA}}$ has been replaced with the LB potential $v_{\rm xc}^{\rm LB}$ with the correct Coulombic behavior and zero asymptotics $v_{\rm xc}(\infty)$=0. The total asymptotically corrected potential $v_{\rm xc}^{\text{LDA-AC}}$ is defined simply as the maximum of those two potentials $v_{\rm xc}^{\text{LDA-AC}}(\mathbf{r}) = max[v_{\rm xc}^{\rm LDA}(\mathbf{r}) - I_p + \varepsilon_N, v_{\rm xc}^{\rm LB}(\mathbf{r})]$. The disadvantage of this simple correction is that, by construction, the potential ${v_{\rm xc}}^{\text{LDA-AC}}$ possesses a discontinuity in its derivative.

In Ref. [176] the unmodified GGA HCTH potential $v_{\rm xc}^{\rm HCTH}$ has been used in the bulk region, while the asymptotics has been provided with the Fermi-Amaldi potential $v^{\rm FA}(\mathbf{r}) = -v_H(\mathbf{r})/N$, which is shifted upwards by $(I_p{+}\varepsilon_N)$. Thus, the resulting asymptotically corrected potential $v_{\rm xc}^{\text{HCTH-AC}}$ asymptotically goes to a positive constant, $v_{\rm xc}^{\text{HCTH-AC}}(\infty)$=$(I_p{+}\varepsilon_N)$. The potential $v_{\rm xc}^{\rm HCTH}$ is retained in the spherical regions around the nuclei $\{A\}$ and the asymptotic correction $[v^{\rm FA}(\mathbf{r}) = -v_H(\mathbf{r})/N + (I_p + \varepsilon_N)]$ is switched on by linear interpolation in the intermediate region. The corresponding interpolation function contains explicit electron-nuclear distances r_A (see below for the corresponding formula), so that $v_{\rm xc}^{\text{HCTH-AC}}$ is defined on a grid. Both the downward shift of the bulk potential in Ref. [177] and the upward shift of the asymptotic potential in Ref. [176] are equivalent in the sense, that they have the same effect on the orbital energy difference $\Delta\varepsilon_{ia}$, while the absolute shift of the total xc potential is immaterial, since the latter is defined up to an arbitrary constant (see the next section for further discussion). The corrections of Refs. [177] and [176] have produced considerable improvement of the calculated molecular response properties. Still, further improvement of model xc potentials is desirable.

Here we propose to use a gradient-regulated asymptotic correction (GRAC), i.e. we employ the standard dimensionless density-gradient argument x

$$x(\mathbf{r}) = \frac{|\nabla\rho(\mathbf{r})|}{\rho^{4/3}(\mathbf{r})} \tag{7.2}$$

as a switching parameter of the interpolation function $f[x(\mathbf{r})]$. The argument x appears to be a natural parameter for this purpose, since in the region of the density tails it diverges, $x(\mathbf{r}) \sim \rho^{-1/3}(\mathbf{r})$, while it remains finite in the bulk region. One can see this from Figure 7.1, where $x(r)$ is plotted for the atoms H, C, N, O. For heavier atoms C, N, O, oscillations of $x(r)$ in the bulk region with maxima of about 10 reflect the atomic shell structure. Starting from r=1 a.u., $x(r)$ diverges monotonically.

Having this behavior of $x(\mathbf{r})$ in mind, we choose the following form for the interpolation function $f[x(\mathbf{r})]$ in Eq. (7.1)

$$f\left[x(\mathbf{r})\right] = \frac{1}{1 + e^{-\alpha[x(\mathbf{r})-\beta]}} \tag{7.3}$$

which turns to 1 at the asymptotics $x(\mathbf{r}) \to \infty$ and, depending on the empirical parameters α and β, can be made vanishing in the bulk region. The parameter β indicates where to switch ($f(x)$=1/2 for x=β), while α determines how fast the switching is (with the condition that their product $\alpha\beta$ should be large enough, so that $\exp(\alpha\beta) \gg 1$). The value β=40 has been chosen from atomic calculations, which is well above maximum x values in the bulk atomic regions (see Figure 7.1). With

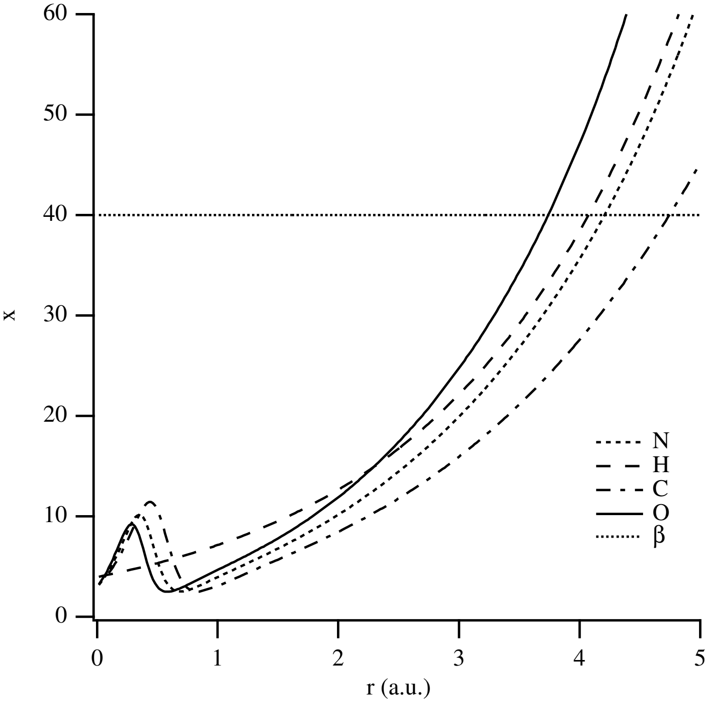

Figure 7.1: Form of the density-gradient function $x(\mathbf{r})$ for the H, C, N, O atoms (the straight line indicates the value of β parameter).

this value a switch to the asymptotic potential v_{xc}^{a} occurs as close to the nucleus as possible, yet without perturbing the energies ε_i of the occupied KS orbitals, i.e. the values ε_i obtained with $v_{\mathrm{xc}}^{b\text{-AC}}$ are virtually the same as those obtained with the bulk potential v_{xc}^{b}. For the parameter α the value α=0.5 has been chosen which, together with β=40, guarantees that $f[x(\mathbf{r})]$ vanishes in the bulk region. The use of the dimensionless argument x has the advantage, that the dimensionless function $f[x(\mathbf{r})]$ does not change scaling properties of the potentials v_{xc}^{a} and v_{xc}^{b} within Eq. (7.1). The advantage of the proposed GRAC procedure is that switching to an asymptotically correct potential v_{xc}^{a} occurs naturally, when the argument x of Eq. (7.2) indicates the asymptotic region of the density tails.

The basic option in this chapter is the GGA BP potential $v_{\mathrm{xc}}^{\mathrm{BP}}(\rho(\mathbf{r}), \nabla\rho(\mathbf{r}); \mathbf{r})$ as the bulk potential and the LB potential $v_{\mathrm{xc}}^{\mathrm{LB}}(\rho(\mathbf{r}), x(\mathbf{r}); \mathbf{r})$ as the asymptotic potential

$$\begin{aligned} v_{\mathrm{xc}}^{\mathrm{BP\text{-}GRAC}}\left(\rho(\mathbf{r}), \nabla\rho\left(\mathbf{r}\right); r\right) = \left(1 - f[x(\mathbf{r})]\right) v_{\mathrm{xc}}^{\mathrm{BP}}\left(\rho(\mathbf{r}), \nabla\rho(\mathbf{r}); \mathbf{r}\right) \\ + f[x(\mathbf{r})]\left[v_{\mathrm{xc}}^{\mathrm{LB}}\left(\rho(\mathbf{r}), \nabla\rho(\mathbf{r}); \mathbf{r}\right) + \left(I_p + \varepsilon_N\right)\right] \end{aligned} \tag{7.4}$$

All components of the asymptotically corrected potential $v_{\mathrm{xc}}^{\mathrm{BP\text{-}GRAC}}$ of Eq. (7.4) are explicit functions of the density ρ and its gradient $\nabla\rho$ (including the second derivatives of ρ with respect to $\mathbf{r}$ in $v_{\mathrm{xc}}^{\mathrm{BP}}$), so that $v_{\mathrm{xc}}^{\mathrm{BP\text{-}GRAC}}$ is a genuine density functional, which has an analytical representation and it is a smooth potential. In Eq. (7.4) the constant shift $(I_p{+}\varepsilon_N)$ is added to the asymptotic part, as in Ref. [176], so that Eq. (7.4) has the asymptotics

$$v_{\mathrm{xc}}^{\mathrm{BP\text{-}GRAC}}(\mathbf{r}) \to -\frac{1}{r} + (I_p + \varepsilon_N)$$

where ε_N is the HOMO energy of the potential Eq. (7.4) and the Coulombic part $-1/r$ is provided by the LB potential $v_{\mathrm{xc}}^{\mathrm{LB}}$. With the choice for positive asymptotics, $v_{\mathrm{xc}}^{\mathrm{BP\text{-}GRAC}}$ has virtually the same ε_N as the bulk BP potential $v_{\mathrm{xc}}^{\mathrm{BP}}$, and the GGA (as well as LDA) ε_N value is substantially smaller (in absolute magnitude) than I_p. However, $v_{\mathrm{xc}}^{\mathrm{BP\text{-}GRAC}}(\mathbf{r})$ is, of course, equivalent to the potential $v_{\mathrm{xc}}^{\mathrm{BP\text{-}GRAC}}(\mathbf{r}){-}(I_p{+}\varepsilon_N)$ (here the shift is applied to the total potential), since v_{xc} is defined only up to an arbitrary constant. This latter potential has zero asymptotics and its HOMO energy is just $-I_p$, as required by the rigorous KS theory for potentials with zero asymptotics. As an alternative to Eq. (7.4) one can apply a shift to the bulk potential, using $v_{\mathrm{xc}}^{b}{=}v_{\mathrm{xc}}^{\mathrm{BP}}{+}\Delta$ where Δ is determined during the SCF cycles. Starting with $\Delta{=}(-I_p + \varepsilon_N^{\mathrm{LDA/GGA}})$ the downward shift of the bulk LDA/GGA potential yields an $\varepsilon_N^{(1)}$ value of the corrected potential, which will be close to $-I_p$. The shift can be updated on subsequent cycles, with increment $(-I_p{+}\varepsilon_N{}^{(n)})$ to be applied on cycle $(n+1)$, to fix the HOMO one-electron energy at $-I_p$. To determine the shift in either the asymptotic or in the bulk potential, the ionization energy I_p should be obtained with additional calculations of a neutral system and its cation with the standard DFT methods. Bearing in mind that calculation of I_p is a separate step, we use here the experimental I_p values as an input.

The explicit use of the ionization energy might create a problem in the case of a weakly bound molecular complex with fragments of different electronegativity. It is clear in this case that, in order to reproduce excitations which are localized within a certain fragment, one should use the ionization energy of this fragment. A possible remedy for this problem could be partitioning of the molecular volume into fragment regions, so that in each region the expression Eq. (7.4) will be calculated with the I_p and ε_N values of the corresponding fragment. However, we advocate the use of methods like the present one that work with the I_p and ε_N values to systems that are sufficiently strongly connected that these are genuinely global quantities of the system.

Besides $v_{\mathrm{xc}}^{\mathrm{LB}}$, we also use the Fermi-Amaldi (FA) potential v^{FA}

$$v^{\mathrm{FA}}(\mathbf{r}_1) = -\frac{v_H(\mathbf{r}_1)}{N} = -\frac{1}{N}\int \frac{\rho(\mathbf{r}_2)}{|\mathbf{r}_1 - \mathbf{r}_2|} d\mathbf{r}_2 \tag{7.5}$$

as the asymptotic potential in Eq. (7.4). From a theoretical point of view, the disadvantage of v^{FA} is that, as follows from Eq. (7.5), it is effectively produced with an “exchange-correlation” hole function $-\rho(\mathbf{r}_2)/N$, which is delocalized over the entire system, while the real xc hole is more or less localized around the reference electron at $\mathbf{r}_1$. Because of this, application of v^{FA} for large molecules should produce underestimation of the exchange-correlation effects in the nearer asymptotic region.

The present chapter also compares the performance of the GRAC interpolation function with the linear interpolation approach of Ref. [176] (which has been characterized before) for the same potentials v^a_{xc} and v^b_{xc}. In the latter approach the asymptotically corrected potential v^{b-AC}_{xc} lacks an uniform analytical representation and it is defined on the grid in the following way: when the distance r_A from a nucleus $\{A\}$ is less than R^A_1, then $v^{b\text{-AC}}_{\mathrm{xc}} = v^b_{\mathrm{xc}}$; when $R^A_1 < r_A < R^B_2$ for M nuclei (and $r_B < R^B_2$ for the others nuclei $\{B\}$), then $v^{b\text{-AC}}_{\mathrm{xc}} = v^b_{\mathrm{xc}} + \mu(v^a_{\mathrm{xc}} - v^b_{\mathrm{xc}})$ with

$$\mu = \sum_{A=1}^{M} \frac{r_A - R^A_2}{R^A_1 - R^A_2} \tag{7.6}$$

when the distances from all atoms are larger than R_2, then $v^{b\text{-AC}}_{\mathrm{xc}} - v^a_{\mathrm{xc}}$. The radii $R_1$and R_2 are determined as follows: $R_1 = \gamma R_{\mathrm{SB}}$ and $R_2 = \delta R_{\mathrm{SB}}$ where R_{SB} is the Slater-Bragg radius of the atom and $\gamma = 3.5$ and $\delta = 4.7$ are the empirical parameters.

Note that, unlike the standard GGA potentials, virtually all the asymptotically corrected potentials (as well as the SAOP potential) are not functional derivatives of known xc energy functionals. The results of molecular response calculations with asymptotically and otherwise corrected potentials, including those to be presented in the next section, demonstrate that for high quality response properties it is of primary importance that the shape of the potential be accurate, rather than that the condition be met of being a functional derivative of a given density functional for the exchange-correlation energy.

7.3 Calculations of excitation energies

Calculations of excitation energies are performed using the RESPONSE [180] module of the Amsterdam Density Functional program (ADF)[78, 93, 181, 182, 183]. In order to get results close to the basis set limit increasing numbers of diffuse functions are added to the standard ADF basis V[1]. We have monitored systematically the improvement of results with increasing numbers of diffuse basis functions and we have selected very large basis sets near to the basis set limit. For all the prototype molecules and pyridine we have added for C, O, and N atoms two $3p$, two $3d$, two $4s$ and two $4f$ diffuse function and for the H atom one $2p$ function. In case of benzene for the C atom an even tempered basis set is used ($7s6p2d1f$, with the orbital exponent Z=$\alpha\beta^i$, i=1,...,n, β=1.7 and α is for the most diffuse $1s$, $2p$, $3d$ respectively 0.7045, 0.3459 and 1.2182). Linear combinations of atomic orbitals have been removed from the basis sets where linear dependency due to adding a large number of diffuse functions was detected. We estimate the error on calculated energies due to the finite basis sets to be always smaller than 0.1 eV and in average of the order of a few hundredths

---

[1] Valence triple zeta plus two polarization functions

Excited state and transition	SAOP	BP	BP acFA	BP gracFA	BP gracLB	Exp[a]
$^3\Pi$, $\sigma \to \pi^*$ (V)	6.28	6.18	6.19	6.20	6.19	6.32
$^3\Sigma^+$, $\pi \to \pi^*$ (V)	8.64	8.44	8.44	8.46	8.45	8.51
$^1\Pi$, $\sigma \to \pi^*$ (V)	8.56	8.36	8.42	8.46	8.45	8.51
$^3\Delta$, $\pi \to \pi^*$ (V)	9.37	9.18	9.20	9.22	9.21	9.36
$^3\Sigma^-$, $\pi \to \pi^*$ (V)	10.03	9.86	9.88	9.91	9.90	9.88
$^1\Sigma^-$, $\pi \to \pi^*$ (V)	10.03	9.86	9.88	9.91	9.90	9.88
$^1\Delta$, $\pi \to \pi^*$ (V)	10.46	10.00	10.34	10.37	10.35	10.23
$^3\Sigma^+$, $\sigma \to 3s$	10.32	8.98	10.14	10.29	10.39	10.40
$1\Sigma^+$, $\sigma \to 3s$	10.69	9.10	10.51	10.63	10.79	10.78
$^3\Sigma^+$, $\sigma \to 3p\sigma$	11.26	9.48	11.14	11.40	11.40	11.30
$^1\Sigma^+$, $\sigma \to 3p\sigma$	11.41	9.49	11.30	11.53	11.59	11.40
$^1\Pi$, $\sigma \to$ $3p\pi$	11.58	9.49	11.28	11.40	11.64	11.53
$^3\Pi$, $\sigma \to 3p\pi$	11.51	9.51	11.23	11.36	11.54	11.55
$^1\Sigma^+$, $\sigma \to 3d\sigma$	12.59	9.93	12.30	12.44	12.67	12.40
MAE	0.09	1.01	0.14	0.10	0.09	
VSMAE	0.11	0.12	0.08	0.08	0.08	
RSMAE	0.07	1.91	0.21	0.12	0.10	
I_p	13.62	9.15	14.01	14.01	14.01	

---

[a] Ref. [111]

Table 7.1: Vertical excitation energies (eV) of CO. MAE is the mean absolute error, VSMAE is the MAE for the V (valence) excitations and RSMAE is the MAE for the Rydberg excitations. Ionization potential I_p corresponds to $-\varepsilon_N$ for SAOP and BP and to the input experimental value for GRAC/AC.

of an eV. Experimental geometries are used for all molecules (see Ref. [111] for the prototype molecules, Ref. [184] for benzene and Ref. [185] for pyridine).

Tables 7.1–7.6 compare the vertical excitation energies ω_i calculated with the standard exchange-correlation BP potential, BP with various asymptotic corrections, and with the SAOP potential for small prototype molecules N_2, CO, CH_2O, C_2H_4 and larger aromatic systems C_5NH_5, C_6H_6.

The ω_i values have been obtained from the solution of the eigenvalue problem (6.11). The ALDA xc kernel (6.15) has been used in all cases and, as follows from the discussion in Chapt. 6, asymptotic corrections to BP alter only the KS orbital energy differences, and to some extent, the form of the unoccupied KS orbitals.

The asymptotically corrected potentials to be compared are BP-GRAC-LB of (7.4), BP-GRAC-FA with the gradient-dependent switching function in (7.3) and the FA asymptotic potential in (7.5) as well as the analogous potential BP-AC-FA with the linear interpolation function (7.6).

The TDDFRT excitation energies are compared with reference data. For N_2,

Excited state and transition	SAOP	BP	BP acFA	BP gracFA	BP gracLB	Exp[a]
$^3\Sigma_u^+$, $\pi_u\to\pi_g$ (V)	7.89	7.91	7.92	7.93	7.92	7.75
$^3\Pi_g$, $\sigma_g\to\pi_g$ (V)	7.81	7.73	7.75	7.75	7.75	8.04
$^3\Delta_u$, $\pi_u\to\pi_g$ (V)	8.82	8.84	8.86	8.86	8.86	8.88
$^1\Pi_g$, $\sigma_g\to\pi_g$ (V)	9.31	9.21	9.25	9.27	9.26	9.31
$^3\Sigma_u^-$, $\pi_u\to\pi_g$ (V)	9.66	9.68	9.70	9.72	9.71	9.67
$^1\Sigma_u^-$, $\pi_u\to\pi_g$ (V)	9.66	9.68	9.70	9.72	9.71	9.92
$^1\Delta_u$, $\pi_u\to\pi_g$ (V)	10.21	10.22	10.25	10.27	10.26	10.27
$^3\Pi_u$, $\sigma_u\to\pi_g$ (V)	10.88	10.69	10.72	10.73	10.73	11.19
$^3\Sigma_g^+$, $\sigma_g\to 3s\sigma_g$	11.85	10.06	11.63	11.87	11.92	12.00
$^1\Sigma_g^+$, $\sigma_g\to 3s\sigma_g$	12.26	10.19	12.01	12.22	12.32	12.20
$^1\Pi_u$, $\sigma_g\to 3p\pi_u$	12.97	10.76	12.67	12.87	13.02	12.90
$^1\Sigma_u^+$, $\sigma_g\to 3p\sigma_u$	12.88	10.46	12.70	13.00	13.07	12.98
$^1\Pi_u$, $\pi_u\to 3s\sigma_g$	13.23	11.43	13.09	12.87	13.36	13.24
$^1\Pi_u$, $\sigma_u\to\pi_g$	13.59	11.59	13.42	13.32	13.49	13.63
$^1\Sigma_u^+$, ...	14.03	11.61	14.01	14.19	14.17	14.25
MAE	0.11	1.10	0.20	0.15	0.13	
VSMAE	0.11	0.13	0.12	0.11	0.11	
RSMAE	0.12	1.92	0.27	0.18	0.15	
I_p	15.19	10.36	15.59	15.59	15.59	

[a] Ref. [111]

Table 7.2: Vertical excitation energies (eV) of N_2. See caption of Table 7.1.

CO, CH_2O, C_2H_4 the same experimental data are used as in Ref. [111], while for C_5NH_5 and C_6H_6 the energies are taken from experiment and from calculations in Refs. [186, 187] with the *ab initio* complete active space multi-configurational self-consistent-field method with addition of second-order perturbation theory corrections (CASPT2). Tables 7.1–7.6 also present the mean absolute error (MAE) with respect to the reference values for all excitations and separately the mean absolute errors for the excitations to valence states (VSMAE) and to Rydberg-like states (RSMAE). In Tables 7.5 and 7.6 we mark with (d) states having contributions from double and higher excitations of more than 8% in the configuration interaction wave functions as reported in Ref. [188] and that are insufficiently described within the adiabatic approximation. In this case also the mean absolute error excluding states marked with a (d) is reported in parentheses beside the MAE value.

The results obtained with the uncorrected BP potential are typical for the standard LDA and GGA methods. BP yields a good estimate of the ω_i excitation energies lower than the ionization energy estimated by BP HOMO $-\varepsilon_N$. This is reflected in low VSMAE values of BP, 0.1–0.3 eV for all molecules. For Rydberg excitation

Excited state and transition	SAOP	BP	BP acFA	BP gracFA	BP gracLB	Exp[a]
$^3A_2$, $n \to \pi^*$ (V)	3.64	3.31	3.31	3.32	3.31	3.50
$^1A_2$, $n \to \pi^*$ (V)	4.24	3.91	3.92	3.93	3.92	4.10
$^3A_1$, $\pi \to \pi^*$ (V)	6.33	6.24	6.25	6.26	6.25	6.00
$^3B_2$, $n \to 3s$	6.92	5.87	6.70	6.83	6.62	7.09
$^1B_2$, $n \to 3s$	7.14	5.92	6.87	7.00	6.81	7.13
$^3B_2$, $n \to 3p_{a_1}$	8.08	6.49	7.66	7.76	7.72	7.92
$^1B_2$, $n \to 3p_{a_1}$	8.21	6.50	7.79	7.90	7.84	7.98
$^3A_1$, $n \to 3p_{b_2}$	8.15	6.51	7.86	7.95	7.80	8.11
$^1A_1$, $n \to 3p_{b_2}$	8.26	6.50	7.96	8.05	7.94	8.14
$^1B_1$, $\sigma \to \pi^*$ (V)	9.01	8.91	8.92	8.93	8.92	9.00
MAE	0.14	0.93	0.22	0.16	0.23	
VSMAE	0.16	0.18	0.18	0.17	0.18	
RSMAE	0.12	1.43	0.26	0.15	0.27	
I_p	11.02	6.35	10.88	10.88	10.88	

[a] Ref. [111]

Table 7.3: Vertical excitation energies (eV) of CH_2O. See caption of Table 7.1.

energies BP fails to reproduce both their absolute values and their relative order. BP consistently and substantially underestimates higher excitations, which leads to large RSMAE values of order of 1 eV for CH_2O, C_2H_4, C_5NH_5 and of 2 eV for CO and N_2. Note the lower (though still appreciable) RSMAE of 0.59 eV for the benzene. As a result, the total MAEs of BP are also large.

Corrections to BP considerably improve its performance. By construction, these corrections have relatively little effect on the lower excitations. Due to this, VSMAE values of all corrected potentials are close to the corresponding BP values. Still, in all those cases where corrections alter VSMAE, they always produce an improvement, which is most appreciable for ethylene (see Table 7.4). But, the most important, corrections dramatically improve the calculated higher excitations. In particular, for ethylene, and benzene RSMAE values of all corrected potentials appear to become even smaller, than the corresponding VSMAE values. As a result, in all cases the total MAE of the corrected potentials is much smaller than that of the standard BP, and in quite a few cases MAE approaches the benchmark accuracy of 0.1 eV for the electronic spectra. One can further analyze the performance of various types of asymptotic correction by comparing the results of the corresponding corrected potentials. In particular, the comparison of the results of BP-GRAC-FA and BP-AC-FA allows to assess the performance of the proposed GRAC function (7.3), since these two potentials differ only in the interpolation functions. On average, BP-GRAC-FA yields somewhat better higher excitations compared to BP-AC-FA. In particular, for N_2, CO and CH_2O BP-GRAC-FA produces higher energy values and, as a result,

Excited state and orbital	SAOP	BP	BP acFA	BP gracFA	BP gracLB	Exp[a]
$^3B_{1u}$, π^* (V)	4.64	4.68	4.69	4.69	4.68	4.36
$^3B_{3u}$, $3s$	7.18	6.51	7.10	7.13	7.01	6.98
$^1B_{3u}$, $3s$	7.29	6.53	7.19	7.22	7.12	7.15
$^1B_{1u}$, π^* (V)	7.62	7.43	7.62	7.65	7.60	7.66
$^3B_{1g}$, $3p_y$	7.91	7.09	7.81	7.84	7.72	7.79
$^3B_{2g}$, $3p_z$	7.81	6.93	7.77	7.84	7.61	7.79
$^1B_{1g}$, $3p_y$	8.00	7.10	7.88	7.91	7.84	7.83
$^1B_{2g}$, $3p_z$	7.94	6.95	7.85	7.92	7.70	8.00
^3A_g, $3p_x$	8.70	7.36	8.22	8.26	8.42	8.15
^1A_g, $3p_x$	8.91	7.36	8.36	8.40	8.61	8.29
$^3B_{3u}$, $3d_{z^2}$	8.96	7.61	8.70	8.73	8.76	8.57
$^1B_{3u}$, $3d_{z^2}$	9.03	7.64	8.74	8.77	8.79	8.62
MAE	0.25	0.72	0.10	0.11	0.16	
VSMAE	0.16	0.28	0.19	0.17	0.19	
RSMAE	0.28	0.81	0.08	0.10	0.16	
I_p	10.92	6.81	10.52	10.52	10.52	

---

[a] Ref. [111]

Table 7.4: Vertical excitation energies (eV, from π-orbital) of C_2H_4. See caption of Table 7.1.

its RSMAEs are 0.08–0.12 eV lower than those of BP-AC-FA. We attribute this difference to the fact, that the Fermi-distribution-type GRAC function in Eq. (7.3) switches faster than the linear interpolation function in Eq. (7.6) to the asymptotic potential, thus effectively producing a less attractive potential in the transition region. It seems also, that the GRAC switching is more flexible, since it occurs naturally when the gradient parameter $x(\mathbf{r})$ indicates the density tail region. Thus, for N_2, for example, the switching (in the direction along the N–N axis) occurs at a distance of less than 4 a.u. from the N atom, whereas for the N atom it occurs at 4.3 a.u. Unlike this, the switching of Ref. [176] in BP-AC-FA is rigidly fixed with the atomic parameters, and it begins at 4.3 a.u. in both cases. Since, as was mentioned before, asymptotic potentials have little influence on the lower excitations, VSMAEs and MAEs of the potentials BP-GRAC-FA and BP-AC-FA are closer to each other than RSMAE, so that the interpolation functions in Eq. (7.3) and in Eq. (7.6) exhibit equally good overall performance. This means, that in practical calculations one can use the explicit function of the density gradient in Eq. (7.3).

To assess the effect of the LB asymptotic correction to BP, one can compare the performance of BP-GRAC-LB with BP-GRAC-FA. Besides the common bulk BP part, these two potentials also have the same switching GRAC function, so that the differences in the results will indicate the difference between the asymptotic LB and FA potentials. On average, both potentials produce results of similar good quality

Excited state and transition	SAOP	BP	BP acFA	BP gracFA	BP gracLB	Exp/ CASPT2[a]
B_2, $\pi \rightarrow \pi^*$ (V)	5.36	5.38	5.35	5.40	5.38	4.99 (d)
A_1, $\pi \rightarrow \pi^*$ (V)	6.23	6.24	6.25	6.26	6.23	6.38
A_1, $\pi \rightarrow \pi^*$ (V)	7.21	7.19	7.22	7.24	7.12	7.22
B_2, $\pi \rightarrow \pi^*$ (V)	7.17	7.09	7.14	7.16	7.08	7.22
B_1, $n \rightarrow \pi^*$ (V)	4.55	4.39	4.39	4.39	4.38	4.59 (d)
A_2, $n \rightarrow \pi^*$ (V)	4.72	4.49	4.50	4.50	4.49	5.43 (d)
A_1, $\pi(\mathrm{a1}) \rightarrow 3s$	6.38	5.46	6.18	6.28	5.80	6.28
A_2, $\pi(\mathrm{a2}) \rightarrow 3s$	6.86	6.53	6.89	6.98	6.51	6.75*
B_2, $\pi(\mathrm{a1}) \rightarrow 3p_x$	7.05	5.86	6.83	6.92	6.40	7.21*
B_1, $\pi(\mathrm{a2}) \rightarrow 3p_x$	7.57	6.59	7.52	7.57	7.13	7.25*
B_1, $n \rightarrow 3s$	7.53	6.8	8.33	7.61	7.14	7.39*
A_1, $\pi(\mathrm{a1}) \rightarrow 3p_y$	7.30	5.95	7.01	7.09	6.61	7.35*
A_2, $\pi(\mathrm{a2}) \rightarrow 3p_y$	7.79	7.09	7.74	7.82	7.34	7.52*
A_2, $\pi(\mathrm{a2}) \rightarrow 3d_{z^2}$	8.22	7.09	8.08	8.13	7.90	7.98*
B_2, $\pi(\mathrm{a2}) \rightarrow 3p_z$	8.36	6.68	7.55	8.00	7.87	7.41*
A_2, $n \rightarrow 3p_x$	8.36		8.15	8.40	7.90	8.03*
B_1, $\pi(\mathrm{a1}) \rightarrow 3p_z$	7.82	5.98	7.18	7.23	7.09	7.45*
B_1, $\pi(\mathrm{a2}) \rightarrow 3d_{xy}$	8.24	7.09	8.19	8.28	7.75	8.03*
MAE	0.25	0.67	0.27	0.27	0.34	
	(0.23)	(0.70)	(0.23)	(0.23)	(0.30)	
VSMAE (V)	0.22	0.31	0.28	0.29	0.32	
RSMAE	0.27	0.86	0.27	0.27	0.34	
I_p	10.24	5.95	9.34	9.34	9.34	

---

[a] Refs. [186, 187], CASPT2 data marked with an asterisk.

Table 7.5: Singlet vertical excitation (eV) of C_5NH_5. Excited states marked with (d) had more than 8% double excitation character, see text. MAE values between parentheses are obtained excluding these states. See also caption of Table 7.1.

with a slightly better performance of FA for formaldehyde and of LB for benzene.

One can also assess the performance of the bulk BP potential from the comparison of the results of BP-AC-FA with those obtained in Ref. [176] with the asymptotically corrected potential HCTH-AC-FA, where HCTH is the GGA potential, the functional derivative of the HCTH energy functional of Ref. [9]. Thus, the present BP-AC-FA and HCTH-AC-FA of Ref. [176] differ only in the bulk part. Both BP-AC-FA and HCTH-AC-FA produce virtually identical MAEs for formaldehyde and ethylene, but for benzene the MAE of 0.14 eV of HCTH-AC-FA is somewhat lower than the 0.21 eV of BP-AC-FA, while for CO and N_2 MAEs of 0.14 and 0.20 eV, respectively, of BP-AC-FA are lower than the corresponding values 0.32 and 0.34 eV of HCTH-AC-FA. From this we can conclude, that BP can be recommended for molecular response calculations.

From Tables 7.1–7.6 one can see also a good performance of the SAOP potential. The quality of its results is similar to that of the asymptotically corrected potentials and SAOP produces the least MAEs for N_2, CO, CH_2O, C_5NH_5. Unlike the schemes of asymptotic correction, SAOP employs neither standard GGA bulk potentials, nor the precalculated ionization energies I_p. Instead, the potential $v_{\mathrm{xc}}^{\mathrm{SAOP}}$ with the zero asymptotics $v_{\mathrm{xc}}^{\mathrm{SAOP}}(\infty)=0$, is constructed with statistical averaging of model orbital potentials [111, 174, 175]. This potential yields HOMO energies $\varepsilon_N^{\mathrm{SAOP}}$, which are much closer to the experimental energies $-I_p$ than the $\varepsilon_N^{\mathrm{GGA}}$ values of standard GGAs (see Tables 7.1–7.6). The largest deviation between $\varepsilon_N^{\mathrm{SAOP}}$ and $-I_p$ occurs for benzene, with the former quantity being appreciably larger (in absolute magnitude) than the latter (see Table 7.6). As a result, SAOP consistently overestimates the energies of the higher excitations, which are not far from I_p, and produces in this particular case the largest MAE, VSMAE and RMAE.

Table 7.7 compares the lowest dipole excitation energies calculated for the alkali dimers Li_2, Na_2, K_2 with experimental reference data (Ref. [189] for excitation energies and Ref. [190] for average static polarizability of Li_2 and Na_2, for K_2 *ab initio* value [191]). The results show the same general trend as for the molecules discussed above. BP reproduces well the lowest excitations to $^1\Sigma_u^+$ and $^1\Pi_u$ states with a somewhat larger error for the $^1\Sigma_u^+$ state of Na_2. On the other hand, BP consistently underestimates higher $2^1\Sigma_u^+$ and $2^1\Pi_u$ excitations. Again, the asymptotic corrections to BP improve the calculated higher excitations, bringing MAE for the dimers close to the benchmark accuracy of 0.1 eV (see Table 7.7). Note the high quality of the excitation energies obtained with SAOP, which is, on average, even slightly better than those of the asymptotically corrected potentials. Note also a slight improvement of the dipole polarizabilities α_d calculated by the potentials BP-GRAC-FA and BP-GRAC-LB with the GRAC interpolation function, while BP-AC-FA with the linear interpolation function of Eq. (7.6) produces virtually the same α_d values as BP.

To sum up, the asymptotic corrections to the BP potential provide high overall quality of the calculated excitation energies and a substantial improvement upon the standard BP potential. The corrections dramatically improve the calculated Rydberg-like excitations, while keeping and, sometimes, improving valence excitations. All asymptotic corrections considered display a similar quality of the results, in particular, the present GRAC interpolation function (7.3) performs well with both the FA and LB as the asymptotic potentials.

7.4 Conclusions

In this chapter corrections to the standard DFT exchange-correlation potentials have been considered with the aim to improve the excitation energies (especially for higher excitations) calculated within TDDFRT. A scheme of gradient-regulated connection between inner and outer parts (GRAC) has been developed. According to this scheme, the interpolation between the bulk and asymptotic potentials is carried out with an interpolation function, which depends on the dimensionless gradient parameter $x(\mathbf{r})$

of Eq. (7.2). Together with a standard GGA potential (as the bulk potential) and with the shifted LB potential (as the asymptotic potential) this interpolation function would constitute a smooth potential $v_{\mathrm{xc}}^{\text{GGA-GRAC}}(\mathbf{r})$ with an analytical representation. $v_{\mathrm{xc}}^{\text{GGA-GRAC}}(\mathbf{r})$ would be an explicit "local" density functional in the sense, that it depends on quantities, such as the electron density $\rho(\mathbf{r})$ and its gradient $\nabla\rho$, which are evaluated at the point $\mathbf{r}$.

The corrections to the GGA BP xc potential produced with the GRAC interpolation function, the linear interpolation function of Ref. [176], and with the LB and FA asymptotic potentials have been employed to calculate the vertical excitation energies of the prototype molecules N_2, CO, CH_2O, C_2H_4, C_5NH_5, C_6H_6 as well as the lowest excitation energies of the alkali dimers Li_2, Na_2, K_2.

The various asymptotic corrections provide a similar high quality of the calculated excitation energies and a substantial improvement upon the standard BP potential. In quite a few cases the corresponding mean absolute errors of the asymptotically corrected potentials approach the benchmark accuracy of 0.1 eV for the electronic spectra. In particular, the shape corrections substantially improve the calculated Rydberg-like excitations, while retaining and, in some cases, improving the quality of the calculated valence excitations. These results allow us to propose for molecular response calculations the combination BP-GRAC-LB, a smooth potential and a genuine local density functional. Its use does not entail any additional computational effort once a GGA "bulk" potential is evaluated. Our results also confirm the conclusion, that for a variety of small and medium-size molecules high quality TDDFRT results can be achieved with the efficient combination of a properly constructed xc potential with the simple ALDA approximation (6.15) for the xc kernel. We stress that asymptotic correction of KS potential is not enough. For instance, the recently developed molecular exact exchange potentials [32, 36] are asymptotically correct but still are not competitive for excitation energy calculations due to general shape deficiencies (lack of the correlation potential contribution).

As discussed also in Sec. 6.4.2 the schemes of correction of the standard LDA/GGA potentials considered in this chapter and in Refs. [176, 177], and the scheme of statistical averaging of (model) orbital potentials (SAOP) offer two alternative ways of improving approximate Kohn-Sham xc potentials. SAOP represents orbital-dependent functionals, it depends on the densities of individual KS orbitals, and the SAOP approach employs essentially differences in spatial localization of these orbitals. As has been shown in Sec. 7.3, SAOP produces high quality results, though from the point of view of implementation and computation orbital-dependent functionals are more demanding than standard "local" DFT functionals. In this sense, the present scheme of asymptotic correction of LDA/GGA potentials offers an alternative. It uses standard DFT potentials and schemes, such as BP-GRAC-LB, and produces local density functionals. BP-GRAC-LB shares with the asymptotically corrected potentials of Refs. [176, 177] the disadvantage that it requires as input the ionization energy of the system, which first has to be evaluated in a separate calculation.

Excited state and transition	SAOP	BP	BP acFA	BP gracFA	BP gracLB	Exp/ CASPT2[a]
$^1B_{2u}$, $\pi \rightarrow \pi^*$ (V)	5.29	5.29	5.32	5.33	5.31	4.90 (d)
$^1B_{1u}$ (V)	6.06	6.05	6.09	6.09	6.06	6.20
$^1E_{1u}$ (V)	6.94	6.55	6.89	6.92	6.86	6.94
$^1E_{2g}$ (V)	8.30	8.31	8.40	8.40	8.38	7.90*(d)
$^1E_{1g}$, $\pi \rightarrow 3s$	6.55	5.96	6.50	6.55	6.22	6.33
$^1A_{2u}$, $\pi \rightarrow 3p_{x/y}$	7.34	6.31	7.12	7.26	6.86	6.93
$^1E_{2u}$	7.33	6.32	7.11	7.25	6.85	6.95
$^1A_{1u}$	7.34	6.35	7.13	7.28	6.85	6.99*
$^1E_{1u}$, $\pi \rightarrow 3p\pi$	8.10	6.93	7.29	7.29	7.28	7.41
$^1B_{1g}$, $\pi \rightarrow 3d_{x^2-y^2/xy}$	7.98	6.79	7.70	8.05	7.61	7.46
$^1B_{2g}$	8.03	6.80	7.72	8.09	7.64	7.46
$^1E_{1g}$	8.01	6.80	7.70	8.08	7.63	7.54
$^1A_{1g}$, $\pi \rightarrow 3d_{zx/zy}$	9.01	7.12	7.95	7.95	8.17	7.74
$^1E_{2g}$	8.91	7.10	7.91	7.91	8.04	7.81
$^1A_{2g}$	8.94	7.14	7.95	7.95	8.10	7.81
$^1E_{1g}$, $\pi \rightarrow 3d_{z^2}$	7.97	7.05	7.59	7.78	7.49	7.57*
$^3B_{2u}$, $\pi \rightarrow \pi^*$ (V)	5.02	5.02	5.06	5.06	5.04	5.60
$^3B_{1u}$ (V)	4.42	4.43	4.47	4.47	4.46	3.94
$^3E_{1u}$ (V)	4.77	4.77	4.81	4.81	4.80	4.76
$^3E_{2g}$ (V)	7.44	7.45	7.51	7.51	7.49	7.12*
$^3E_{1g}$, $\pi \rightarrow 3s$	6.51	5.95	6.45	6.53	6.19	6.34*
$^3A_{2u}$, $\pi \rightarrow 3p_{x/y}$	7.28	6.30	7.10	7.24	6.83	6.80*
$^3E_{2u}$	7.31	6.32	7.12	7.26	6.85	6.90*
$^3A_{1u}$	7.34	6.33	7.13	7.28	6.88	7.00*
$^3E_{1u}$, $\pi \rightarrow 3p\pi$	8.02	6.59	7.22	7.21	7.16	6.98*
$^3B_{1g}$, $\pi \rightarrow 3d_{x^2-y^2/xy}$	7.98	6.80	7.71	8.06	7.62	7.53*
$^3B_{2g}$	7.93	6.80	7.70	8.05	7.60	7.53*
$^3E_{1g}$	7.95	6.80	7.70	8.05	7.61	7.57*
$^3E_{2g}$, $\pi \rightarrow 3d_{zx/zy}$	8.29	7.12	7.93	7.93	8.06	7.55*
$^3A_{1g}$	8.85	7.12	7.91	7.91	8.01	7.62*
$^3A_{2g}$	8.94	7.14	7.95	7.95	8.10	7.70*
$^3E_{1g}$, $\pi \rightarrow 3d_{z^2}$	7.87	7.03	7.54	7.69	7.41	7.56*
MAE	0.53	0.53	0.21	0.32	0.21	
	(0.54)	(0.54)	(0.20)	(0.31)	(0.19)	
VSMAE	0.29	0.34	0.32	0.32	0.33	
RSMAE	0.61	0.59	0.18	0.32	0.17	
I_p	10.32	6.26	9.25	9.25	9.25	

---

[a] Refs. [186, 187], CASPT2 data marked with an asterisk.

Table 7.6: Vertical excitation energies (eV) of C_6H_6. See caption of Tables 7.1 and 7.5

	Exp[a]	SAOP	BP	BP acFA	BP gracFA	BP gracLB
Li_2						
$^1\Sigma_u^+$ (LL)	1.74	1.98	1.99	1.99	1.98	1.96
$^1\Pi_u$ (LL)	2.53	2.46	2.62	2.59	2.55	2.55
$^1\Sigma_u^+$	3.78	3.71	3.06	3.63	3.62	3.33
α_{av}	221[b]	223.90	196.90	200.00	204.40	205.06
Na_2						
$^1\Sigma_u^+$ (LL)	1.82	1.96	2.06	2.06	2.04	2.02
$^1\Pi_u$ (LL)	2.52	2.51	2.63	2.64	2.59	2.59
$^1\Sigma_u^+$	3.64	3.64	3.23	3.49	3.52	3.60
α_{av}	270[b]	233.50	238.00	238.00	243.00	246.00
K_2						
$^1\Sigma_u^+$ (LL)	1.45	1.57	1.54	1.54	1.53	1.50
$^1\Pi_u$ (LL)	1.91	2.02	2.00	1.99	1.94	1.92
$^1\Sigma_u^+$	2.85	2.62	2.57	2.69	2.69	2.62
$^1\Pi_u$	2.85	2.82	2.70	2.85	2.82	2.78
α_{av}	462.6[c]	436.10	451.30	451.35	463.32	474.42
MAE		0.10	0.24	0.13	0.11	0.14
MAE (LL)		0.12	0.22	0.21	0.17	0.14
MAE(HL)		0.08	0.39	0.12	0.12	0.20

---

[a] Ref. [189]

[b] Ref. [190]

[c] *ab initio*[191]

Table 7.7: Lowest dipole-allowed excitation energies and average static polarizabilities α_{av} for alkali dimers. MAE is the mean absolute error of the all excitation energies in this table, MAE(LL) is the mean absolute error for the all lowlying (LL) excitation energies and MAE(HL) for the highlying.

Chapter

8

Shape corrections to the GGA potentials for molecular response calculations

The performance is assessed of two shape-corrected Kohn-Sham potentials, the SAOP and the gradient-regulated asymptotic connection procedure applied to the Becke-Perdew potential (BP-GRAC), versus LDA and GGA potentials, in molecular response calculations of the static average polarizability α, the Cauchy coefficient S_{-4}, and the static average hyperpolarizability β. The nature of the distortions of the LDA/GGA potentials is highlighted and it is shown that they introduce many spurious excited states at too low energy which may mix with valence excited states, resulting in wrong excited state compositions. They also lead to wrong oscillator strengths and thus to a wrong spectral structure of properties like the polarizability. LDA, Becke-Lee-Yang-Parr (BLYP), and Becke-Perdew (BP) characteristically underestimate contributions to α and S_{-4} from bound Rydberg-like states and overestimate those from the continuum. Cancellation of the errors in these contributions occasionally produces fortuitously good results. The distortions of the LDA, BLYP, and BP spectra are related to the deficiencies of the LDA/GGA potentials in both the bulk and outer molecular regions. In contrast, both SAOP and BP-GRAC potentials produce high quality polarizabilities for 21 molecules and also reliable Cauchy moments and hyperpolarizabilities for the selected molecules. The analysis for the N_2 molecule shows, that both SAOP and BP-GRAC yield reliable energies ω_i and oscillator strengths f_i of individual excitations, so that they reproduce well the spectral structure of α and S_{-4}.

8.1 Introduction

The importance of shape corrections to the LDA/GGA Kohn-Sham potentials, consisting of asymptotic correction to yield $-1/r$ behavior [89], as well as correction in the bulk molecular region, to put e.g. the HOMO level at the first IP, for the calculation

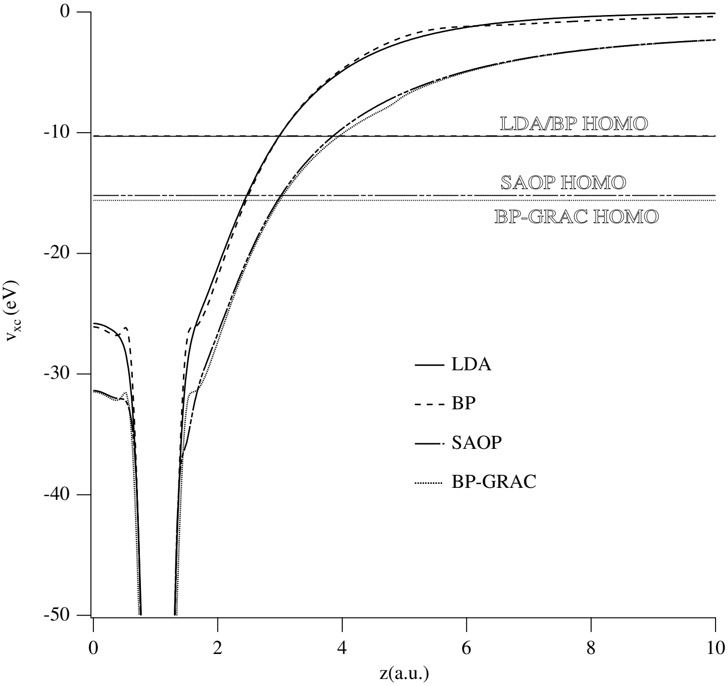

Figure 8.1: The SAOP and BP-GRAC xc potentials are plotted along the main axis for the N_2 molecule. LDA and BP xc potentials are also plotted for comparison.

of response properties, discussed in Chapt. 6, has been demonstrated with various novel model xc potentials for quadrupole polarizabilities in Ref. [192], and for a range of response properties including excitation energies in Refs. [111, 132, 176, 178, 193] and in Chapter 7.

A common feature of the model potentials is their effectively more attractive character (with respect to the long-range asymptotics $v_{\text{xc}}(\infty)$) in the bulk and outer valence regions compared to the standard potentials of the LDA and GGAs. This feature is illustrated with Fig. 8.1 where the xc potentials constructed by SAOP [111, 174, 175] and by gradient-regulated asymptotic connection procedure (see Chapt. 7) applied to the GGA BP xc potential [4, 6] (BP-GRAC) are plotted along the main axis of the molecule N_2. They are compared with the LDA potential and with the uncorrected BP potential. Both SAOP and BP-GRAC potentials are shifted downward in the bulk valence region by (roughly) a constant compared to the LDA and BP ones. Note, that in the BP-GRAC case this shift is explicitly introduced in the GRAC procedure. In the outer region both SAOP and BP-GRAC potentials have the Coulombic asymptotics $-1/r$, while the LDA potential decays exponentially and the BP potential decays as $-c/r^2$.

These features of the model potentials bring a substantial improvement compared to the standard approximations of the energy gaps $\Delta\varepsilon_{ia} = \varepsilon_a - \varepsilon_i$ between the occupied valence ψ_i and the unoccupied ψ_a KS orbitals. The correct Coulombic asymptotics of the improved potentials leads to a relative stabilization of bound Rydberg-like states compared to the LDA/GGA potentials. This stabilization is however smaller than the downshift of the occupied orbitals due to the downshift of the SAOP and BP-GRAC potentials in the molecular region. Therefore, for higher-lying bound unoccupied Rydberg-like orbitals a the energy differences $\Delta\varepsilon_{ia}$ are substantially increased. This is important for the excitation spectra calculated with TDDFT, since $\Delta\varepsilon_{ia}$ serve in this theory as the zero order estimates of excitation energies. In addition, the correct Coulombic asymptotics of the improved potentials leads to an improved spatial extent of bound Rydberg-like states, which will affect the transition dipole matrix elements. We stress that the new potentials, as well as the older LB94 [89], are not only asymptotically corrected, but the shape correction in the molecular region is at least as important. If the unoccupied orbital a is a lowlying one which has its amplitude mostly in the same region as the HOMO, it will be downshifted by about the same amount, so we do not expect a large change in the excitation energies to such an orbital. These effects of the new potentials appear to be essential (see results in Sec. 8.3 and the analysis in Sec. 8.4) for the correct description of both the excitation energies and of other characteristics of the excitations such as their composition in terms of contributing orbital excitations and their relative contributions to the calculated polarizabilities. In this chapter the performance of the SAOP and BP-GRAC potentials is assessed in TDDFT calculations of the static average polarizability α of 21 light molecules and also in calculations of the related properties such as the anisotropy of α, the Cauchy coefficient S_{-4} and the hyperpolarizability β. In Sec. 8.1 the main features in the shape of these potentials versus the traditional LDA/GGAs are discussed. In Sec. 8.2 the methodical and computational details are given. In Sec. 8.3 the results of the SAOP and BP-GRAC molecular response calculations are compared with those of LDA and GGAs (BP and Becke-Lee-Yang-Parr, BLYP [4, 7] approximations) as well as with the experimental data. SAOP, BP-GRAC and BP yield polarizabilities of a similar good quality and they substantially improve upon LDA and BLYP. Furthermore, SAOP and BP-GRAC perform definitely better than either BP or LDA and BLYP in calculation of the S_{-4} Cauchy coefficients and, especially, in calculation of the hyperpolarizabilities. In Sec. 8.4 the analysis of contributions from individual excitations to α and S_{-4} is performed for the case of the N_2 molecule, for which the corresponding experimental data are available. While SAOP and BP-GRAC reproduce very well the spectral structure of α and S_{-4}, LDA, BLYP, and BP considerably distort it, so that a good quality of the total BP α values appears to be the result of an error cancellation. The distortions of the LDA/GGA spectra are related to the deficient form of the corresponding potentials in both bulk and outer regions. Finally, conclusions are drawn in Sec. 8.5.

Atom	$1s$	$2p$	$3d$	$4f$
H($7s5p4d$)	0.057513	0.156109	0.239461	
C($9s7p5d4f$)	0.078929	0.108203	0.202024	0.395110
N($9s7p5d4f$)	0.092674	0.124531	0.202024	0.395110
O($9s7p5d4f$)	0.106588	0.140372	0.183658	0.359191
F($11s7p5d4f$)	0.042280	0.157918	0.183658	0.359191
Si($11s9p7d4f$)	0.067811	0.070834	0.123252	0.227488
P($11s9p7d4f$)	0.071779	0.075893	0.133816	0.239461
S($11s9p7d4f$)	0.076097	0.082302	0.147902	0.251434
Cl($11s9p7d4f$)	0.080357	0.087446	0.140859	0.239461

Table 8.1: Even-tempered basis set for the H,C, O, F, Si, P, S, Cl atoms (in parentheses the number n of $1s$, $2p$, $3d$ and $4f$) with the orbital exponent $Z = ab^i$, $i = 1, ..., n$, $b = 1.7$. The value of for the most diffuse $1s$, $2p$, $3d$ and $4f$ for each atom is indicated.

8.2 Computational details

The RESPONSE module of the Amsterdam Density Functional program (ADF2000 modified/development version) [93, 181, 182, 183] has been used to perform TDDFT calculations of molecular response properties [180] with the SAOP, BP-GRAC[1], LDA, and GGA potentials and with the ALDA xc kernel. We used the even tempered (ET) basis sets [194, 195] of Slater-type orbitals (STOs) consisting of the $1s$, $2p$, $3d$,... functions with the orbital exponents $Z = ab^i$, $i = 1, .., n$, $b = 1.7$. Table 8.1 presents the number n of $1s$, $2p$, $3d$ and $4f$ functions for each atom and the a values for the most diffuse functions. These ET basis sets were selected monitoring the quality of results with the number of diffuse functions added to standard ET basis sets. To avoid numerical problems, linear combinations of atomic orbitals have been removed from the basis sets, for which the linear dependence due to the addition of a large number of diffuse functions was detected. The results obtained with the present basis appear to be close to the basis set limit.

The calculated average static polarizability and hyperpolarizability are given by (the indices ab... label the Cartesian axes x, y, z):

$$\alpha = \frac{1}{3}\sum_a \alpha_{aa} \tag{8.1}$$

$$\beta = \frac{1}{5}\sum_b (\beta_{abb} + \beta_{bab} + \beta_{bba}) \tag{8.2}$$

(in Eq. 8.2 a is the dipolar axis), while the anisotropy of the polarizability $\Delta\alpha$ is

$$|\Delta\alpha|^2 = \frac{1}{2}\sum_{a<b} (\alpha_{aa} - \alpha_{bb})^2 \tag{8.3}$$

---

[1] The ionization potentials I_p required in the calculation of this potential are taken from experiment and presented in Table 8.2.

The components of the dipole polarizability α_{ab} and hyperpolarizability β_{abc} tensors can be defined through an expansion of the dipole moment μ_a into different orders of the external fields E_b

$$\mu_a = \mu_a (E = 0) + \sum_b \alpha_{ab} E^b + \frac{1}{2!} \sum_{bc} \beta_{abc} E^b E^c + \frac{1}{3!} \sum_{bcd} \gamma_{abcd} E^b E^c E^d + ...$$

The S_{-4} Cauchy coefficient relates to the frequency dispersion in the average dipole polarizability $\alpha(\omega)$

$$\alpha_d (\omega) = \alpha_d (0) + S_{-4}\omega^2 + S_{-6}\omega^4 + ...$$

The Cauchy coefficients S_{-2k} are calculated from all oscillator strengths f_i, weighted by an even power of the excitation energies ω_i

$$S_{-2k} = \sum_i \omega_i^{-2k} f_i. \tag{8.4}$$

The S_{-2} coefficient is equal to the average static polarizability while the S_0 coefficient should be equal to the number of electrons in the basis set limit.

8.3 Results of molecular response calculations

A key feature of the SAOP potential (see Chapter 6), its more attractive character compared to the LDA and GGA potentials, is illustrated with Table 8.2 where the corresponding energies ε_N of the highest occupied molecular orbital (HOMO) are compared with the first VIP I_p. Note, that the rigorous KS theory requires $\varepsilon_N = -I_p$ for potentials with the zero asymptotics $v_{\text{xc}}(\infty) = 0$. The LDA and GGA $-\varepsilon_N$ values are substantially smaller than I_p, with the BLYP energies being, as a rule, the smallest ones. The BP error in the fourth column of Table 8.2 is, actually, the downward shift $-(I_p + \varepsilon_N)$ in the bulk region (with respect to $v_{\text{xc}}^{\text{BP}}$) of the GRAC potential $v_{\text{xc}}^{\text{BP-GRAC}}(\mathbf{r}) - (I_p + \varepsilon_N)$ presented in Fig. 8.1. Its average value for the considered molecules amounts to -4.3 eV. Due to the more attractive character of the SAOP potential, its $-\varepsilon_N$ values are much larger than LDA and GGA ones and they are rather close to I_p. The corresponding SAOP average error is only 0.39 eV. Note, that the same average error of 0.4 eV has been reported in Ref. [196] where the SAOP energies $-\varepsilon_i$ have been used to estimate not only the first, but also other valence ionization potentials I_i for 64 molecules.

Table 8.3 compares the average static polarizabilities of 21 small molecules at the experimental geometry [67, 197] calculated with SAOP, BP-GRAC and the standard LDA and GGA (BP, BLYP) potentials with the experimental α values (Expt.) [198, 199, 200, 201, 202, 203, 204]. The molecules in Table 8.3 are placed in the order of increasing polarizability. LDA systematically overestimates α, it has the same average of the relative $(\alpha - \alpha_{\text{exp}})$ and absolute $|\alpha - \alpha_{\text{exp}}|$ errors, which amount to 5%. The performance of GGA appears to depend substantially on the type of the functional.

	SAOP	err.	BP	err.	BLYP	err.	LDA	err.	Expt.
CS_2	10.72	0.65	6.86	−3.21	6.58	−3.49	6.89	−3.18	10.07
H_2S	10.25	−0.21	6.37	−4.09	6.12	−4.34	6.36	−4.10	10.46
C_2H_4	10.94	0.43	6.78	−3.73	6.53	−3.908	6.9	−3.61	10.51
PH_3	10.53	−0.06	6.78	−3.09	6.56	−3.31	6.73	−3.14	10.59
NH_3	10.70	−0.10	6.26	−4.54	6.08	−4.72	6.25	−4.55	10.80
OCS	11.76	0.58	7.54	−3.64	7.28	−3.9	7.60	−3.58	11.18
Cl_2	11.65	0.17	7.37	−4.11	7.15	−4.33	7.40	−4.08	11.48
C_2H_6	12.52	0.52	8.22	−3.78	8.06	−3.94	8.11	−3.89	12.00
SiH_4	12.49	0.19	8.63	−3.67	8.44	−3.86	8.53	−3.77	12.3
SO_2	12.85	0.50	8.14	−4.21	7.97	−4.38	8.23	−4.12	12.35
H_2O	12.36	−0.26	7.35	−5.27	7.21	−5.41	7.40	−5.22	12.62
HCl	12.42	−0.32	8.11	−4.63	7.89	−4.85	8.13	−4.61	12.74
N_2O	13.48	0.59	8.49	−4.40	8.29	−4.6	8.62	−4.27	12.89
CH_4	13.90	0.30	9.55	−4.05	9.37	−4.23	9.46	−4.14	13.60
CO_2	14.36	0.58	9.14	−4.64	8.95	−4.83	9.28	−4.50	13.78
CO	13.74	−0.27	9.14	−4.87	9.00	−5.01	9.11	−4.90	14.01
H_2	14.80	−0.63	10.50	−4.93	10.39	−5.04	10.26	−5.17	15.43
N_2	15.28	−0.3	10.39	−5.19	10.26	−5.32	10.41	−5.17	15.58
SF_6	16.22	0.52	10.07	−5.63	9.93	−5.77	10.23	−5.47	15.70
F_2	15.69	−0.01	9.52	−6.18	9.44	−6.26	9.62	−6.08	15.70
HF	15.60	−0.43	9.74	−6.29	9.62	−6.41	9.81	−6.22	16.03
av		0.12		−4.52		−4.70		−4.50	
abs		0.36		4.52		4.70		4.50	

Table 8.2: First ionisation potential: for BP-GRAC the experimental value (Expt.) given as input, for SAOP and BP respectively $-\varepsilon_N^{\mathrm{SAOP}}$ and $-\varepsilon_N^{\mathrm{BP}}$; err. is the difference between SAOP/BP and experimental (GRAC) values.

	SAOP	BP-GRAC	BP	BLYP	LDA	Expt.
H_2	5.63	5.34	5.55	5.78	5.91	5.43
HF	5.40	5.71	6.10	6.47	6.23	5.60
F_2	8.08	8.47	8.75	9.13	8.87	8.38
H_2O	9.45	9.80	10.33	10.95	10.60	9.64
N_2	11.82	11.78	12.06	12.55	12.28	11.74
CO	13.01	13.07	13.38	13.95	13.71	13.08
NH_3	14.21	14.53	15.11	15.94	15.57	14.56
CH_4	17.32	17.03	17.07	17.67	17.71	17.27
HCl	17.99	17.62	18.11	19.13	18.63	17.39
CO_2	16.79	17.39	17.48	18.17	17.74	17.51
N_2O	19.07	19.60	19.70	20.45	19.96	19.70
H_2S	25.72	25.10	25.65	27.03	26.50	24.71
SO_2	24.98	25.69	25.82	26.89	26.20	25.61
C_2H_4	28.09	28.14	28.14	29.31	28.88	27.70
C_2H_6	29.87	29.54	29.45	30.42	30.46	29.61
SF_6	29.00	31.06	31.38	32.27	31.96	30.04
Cl_2	31.56	31.15	31.35	32.74	32.00	30.35
PH_3	31.62	30.75	31.05	32.36	32.27	30.93
SiH_4	32.71	32.02	32.00	32.86	33.69	31.90
OCS	34.18	34.49	34.37	35.83	34.92	33.72
CS_2	56.50	55.98	55.39	57.75	56.28	55.28
av%	0.07	0.69	2.40	6.86	5.16	
abs%	2.48	1.20	2.59	6.86	5.16	

Table 8.3: Static isotropic polarizabilities α (in a.u.)

BLYP produces the worst α values with the larger average error of 7%. On the other hand, BP substantially improves upon LDA, with the average absolute error being reduced to 2.6%. Both BP-GRAC and SAOP definitely improve further upon BP for molecules with smaller polarizabilities at the top of Table 8.3 (the only exception is the SAOP α value for H_2, which is slightly worse than the BP one). For molecules with larger polarizabilities the trend is not so uniform. The BP-GRAC average absolute error is further reduced to 1.2%, while the SAOP produces almost the same error (2.5%) as BP. Compared to other potentials, SAOP has the much smaller average α error of only 0.07%. This means that, while LDA and GGAs tend to overestimate, SAOP lacks this systematic overestimation and its values are distributed around the experimental ones.

Table 8.4 presents the anisotropies (8.3) of the static polarizabilities of 11 molecules. One can see from Table 8.4 that LDA, BLYP and BP yield similar anisotropies. BP-GRAC improves upon BP, especially for the molecules H_2O and H_2S with small anisotropies, while the results of SAOP for this quantity are somewhat worse than the BP-GRAC ones.

	SAOP	BP-GRAC	BP	BLYP	LDA	Expt.
H_2O	0.84	0.43	0.07	0.18	0.04	0.67
H_2S	0.13	0.42	1.08	1.70	1.17	0.67
HF	1.20	1.09	0.96	0.92	0.93	1.33
HCl	1.80	1.48	1.21	1.01	1.18	1.51
NH_3	1.10	1.94	2.67	3.15	2.83	1.94
CO	3.32	3.40	3.42	3.45	3.29	3.57
N_2	4.78	4.69	4.74	4.78	4.67	4.59
C_2H_4	12.40	11.78	11.61	11.60	11.88	11.40
SO_2	11.95	12.61	12.57	12.81	12.55	13.00
CO_2	12.63	13.20	13.24	13.39	13.35	13.83
Cl_2	16.77	16.41	16.35	16.49	16.44	17.53
av%:	−9.55	−9.67	−4.78	6.47	−3.70	
abs%:	19.92	−10.67	23.63	34.01	26.65	

Table 8.4: Anisotropy of static polarizability $\Delta\alpha$ (in a.u.)

Table 8.5 presents the S_{-4} Cauchy coefficients for 13 molecules. As in the case of polarizabilities, LDA systematically overestimates the S_{-4} coefficient with an average relative $|S_{-4}|$ error of 21% and BLYP increases further this error. On the other hand, BP improves upon LDA and the BP error is reduced to 14%. Both BP-GRAC and SAOP definitely improve further upon BP, in particular, the BP-GRAC S_{-4} values are better than the BP ones in all cases except CO_2. This brings both SAOP and BP-GRAC $|S_{-4}|$ errors down to 7.3% and 3.9%, respectively (see Table 8.8). SAOP produces also a very small average S_{-4} error of only −0.05%.

Table 8.6 compares the average static hyperpolarizabilities β (8.2) of the molecules NH_3, CO, H_2O, and HF calculated with SAOP, BP-GRAC, LDA, and GGA with the *ab initio* ones obtained in Refs. [205] with the coupled cluster CCSD and CCSD(T) methods. Again, LDA produced overestimated values with the average $|\beta|$ error [with respect to CCSD(T)] of 35% and BLYP increases further the error to 41%. In this case, however, BP does not improve substantially upon LDA, the BP values appear to be rather close to the LDA ones with the average error of 26%. Both SAOP and BP-GRAC improve substantially upon BP, with the average $|\beta|$ error being reduced to 3% and 5%, respectively. Thus, application of the SAOP and BP-GRAC potentials bring the DFT hyperpolarizabilities rather close to those obtained with the most advanced *ab initio* coupled cluster methods. It should be cautioned, however, that at this point the comparison is not definitive, errors in either the CCSD(T) values (due to basis set deficiencies, for instance) or in the SAOP or BP-GRAC values may be as large as their difference.

To sum up, SAOP, BP-GRAC, and BP produce polarizabilities α of the same good quality and they substantially improve upon LDA and BLYP. However, SAOP and BP-GRAC perform definitely better than BP in calculation of the S_{-4} Cauchy

	SAOP	BP-GRAC	BP	BLYP	LDA	Expt.
HF	11.74	13.01	17.08	20.32	17.88	14.40
F_2	16.29	17.59	20.01	22.48	20.39	17.161
N_2	30.48	30.20	32.99	36.92	34.50	30.11
H_2O	33.00	36.05	45.66	55.03	48.82	35.42
CO	48.71	48.84	53.30	59.38	57.47	48.26
CO_2	44.67	48.94	50.22	55.96	51.96	50.99
CH_4	63.61	62.69	63.93	71.22	69.48	62.41
HCl	74.22	71.50	80.93	96.11	87.02	67.12
NH_3	67.70	74.23	91.03	109.79	97.83	71.44
Cl_2	133.84	133.39	138.65	159.51	145.84	125.8
H_2S	150.31	145.00	161.94	193.58	176.04	138.3
SiH_4	189.42	183.71	185.3	202.1	206.78	178.4
PH_3	211.59	201.68	212.53	243.30	232.06	189.8
av%	−0.05	1.78	13.55	30.93	21.21	
abs%:	7.34	3.88	13.79	30.93	21.21	

Table 8.5: S_{-4} Cauchy moments (a.u.)

	SAOP	BP-GRAC	BP	BLYP	LDA	CCSD	CCSD(T)
NH_3	−33.9	−37.87	−48.4	−56.00	−51.4	−30.0	−34.3
CO	22.18	21.90	28.83	31.8	30.5	23.00	23.5
H_2O	−17.3	−18.2	−22.2	−25.0	−24.6	−16.2	−18.0
HF	−7.2	−7.2	−8.5	−9.3	−9.0	−6.8	−7.3
abs%	3.01	4.92	25.9	41.2	34.9		

Table 8.6: Hyperpolarizability β

coefficients and, especially, in calculation of the hyperpolarizabilities β. These trends will be rationalized in the next section with the spectral analysis of the response properties of the N_2 molecule.

8.4 Spectral analysis of the response properties of the N_2 molecule

A physically sound TDDFT approach should reproduce not only total response quantities, such as and S_{-4}, but also their spectral structure, i.e. the oscillator strengths f_i and energies ω_i of individual excitations, which determine α and S_{-4} through the sum rules (i.e. particular cases of Eq. (8.4))

$$\alpha = \sum_i \frac{f_i}{\omega_i^2} \tag{8.5}$$

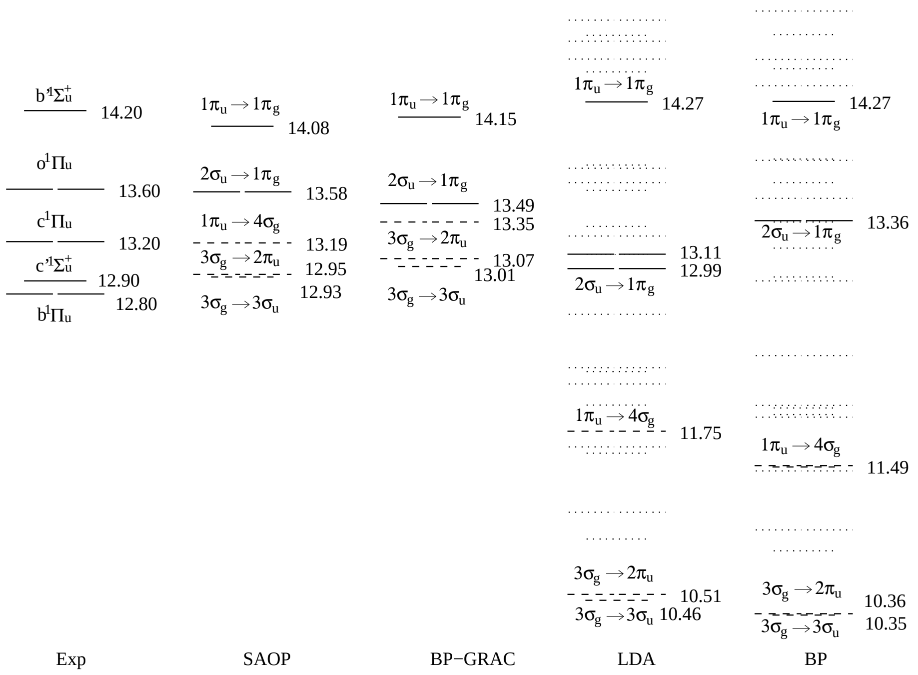

Figure 8.2: The experimentally observed[206] excited state levels are given to the left (for N_2). The levels correspond to the Franck-Condon maximum in the absorption. The calculated levels according to the various model Kohn-Sham potentials are given in the other columns. The valence excited states are indicated with drawn lines, and the Rydberg states with broken lines. The many spurious Rydberg states occurring for the LDA and the BP potentials are indicated with dotted lines.

$$S_{-4} = \sum_i \frac{f_i}{\omega_i^4} \tag{8.6}$$

$$N = \sum_i f_i \tag{8.7}$$

Fig. 8.2 compares the molecular state diagram produced from the experimental data for the 5 lowest (below 15 eV) dipole allowed excitations of the N_2 molecule [206, 207] with the diagrams obtained with the SAOP, BP-GRAC, BP, and LDA potentials.

The corresponding excitation energies ω_i are presented in Table 8.7. There are also presented (in parentheses, below the experimental ω_i values) as representative accurate *ab initio* values the excitation energies obtained recently with the size-consistent self-consistent configuration interaction operator $(SC)^2$CI applied to the complete active space single and double CI (CAS-SDCI). We note that the experimental spectra exhibit strongly overlapping progressions of vibronic states, which sometimes are perturbed due to interaction. Since we calculate vertical transitions we cite in the table

	SAOP	BP-GRAC	BP	BLYP	LDA	Expt.
$\boldsymbol{3\sigma_g \to 3\sigma_u}$	98%	98%	100%	100%	100%	$c'^1\Sigma_u^+$
ω	12.93	13.01	10.35	10.20	10.46	12.9 (12.83)
f	0.219	0.216	0.003	0.004	0.003	0.279
f/ω^2	0.97	0.95	0.02	0.03	0.02	1.24
f/ω^4	4.31	4.14	0.13	0.22	0.13	5.76
$\boldsymbol{3\sigma_g \to 2\pi_u}$	99%	99%	100%	100%	100%	$b^1\Pi_u$
ω	12.95	13.07	10.36	10.24	10.51	12.8 (12.86)
f	0.122	0.100	0.004	0.006	0.005	0.243
f/ω^2	0.54	0.44	0.03	0.02	0.04	1.10
f/ω^4	2.36	1.86	0.19	0.17	0.24	4.97
$\boldsymbol{1\pi_u \to 4\sigma_g}$	96%	59%	99%	100%	100%	$c^1\Pi_u$
ω	13.19	13.35	11.49	11.22	11.75	13.2 (13.45)
f	0.189	0.374	0.013	0.033	0.019	0.145
f/ω^2	0.80	1.54	0.09	0.20	0.15	0.63
f/ω^4	3.42	6.44	0.48	1.16	0.84	2.47
$\boldsymbol{2\sigma_u \to 1\pi_g}$	91%	55%	85%	75%(12%)	78%(10%)	$o^1\Pi_u$
ω	13.58	13.49	13.36	13.21(13.11)	12.99(13.11)	13.6 (13.52)
f	0.166	0.02	0.292	0.094(0.19)	0.094(0.20)	0.080
f/ω^2	0.67	0.08	1.21	0.40(0.82)	0.41(0.86)	0.32
f/ω^4	1.70	0.34	5.02	1.70(3.54)	1.84(3.70)	1.28
$\boldsymbol{1\pi_u \to 1\pi_g}$	59%	58%	26%	26%	22%	$b'^1\Sigma_u^+$
ω	14.08	14.15	14.27	14.00	14.27	14.2 (14.33)
f	0.432	0.431	0.245	0.239	0.212	0.278
f/ω^2	1.61	1.59	0.90	0.90	0.77	1.03
f/ω^4	6.02	5.98	3.25	3.4	2.81	3.81
$\sum f$	1.13	1.14	0.557	0.376(0.566)	0.333(0.533)	1.025
$\sum f/\omega^2$	4.60	4.61	2.25	1.55(2.37)	1.39(2.25)	4.30
$\sum f/\omega^4$	18.82	18.68	9.07	5.65(9.19)	5.86(9.50)	18.13

Table 8.7: The oscillator strengths f, the corresponding excitation energy and the assigned orbital transition $\psi_i \to \psi_a$ for the 5 lowest experimental (Expt.) excitations of N$_2$ are compared with the f and ω obtained with SAOP, BP-GRAC and LDA/GGA calculations for these excitations (see Sec. 8.4 for discussion of assignment). Below the experimental excitation energies a representative value from recent very accurate *ab initio* calculations is given, see text. Also the contributions $\sum f/\omega^2$, $\sum f/\omega^4$ to the polarizability and to the Cauchy coefficient are reported for each excited state as well as their sum over these states.

the experimental transition energies to the vibrational states with maximum intensity. These do not always stand out unambiguously, and in view of the vibrational level splittings ranging from 0.1 to 0.25 eV we should take the "experimental" benchmark levels to have an uncertainty of ca. 0.1 eV.

There are two $^1\Sigma_u^+$ states and three $^1\Pi_u$ states. The assignment of the two $^1\Sigma_u^+$ states to $3\sigma_g \rightarrow 3\sigma_u$ and $1\pi_u \rightarrow 1\pi_g$ orbital transitions agrees with what has been inferred from experiment and the SAOP/BP-GRAC energies of these excitations agree perfectly with the corresponding experimental and *ab initio* values. The excitation to the $b^1\Sigma_u^+$ state has valence character ($\pi \rightarrow \pi^*$), while the $c^1\Sigma_u^+$ ($3\sigma_g \rightarrow 3\sigma_u$) state is usually referred to as the lowest Rydberg state in N_2 (we indicate valence excited states in Fig. 8.2 with drawn lines, the Rydberg states with broken lines). This indicates that the $3\sigma_u$ is not simply the expected antibonding combination of $2p\sigma$ AO's on the N atoms (in which case we would be dealing with a valence excitation). Indeed, because of the short N–N distance the $2p\sigma - 2p\sigma$ is extremely antibonding and very highlying, and we find the $3\sigma_u$ to be a very diffuse strongly hybridized (so as to reduce antibonding character) combination of notably atomic $4s$ and $4p$ character. This confirms the experimental assignment of Rydberg character.
For the three $^1\Pi_u$ states we obtain almost perfect agreement with experiment for both the SAOP and BP-GRAC potentials when we assign the three calculated $^1\Pi_u$ states with $3\sigma_g \rightarrow 2\pi_u$, $1\pi_u \rightarrow 4\sigma_g$ and $2\sigma_u \rightarrow 1\pi_g$ character to the $b^1\Pi_u$, $c^1\Pi_u$, and $o^1\Pi_u$ states respectively. The SAOP/BP-GRAC ω_i values are very close to the *ab initio* ones for the same type of excitation. This assignment would imply that the highest state of $^1\Pi_u$ symmetry, $o^1\Pi_u$, has valence character ($2\sigma_u \rightarrow 1\pi_g$), while the other ones have Rydberg character. However, in the experimental work [207] the $2\sigma_u \rightarrow 1\pi_g$ valence character has been ascribed to the lowest state of $^1\Pi_u$ symmetry, the $b^1\Pi_u$. This latter assignment would lead to a discrepancy between experiment and theory in the sense, that SAOP and BP-GRAC as well as the cited $(SC)^2$CAS-SDCI method and other *ab initio* methods [208, 209] all overestimate the energy of the valence $2\sigma_u \rightarrow 1\pi_g$ vertical excitation by 0.7–0.8 eV. Furthermore, we have calculated the potential curve for this excited state with SAOP and found that it corresponds better to the curve fitted from the experimental data for the $o^1\Pi_u$ state in the sense that it gives similar high vibration frequency and it does not exhibit the considerable softening of the curve that is typical for the lowest excited state, $b^1\Pi_u$. It is clear from our potential energy curves that our lowest excitation energies at the various bond distances would indeed correspond to a rather soft vibration, as found in the experiment for $b^1\Pi_u$. These lowest excitations change character from $3\sigma_g \rightarrow 2\pi_u$ to $1\pi_u \rightarrow 4\sigma_g$, i.e. the calculated lowest $^1\Pi_u$ state ($b^1\Pi_u$) exhibits an avoided crossing with the $c^1\Pi_u$. It is clear that further detailed calculations of the potential curves of all involved $^1\Pi_u$ states with the proper non-Born-Oppenheimer treatment of their vibronic interaction are required to fully resolve the issue of experimental assignment versus theoretical calculations.

Comparing now to the BP and LDA calculations, we note that these produce similar to each other and qualitatively incorrect excitation spectra. First of all, the considered three Rydberg-like states (broken lines in Fig. 8.2) are shifted downward by

2.2–2.8 eV in the BP and LDA diagrams compared to the experiment. Furthermore, as many as 25 other Rydberg and mixed states (dotted lines in Fig. 8.2) are placed by BP and LDA below 15 eV. The excitations with valence character ($2\sigma_u \rightarrow 1\pi_g$ and $1\pi_u \rightarrow 1\pi_g$), however, are not shifted much in the LDA/GGA calculations and remain in good agreement with the experimental, SAOP and BP-GRAC $o^1\Pi_u$ and $b^1\Sigma_u^+$ states.

The incorrect LDA/GGA spectra are, clearly, artefacts of the deficient LDA/GGA potentials, specifically, of their upward shift in the bulk region displayed in Fig. 8.1. This shift does not influence valence excitations, since the participating occupied and unoccupied valence orbitals, which are localized in the bulk region, both experience approximately the same upward shift. However, in the outer region the difference between the LDA/GGA and SAOP/BP-GRAC potentials is reduced, since all potentials approach (though in a different way) the zero asymptotics. Because of this, the LDA/GGA upward shift for Rydberg orbitals in the outer region is substantially smaller, than that for valence orbitals in the bulk region. This causes an artificial stabilization of the Rydberg orbitals with respect to the valence ones, which produces the underestimated LDA/GGA energies ω_i of the Rydberg excitations (see Table 8.7) and, as a result, the incorrect LDA/GGA spectra with many Rydberg-like states below 15 eV presented in Fig. 8.2.

Besides the excitation energy ω_i, Table 8.7 presents also the oscillator strength f_i and the percentage of the main orbital transition $\psi_i \rightarrow \psi_a$ for each considered excited state, obtained with the SAOP, BP-GRAC, BP, BLYP and LDA potentials. In the case of the SAOP and BP-GRAC calculations, as well as for the experimental data, we are simply dealing with the five lowest excited states, but for the LDA and GGA potentials we have to identify the appropriate excited states among the many spurious Rydberg states. In almost all cases (with a caveat for $b^1\Sigma_u^+$, see below) it was possible for each of the potentials to unambiguously identify the excited state with the main contribution from a given orbital transition. In the table are also presented individual and overall contributions from the lowest excitations to and S_{-4}.

We consider, first, the valence excitations $2\sigma_u \rightarrow 1\pi_g$ and $1\pi_u \rightarrow 1\pi_g$ which are associated according to our assignment with the two highest states, $b^1\Sigma_u^+$ and $o^1\Pi_u$. The excitation energies of SAOP are in excellent agreement with experiment, as are the oscillator strengths f_i. We note that the oscillator strengths are very difficult to calculate to high accuracy, being very sensitive to small changes in orbital composition of transitions, basis set etc. Agreement within a factor of two with experiment can be considered very satisfactory. The energies of BP-GRAC are also very good, but the $2\sigma_u \rightarrow 1\pi_g$ excitation being a bit low and the next lower $1\pi_u \rightarrow 4\sigma_g$ excitation being a bit high leads to strong mixing between these orbital excitations (almost fifty-fifty). As a result the oscillator strength of the BP-GRAC $2\sigma_u \rightarrow 1\pi_g$ ($o^1\Pi_u$) is rather low and that of $1\pi_u \rightarrow 4\sigma_g$ ($c^1\Pi_u$) rather high. The contributions from the $2\sigma_u \rightarrow 1\pi_g$ and $1\pi_u \rightarrow 4\sigma_g$ transitions to the f_i partially cancel each other for the former state and they add up for the latter state.

Turning to the LDA/GGA calculations, we have already noted that LDA, BP, and BLYP energies ω_i are not very different from the SAOP and BP-GRAC ones and accordingly also reproduce the experimental excitation energies reasonably well. It appears, however, that LDA/GGAs distort seriously the orbital structure of the TDDFT solution for these excitations. Indeed, although the contribution of the valence orbital transition $1\pi_u \rightarrow 1\pi_g$ to the excitation associated with the $b^1\Sigma_u^+$ state is the largest of all contributing orbital transitions, it is only 25% according to LDA, BLYP, and BP. Many smaller contributions come from numerous Rydberg-like orbital transitions $\psi_i \rightarrow \psi_a$ which, in turn, bring their dominant contributions to the corresponding Rydberg-like states with have energies close to that of the $b^1\Sigma_u^+$ state (see Fig. 8.2). As for the $o^1\Pi_u$ state, although LDA and BLYP still have the orbital transition $2\sigma_u \rightarrow 1\pi_g$ as dominant contribution, they produce also an appreciable contribution of $2\sigma_u \rightarrow 1\pi_g$ to another excitation with the energy 13.1 eV, which is very close to the 12.99 eV they obtain for the $o^1\Pi_u$ state. The ω_i and f_i values for this additional excitation are given in parentheses in the corresponding columns of Table 8.7. This situation, where a strong mixture of the valence and Rydberg orbital transitions occurs because of the presence of a multitude of Rydberg excitations with energies close to the valence excitations, as presented in Fig. 8.2, occurs for both the $1\pi_u \rightarrow 1\pi_g$ and the $2\sigma_u \rightarrow 1\pi_g$ excitations and creates a serious problem for the proper interpretation of the LDA/GGA TDDFT spectrum. The latter is, clearly, an artefact of the relative stabilization of the Rydberg-like orbitals in the deficient LDA/GGA potentials discussed above.

Note, that the SAOP TDDFT solution for the valence excitations does not present such an interpretation problem. Indeed, with SAOP the excitation associated with the $o^1\Pi_u$ state is produced predominantly (91%) with the assigned orbital transition $2\sigma_u \rightarrow 1\pi_g$ (see Table 8.7). In the other valence excitation associated with the $b^1\Sigma_u^+$ state the assigned orbital transition $1\pi_u \rightarrow 1\pi_g$ is mixed with Rydberg transitions according to both SAOP and BP-GRAC, but these Rydberg orbital transitions are the predominant contributions to Rydberg-like states, which are lying much higher than the $b^1\Sigma_u^+$ state, so that this does not present a problem for the assignment of the SAOP and BP-GRAC spectra.

We proceed our spectral analysis with the discussion of the lowest Rydberg-like excitations in Table 8.7. In this case for all potentials the assigned orbital transitions bring dominant contributions to the corresponding excitations, with the above-mentioned exception of the contribution of the $1\pi_u \rightarrow 4\sigma_g$ excitation to the $c^1\Pi_u$ state for BP-GRAC, where it gets mixed with the valence $2\sigma_u \rightarrow 1\pi_g$. However, there is a remarkable difference between the oscillator strengths f_i calculated for these Rydberg excitations with the SAOP and BP-GRAC potentials, on the one side, and with the LDA, BLYP, and BP potentials, on the other side. LDA/GGAs produce very low f_i, which are much smaller than the experimental values for all three Rydberg-like excitations of Table 8.7. SAOP and BP-GRAC produce much larger f_i, in particular, for the lowest $3\sigma_g \rightarrow 3\sigma_u$ excitation the SAOP/BP-GRAC f_i are 50–70 times as large and for the next $3\sigma_g \rightarrow 2\pi_u$ excitation they are 20–30 times as large as the LDA/GGA f_i. On the other hand, these SAOP/BP-GRAC f_i are rather close to the experimental values.

The reason for these very different f_i values appears to be the different size of the relevant Rydberg-like molecular orbitals (MOs) calculated with the SAOP/BP-GRAC and with the LDA/GGA potentials. The analysis of these MOs in terms of the atomic orbitals (AOs) of the N atoms reveals that, while the $3\sigma_u$, $2\pi_u$, and $4\sigma_g$ MOs calculated with LDA/GGA consist, predominantly, of the $3s$, $3p$ AOs, the same MOs calculated with SAOP/BP-GRAC consist, mainly, of the substantially more diffuse $4s$, $4p$ and higher-lying AOs. The resultant more diffuse SAOP/BP-GRAC $3\sigma_u$, $2\pi_u$, and $4\sigma_g$ MOs yield larger orbital transition moments $r^{\mu}_{ia} = \langle\psi_i|\, r^{\mu}\, |\psi_a\rangle$ (r^{μ} is x,y or z) than those calculated with LDA/GGAs. This difference is further amplified for the oscillator strengths f_i, which include the squares of r^{μ}_{ia}.

The physical reason for the different size of the Rydberg-like orbitals obtained with the SAOP/BP-GRAC and LDA/GGA potentials is, again, the deficient form of the latter potentials, this time in the outer region. Indeed, as can be clearly seen from Fig. 8.1, the LDA/GGA potentials with their fast decay differ appreciably from zero in a much more restricted area than the SAOP and BP-GRAC potentials with their correct Coulombic asymptotics. Because of this, the former potentials confine bound Rydberg MOs in the restricted area, making them more localized, while the latter potentials support more diffuse Rydberg MOs. These more diffuse MOs produce much larger SAOP/BP-GRAC oscillator strengths f_i, as was explained above.

The above-mentioned low f_i for the three Rydberg-like excitations make partial LDA/GGA sums $\sum_i f_i$ over our five states in Table 8.7 much smaller compared to the experimental ones. The sums calculated with LDA and BLYP are especially low, but if we add (in parentheses in the corresponding columns of Table 8.7) the additional excitation with an appreciable contribution from the $2\sigma_u \rightarrow 1\pi_g$ orbital transition (see the discussion above), the LDA and BLYP sums become close to the BP one. The factors, by which the f_i (which are in the numerators of Eqs. (8.5) and (8.6)) are too low, are more significant than the too large factors $1/\omega_i^2$ and $1/\omega_i^4$ due to the smaller energies ω_i in the denominators, thus producing low LDA/GGA partial α and S_{-4} values, which are 2 to 3 times smaller than the corresponding experimental values. In contrast, the SAOP and BP-GRAC overall pictures for the lowest dipole allowed excitations agree very well with the experiment. SAOP and BP-GRAC yield practically the same partial f sums, which are close to the experimental estimate and, as was discussed above, they reproduce the experimental excitation energies ω_i. As a result, the SAOP and BP-GRAC partial and S_{-4} values appear to be close to each other and to the experimental values (see Table 8.7).

Interesting enough, the above-mentioned LDA/GGA underestimation of the contributions from the lowest excitations is more than compensated with overestimated contributions from higher excitations, the summation over which (to obtain α and S_{-4}) is supposed to represent integration (in a Stieltjes sense) over the underlying ionization continuum. Table 8.8 presents the f_i and ω_i values calculated for excitations with energies ω_i, which are higher than the N_2 ionization energy $I_p = 15.6$ eV and lower than the threshold of 22 eV, and which have oscillator strengths f_i higher than 0.1. Just as in Table 8.7, the LDA/GGA energies ω_i of Table 8.8 are consistently lower than the SAOP and BP-GRAC ones. However, unlike in Table 8.7, the LDA/GGA oscillator strengths f_i for the excitations in Table 8.8 appear to be system-

	SAOP	BP-GRAC	BP	BLYP	LDA
$\mathbf{1\pi_u \rightarrow 2\delta_g}$	96%	94%	94%	87%	87%
ω	17.06	17.16	14.59	14.20	14.73
f	0.113	0.140	0.16	0.20	0.154
f/ω^2	0.28	0.35	0.56	0.76	0.52
f/ω^4	0.72	0.88	1.94	2.76	1.80
$\mathbf{3\sigma_g \rightarrow 8\sigma_u}$	100%	100%	99%	99%	99%
ω	17.64	17.58	15.20	14.85	15.19
f	0.142	0.132	0.167	0.148	0.160
f/ω^2	0.34	0.32	0.54	0.50	0.51
f/ω^4	0.81	0.75	1.72	1.66	1.65
$\mathbf{1\pi_u \rightarrow 11\sigma_g}$	96%	97%	99%	99%	99%
ω	20.36	20.44	18.69	18.33	18.78
f	0.100	0.109	0.174	0.160	0.160
f/ω^2	0.18	0.19	0.36	0.36	0.34
f/ω^4	0.32	0.34	0.78	0.80	0.70
$\mathbf{1\pi_u \rightarrow 4\sigma_g}$	91%	80%	94%	95%	94%
ω	21.54	21.65	20.55	20.13	20.55
f	0.704	0.600	0.84	0.82	0.80
f/ω^2	1.12	0.94	1.48	1.50	1.42
f/ω^4	1.80	1.50	2.60	2.76	2.48
$\sum f$	1.059	0.981	1.341	1.328	1.274
$\sum f/\omega^2$	1.92	1.90	2.94	3.12	2.79
$\sum f/\omega^4$	3.65	3.47	7.04	7.98	6.63

Table 8.8: Oscillator strength f and excitation energy ω calculated for the excitations which have energies higher than the N_2 ionization potential and lower than 22 eV and oscillator strengths larger than 0.1. The contributions $\sum f/\omega^2$, $\sum f/\omega^4$ the polarizability and to the Cauchy coefficient are reported, as well as their sums over these states.

atically larger than the SAOP/BP-GRAC ones. This latter trend can be understood qualitatively from the sum rule, which requires the sum over f_i to be the constant N, the total number of electrons. Then, underestimation of the partial sum $\sum_i f_i$ over the lowest excitations in Table 8.7 must be compensated with a corresponding overestimation for higher excitations, which can be seen from Table 8.8. In this latter case, the LDA/GGA underestimation of ω_i and overestimation of f_i work in the same direction, so that the LDA/GGA partial and S_{-4} values for the "continuum" states are substantially larger than the SAOP/BP-GRAC ones (see Table 8.8).

Thus, BP as well as LDA and BLYP substantially underestimate contributions to and S_{-4} from the Rydberg-state excitations and they overestimate those from the "continuum" states. Contrary to this, SAOP and BP-GRAC yield a more balanced "excitation structure" of and S_{-4}, which is remarkably similar for both methods and which agrees well with the experimental data for the lowest excitations. Due to the partial compensation of the above-mentioned LDA/GGA errors of opposite signs, the total LDA/GGA polarizabilities for N_2 are in better agreement with experiment than the corresponding partial sums over the lowest excitations (compare Table 8.3 and Table 8.7). An especially lucky error compensation occurs for BP with =12.06 a.u., which is not much larger than the experimental value α=11.74 a.u., though the SAOP α=11.82 a.u. and BP-GRAC α=11.78 a.u. still have smaller errors. Then, bearing in mind that BP underestimates the higher excitation energies ω_i and that the S_{-4} sum has the additional ω_i^2 factor in the denominator compared to the α sum, one can expect a larger BP overestimation for the S_{-4} Cauchy coefficient. Indeed, as follows from Table 8.5, the BP value S_{-4}=32.99 a.u. is appreciably larger than the experimental S_{-4}=30.11 a.u., while the SAOP S_{-4}=30.48 a.u. and the BP-GRAC S_{-4}=30.20 a.u. are close to the experiment.

The spectral analysis of the polarizability α and the S_{-4} Cauchy coefficient of N_2 performed in this section shows that LDA and GGAs all produce a distorted picture of the contributions to and S_{-4} from individual excitations. In contrast, SAOP and BP-GRAC both yield a qualitatively correct structure of and S_{-4}. General conclusions from this analysis will be drawn in the next section.

8.5 Conclusions

It has often been observed that in particular excitations to Rydberg states are affected by the shape corrections to the LDA and GGA xc potentials, while valence excitations are believed to be represented reasonably well by LDA and GGA calculations. In this chapter the performance of the approximate SAOP [111] and BP-GRAC [87] xc potentials has been assessed in molecular TDDFT calculations of the static average polarizability α, and its frequency dispersion in the form of the S_{-4} Cauchy coefficient, and the static average hyperpolarizability β. The results have been compared with those obtained with the standard LDA and some GGA (BP and BLYP) potentials, and the performance of these potentials has been more closely examined by explicitly considering the spectral structure of α and S_{-4}.

Due to their correct form, the SAOP and BP-GRAC potentials reproduce well the characteristics of the molecular excitation spectra, such as individual excitation energies ω_i and oscillator strengths f_i. In contrast, standard LDA and GGA potentials produce a distorted spectral structure of and S_{-4}. They tend to underestimate the energies ω_i and they also appear to underestimate the oscillator strengths f_i of excitations to bound Rydberg-like states and overestimate those for excitations to the "continuum" states. As a result, LDA and GGAs tend to underestimate contributions to and S_{-4} from Rydberg-like states and to overestimate those from the continuum, so that these errors of opposite signs partially compensate each other.

These distortions of the LDA/GGA spectra have been related to the deficient form of the corresponding potentials in both bulk and outer regions. In particular, artificial stabilization (low energies ω_i) of the Rydberg-like states is due to the upward shift of the LDA/GGA potentials in the bulk region. In turn, artificial localization of bound

Rydberg-like states, which results in low oscillator strengths f_i, is due to the fast decay of the LDA/GGA potentials in the outer region, which makes the LDA/GGA potential well considerably more narrow than the asymptotically corrected SAOP and BP-GRAC potentials, see Fig. 8.1. The distortions create a serious problem for the assignment of the LDA/GGA TDDFT spectra. The SAOP and BP-GRAC potentials, which are free from the above-mentioned deficiencies, produce a balanced spectral structure of the molecular response quantities.

Both SAOP and BP-GRAC yield high quality molecular polarizabilities α, Cauchy coefficients S_{-4}, and hyperpolarizabilities β for the considered molecules. The SAOP and BP-GRAC average errors for these properties are only a few percent and they improve substantially upon LDA and BLYP. Due to somewhat reduced errors from individual excitations and their lucky cancellation, BP also reproduces well the polarizabilities. However, the distorted BP spectral structure of the response properties manifests itself in a worsening quality of the BP Cauchy coefficients and hyperpolarizabilities.

Further refinement of the SAOP and BP-GRAC potentials can further enhance the quality of the TDDFT results. Within SAOP, for example, one can apply statistical averaging separately to the xc-hole and "response" [73] parts of a model xc potential. Within the GRAC procedure, one can use, instead of the BP potential, the derivative of an exchange-correlation energy functional with parameters which would be directly fitted to reproduce molecular response properties calculated with the resultant GRAC potential. Further improvement of the TDDFT results might also require (especially for larger, more polarizable molecules) refinement of the xc kernel beyond the ALDA f_{xc} employed in this chapter.

Chapter

9

(Hyper)polarizabilities of molecular chains

An approximate Kohn-Sham (KS) exchange potential $v_{x\sigma}^{\mathrm{CEDA}}$ is developed, based on the common energy denominator approximation (CEDA) for the static orbital Green's function, which preserves the essential structure of the density response function. $v_{x\sigma}^{\mathrm{CEDA}}$ is an explicit functional of the occupied KS orbitals, which has the Slater $v_{S\sigma}$ and response $v_{\mathrm{resp}\sigma}^{\mathrm{CEDA}}$ potentials as its components. The latter exhibits the characteristic step structure with "diagonal" contributions from the orbital densities $\psi_{i\sigma}^2$, as well as "off-diagonal" ones from the occupied-occupied orbital products $\psi_{i\sigma}\psi_{j\neq i\sigma}^*$. Comparison of the results of atomic and molecular ground-state CEDA calculations with those of the Krieger-Li-Iafrate (KLI), exact exchange (EXX), and Hartree-Fock (HF) methods show, that both KLI and CEDA potentials can be considered as very good analytical "closure approximations" to the exact KS exchange potential. The total CEDA and KLI energies nearly coincide with the EXX ones and the corresponding orbital energies $\varepsilon_{i\sigma}$ are rather close to each other for the light atoms and small molecules considered. The CEDA, KLI, EXX $-\varepsilon_{i\sigma}$ values provide the qualitatively correct order of ionizations and they give an estimate of VIPs comparable to that of the HF Koopmans' theorem. However, the additional off-diagonal orbital structure of $v_{x\sigma}^{\mathrm{CEDA}}$ appears to be essential for the calculated response properties of molecular chains. KLI already considerably improves the calculated (hyper)polarizabilities of the prototype hydrogen chains H_n over local density approximation (LDA) and standard generalized gradient approximations (GGAs), while the CEDA results are definitely an improvement over the KLI ones. The reasons of this success are the specific orbital structures of the CEDA and KLI response potentials, which produce in an external field an ultra-nonlocal field-counteracting exchange potential.

9.1 Introduction

The success of the KS DFT in calculations of molecular response properties is due to the efficient inclusion of the electron Coulomb correlation into the KS potentials and kernels as well as due to favorable features of the KS orbital spectrum. Unlike the canonical Hartree-Fock (HF) unoccupied orbitals of an N electron system, which resemble one-electron states of the anionic $(N+1)$ system, the KS unoccupied orbitals represent approximately one-electron excitations of the N electron system. Because of this, the quality of the results obtained within time dependent DFT with xc potentials v_{xc} of LDA and GGAs as well as with the xc kernel f_{xc} of ALDA is often superior to that of HF and it is competing with the quality of the results of the correlated *ab initio* methods [36, 129, 130, 180, 210, 211, 212, 213]. Asymptotic corrections to the GGA potentials improve further the results for compact molecules [87, 89, 176, 177, 192] and a balanced description of the atomic shell structure and asymptotic behavior of v_{xc} within SAOP [111, 174, 175] produces a good quality of the calculated response properties for a variety of molecules from diatomic and small organic molecules [111] (see also previous chapters) to metal clusters [214] to complexes of the transition metals [215, 216, 217].

Notwithstanding this success, there were also identified some notoriously difficult problem cases for DFT methods. Among these are the response properties of molecular chains. As was found in Refs. [147, 148] LDA and GGAs dramatically overestimate the linear and nonlinear polarizabilities of finite polyacetylene chains of varying length and of the hydrogen chains H_n. It was recognized that, in order to adequately describe these properties, DFT potentials should possess a characteristic orbital structure [40, 148, 149], which produces an ultra-nonlocal term counteracting an external field. LDA and GGA potentials, which depend explicitly on the electron density ρ and its derivatives, lack this structure. On the other hand, the exchange-only approximation of Krieger, Li, and Iafrate (KLI) [38] with its orbital-dependent potential v_x improves considerably upon LDA and GGAs. Still, the KLI polarizabilities α and second hyperpolarizabilities γ for H_n are definitely inferior to the HF ones [148] (see also 9.5). This clearly requires further improvement at the exchange-only level of the orbital structure of the potential v_x beyond KLI.

In this chapter an approximate exchange potential $v_{x\sigma}^{\mathrm{CEDA}}$ is presented, which is explicitly expressed in terms of the occupied KS orbitals $\psi_{i\sigma}$. It is developed with the common energy denominator approximation (CEDA) for the static orbital Green's function $G_{i\sigma}$, which preserves the essential structure of the response theory. CEDA is characterized in Sec. 9.2 and it is compared with the Sharp-Horton approximation for $G_{i\sigma}$ [218]. In Sec. 9.3 the derivation of the potential $v_{x\sigma}^{\mathrm{CEDA}}$ is given, which possesses an additional "off-diagonal" orbital structure compared to the KLI potential $v_{x\sigma}^{\mathrm{KLI}}$. In Sec. 9.4 atomic and molecular ground-state total and orbital energies are calculated with CEDA, KLI, HF as well as with the exact exchange (EXX) method [32]. The orbital energies of the above-mentioned exchange-only methods are compared with those of the rather accurate KS solutions obtained from the correlated *ab initio* electron densities ρ [89] and with the experimental vertical ionization potentials (VIPs). In 9.5 the comparison is made of the static polarizabilities and second hyperpolarizabilities of the prototype hydrogen linear chains H_6, H_{12}, and H_{18} calculated within the finite-field approach with CEDA, KLI, HF, LDA, GGAs as well as with the Møller-Plesset (MP2 and MP4) perturbation theory and coupled cluster

(CCSDT) method. While LDA and GGA greatly overestimate (hyper)polarizabilities of the lengthier chains, KLI performs much better and, in turn, CEDA improves considerably upon KLI, thus bringing DFT (hyper)polarizabilities rather close to the *ab initio* ones. The reason of this relative success of CEDA is established: it is the more adequate representation with CEDA of the orbital structure responsible for the field-counteracting exchange effect. In Sec. 9.6 the implication of the present results for the KS theory, its development and its applications are discussed and the conclusions are drawn.

9.2 The common energy denominator approximation for $G_{i\sigma}$

The KS exchange potential $v_{x\sigma}$ (σ is the electron spin index) can be obtained from the equations of the optimized potential method (OPM) [31]

$$\sum_i n_{i\sigma} \int d\mathbf{r}_2 \left[v_{x\sigma}(\mathbf{r}_2) - v^i_{x\sigma}(\mathbf{r}_2)\right] G_{i\sigma}(\mathbf{r}_2, \mathbf{r}_1)\, \psi^*_{i\sigma}(\mathbf{r}_2)\, \psi_{i\sigma}(\mathbf{r}_1) + \text{c.c.} = 0 \tag{9.1}$$

with the static orbital Green's function $G_{i\sigma}$

$$G_{i\sigma}(\mathbf{r}_1, \mathbf{r}_2) = \sum_{j \neq i} \frac{\psi_{j\sigma}(\mathbf{r}_1)\, \psi^*_{j\sigma}(\mathbf{r}_2)}{\varepsilon_{j\sigma} - \varepsilon_{i\sigma}} \tag{9.2}$$

and the Hartree-Fock orbital potentials $v^i_{x\sigma}$ calculated with the OPM orbitals,

$$v^i_{x\sigma}(\mathbf{r}_1) = -\frac{1}{\psi^*_{i\sigma}(\mathbf{r}_1)} \sum_{j=1} n_{j\sigma} \psi^*_{j\sigma}(\mathbf{r}_1) \int \frac{\psi^*_{i\sigma}(\mathbf{r}_2)\, \psi_{j\sigma}(\mathbf{r}_2)}{|\mathbf{r}_1 - \mathbf{r}_2|} d\mathbf{r}_2.$$

To obtain an explicit expression for $v_{x\sigma}$ in terms of the occupied orbitals, one has to insert in (9.1) some "closure approximation" to the Green's function $G_{i\sigma}$. It is, of course, desirable that an approximate $G_{i\sigma}$ would reproduce the basic properties of the exact function (9.2), in particular, the structure of the corresponding static KS linear response function $\chi_{s\sigma}$

$$\begin{aligned}
\chi_{s\sigma}(\mathbf{r}_2, \mathbf{r}_3) &= -\sum_{i=1}^{N_\sigma} n_{i\sigma} \psi^*_{i\sigma}(\mathbf{r}_2)\, G_{i\sigma}(\mathbf{r}_2, \mathbf{r}_3)\, \psi_{i\sigma}(\mathbf{r}_3) + \text{c.c.} \\
&= -\sum_{i=1}^{N_\sigma} n_{i\sigma} \psi^*_{i\sigma}(\mathbf{r}_2)\, \psi_{i\sigma}(\mathbf{r}_3) \sum_{j \neq i} \frac{\psi_{j\sigma}(\mathbf{r}_2)\, \psi^*_{j\sigma}(\mathbf{r}_3)}{\varepsilon_{j\sigma} - \varepsilon_{i\sigma}} + \text{c.c.} \\
&= -\sum_{i=1}^{N_\sigma} n_{i\sigma} \psi^*_{i\sigma}(\mathbf{r}_2)\, \psi_{i\sigma}(\mathbf{r}_3) \sum_{c > N_\sigma} \frac{\psi_{c\sigma}(\mathbf{r}_2)\, \psi^*_{c\sigma}(\mathbf{r}_3)}{\varepsilon_{c\sigma} - \varepsilon_{i\sigma}} + \text{c.c.}
\end{aligned} \tag{9.3}$$

Note the well-known fact [32], that in the double sum of Eq. (9.3) the contributions from the pairs of the occupied orbitals $\psi_{i\sigma}$ and $\psi_{j\sigma}$ cancel each other, since they contain the orbital energy differences $\Delta\varepsilon_{ij\sigma} = \varepsilon_{j\sigma} - \varepsilon_{i\sigma}$ and $\Delta\varepsilon_{ji\sigma} = \varepsilon_{i\sigma} - \varepsilon_{j\sigma} = -\Delta\varepsilon_{ij\sigma}$ of opposite signs. Thus, the occupied-occupied orbital mixing does not contribute to the response function $\chi_{s\sigma}$, which contains only contributions corresponding to excitations from an occupied orbital $\psi_{j\sigma}$ to an unoccupied one $\psi_{c\sigma}$. Strictly speaking, the above-mentioned cancellation is possible, if $n_{i\sigma}$ of all occupied orbitals are equal to each other, for instance, $n_{i\sigma} = 1$ as for a pure KS state. This cancellation will be the physical basis for our further derivation, so that throughout this chapter we assume that for all occupied orbitals $n_{i\sigma} = n_{j\sigma}$.

In KLI the simple Sharp-Horton (SH) approximation [38, 218] has been employed, according to which various differences $\Delta\varepsilon_{ij\sigma} = \varepsilon_{j\sigma} - \varepsilon_{i\sigma}$ in (9.2) are represented by a single constant $\varepsilon_{j\sigma} - \varepsilon_{i\sigma} \approx \Delta\tilde{\varepsilon}_\sigma$. With this approximation, summation over the complete spectrum produces a delta-function and the functions $G_{i\sigma}$ and $\chi_{s\sigma}$ assume the form

$$G_{i\sigma}^{SH}(\mathbf{r}_1, \mathbf{r}_2) = \frac{1}{\Delta\tilde{\varepsilon}_\sigma}\left\{\delta(\mathbf{r}_1 - \mathbf{r}_2) - \psi_{i\sigma}(\mathbf{r}_1)\psi_{i\sigma}^*(\mathbf{r}_2)\right\} \tag{9.4}$$

$$\chi_{s\sigma}^{SH}(\mathbf{r}_1, \mathbf{r}_2) = -\frac{2}{\Delta\tilde{\varepsilon}_\sigma}\left\{\delta(\mathbf{r}_1 - \mathbf{r}_2)\rho_\sigma(\mathbf{r}_1) - \sum_{i=1}^{N_\sigma} n_{i\sigma}\left|\psi_{i\sigma}(\mathbf{r}_1)^2\right|\left|\psi_{i\sigma}(\mathbf{r}_2)^2\right|\right\} \tag{9.5}$$

The approximation (9.4) appears to be a crude one and it violates the physical spirit of the Unsöld approximation [219] of the conventional state based many-electron perturbation theory [220, 221, 222], which also employs the common energy denominator. Indeed, within the Unsöld approximation, the energy differences $\Delta E_i = E_i - E_0$ between the many-electron ground state Ψ_0 and excited states Ψ_i are represented by a single constant ΔE, which is justified in this case, since all ΔE_i are positive and ΔE_i for the most important lowest excited states Ψ_i are expected to be not far from each other. In contrast, the orbital based SH approximation (9.4) levels large energy differences $\Delta\varepsilon_{ic\sigma}$ for the occupied-unoccupied orbital pairs and relatively small differences $\Delta\varepsilon_{ij\sigma}$ for the occupied-occupied pairs. In the latter case it even neglects the change of the sign when going from $\Delta\varepsilon_{ij\sigma}$ to $\Delta\varepsilon_{ji\sigma}$. Because of this, in the SH density response function (9.5) only the self-interaction is excluded and it effectively contains contributions from mixing of different occupied orbitals, unlike the exact KS function (9.3).

Recently, a more physically motivated common energy denominator approximation (CEDA) for $G_{i\sigma}$ has been proposed [40], which restores the essence of the Unsöld approximation in the present orbital based perturbation approach. Within this approximation, only the energy differences $\Delta\varepsilon_{ic\sigma}$ for the occupied-unoccupied orbital pairs are approximated with the mean energy $\Delta\tilde{\varepsilon}_\sigma$

$$\Delta\varepsilon_{ic\sigma} = \varepsilon_{c\sigma} - \varepsilon_{i\sigma} \approx \Delta\tilde{\varepsilon}_\sigma, i \leq N_\sigma, c > N_\sigma$$

while the true differences $\Delta\varepsilon_{ij\sigma}$ for the occupied-occupied pairs are retained. This gives for $G_{i\sigma}^{\mathrm{CEDA}}$

$$G_{i\sigma}^{\mathrm{CEDA}}\left(\mathbf{r}_1,\mathbf{r}_2\right)=\sum_{j\neq i}^{N_\sigma}\frac{1}{\Delta\varepsilon_{ij\sigma}}\psi_{j\sigma}\left(\mathbf{r}_1\right)\psi_{j\sigma}^*\left(\mathbf{r}_2\right)+\frac{1}{\Delta\tilde{\varepsilon}_\sigma}\sum_{c>N_\sigma}\psi_{c\sigma}\left(\mathbf{r}_1\right)\psi_{c\sigma}^*\left(\mathbf{r}_2\right) \tag{9.6}$$

Adding and subtracting to the r.h.s. of (9.6) contributions of the occupied orbitals with the common denominator $\Delta\tilde{\varepsilon}_\sigma$, we obtain the expressions for $G_{i\sigma}^{\mathrm{CEDA}}$

$$\begin{aligned}G_{i\sigma}^{\mathrm{CEDA}}\left(\mathbf{r}_1,\mathbf{r}_2\right)=&\frac{\delta\left(\mathbf{r}_1-\mathbf{r}_2\right)}{\Delta\tilde{\varepsilon}_\sigma}-\frac{1}{\Delta\tilde{\varepsilon}_\sigma}\sum_{j}^{N_\sigma}\psi_{j\sigma}\left(\mathbf{r}_1\right)\psi_{j\sigma}^*\left(\mathbf{r}_2\right)\\&+\sum_{j\neq i}^{N_\sigma}\frac{1}{\Delta\varepsilon_{ij\sigma}}\psi_{j\sigma}\left(\mathbf{r}_1\right)\psi_{j\sigma}^*\left(\mathbf{r}_2\right)\end{aligned} \tag{9.7}$$

and for the corresponding density response function

$$\begin{aligned}&\chi_{s\sigma}^{\mathrm{CEDA}}\left(\mathbf{r}_1,\mathbf{r}_2\right)=-\frac{1}{\Delta\tilde{\varepsilon}_\sigma}\delta\left(\mathbf{r}_1-\mathbf{r}_2\right)\rho_\sigma\left(\mathbf{r}_1\right)\\&+\frac{1}{\Delta\tilde{\varepsilon}_\sigma}\sum_{i}^{N_\sigma}n_{i\sigma}\psi_{i\sigma}^*\left(\mathbf{r}_1\right)\psi_{i\sigma}\left(\mathbf{r}_2\right)\sum_{j}^{N_\sigma}\psi_{j\sigma}\left(\mathbf{r}_1\right)\psi_{j\sigma}^*\left(\mathbf{r}_2\right)\\&-\sum_{i}^{N_\sigma}n_{i\sigma}\psi_{i\sigma}^*\left(\mathbf{r}_1\right)\psi_{i\sigma}\left(\mathbf{r}_2\right)\sum_{j\neq i}^{N_\sigma}\frac{1}{\Delta\varepsilon_{ij\sigma}}\psi_{j\sigma}\left(\mathbf{r}_1\right)\psi_{j\sigma}^*\left(\mathbf{r}_2\right)+\mathrm{c.c.}\\&=-\frac{1}{\Delta\tilde{\varepsilon}_\sigma}\sum_{i}^{N_\sigma}n_{i\sigma}\psi_{i\sigma}^*\left(\mathbf{r}_1\right)\psi_{i\sigma}\left(\mathbf{r}_2\right)\sum_{c>N_\sigma}\psi_{c\sigma}\left(\mathbf{r}_1\right)\psi_{c\sigma}^*\left(\mathbf{r}_2\right)+\mathrm{c.c.}\end{aligned} \tag{9.8}$$

One can see from (9.8) that, just as for the exact function (9.3), the terms with the occupied-occupied mixing are properly excluded from the approximate $\chi_{s\sigma}^{\mathrm{CEDA}}$ of Eq. (9.8). In particular, the second sum in the r.h.s. of (9.8) disappears due to the mutual cancellation of its terms (under the assumption, that $n_{i\sigma}=n_{j\sigma}$) and the first sum cancels the corresponding contribution to the delta-function. As a result, only the terms with the occupied-unoccupied mixing are properly retained within the common energy denominator approximation. In this sense, the CEDA (9.7) preserves the proper orbital structure of the density response function. In the next section this approximation will be used to obtain the approximate exchange potential $v_{x\sigma}^{\mathrm{CEDA}}$.

9.3 Approximate exchange potential $v_{x\sigma}^{\mathrm{CEDA}}$

To obtain the explicit expression for the exchange potential in terms of the occupied KS orbitals, we insert the CEDA Green's function (9.7) in the OPM equation (9.1), thus obtaining the equation for the potential $v_{x\sigma}^{\mathrm{CEDA}}$

$$\begin{aligned}&\frac{1}{\Delta\tilde{\varepsilon}_\sigma}\{\sum_i n_{i\sigma}\left[v_{x\sigma}^{\mathrm{CEDA}}(\mathbf{r}_1)-v_{x\sigma}^{i}(\mathbf{r}_1)\right]\left|\psi_{i\sigma}(\mathbf{r}_1)\right|^2\\ &-\sum_{i,j\le N_\sigma} n_{i\sigma}\left[1-\frac{\Delta\tilde{\varepsilon}_\sigma(1-\delta_{ij})}{\Delta\varepsilon_{ij\sigma}}\right]\left[\bar{v}_{x\sigma,ij}^{\mathrm{CEDA}}-\bar{v}_{x\sigma,ij}^{i}\right]\psi_{i\sigma}(\mathbf{r}_1)\,\psi_{j\sigma}^{*}(\mathbf{r}_1)+\text{c.c.}\}=0\end{aligned} \tag{9.9}$$

where $\bar{v}_{x\sigma,ij}^{\mathrm{CEDA}}$ and $\bar{v}_{x\sigma,ij}^{i}$ are the matrix elements of the potentials $v_{x\sigma}^{\mathrm{CEDA}}$ and $v_{x\sigma}^{i}$ for the orbitals $\psi_{i\sigma}$ and $\psi_{j\sigma}$

$$\begin{aligned}\bar{v}_{x\sigma,ij}^{\mathrm{CEDA}}&=\int\psi_{i\sigma}^{*}(\mathbf{r}_2)\,\psi_{j\sigma}(\mathbf{r}_2)\,v_{x\sigma}^{\mathrm{CEDA}}(\mathbf{r}_2)\,d\mathbf{r}_2,\\ \bar{v}_{x\sigma,ij}^{i}&=\int\psi_{i\sigma}^{*}(\mathbf{r}_2)\,\psi_{j\sigma}(\mathbf{r}_2)\,v_{x\sigma}^{i}(\mathbf{r}_2)\,d\mathbf{r}_2.\end{aligned}$$

To make (9.9) more compact, we have combined two sums in (9.7). From (9.9) follows

$$\begin{aligned}&v_{x\sigma}^{\mathrm{CEDA}}(\mathbf{r}_1)=v_{S\sigma}(\mathbf{r}_1)\\ &+\frac{1}{2}\sum_{i,j\le N_\sigma}\left\{n_{i\sigma}\left[1-\frac{\Delta\tilde{\varepsilon}_\sigma(1-\delta_{ij})}{\Delta\varepsilon_{ij\sigma}}\right]\left[\bar{v}_{x\sigma,ij}^{\mathrm{CEDA}}-\bar{v}_{x\sigma,ij}^{i}\right]\frac{\psi_{i\sigma}(\mathbf{r}_1)\,\psi_{j\sigma}^{*}(\mathbf{r}_1)}{\rho_\sigma(\mathbf{r}_1)}+\text{c.c.}\right\},\end{aligned} \tag{9.10}$$

where $v_{S\sigma}$ is the Slater potential [164]

$$v_{S\sigma}(\mathbf{r}_1)=\frac{\sum\limits_i n_{i\sigma}\left|\psi_{i\sigma}(\mathbf{r}_1)\right|^2 v_{x\sigma}^{i}(\mathbf{r}_1)}{\rho_\sigma(\mathbf{r}_1)}.$$

Due to the symmetry of the quantities and summations in (9.10), the term containing the orbital energy difference $\Delta\varepsilon_{ij\sigma}$ cancels with the corresponding term in the complex conjugate part with $\Delta\varepsilon_{ji\sigma}=-\Delta\varepsilon_{ij\sigma}$ under our assumption $n_{j\sigma}=n_{i\sigma}$. This gives the equation

$$v_{x\sigma}^{\mathrm{CEDA}}(\mathbf{r}_1)=v_{S\sigma}(\mathbf{r}_1)+\sum_{i,j\le N_\sigma}\left[\bar{v}_{x\sigma,ij}^{\mathrm{CEDA}}-\bar{v}_{x\sigma,ij}^{i}\right]\frac{n_{i\sigma}\psi_{i\sigma}(\mathbf{r}_1)\,\psi_{j\sigma}^{*}(\mathbf{r}_1)}{\rho_\sigma(\mathbf{r}_1)}. \tag{9.11}$$

Equation (9.11) can be solved in the same way as the corresponding equation for the KLI potential [38] after exclusion of the contribution of the density $|\psi_{N\sigma}(\mathbf{r}_1)|^2$ of the highest occupied molecular orbital (HOMO) $\psi_{N\sigma}$ from the sum in (9.11)

$$v_{x\sigma}^{\mathrm{CEDA}}(\mathbf{r}_1)=v_{S\sigma}(\mathbf{r}_1)+{\sum}'_{i,j\le N_\sigma}\left[\bar{v}_{x\sigma,ij}^{\mathrm{CEDA}}-\bar{v}_{x\sigma,ij}^{i}\right]\frac{n_{i\sigma}\psi_{i\sigma}(\mathbf{r}_1)\,\psi_{j\sigma}^{*}(\mathbf{r}_1)}{\rho_\sigma(\mathbf{r}_1)} \tag{9.12}$$

The primed sum in (9.12) indicates this exclusion, which fixes the zero long-range asymptotics of the potential $v_{x\sigma}^{\mathrm{CEDA}}$. Multiplying both sides of (9.11) by $\psi_{k\sigma}^{*}\psi_{l\sigma}$ (again, $\psi_{k\sigma}^{*}\psi_{l\sigma} \neq |\psi_{N\sigma}|^2$), integrating over $\mathbf{r}_1$, and subtracting $\bar{v}_{x\sigma,kl}^{k}$, one obtains the equations for the matrix elements $\bar{v}_{x\sigma,ij}^{\mathrm{CEDA}}$

$$\sum\nolimits'_{i,j\leq N_\sigma} \left(\delta_{ik}\delta_{jl} - M_{klij}^{\sigma}\right)\left[\bar{v}_{x\sigma,ij}^{\mathrm{CEDA}} - \bar{v}_{x\sigma,ij}^{i}\right] = \bar{v}_{S\sigma,kl} - \bar{v}_{x\sigma,kl}^{k} \tag{9.13}$$

where M_{klij}^{σ} is the weighted overlap between the orbital products $\psi_{k\sigma}^{*}\psi_{l\sigma}$ and $\psi_{i\sigma}^{*}\psi_{j\sigma}$

$$M_{klij}^{\sigma} = n_i \int \frac{\psi_{k\sigma}^{*}(\mathbf{r}_1)\,\psi_{l\sigma}(\mathbf{r}_1)\,\psi_{i\sigma}(\mathbf{r}_1)\,\psi_{j\sigma}^{*}(\mathbf{r}_1)}{\rho_\sigma(\mathbf{r}_1)} d\mathbf{r}_1.$$

Eqs.(9.13) are formally solved by inversion of the matrix $(\mathbf{I}-\mathbf{M})$

$$\bar{v}_{x\sigma,ij}^{\mathrm{CEDA}} - \bar{v}_{x\sigma,ij}^{i} = \sum_{kl}^{N_\sigma} \xi_{ij,kl}^{\sigma}\left[\bar{v}_{S\sigma,kl} - \bar{v}_{x\sigma,kl}^{k}\right] \tag{9.14}$$

where

$$\xi_{ij,kl}^{\sigma} = \left(I - M^{\sigma}\right)_{ij,kl}^{-1}, \; \xi_{ij,N\sigma N\sigma}^{\sigma} = \xi_{N\sigma N\sigma,kl}^{\sigma} = 0$$

Finally, inserting (9.14) in (9.12), we obtain for $v_{x\sigma}^{\mathrm{CEDA}}$ the following expression

$$v_{x\sigma}^{\mathrm{CEDA}}(\mathbf{r}_1) = v_{S\sigma}(\mathbf{r}_1) + v_{\mathrm{resp}\sigma}^{\mathrm{CEDA}}(\mathbf{r}_1) \tag{9.15}$$

where $v_{\mathrm{resp}\sigma}^{\mathrm{CEDA}}$ is the response potential [73]

$$v_{\mathrm{resp}\sigma}^{\mathrm{CEDA}}(\mathbf{r}_1) = \sum_{i}^{N_\sigma-1} w_{ii}^{\sigma}\frac{|\psi_{i\sigma}(\mathbf{r}_1)|^2}{\rho_\sigma(\mathbf{r}_1)} + \sum_{i,j\neq i}^{N_\sigma} w_{ij}^{\sigma}\frac{\psi_{i\sigma}(\mathbf{r}_1)\,\psi_{j\sigma}^{*}(\mathbf{r}_1)}{\rho_\sigma(\mathbf{r}_1)} \tag{9.16}$$

$$w_{ij}^{\sigma} = \sum_{kl}^{N_\sigma} n_{i\sigma}\xi_{klij}^{\sigma}\left\{\bar{v}_{S\sigma,kl} - \bar{v}_{x\sigma,kl}^{k}\right\}, \; w_{N\sigma N\sigma}^{\sigma} = 0 \tag{9.17}$$

With (9.15) $v_{x\sigma}^{\mathrm{CEDA}}$ is subdivided naturally into two physically meaningful components, an attractive long-range Slater potential v_{S_σ} and a repulsive short-range response potential $v_{\mathrm{resp}\sigma}^{\mathrm{CEDA}}$. The former is the potential of the Fermi (exchange) hole density distribution $\rho_{x\sigma}(\mathbf{r}_2|\mathbf{r}_1)$

$$v_S(\mathbf{r}_1) = \int \frac{\rho_{x\sigma}(\mathbf{r}_2|\mathbf{r}_1)}{|\mathbf{r}_1 - \mathbf{r}_2|} d\mathbf{r}_2$$

$$\rho_{x\sigma}(\mathbf{r}_2|\mathbf{r}_1) = -\sum_{ij}^{N_\sigma} n_{i\sigma}n_{j\sigma}\frac{\psi_{i\sigma}(\mathbf{r}_1)\,\psi_{j\sigma}^{*}(\mathbf{r}_1)\,\psi_{i\sigma}^{*}(\mathbf{r}_2)\,\psi_{j\sigma}(\mathbf{r}_2)}{\rho_\sigma(\mathbf{r}_1)}$$

System	HF[a]	EXX[b]	KLI	CEDA
Be	−14.57301	0.00058	0.00060	0.00060
Ne	−128.5467	0.0017	0.0022	0.0022
Ar	−526.8173	0.0051	0.0048	0.0052
N_2	−108.9913	0.0052	0.0078	0.0077
CO	−112.7893	0.0051	0.0076	0.0076
H_2O	−76.05710	0.00230	0.00392	0.00364

[a] This work
[b] Ref. [32]

Table 9.1: The atomic and molecular HF total energies and the differences between the EXX, KLI, CEDA and HF total energies (in Hartrees).

and it has Coulombic long-range asymptotics $v_{S_\sigma}(\mathbf{r}_1) \to -1/|\mathbf{r}_1|$ at $|\mathbf{r}_1| \to \infty$. The second component of (9.15), the potential $v^{\text{CEDA}}_{\text{resp}\sigma}$ of (9.16), (9.17) has the characteristic orbital step structure with the step heights w^σ_{ij} corresponding to the individual products $\psi_{i\sigma}\psi^*_{j\sigma}$ of the occupied orbitals. It follows from (9.16) that in the region, where a particular orbital density $|\psi_{i\sigma}|^2$ brings a dominant contribution to the total density ρ_σ, the potential $v^{\text{CEDA}}_{\text{resp}\sigma}$ is close to the corresponding weight w^σ_{ii}, thus producing the step structure of $v^{\text{CEDA}}_{\text{resp}\sigma}$. As a consequence of the fixing of the asymptotics (9.12), the HOMO density $|\psi_{N\sigma}|^2$ is removed from the numerator of (9.16). Since $|\psi_{N\sigma}|^2$ is present in the total density ρ_σ in the denominator and it dominates the density at $|\mathbf{r}_1| \to \infty$, $v^{\text{CEDA}}_{\text{resp}\sigma}$ is a short-range potential, which decays asymptotically faster than the Coulombic asymptotics. The first sum in (9.16) with the "diagonal steps" has the same form as the response potential $v^{\text{KLI}}_{\text{resp}\sigma}$ of the KLI method [38]. However, due to the complete exclusion of the occupied-occupied orbital mixing from (9.8) in our CEDA, $v^{\text{CEDA}}_{\text{resp}\sigma}$ contains also "off-diagonal steps" in the second sum in (9.16). Thus, $v^{\text{CEDA}}_{\text{resp}\sigma}$ provides a more detailed orbital structure compared to the KLI potential $v^{\text{KLI}}_{\text{resp}\sigma}$. The importance of the additional CEDA orbital structure for the calculated molecular response properties will be shown in Sec. 9.5.

9.4 Atomic and molecular ground-state calculations with $v^{\text{CEDA}}_{x_\sigma}$

In this section the results of the ground-state atomic and molecular calculations with the potential $v^{\text{CEDA}}_{x\sigma}$ will be presented and discussed. Table 9.1 presents the total HF energies and their differences with the CEDA and KLI energies for the closed-shell atoms Be, Ne, Ar and molecules N_2, CO, H_2O. All energies have been calculated with the same one-determinantal expression, in which the HF, KLI orbitals and the CEDA ones obtained with $v^{\text{CEDA}}_{x\sigma}$of (9.15) were plugged in. All calculations have been performed by means of a Gaussian orbital density functional code [46, 77] based on the ATMOL package [62]. For the atoms and for CO the 5-zeta *cc*-pCV5z (*cc*-pV5z for Be), for N_2 the quadruple-zeta *cc*-pCVQz, and for H_2O the triple-zeta *cc*-pCVTz correlation-consistent basis sets of Gaussian-type orbitals [65] have been used for all methods. Both CEDA and KLI can be considered as "closure approximations" to the exact exchange (EXX) KS approach [32, 36], thus the EXX vs. HF energy differences taken from Ref. [32] are also presented in Table 9.1.

It appears that the CEDA and KLI energies shown in Table 9.1 practically coincide and they are very close to the EXX ones. All three approaches reproduce excellently the HF energies, which is not entirely surprising, because of the minimum property of the one-determinantal energy. Since the HF method yields the absolute minimum in this case, CEDA, KLI and EXX produce slightly higher energies. Still, the corresponding energy differences do not exceed few milliHartrees (see Table 9.1). Also, the EXX total energy should be lower than the KLI and CEDA energies, since they are the lowest one-determinantal energies attainable under the constraint of a local potential. This is actually the case, if only very little, except for Ar, where the EXX solution may not have been numerically sufficiently precise. Therefore, judging from the total energy criterion, EXX, KLI, CEDA and HF orbitals appear to be close to each other.

Table 9.2 compares the HF, EXX, KLI, and CEDA energies of the frontier occupied orbitals of the molecules N_2, CO, and H_2O. There are also presented the orbital energies of the rather accurate KS exchange-correlation potentials v_{xc} obtained from the *ab initio* correlated densities by the iterative local updating scheme of van Leeuwen and Baerends (LB) [89] as well as the experimental vertical ionization potentials (VIPs) I_i [223, 224, 225]. One can see from Table 9.2, that the HOMO energies of EXX, KLI, and CEDA are close to the HF ones (close to HF $\varepsilon_{N\sigma-1}$ in the case of N_2, see below). This behavior is enforced by the fixing of the long-range asymptotics of the EXX, KLI, and CEDA potentials. In particular, in the latter case the zero asymptotics condition $w_{N\sigma N\sigma}^{\sigma} = 0$ in (9.17) enforces equality of the HOMO matrix elements for the CEDA and HF potentials

$$n_{N\sigma}\left(\bar{v}_{x\sigma,N\sigma N\sigma}^{\mathrm{CEDA}} - \bar{v}_{x\sigma,N\sigma N\sigma}^{N\sigma}\right) = w_{N\sigma N\sigma}^{\sigma} = 0 \tag{9.18}$$

which, in turn, leads to the equality of the corresponding orbital energies if calculated with the same KS orbitals $\psi_{i\sigma}^{s}$

$$\varepsilon_{N\sigma}^{\mathrm{CEDA}} = \varepsilon_{N\sigma}^{\mathrm{HF}}\left[\{\psi_{i\sigma}^{s}\}\right] \approx \varepsilon_{N\sigma}^{\mathrm{HF}}\left[\{\psi_{i\sigma}^{\mathrm{HF}}\}\right] \tag{9.19}$$

The equality analogous to (9.18) is also valid for the KLI [38] and in EXX the condition $\bar{v}_{x\sigma,N\sigma N\sigma}^{\mathrm{EXX}} = \bar{v}_{x\sigma,N\sigma N\sigma}^{N\sigma}$ is imposed on the EXX potential [32]. As was reported in Ref. [226], without such an explicit imposition EXX faces numerical problems in providing the reliable $\varepsilon_{N\sigma}$ values. Since the EXX, KLI, CEDA and HF orbitals are close to each other, the equality (9.19) explains the close correspondence of $\varepsilon_{N\sigma}$ and $\varepsilon_{N\sigma}^{\mathrm{HF}}\{\psi_i^{\mathrm{HF}}\}$ in Table 9.2. Note the curious detail that, in spite of (9.19), for certain systems the HOMOs of the HF and the exchange-only KS methods could be orbitals of different type, and this happens in the case of N_2. In this case Koopmans' theorem

System	Method	$-\varepsilon_{N_\sigma}$	$-\varepsilon_{N_\sigma-1}$	$-\varepsilon_{N_\sigma-2}$
N_2		$3\sigma_g$	$1\pi_u$	$2\sigma_u$
	KLI	17.12	18.51	20.27
	CEDA	17.05	18.46	20.14
	EXX[a]	17.16	18.12	20.23
	HF	16.69 ($1\pi_u$)	17.24 ($3\sigma_g$)	21.18
	KS	15.57	16.68	18.77
	Exp(VIP)[b]	15.58	16.93	18.75
CO		5σ	1π	4σ
	KLI	15.04	18.33	20.68
	CEDA	14.97	18.31	20.58
	EXX[a]	15.03	17.99	20.57
	HF	15.10	17.43	21.90
	KS	14.01	16.77	19.33
	Exp(VIP)[c]	14.01	16.91	19.72
H_2O		$1b_1$	$3a_1$	$1b_2$
	KLI	13.62	15.75	19.31
	CEDA	13.69	15.78	19.54
	EXX[a]	13.71	15.74	19.28
	HF	13.73	15.75	19.26
	KS	12.63	14.78	18.46
	Exp(VIP)[d]	12.62	14.74	18.55

---

[a] Ref. [32]
[b] Ref. [223]
[c] Ref. [224]
[d] Ref. [225]

Table 9.2: Comparison of the KLI, CEDA, EXX, HF, KS energies (in eV) of frontier occupied orbitals and the experimental vertical ionization potentials (VIPs). For N_2 $\varepsilon_{N\sigma}$ and $\varepsilon_{N\sigma-1}$ refer to $3\sigma_g$ and $1\pi_u$ resp. in all cases except for HF where the order of these orbitals is reversed.

fails to predict the experimentally observed ordering of the electronic states making $1\pi_u$ the HOMO in HF. EXX, KLI and CEDA improve upon HF: the (exchange-only) KS HOMOs have the proper $3\sigma_g$ type and an energy which, by virtue of (9.19), is close to the HF $3\sigma_g$ (which is in the column $\varepsilon_{N\sigma-1}$).

We also address the question of how closely the experimental VIPs can be estimated with $-\varepsilon_{i\sigma}$ values of one-electron theories, which is the issue of Koopmans' theorem [227]. One can see from Table 9.2, that the HF Koopmans' theorem overestimates consistently VIPs ($-\varepsilon_{i\sigma}^{\mathrm{HF}}$ are higher than I_i), which can be attributed to the neglect of electron relaxation in cationic states. The only exception is the abovementioned ionization from the $1\pi_u$ MO of N_2 where the wrong ordering produces underestimation of the second VIP (column $\varepsilon_{N\sigma-1}$) with the corresponding HF energy (column $\varepsilon_{N\sigma}$).

It is interesting to note, that $-\varepsilon_{i\sigma}$ values of the exchange-only KS methods provide an estimate of VIPs comparable in quality to that of the HF Koopmans' theorem. The EXX, KLI and CEDA orbital energies $-\varepsilon_{i\sigma}$, being rather close to each other, are also consistently higher than VIPs (see Table 9.2). For N_2 and CO the second VIP is better estimated with the HF Koopmans' theorem, while the EXX, KLI and CEDA $-\varepsilon_{i\sigma}$ values yield a better estimate of the third VIP. For H_2O the orbital energies of all exchange-only methods appear to be close to each other, equally overestimating VIPs. Remarkably, $-\varepsilon_{i\sigma}$ values of the accurate KS xc potential v_{xc} produce a very good estimate of VIPs with an average deviation which approaches 0.1 eV. This striking result can be explained with the analysis of the exact linear relations between the KS orbital energies and VIPs [196].

The results of this section show, that for the considered free atoms and molecules both CEDA and KLI provide very good and still relatively simple "closure approximations" to the exact exchange-only KS potential. In this case the additional off-diagonal structure of $v_{\mathrm{resp}\sigma}^{\mathrm{CEDA}}$ of Eq. (9.16) appears to be not essential, which is manifested with the close correspondence of the CEDA and KLI total and orbital energies. In particular, for the cross-product $\psi_{i\sigma}\psi_{j\sigma}^*$ of the orbitals $\psi_{i\sigma}$ and $\psi_{j\sigma}$ of different symmetry the corresponding off-diagonal step weights w_{ij}^{σ} in (9.16),(9.17) vanish because of the symmetry of the ground-state potential $v_{\mathrm{resp}\sigma}^{\mathrm{CEDA}}$. However, the incorporation of the occupied-occupied orbital mixing in $v_{\mathrm{resp}\sigma}^{\mathrm{CEDA}}$ could be essential for the molecular response properties, such as polarizabilities and hyperpolarizabilities. This will be demonstrated in the next section.

9.5 Calculations of (hyper)polarizabilities of the hydrogen chains H_n

A failure of standard LDA and GGA methods in application to the response properties of molecular chains can be illustrated for the prototype case of linear hydrogen chains H_n. They serve as a simple prototype of molecular chains with a "half-filled band" and they were extensively studied with the HF as well as with the correlated Møller-

α	H_6	H_{12}	H_{18}
LDA	72.7	210.6	367.3
BLYP	68.98	194.80	334.85
BP	69.18	196.68	339.10
PW	68.96	195.84	337.47
KLI	60.50	157.15	260.66
CEDA	59.28	149.35	244.24
HF	56.38	137.64	222.31
MP2[a]	54.16	134.00	217.42
MP4[a]	51.59	126.90	205.39
CCSDT[a]	50.54	123.63	199.65

---

[a] Ref. [228]

Table 9.3: Comparison of the LDA, GGA, KLI, CEDA, HF, MP2, MP4, and CCSDT static longitudinal polarizabilities α (in a.u.) of linear hydrogen chains H_n

Plesset (MP2 and MP4) and coupled cluster (CCSDT) approaches [228, 229]. With the H–H distances of 2 Bohr between the closest H atoms and of 3 Bohr between the neighboring H_2 units adopted in Refs. [228, 229], H_n represents weakly bounded systems with Peierls' distortion.

Table 9.3 compares the static longitudinal polarizabilities α of the hydrogen chains H_6, H_{12}, and H_{18} calculated within the finite-field approach with $v_{x\sigma}^{\text{CEDA}}$ of Eq. (9.15) with those obtained with the LDA, GGA, and HF methods. The GGA functionals considered are the exchange-correlation functional of Perdew and Wang (PW91) [5, 75, 76], the combination BP of the exchange functional of Becke [4] and the correlation functional of Perdew (P86) [6], and the combination of the same exchange functional of Becke with the correlation functional of Lee, Yang, and Parr [7]. The 6-311++G** basis of the Gaussian-type have been used for the H atoms. Comparison is also made with α values obtained in Ref. [228] with the MP2, MP4, and CCSDT methods in the 6-311G(*)* basis.

As was already established for small molecules [205] and for the considered hydrogen chains in Refs. [147, 148, 228], the HF method yields rather satisfactory α values compared to the correlated MP2, MP4, and CCSDT methods. The calculated polarizability decreases consistently with a more complete inclusion of the electron Coulomb correlation in the series HF>MP2>MP4>CCSDT, so that the CCSDT α values are lower by 10% than the HF ones in all three cases. On the other hand, LDA greatly overestimates α, the LDA error increases with the length of the chain. While for H_6 the LDA α value is 1.4 times higher than that of CCSDT, for H_{18} this ratio grows to 1.8. GGAs improve only slightly upon LDA: α values of different GGAs are very close to each other, and for H_{18} GGAs lower the LDA α only by 8%.

The orbital-dependent KLI and CEDA potentials improve dramatically upon LDA/GGAs (see Table 9.3). Still the KLI α deviates appreciably from the HF one

γ	H$_6$	H$_{12}$	H$_{18}$
LDA	102.9	1271	4172
BLYP	95.2	1079	3286
BP	93.7	1097	3397
PW	93.9	1097	3376
KLI	36.9	277.2	778.1
CEDA	34.7	209.2	468.4
HF	29.8	146.9	301.3
MP2[a]	31.2	182.3	390.8
MP4[a]	31.3	178.8	381.7

---

[a] Ref. [228]

Table 9.4: Comparison of the LDA, GGA, KLI, CEDA, HF, MP2, and MP4 static longitudinal second hyperpolarizabilities γ (in a.u.*10^{-3}) of linear hydrogen chains H$_n$

and the corresponding error increases with the chain length. While for H$_6$ KLI overestimates α by 7% compared to HF, for H$_6$ the KLI vs. HF overestimation amounts to 17%. In turn, CEDA improves upon KLI, the corresponding improvement becomes more pronounced for the longer chain. The CEDA α is 5% higher than the HF one for H$_6$ and it is 10% higher for H$_{18}$. Thus, CEDA removes 43% of the KLI vs. HF error for the longest chain considered. The CEDA error with respect to HF becomes close to the HF error with respect to MP4.

The trends observed for α become much more pronounced for the calculated static longitudinal second hyperpolarizabilities γ presented in Table 9.4. While the LDA γ is 3.2 times larger than the MP4 one (the highest correlated *ab initio* level reported in Ref. [229]) and 3.5 times larger than the HF one for H$_6$, the corresponding errors for H$_{18}$ grow to 11 and 14 times, respectively, for H$_{18}$. The GGA errors with $\gamma^{\mathrm{GGA}}/\gamma^{\mathrm{MP4}} \approx 9$ and $\gamma^{\mathrm{GGA}}/\gamma^{\mathrm{HF}} \approx 11$ for H$_{18}$ are still extremely large. The KLI performs much better with $\gamma^{\mathrm{KLI}}/\gamma^{\mathrm{HF}} = 1.24$ for H$_6$, while for H$_{18}$ the KLI error is still considerable, $\gamma^{\mathrm{KLI}}/\gamma^{\mathrm{HF}} = 2.58$. In turn, CEDA improves considerably upon KLI with $\gamma^{\mathrm{CEDA}}/\gamma^{\mathrm{HF}} = 1.16$ for H$_6$ and $\gamma^{\mathrm{CEDA}}/\gamma^{\mathrm{HF}} = 1.55$ for H$_{18}$. Thus, CEDA with its additional off-diagonal structure brings the calculated DFT α and γ values rather close to the *ab initio* ones.

The LDA/GGA α and γ errors for molecular chains are much larger than the corresponding errors for "standard molecules", for which LDA/GGAs also tend to overestimate (hyper)polarizabilities. In the latter case this is attributed to the fact, that (judging from the LDA/GGA orbital energies) the LDA/GGA xc potentials are not attractive enough. Apparently, for molecular chains another electronic factor plays a major role. This factor, as was established in Refs. [148, 149], is a characteristic ultra-nonlocal term induced in the KS exchange and exchange-correlation potentials by an applied uniform electric field, which spans the entire system and counteracts the field. LDA and standard GGAs all fail to produce the counteracting potential, while

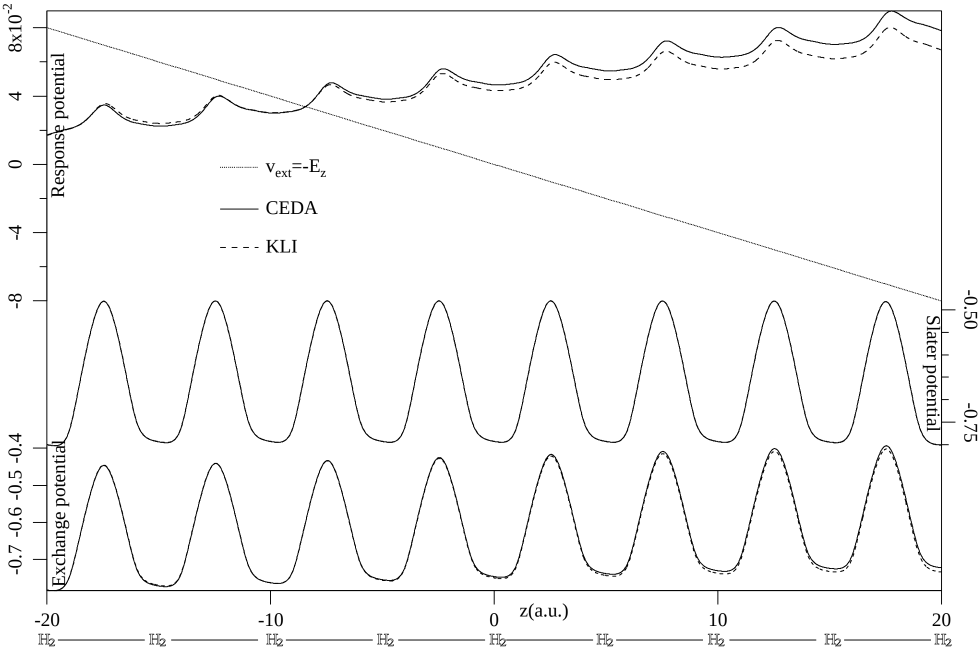

Figure 9.1: The CEDA (drawn line) and the KLI (broken line) total exchange potential (bottom) and the response (top) and Slater (middle) components are plotted along the main axis for the chain H_{18} in an electric field of 0.004 a.u. (the external field-induced potential is displayed with a dotted line in the panel of the response components).

it is generated in the orbital-dependent KLI and CEDA potentials, more precisely, in their response parts. This field-counteracting behavior of the KLI and CEDA potentials is illustrated with Figure 9.1, which display $v_{x\sigma}^{\mathrm{CEDA}}$ and $v_{x\sigma}^{\mathrm{KLI}}$ together with their Slater and response components calculated for the chain H_{18} in an electric field of 0.004 a.u. (the dotted line in Figure 9.1 indicates the external field-induced potential). The KLI and CEDA Slater potentials in Figure 9.1 coincide with each other and they remain the same at both up-field and down-field ends of the hydrogen chain, so that they exhibit only periodical variations which characterize individual H_2 units. Unlike to this, the KLI and CEDA response potentials $v_{\mathrm{resp}\sigma}^{\mathrm{CEDA}}$ and $v_{\mathrm{resp}\sigma}^{\mathrm{KLI}}$ counteract the external field-induced potential, i.e. they become more positive at the down-field end of H_{18}. This determines the overall field-counteracting effect of $v_{x\sigma}^{\mathrm{CEDA}}$and $v_{x\sigma}^{\mathrm{KLI}}$. From the upper part of Figure 9.1, one can clearly see that CEDA develops a larger field-counteracting response potential than KLI.

This can be understood qualitatively from the expression for a linear response $\delta v_{\mathrm{resp}\sigma}^{\mathrm{CEDA}}$ of the potential (9.16) due to an applied external field δv_{ext} inducing a change in the density $\delta\rho_\sigma$

$$\begin{aligned}\delta v^{\mathrm{CEDA}}_{\mathrm{resp}\sigma}(\mathbf{r}_1) &= \int \frac{\delta v^{\mathrm{CEDA}}_{\mathrm{resp}\sigma}(\mathbf{r}_1)}{\delta\rho_\sigma(\mathbf{r}_2)}\delta\rho_\sigma(\mathbf{r}_2)\,d\mathbf{r}_2 \\ &= \sum_i^{N_\sigma-1} \frac{\left|\psi_{i\sigma}(\mathbf{r}_1)\right|^2}{\rho_\sigma(\mathbf{r}_1)} \int \frac{\delta w^\sigma_{ii}}{\delta\rho_\sigma(\mathbf{r}_2)}\delta\rho_\sigma(\mathbf{r}_2)\,d\mathbf{r}_2 \\ &\quad + \sum_i^{N_\sigma-1} w^\sigma_{ii} \int \frac{\delta}{\delta\rho_\sigma(\mathbf{r}_2)}\left[\frac{\left|\psi_{i\sigma}(\mathbf{r}_1)\right|^2}{\rho_\sigma(\mathbf{r}_1)}\right]\delta\rho_\sigma(\mathbf{r}_2)\,d\mathbf{r}_2 \\ &\quad + \sum_{i,j\neq i}^{N_\sigma} w^\sigma_{ij} \int \frac{\delta}{\delta\rho_\sigma(\mathbf{r}_2)}\left[\frac{\psi_{i\sigma}(\mathbf{r}_1)\,\psi^*_{j\sigma}(\mathbf{r}_1)}{\rho_\sigma(\mathbf{r}_1)}\right]\delta\rho_\sigma(\mathbf{r}_2)\,d\mathbf{r}_2 \\ &\quad + \sum_{i,j\neq i}^{N_\sigma} \frac{\psi_{i\sigma}(\mathbf{r}_1)\,\psi^*_{j\sigma}(\mathbf{r}_1)}{\rho_\sigma(\mathbf{r}_1)} \int \frac{\delta w^\sigma_{ij}}{\delta\rho_\sigma(\mathbf{r}_2)}\delta\rho_\sigma(\mathbf{r}_2)\,d\mathbf{r}_2\end{aligned} \tag{9.20}$$

An analogous change of the KLI potential $\delta v^{\mathrm{KLI}}_{\mathrm{resp}\sigma}$ can be expressed formally with the first two sums of (9.20), while the third and the fourth sums represent the change of the "off-diagonal steps" specific for $v^{\mathrm{CEDA}}_{\mathrm{resp}\sigma}$. Let us consider now the case of a symmetric molecular chain X$_n$, which (just as the hydrogen chains H$_n$) has a mid-molecule center of inversion or a mirror plane (or both) as the symmetry element, to which an antisymmetric external field $\delta v_{\mathrm{ext}}(\mathbf{r}_1) = -Ez$ is applied (z is the main symmetry axis of the chain, with $z = 0$ being the molecular midpoint). Then, the field-counteracting exchange effect should manifest itself in the appearance of the term $\delta v^{(\mathrm{fc})}_{\mathrm{resp}\sigma}$ in (9.20), which counters $\delta v_{\mathrm{ext}}(\mathbf{r}_1)$, i.e. it should be an antisymmetric function of z.

It is clear, that the first sum of (9.20) does not contribute to $\delta v^{(\mathrm{fc})}_{\mathrm{resp}\sigma}$, since all its orbital-density terms $\left|\psi_{i\sigma}(\mathbf{r}_1)\right|^2/\rho_\sigma(\mathbf{r}_1)$ are symmetric functions of z. As was shown in Refs. [40, 149], a common contribution for both KLI and CEDA to $\delta v^{(\mathrm{fc})}_{\mathrm{resp}\sigma}$ comes from the second sum of (9.20). In the third sum, as was already mentioned in the previous section, the off-diagonal weights w^σ_{ij} for the orbitals $\psi_{i\sigma}$ and $\psi_{j\sigma}$ of different symmetry are zero due to the symmetry, but the corresponding derivatives $\delta w^\sigma_{ij}/\delta\rho_\sigma(\mathbf{r}_2)$ in the fourth sum of (9.20) will be, in general, non-zero functions of $\mathbf{r}_2$. Thus, this latter sum is expected to be responsible for the observed additional build-up of the field-counteracting CEDA potential as compared to KLI. Its spatial form as an antisymmetric function of $\mathbf{r}_1$ is determined with the occupied-occupied products $\psi_{i\sigma}(\mathbf{r}_1)\psi^*_{j\sigma}(\mathbf{r}_1)$ of orbitals of the appropriate symmetry.

The established field-counteracting terms of the CEDA and KLI exchange potentials effectively compensate an external field-induced potential. The LDA and standard GGA potentials all lack the above-mentioned orbital structure and, in the absence of the compensation effect, they produce the observed dramatic overestimation of (hyper)polarizabilities of molecular chains. Contrary to this, both CEDA and

KLI benefit from the field-counteracting compensation effect, which greatly reduces the calculated (hyper)polarizability. Due to the additional off-diagonal orbital structure and the additional build-up of the field-counteracting potential, CEDA improves considerably upon KLI.

9.6 Conclusions

In this chapter an approximate KS exchange potential $v_{x\sigma}^{\mathrm{CEDA}}$ is developed, based on the common energy denominator approximation (CEDA) for the static orbital Green's function, which preserves the essential orbital structure of the density response function. $v_{x\sigma}^{\mathrm{CEDA}}$ is an explicit functional of the occupied KS orbitals, which has the Slater $v_{S\sigma}$ and response $v_{\mathrm{resp}\sigma}^{\mathrm{CEDA}}$ potentials as its components. The latter potential exhibits the characteristic step structure produced by the orbital densities $|\psi_{i\sigma}|^2$, similar to that of the KLI potential. In addition, due to the complete exclusion of the occupied-occupied orbital mixing from the CEDA density response function, $v_{\mathrm{resp}\sigma}^{\mathrm{CEDA}}$ contains also "off-diagonal steps" produced by the orbital cross-products $\psi_{i\sigma}\psi_{j(\neq i)\sigma}^{*}$.

Comparison of the results of atomic and molecular ground-state CEDA, KLI, EXX, and HF calculations show, that both KLI and CEDA potentials can be considered as very good analytical "closure approximations" to the exact KS exchange potential. The total CEDA and KLI energies nearly coincide with the EXX ones and the corresponding orbital energies are rather close to each other for the light atoms and small molecules considered. The CEDA, KLI, EXX $-\varepsilon_{i\sigma}$ values provide the qualitatively correct order of ionizations and they give an estimate of VIPs comparable to that of the HF Koopmans' theorem.

The additional off-diagonal orbital structure of the CEDA potential appears to be essential for the calculated response properties of molecular chains. CEDA and KLI greatly improve the calculated (hyper)polarizabilities of the hydrogen chains H_n upon LDA and standard GGAs, with the CEDA results being definitely better than the KLI ones. The reason of this success are the specific orbital structures of the CEDA and KLI response potentials, which produce in an external field an ultra-nonlocal field-counteracting exchange potential.

With this, CEDA holds promise for the calculation of molecular response properties. Furthermore, the present CEDA can serve as a basis for simpler approximations which, nevertheless, would retain its orbital structure. An important further development would also be an extension of the present exchange-only CEDA to a full exchange-correlation theory. Since CEDA appears to recover to high accuracy the counteracting field in the KS potential in as much as it originates in the exchange part of the potential, the remaining deficiency for the calculated hyperpolarizability is probably due to the neglect of the counteracting field effect embodied in the KS correlation potential. One consistent way to include correlation effects is the extension of CEDA (which in this chapter operates with n_σ occupied KS orbitals) to the general case $M_\sigma \geq n_\sigma$ with both occupied and unoccupied KS orbitals (Chapt. 5).

Summary and concluding remarks

The Kohn-Sham (KS) approach to density functional theory (DFT) is a very efficient tool in theoretical chemistry, but its success in making predictions and interpreting chemical data relies on the approximation for the exchange and correlation functional. The latter has to account for the correlation effects due to the interactions between electrons that are neglected in the "noninteracting particles" picture.

The standard generalized gradient approximations (GGAs) are quite successful, often providing, in spite of their simplicity, a remarkable accuracy. Nevertheless, beside the many successful calculations, there are still cases reported in the literature which are clearly problematic for DFT at this level of approximation.

In this thesis a number of these "problematic" cases have been considered, the reasons for the failure of the GGAs have been analyzed and possible improvements have been tested. Two alternatives have been explored, either to remain within the GGAs or to develop functionals explicitly dependent on the KS orbitals.

The first part of this thesis has been dedicated to the problem of the approximation of the exchange and correlation energy functional in relation to chemical reactions and molecular dissociation processes.

The problematic case of the prototype system with two-center three-electron bond He_2^+, for which the GGAs overestimate the dissociation energy by 25–30 kcal/mol, has been analyzed in Chapt. 3 comparing the approximate with the accurate KS results. It emerges that the major restriction of GGA energy functionals is the localized nature of their exchange and correlation hole. This restriction turns out to be an advantage in the case of covalent bond systems that are efficiently described by GGAs: the approximated exchange takes into account both exchange and nondynamical correlation effects while the approximated correlation covers the dynamical part of correlation. For He_2^+ instead, the occupation of the valence orbital with antibonding character hampers the nondynamical correlation effects and the GGA exchange produces spurious nondynamical correlation. This result can be generalized for all systems with weak nondynamical correlation, such systems can be recognized by the non-integer ratio between the number of electrons involved in a bond and the number of centers on which the bond is delocalized. In fact as has been established in Chapt. 4, the main argument of gradient corrections to the local density approximation functional, the dimensionless gradient argument s_σ^2, presents in the bonding region of these systems local maxima that can be traced back to the orbital structure of the bond (for comparison s_σ^2 is practically zero in the bonding region of strong covalent systems like N_2). To this local enhancement of s_σ^2 has been attributed the built-in of spurious correlation and therefore the overestimation of the stability of these molecular systems.

The performance of several meta-GGAs and "modified" GGAs has been then assessed (Chaps. 4 and 3) for those systems that are, following our analysis, problematic for standard GGAs. In particular the dissociation of He_2^+, $(HF)_2^+$, $(H_2O)_2^+$, $(NH_3)_2^+$ and the central barrier of the symmetrical S_N2 reactions have been considered. The differences between these functionals and the standard GGAs have been also discussed in those chapters.

The "modified" GGA exchange functionals differ from the "standard" GGAs because they do not satisfy the uniform gas limit and instead they reduce in the zero gradient limit to the $X\alpha$ exchange with α that enhances the LDA exchange by a factor $\sim$1.05. Moreover for values of the gradient argument s_σ between 0 and 1, typical for the bonding region of molecules, they have a s_σ^4 main gradient correction versus s_σ^2 of the "standard" functionals. For this reason they are less sensitive to the local maxima of s_σ^2 in the bonding region of problematic systems.

The meta-GGAs depend, as well as on the spin densities and their gradients, on the kinetic energy density of KS orbitals. The latter can help to detect where the localized description of the exchange and correlation hole might fail. In particular, as pointed out in Chapt. 4, the ratio of the LDA and KS kinetic energy density, employed in several meta-GGAs, has a dominant $1/s_\sigma^2$ behavior and can therefore reduce the overestimation coming from local maxima of s_σ^2 in the bonding regions of problematic systems.

As a matter of fact both the meta-GGAs and the GGAs improve the results for the central barrier of symmetrical S_N2 reactions and for the dissociation energy of bifragmental radical cations with two-center three-electron bond. For the S_N2 reactions in particular the combination of the optimal exchange (OPTX) functional[1] and the LAP3 correlation functional[2] provides rather good results: the calculated central barriers differ on average only by 1 kcal/mol from reference data, while the difference for the standard GGA is on average 7 kcal/mol. On the other hand, for the dissociation energy of the two-center three-electron bond the meta-GGAs and the modified GGAs lower the error by 5–10%, but the difference with respect to reference data remains rather large.

Furthermore in Chapt. 4 GGAs and meta-GGAs with improved correlation functionals with the parallel and opposite spin correlation modeled separately have been

---

[1] N.C. Handy and A.J. Cohen, Mol. Phys. **99** (2001) 403

[2] E.I. Proynov, S. Sirois, and D.R. Salahub, Intern. J. Quantum Chem. **64** (1997) 427

shown to provide rather good results for reaction barrier of hydrogen abstraction and hydrogen exchange reactions. Again the combination of OPTX and LAP3 provides the best results with a mean absolute error of about 3 kcal/mol on the energy barriers.

The GGA, in its spin restricted form, fails also to describe the extreme nondynamical correlation in the dissociating electron pair bond. In this case the approximated exchange hole (that should cover also nondynamical correlation effects) is too shallow to describe the strong left-right correlation as has been discussed in Chapt. 5.

In the same chapter the entire potential curve of H_2 has been very well reproduced by self-consistent KS DFT calculations using the exchange-correlation functional proposed by Buijse and Baerends[3]. The latter describes correctly the dissociation limit of the H_2 molecule employing both the bonding highest occupied and the antibonding lowest unoccupied molecular orbitals. For finite bond distances the effective weights, or “fictitious occupation numbers”, of occupied and virtual orbitals (virtual orbitals other than the lowest unoccupied molecular orbital have been included in order to simulate dynamical correlation effects) have been calculated with a two parameters Fermi-type distribution depending on the KS orbital energies. The two parameters however have been fitted to reproduce the H_2 potential curve and therefore are far from being “universal”; in the future a better guess for the “fictitious occupation numbers” has to be found that takes into account not only the relative energies, but also the spatial localization of the molecular orbitals.

The bottleneck in the construction of a “universal” functional is thus the modeling of the nondynamical correlation effects. In fact while the exchange can be calculated from the exact orbital expression and the dynamical part is efficiently and rather accurately approximated by the GGA or meta-GGA correlation functionals, there is still no functional that is able to describe both the strong left-right correlation of dissociating electron pair bonds and the absence of/weak nondynamical correlation in systems like He_2^+. Future works should therefore study how to model such effects possibly using, as suggested by the results of this work, the information from both occupied and virtual orbitals.

The second part of this thesis has been dedicated to the xc potential. The xc potentials derived from GGA energy functionals suffer, as discussed in Chapts. 7 and 8, of two main shortcomings. First in the bulk region they are systematically too repulsive and the energies of the valence orbitals, in particular of the highest occupied molecular orbital that for a potential with a zero asymptotic should be equal to minus the first vertical ionization potential, are underestimated (in absolute value). The generalized gradient approximations in fact underestimate the first ionization potential by 3–6 eV. This error influences the energy differences, in particular between valence and highlying orbital energies close to zero energy. As a consequence, excitation energies, given at the zero order by orbital energies differences, to Rydberg states are also underestimated by 2–5 eV. Second the GGAs do not have the correct asymptotic behavior, but decay too rapidly being too repulsive also in the outer region.

---

[3] Molec. Phys. **100** (2002) 401; Phys. Rev. Lett. **87** (2001) 133004

This affects mainly the oscillator strengths of Rydberg states that are systematically underestimated. The distortions of excitation spectra calculated with GGAs have been shown in Chapt. 8 for the dipole allowed excitations of the N_2 molecule. The Rydberg states are artificially stabilized with respect to the valence states and the calculated excitation spectra show, under 15 eV, 25 "spurious" Rydberg states. The excitation energy of the valence states are in general in quite good agreement with the experiment, but their orbital composition can be wrong due to the mixing with the "spurious" transition to the Rydberg states. Moreover the oscillator strengths of the Rydberg states are underestimated by 1 or 2 orders of magnitude. This example makes clear that DFT at this level of approximation is not an adequate tool for reproducing and interpreting molecular excitation spectra.

In this thesis a scheme has been proposed to correct both shortcomings of the approximated potentials. The original GGA potential is shifted in the bulk in order to satisfy the equality between minus the highest occupied molecular orbital and the first vertical ionization potential, in the outer region a potential is employed that provides the correct Coulomb decay. The connection between the shifted GGA potential in the bulk and the potential with the correct asymptotic decay is regulated by the gradient of the density. This consistent DFT scheme has been applied to the combination of Becke (B) exchange and Perdew (P) correlation potentials, corrected with the potential of van Leeuwen and Baerends[4], to calculate the excitation spectra of small and organic molecules. Like other asymptotic corrected potential proposed in the literature[5], the gradient regulated asymptotic corrected (GRAC) BP potential improves substantially the results for Rydberg excitations energies and oscillator strengths and on the whole it reproduces quantitatively and qualitatively the experimental molecular excitation spectra. The quality of the results for these molecules is comparable to the quality one can obtain with the exchange-correlation potential constructed as statistical average of orbital model potentials[6] (SAOP).

Both the GRAC-BP and SAOP potentials have been tested for the static average polarizability and related quantities for 21 small molecules demonstrating that the improvement in the description of the spectra leads to an improvement of the static average polarizability and a substantial improvement of the second Cauchy coefficient (related to the frequency dispersion of the polarizability) and of the static average hyperpolarizability.

These approximations for the exchange-correlation potential can then be recommended for calculating excitation energies and response properties of small and organic molecules. The main disadvantage of the GRAC scheme is that the first vertical ionization potential has to be given as a input in order to shift the potential in the bulk, while the SAOP, due to its orbital structure provides by itself a good estimate of the first vertical ionization potential (mean absolute error ~ 0.4 eV). Further tests are needed to assess the performance of these potentials, for example for response properties of transition metals and transition metal complexes.

---

[4] Phys. Rev. A, **49** (1994) 2421

[5] J. Chem. Phys. **108** (1998) 4439; J. Chem. Phys. **109** (1998) 10180

[6] J. Chem. Phys. **112** (2000) 1344

The problem of the response of the exchange-correlation potential to an external field for molecular chains has been finally considered. The exact exchange-correlation potential has a linear term counteracting the external field. The generalized gradient approximation exchange-correlation potentials miss this term and as a consequence they overestimate badly the polarizability of extended systems such as molecular chains. For the prototype hydrogen chain H_{18} for example, as has been shown in Chapt. 9, the hyperpolarizability calculated with the GGA is one order of magnitude larger than with accurate *ab initio* methods. A term counteracting the external field, instead, is present in the approximated exchange potential proposed by Krieger, Li and Iafrate[7] (KLI). In particular the counteracting term comes from the orbital structure of its response part. This potential improves the results for the polarizability and hyperpolarizability of the H_{2n} molecular chains, but still the hyperpolarizability of H_{18} is overestimated by a factor 3 with respect to Hartree-Fock calculations. In this thesis the calculations of the polarizability and hyperpolarizability of the H_{2n} molecular chains have been repeated with the orbital-dependent exchange potential constructed with the common energy denominator approximation (CEDA) for the Green function of the KS system. This potential shares with the KLI potential the exchange hole (or Slater) potential, but the response part has an additional orbital structure containing not only orbital densities, but also off-diagonal orbital products. This additional structure contributes to the counteracting term removing 43% of the error of the KLI potential (versus Hartree-Fock).

To conclude, the cases studied in this thesis suggest that though it is possible to construct improved functionals within the GGA, a real qualitative and quantitative breakthrough is possible only considering explicitly the dependence on KS orbitals.

---

[7] Phys. Rev. A **45** (1992) 101

Samenvatting

Dichtheidsfunctionaaltheorie met verbeterde gradiënt- en orbitaal-afhankelijke functionalen

Het Kohn-Sham (KS) formalisme van de dichtheidsfunctionaaltheorie is een zeer efficiënt werktuig in de theoretische chemie, maar zijn succes in het voorspellen en interpreteren van resultaten uit chemische experimenten hangt af van de benadering van de exchange-correlatie (xc) functionaal. Deze functionaal zou de correlatie effecten (ten gevolge van interactie tussen elektronen) moeten reproduceren, welke in het onafhankelijke deeltjes model verwaarloosd worden.

De standaard gegeneraliseerde gradiënt benaderingen (GGA) zijn vrij succesvol en vaak geven ze nauwkeurige resultaten ondanks hun eenvoud. Toch zijn er, naast vele succesvolle berekeningen, gevallen bekend die duidelijk problematisch zijn voor DFT op het benaderingsniveau van GGA's.

In dit proefschrift zijn een aantal van deze probleemgevallen beschouwd, de oorzaken voor de mislukkingen zijn onderzocht en mogelijke verbeteringen zijn voorgesteld en getest. Twee opties zijn onderzocht, namelijk het aanbrengen van verbeteringen op het niveau van GGA's en het ontwikkelen van functionalen die expliciet afhankelijk zijn van KS orbitalen.

Het eerste deel van dit proefschrift is gewijd aan het probleem van de benadering van de xc energiefunctionaal voor chemische reacties en moleculaire dissociaties.

Het probleemgeval van het prototype systeem met twee-centra drie-elektronen binding He_2^+, waarvoor de GGA aanpak de dissociatie-energie overschat met 25–30 kcal/mol, is geanalyseerd in Hoofdstuk 3 met een vergelijking tussen de benaderde en zeer nauwkeurige KS resultaten.

Het blijkt dat de grootste beperking van de GGA energiefunctionalen het lokale karakter van het xc "hole" is. Deze beperking blijkt een voordeel te zijn in het geval van moleculen met een covalente binding die efficiënt beschreven wordt door de GGA's: de benaderde exchange omvat zowel de exchange als de niet-dynamische correlatie, terwijl de benaderde correlatie de dynamische correlatie weergeeft. Daarentegen geldt voor He_2^+ dat de bezetting van de valentie-orbitaal met anti-bindend karakter de niet-dynamische effecten tegenwerkt, waardoor de GGA valse niet-dynamische correlatie produceert. Dit resultaat kan worden gegeneraliseerd voor alle systemen met zwakke niet-dynamische correlatie. Deze systemen kunnen herkend worden aan de niet-gehele verhouding tussen het aantal elektronen die bij de binding betrokken zijn en het aantal centra waarover de binding is gedelokaliseerd. Zoals bewezen is in Hoofdstuk 4, heeft de belangrijkste variabele van de gradiënt correcties op de functionaal van de lokale dichtheid benadering (local density approximation, LDA), de dimensieloze variabele s_σ^2, lokale maxima in het gebied van de binding van deze moleculen. Deze lokale maxima kunnen worden herleid tot de orbitaalstructuur van de binding (ter vergelijking, s_σ^2 is bijna nul in het gebied van de binding van het sterk covalent gebonden molecuul N_2). De valse niet-dynamische correlatie en de hiermee samenhangende overschatting van de stabiliteit van deze systemen is toegeschreven aan de lokale maxima van s_σ^2.

De prestaties van verschillende meta-GGA's en gemodificeerde GGA's zijn getest (Hoofdstukken 3 en 4) voor de moleculen die volgens onze analyse problematisch zijn voor standaard GGA's. Met name de dissociatie van He_2^+, $(HF)_2^+$, $(H_2O)_2^+$, $(NH_3)_2^+$ en de centrale overgangsbarrière van de bimoleculaire nucleofiele substitutie reacties (S_N2) zijn beschouwd. De verschillen tussen deze functionalen en de standaard GGA's zijn ook behandeld in deze hoofdstukken.

De gemodificeerde GGA exchange functionalen verschillen van de standaard GGA, omdat ze niet voldoen aan de uniforme gas limiet. In de limiet dat de gradiënt naar nul gaat, worden ze gelijk aan $X\alpha$ exchange met α zó dat het de LDA met een factor 1.05 verhoogt. Verder is voor waarden van s_σ tussen 0 en 1, typisch voor het gebied van de binding in moleculen, de belangrijkste gradiënt correctie van de gemodificeerde GGA's s_σ^4 in plaats van de s_σ^2 van de "standaard" functionalen. Hierdoor zijn ze minder gevoelig voor de lokale maxima van s_σ^2 in het gebied van de binding in de problematische systemen.

De meta-GGA's zijn, behalve afhankelijk van de spindichtheid en de gradiënten hiervan, ook afhankelijk van de kinetische energiedichtheid van de KS orbitalen. De kinetische energiedichtheid helpt om de gevallen op te sporen waarin de gelokaliseerde beschrijving van het exchange-correlatie "hole" fout kan zijn. In het bijzonder, zoals opgemerkt in Hoofdstuk 4, heeft de verhouding tussen de LDA en KS kinetische energiedichtheid, die gebruikt wordt in verschillende meta-GGA's, een dominant $1/s_\sigma^2$ gedrag. Daarom vermindert deze variabele de overschatting die veroorzaakt wordt door de lokale maxima van s_σ^2 in het gebied van de binding in de problematische systemen.

Feitelijk verbeteren zowel meta-GGA's als GGA's de resultaten voor de centrale overgangsbarrière van S_N2 reacties en voor de dissociatie energie van moleculen met een twee-centra drie-elektronen binding. Met name de combinatie van de "optimal exchange" (OPTX) functionaal[1] en de LAP3 correlatie functionaal[2] geeft vrij goede resultaten voor de S_N2 reacties. De berekende overgangsbarrière wijkt gemiddeld slechts 1 kcal/mol van de referentie data af, terwijl dit verschil voor de GGA gemiddeld 7 kcal/mol is. Aan de andere kant, voor de dissociatie energie van moleculen met een twee-centra drie-elektronen binding verlagen de meta-GGA's en gemodificeerde GGA's de fout met 5–10%, maar het verschil ten opzichte van de referentie data blijft groot.

Bovendien is gebleken in Hoofdstuk 4 dat GGA's en meta-GGA's met verbeterde correlatie functionalen die parallele en tegengestelde spin correlatie afzonderlijk behandelen, goede resultaten leveren voor de overgangsbarrière van waterstof abstractie en waterstof uitwisselingreacties. Nogmaals geeft de combinatie van LAP3 en OPTX het beste resultaat met een gemiddelde absolute fout van ongeveer 3 kcal/mol op de overgangsbarrière.

De GGA, in de "spin restricted" variant, kan niet goed de extreme niet-dynamische correlatie in de dissocierende elektronen-paar binding beschrijven. In dit geval is het benaderde exchange "hole" (dat ook de niet-dynamische correlatie-effecten zou moeten omvatten) te ondiep om de sterke links-rechts correlatie te beschrijven zoals besproken is in Hoofdstuk 5.

In hetzelfde hoofdstuk is de potentiaalcurve erg goed weergegeven door zelfconsistente KS DFT berekeningen die gebruik maken van de Buijse-Baerends[3] xc functionaal. Deze functionaal beschrijft goed de dissociatielimiet van het H_2 molecuul gebruikmakend van zowel de hoogste bezette bindende als de laagste onbezette antibindende moleculaire orbitalen. De effectieve gewichten, of "fictieve bezettingsgetallen", van de bezette en onbezette orbitalen (onbezette orbitalen anders dan de laagste onbezette orbitaal zijn inbegrepen om dynamische correlatie-effecten te simuleren) zijn berekend voor eindige afstanden met een twee-parameters Fermi-type verdeling afhankelijk van de KS orbitaalenergie. De twee parameters zijn desondanks aangepast om de H_2 potentiaal curve te reproduceren en zijn daarom niet universeel. In de toekomst zal men een betere schatting voor de fictieve bezetting moeten vinden die niet alleen rekening houdt met de relatieve energieën, maar ook met de ruimtelijke lokalisering van moleculaire orbitalen.

Het knelpunt in de opbouw van een "universele" functionaal is dus het modeleren van de niet-dynamische correlatie-effecten. Hoewel de exchange berekend kan worden uit de exacte orbitaal uitdrukking en het dynamische deel efficiënt en nauwkeurig benaderd wordt door de GGA of meta-GGA correlatiefunctionalen, is er nog steeds geen functionaal die in staat is om zowel de sterke links-rechts correlatie van de dissociërende elektronen-paar binding, als het gebrek aan (of zwakke) niet-dynamische correlatie zoals in systemen als He_2^+ te beschrijven. In toekomstig werk zou men dus moeten onderzoeken hoe deze effecten te modeleren, mogelijk met gebruik van de informatie uit èn de bezette èn de virtuele orbitalen, zoals gesuggereerd wordt door de resultaten van dit proefschrift.

---

[1] N.C. Handy and A.J. Cohen, Mol. Phys. **99** (2001) 403

[2] E.I. Proynov, S. Sirois, and D.R. Salahub, Intern. J. Quantum Chem. **64** (1997) 427

[3] Molec. Phys. **100** (2002) 401; Phys. Rev. Lett. **87** (2001) 133004

Het tweede deel van dit proefschrift is besteed aan de xc potentiaal. De xc potentialen, die afgeleid zijn van de GGA energiefunctionalen zoals behandeld in Hoofdstukken 7 en 8, lijden aan twee belangrijke tekortkomingen. Ten eerste zijn ze in het bulk gebied systematisch te repulsief en de energieën van valentie-orbitalen worden onderschat, met name van de hoogste bezette orbitaal die, voor een potentiaal die asymptotisch naar nul gaat, minus de eerste verticale ionisatie-energie zou moeten zijn. De GGA's onderschatten inderdaad de eerste verticale ionisatiepotentiaal met 3–6 eV. Deze fout beïnvloedt de energie verschillen, in het bijzonder die tussen valentie- en hoogliggende orbitalen met energieën dichtbij nul. Dientengevolge worden excitatie energieën, die in de nulde orde gegeven worden door de energieverschillen, naar Rydberg toestanden ook onderschat met 2–5 eV. Ten tweede hebben de GGA's een verkeerd asymptotisch gedrag: ze vallen te snel af en ze zijn, ook in het buitengebied, te repulsief. Dit heeft grote invloed op oscillatorsterktes van Rydberg toestanden, die hierdoor systematisch onderschat worden. De vervormingen van de excitatiespectra die berekend zijn met GGA's zijn beschouwd in Hoofdstuk 8 voor de dipool toegestane excitatie van het N_2 molecuul. De Rydberg toestanden worden kunstmatig te stabiel ten opzichte van de valentietoestanden en de berekende excitatiespectra vertonen onder de 15 eV 25 valse Rydberg toestanden. De excitatie-energieën van de valentietoestanden komen in het algemeen vrij goed overeen met het experiment, hoewel de orbitaalsamenstelling verkeerd kan zijn door het mengen met de overgangen naar de valse Rydberg toestanden. Bovendien worden de oscillatorsterktes onderschat met een factor tien tot honderd. Dit voorbeeld maakt duidelijk dat DFT op dit benaderingsniveau niet een geschikt werktuig is om excitatiespectra te reproduceren en interpreteren.

In dit proefschrift is een schema voorgesteld om beide tekortkomingen van de benaderde potentialen te corrigeren. De originele GGA potentiaal wordt verschoven in de bulk om te voldoen aan de gelijkheid tussen de eerste verticale ionisatiepotentiaal en minus de hoogste bezette moleculaire orbitaal, terwijl in het buitengebied een potentiaal wordt gebruikt die het correcte Coulombische verval geeft. De verbinding tussen de verschoven GGA potentiaal in de bulk en de potentiaal met het correcte asymptotisch gedrag wordt geregeld door de gradiënt van de dichtheid. Dit consequente DFT schema is toegepast op de combinatie van Becke (B) exchange- en Perdew (P) correlatiepotentialen, gecorrigeerd met de potentiaal van Van Leeuwen en Baerends[4], om de excitatiespectra van kleine organische moleculen te berekenen. Net zoals asymptotisch gecorrigeerde potentialen uit de literatuur[5], verbetert de gradiënt gereguleerde asymptotisch gecorrigeerde (GRAC) BP potentiaal substantiëel de resultaten voor Rydberg excitatie-energieën en oscillatorsterktes. Alles bij elkaar reproduceert deze potentiaal kwantitatief en kwalitatief de experimentele moleculaire excitatiespectra. De kwaliteit van de resultaten is vergelijkbaar met de kwaliteit die men kan bereiken met de xc potentiaal die opgebouwd is als statistisch gemiddelde van orbitaal-modelpotentialen[6] (SAOP).

---

[4] Phys. Rev. A, **49** (1994) 2421

[5] J. Chem. Phys. **108** (1998) 4439; J. Chem. Phys. **109** (1998) 10180

[6] J. Chem. Phys. **112** (2000) 1344

De GRAC-BP en SAOP potentialen zijn beide gebruikt om de statische gemiddelde polariseerbaarheid en gerelateerde grootheden voor 21 kleine moleculen uit te rekenen. De resultaten tonen aan dat een verbetering in de beschrijving van de excitatiespectra leidt tot een verbetering van de statische gemiddelde polariseerbaarheid en een aanzienlijke verbetering van de tweede Cauchy coëfficiënt, die gerelateerd is aan de frequentie-afhankelijkheid van de polariseerbaarheid, en van de statische gemiddelde hyperpolariseerbaarheid.

Deze benaderingen van de xc potentiaal worden aanbevolen om excitatiespectra en responseigenschappen te berekenen van kleine en organische moleculen. Het grootste nadeel van het GRAC schema is dat de verticale ionisatiepotentiaal als input gegeven moet worden voor de verschuiving in het bulk gebied, terwijl SAOP, vanwege zijn orbitaalstructuur, op zichzelf al een goede schatting geeft van de verticale ionisatiepotentiaal (gemiddelde absolute fout ~ 0.4 eV). Verdere tests zijn nodig om de werking van deze potentialen te onderzoeken, bijvoorbeeld op het gebied van responseigenschappen van overgangsmetalen en overgangsmetaalcomplexen.

Ten slotte is het probleem van de respons van de xc potentiaal op een extern veld voor moleculaire ketens beschouwd. De exacte xc potentiaal heeft een lineaire term die het externe veld tegenwerkt. De GGA xc potentialen missen deze term en overschatten daarom aanzienlijk de polariseerbaarheid van uitgebreide systemen zoals moleculaire ketens. Zoals aangetoond in Hoofdstuk 9 voor bijvoorbeeld de prototype waterstofketen H_{18}, is de hyperpolariseerbaarheid die berekend is met de GGA, een factor tien groter dan die berekend met nauwkeurige *ab initio* methodes. Een term die het externe veld tegenwerkt is daarentegen wel aanwezig in de benaderde exchange potentiaal die voorgesteld is door Krieger, Li en Iafrate[7] (KLI). Met name de term die het elektrische veld tegenwerkt, komt uit het respons deel van zijn orbitaalstructuur. Deze potentiaal verbetert de resultaten voor de polariseerbaarheid en de hyperpolariseerbaarheid van de H_{2n} moleculaire ketens, maar de hyperpolariseerbaarheid wordt nog overschat met een factor drie ten opzichte van Hartree-Fock (HF) berekeningen. In dit proefschrift zijn de berekeningen voor de polariseerbaarheid en de hyperpolariseerbaarheid van de H_{2n} moleculaire ketens herhaald met de orbitaalafhankelijke exchangepotentiaal die afgeleid is van de "common energy denominator approximation" (CEDA) voor de Green functie van het KS systeem. Deze potentiaal heeft hetzelfde exchange "hole" als de KLI potentiaal, maar het respons deel heeft een extra orbitaalstructuur die niet alleen orbitaaldichtheden bevat, maar ook niet-diagonale orbitaalproducten. Deze extra structuur draagt bij aan de tegenwerkende term en verlaagt de fout van de KLI potentiaal (ten opzichte van HF) met 43%.

Tot besluit, de gevallen die onderzocht zijn in dit proefschrift wijzen erop dat hoewel het mogelijk is om verbeterde GGA functionalen te ontwikkelen, een echte kwalitatieve en kwantitatieve doorbraak alleen mogelijk is, wanneer de orbitaalafhankelijkheid van de potentiaal nadrukkelijk wordt meegenomen.

---

[7] Phys. Rev. A **45** (1992) 101

Bibliography

[1] P. Hohenberg and W. Kohn, Phys. Rev. **136**, B864 (1964).

[2] W. Kohn and L. J. Sham, Phys. Rev. **140**, A1133 (1965).

[3] S. Lundqvist and N. H. March, eds., *Theory of Inhomogeneous Electron Gas* (Plenum, New York, 1983).

[4] A. D. Becke, Phys. Rev. A **38**, 3098 (1988).

[5] J. P. Perdew, K. Burke, and Y. Wang, Phys. Rev. B **54**, 16533 (1996).

[6] J. P. Perdew, Phys. Rev. B **33**, 8822 (1986), erratum: 34, 7406 (1986).

[7] C. T. Lee, W. T. Yang, and R. G. Parr, Phys. Rev. B **37**, 785 (1988).

[8] N. C. Handy and A. J. Cohen, Mol. Phys. **99**, 403 (2001).

[9] F. A. Hamprecht, A. J. Cohen, D. J. Tozer, and N. C. Handy, J. Chem. Phys. **109**, 6264 (1998).

[10] R. D. Adamson, P. M. W. Gill, and J. A. Pople, Chem. Phys. Lett. **284**, 6 (1998).

[11] T. Bally and G. N. Sastry, J. Phys. Chem. A **101**, 7923 (1997).

[12] B. Braida, P. C. Hiberty, and A. Savin, J. Phys. Chem. A **102**, 7872 (1998).

[13] M. Sodupe, J. Bertran, L. Rodriguez-Santiago, and E. J. Baerends, J. Phys. Chem. A **103**, 166 (1999).

[14] B. G. Johnson, C. A. Gonzales, P. M. W. Gill, and J. A. Pople, Chem. Phys. Lett. **221**, 100 (1994).

[15] D. Porezag and M. R. Pederson, J. Chem. Phys. **102**, 9345 (1995).

[16] S. Skokov and R. A. Wheeler, Chem. Phys. Lett. **271**, 251 (1997).

[17] M. N. Glukhovtsev, R. D. Bach, A. Pross, and L. Radom, Chem. Phys. Lett. **260**, 558 (1996).

[18] A. Streitwieser, G. S. C. Choy, and F. AbuHasanayn, J. Am. Chem. Soc. **119**, 5013 (1997).

[19] P. R. T. Schipper, O. V. Gritsenko, and E. J. Baerends, Phys. Rev. A **57**, 1729 (1998).

[20] O. V. Gritsenko, B. Ensing, P. R. T. Schipper, and E. J. Baerends, J. Phys. Chem. A **104**, 8558 (2000).

[21] P. R. T. Schipper, O. V. Gritsenko, and E. J. Baerends, J. Chem. Phys. **111**, 4056 (1999).

[22] A. D. Becke, J. Chem. Phys. **112**, 4020 (2000).

[23] H. L. Schmider and A. D. Becke, Theochem-J. Mol. Struct. **527**, 51 (2000).

[24] A. D. Becke and K. E. Edgecombe, J. Chem. Phys. **92**, 5397 (1990).

[25] J. P. Perdew and A. Zunger, Phys. Rev. B **23**, 5048 (1981).

[26] S. Patchkovskii and T. Ziegler, J. Chem. Phys. **116**, 7806 (2002).

[27] A. D. Becke, J. Chem. Phys. **98**, 1372 (1993).

[28] A. D. Becke, J. Chem. Phys. **98**, 5648 (1993).

[29] J. Jaramillo, G. E. Scuseria, and M. Ernzerhof, J. Chem. Phys. **118**, 1068 (2003).

[30] E. J. Baerends, Phys. Rev. Lett. **87**, 133004 (2001).

[31] J. D. Talman and W. F. Shadwick, Phys. Rev. A **14**, 36 (1976).

[32] S. Ivanov, S. Hirata, and R. J. Bartlett, Phys. Rev. Lett. **83**, 5455 (1999).

[33] M. Stadele, M. Moukara, J. A. Majewski, P. Vogl, and A. Görling, Phys. Rev. B **59**, 10031 (1999).

[34] A. Görling, Phys. Rev. B **53**, 7024 (1996).

[35] A. Görling, Phys. Rev. B **59**, 10370 (1999).

[36] A. Görling, Phys. Rev. Lett. **83**, 5459 (1999).

[37] S. Kummel and J. P. Perdew, Phys. Rev. Lett. **90**, 43004 (2003).

[38] J. B. Krieger, Y. Li, and G. J. Iafrate, Phys. Rev. A **45**, 101 (1992).

[39] R. van Leeuwen, O. V. Gritsenko, and E. J. Baerends, Z. Phys. D. **33**, 8955 (1995).

[40] O. V. Gritsenko and E. J. Baerends, Phys. Rev. A **6404**, 42506 (2001).

[41] W. Kohn, A. D. Becke, and R. G. Parr, J. Phys. Chem. **100**, 12974 (1996).

[42] Q. S. Zhao, R. C. Morrison, and R. G. Parr, Phys. Rev. A **50**, 2138 (1994).

[43] R. C. Morrison and Q. S. Zhao, Phys. Rev. A **51**, 1980 (1995).

[44] C.-O. Almbladh and A. C. Pedroza, Phys. Rev. A **29**, 2322 (1984).

[45] F. Aryasetiawan and M. J. Stoll, Phys. Rev. B **34**, 4401 (1986).

[46] M. A. Buijse, E. J. Baerends, and J. G. Snijders, Phys. Rev. A **40**, 4190 (1989).

[47] O. V. Gritsenko, R. van Leeuwen, and E. J. Baerends, Phys. Rev. A **52**, 1870 (1995).

[48] O. V. Gritsenko, P. R. T. Schipper, and E. J. Baerends, J. Chem. Phys. **107**, 5007 (1997).

[49] V. E. Ingamells and N. C. Handy, Chem. Phys. Lett. **248**, 373 (1996).

[50] D. J. Tozer, V. E. Ingamells, and N. C. Handy, J. Chem. Phys. **105**, 9200 (1996).

[51] P. R. T. Schipper, O. V. Gritsenko, and E. J. Baerends, Theor. Chem. Acc. **99**, 329 (1998).

[52] J. Baker, M. Muir, and J. Andzelm, J. Chem. Phys. **102**, 2063 (1995).

[53] H. Chermette, H. Razafinjanahary, and L. Carrion, J. Chem. Phys. **107**, 10643 (1997).

[54] G. I. Csonka and B. G. Johnson, Theor. Chem. Acc. **99**, 158 (1998).

[55] M. Filatov and W. Thiel, Chem. Phys. Lett. **295**, 467 (1998).

[56] L. Q. Deng, V. Branchadell, and T. Ziegler, J. Am. Chem. Soc. **116**, 10645 (1994).

[57] B. S. Jursic, Theor. Comput. Chem. **4**, 709 (1996).

[58] E. I. Proynov, S. Sirois, and D. R. Salahub, Int. J. Quantum Chem. **64**, 427 (1997).

[59] T. van Voorhis and G. E. Scuseria, J. Chem. Phys. **109**, 400 (1998).

[60] J. P. Perdew, S. Kurth, A. Zupan, and P. Blaha, Phys. Rev. Lett. **82**, 2544 (1999).

[61] M. Filatov and W. Thiel, Phys. Rev. A **57**, 189 (1998).

[62] V. Saunders and J. van Lenthe, Mol. Phys. **48**, 923 (1983).

[63] J. A. Pople, R. Seeger, and R. Krishnan, Int. J. Quantum Chem. Symp. **11**, 149 (1977).

[64] D. E. Woon and T. H. Dunning, J. Chem. Phys. **100**, 2975 (1994).

[65] D. E. Woon and T. H. Dunning, J. Chem. Phys. **103**, 4572 (1995).

[66] T. H. Dunning, J. Chem. Phys. **90**, 1007 (1989).

[67] K. P. Huber and G. Herzberg, *Constants of diatomic molecules* (Van Nostrand-Reinhold, New York, 1979).

[68] P. M. W. Gill and L. Radom, J. Am. Chem. Soc. **110**, 4931 (1988).

[69] M. A. Buijse and E. J. Baerends, in *Electronic Density Functional Theory of molecules*, edited by D. E. Ellis (Kluwer Academic Publishers, Dordrecht, 1995), p. 1.

[70] E. R. Davidson, S. A. Hagstrom, S. J. Chakravorty, V. M. Umar, and C. F. Fischer, Phys. Rev. A **44**, 7071 (1991).

[71] A. Szabo and N. S. Ostlund, *Modern Quantum Chemistry*, vol. 2 (McGraw-Hill, 1989).

[72] P. R. T. Schipper, O. V. Gritsenko, and E. J. Baerends, Theor. Chem. Acc. **98**, 16 (1997).

[73] E. J. Baerends and O. V. Gritsenko, J. Phys. Chem. A **101**, 5383 (1997).

[74] O. V. Gritsenko, R. van Leeuwen, and E. J. Baerends, J. Chem. Phys. **104**, 8535 (1996).

[75] J. P. Perdew, in *Electronic Structure of Solids*, edited by P. Ziesche and H. Eschrig (Akademie Verlag, Berlin, 1991), p. 11.

[76] J. P. Perdew, J. A. Chevary, S. H. Vosko, K. A. Jackson, M. R. Pederson, D. J. Singh, and C. Fiolhais, Phys. Rev. B **46**, 6671 (1992).

[77] M. A. Buijse, Ph.D. thesis, Vrije Universiteit (1991).

[78] E. J. Baerends, A. Bérces, C. Bo, P. M. Boerrigter, L. Cavallo, L. Deng, R. M. Dickson, D. E. Ellis, L. Fan, T. H. Fischer, et al., *ADF 2000.01*, SCM, Theoretical Chemistry, Vrije Universiteit, Amsterdam, The Netherlands (2000), development-modified.

[79] J. P. Perdew, K. Burke, and M. Ernzerhof, Phys. Rev. Lett. **77**, 3865 (1996).

[80] Y. K. Zhang and W. T. Yang, Phys. Rev. Lett. **80**, 890 (1998).

[81] M. Filatov and W. Thiel, Mol. Phys. **91**, 847 (1997).

[82] A. D. Boese, N. L. Doltsinis, N. C. Handy, and M. Sprik, J. Chem. Phys. **112**, 1670 (2000).

[83] T. Tsuneda, T. Suzumura, and K. Hirao, J. Chem. Phys. **110**, 10664 (1999).

[84] R. Colle and O. Salvetti, Theor. Chim. Act. **37**, 329 (1975).

[85] E. Proynov, H. Chermette, and D. R. Salahub, J. Chem. Phys. **113**, 10013 (2000).

[86] J. B. Krieger, J. Chen, G. J. Iafrate, and A. Savin, in *Electron Correlation and Material Properties*, edited by A. Gonis and N. Kioussis (Plenum Press, New York, 1999).

[87] M. Grüning, O. V. Gritsenko, S. J. A. van Gisbergen, and E. J. Baerends, J. Chem. Phys. **114**, 652 (2001).

[88] F. Herman, J. P. van Dijke, and I. B. Ortenburger, Phys. Rev. Lett. **22**, 807 (1969).

[89] R. van Leeuwen and E. J. Baerends, Phys. Rev. A **49**, 2421 (1994).

[90] A. D. Becke and M. R. Roussel, Phys. Rev. A **39**, 3761 (1989).

[91] A. D. Becke, J. Chem. Phys. **88**, 1053 (1988).

[92] A. D. Becke, Int. J. Quantum Chem. pp. 625–632 (1994), suppl. 28.

[93] C. F. Guerra, J. G. Snijders, G. te Velde, and E. J. Baerends, Theor. Chem. Acc. **99**, 391 (1998).

[94] G. T. Velde, F. M. Bickelhaupt, E. J. Baerends, C. Fonseca-Guerra, S. J. A. van Gisbergen, J. G. Snijders, and T. Ziegler, J. Comput. Chem. **22**, 931 (2001).

[95] J. A. Baerends, E. J. Autschbach, A. Bérces, C. Bo, P. M. Boerrigter, L. Cavallo, D. P. Chong, L. Deng, M. Dickson, D. E. Ellis, L. Fan, et al., *ADF 2002.01*, SCM, Theoretical Chemistry, Vrije Universiteit, Amsterdam, The Netherlands (2002), development-modified.

[96] M. N. Glukhovtsev, A. Pross, and L. Radom, J. Am. Chem. Soc. **117**, 9012 (1995).

[97] B. D. Wladkowski, W. D. Allen, and J. I. Brauman, J. Phys. Chem. **98**, 13532 (1994).

[98] S. E. Barlow, J. M. Vandoren, and V. M. Bierbaum, J. Am. Chem. Soc. **110**, 7240 (1988).

[99] J. W. Larson and T. B. McMahon, J. Am. Chem. Soc. **107**, 766 (1985).

[100] R. C. Dougherty, J. Dalton, and J. Roberts, Organic Mass Spectrometry **8**, 77 (1974).

[101] J. L. Wilbur, B. D. Wladkowski, and J. I. Brauman, J. Am. Chem. Soc. **115**, 10823 (1993).

[102] J. I. Pellerite, M. J. snd Braman, J. Am. Chem. Soc. **105**, 2672 (1983).

[103] B. J. Lynch and D. G. Truhlar, J. Phys. Chem. A **106**, 842 (2002).

[104] M. R. Hand, C. F. Rodriquez, I. H. Williams, and G. G. Balint-Kurti, J. Phys. Chem. A **102**, 5958 (1998).

[105] M. A. Buijse and E. J. Baerends, Mol. Phys. **100**, 401 (2002).

[106] J. P. Perdew, in *DFT 2000, Satellite Symposium of the 10th International Congress of Quantum Chemistry* (Menton, France, 2000).

[107] H. Herman, J. P. van Dyke, and I. B. Ortenburger, Phys. Rev. Lett. **22**, 807 (1969).

[108] H. Herman, I. B. Ortenburger, and J. P. van Dyke, Int. J. Quantum Chem. Symp. **3**, 827 (1970).

[109] F. Della Sala and A. Görling, J. Chem. Phys. **115**, 5718 (2001).

[110] M. Grüning, O. V. Gritsenko, and E. J. Baerends, J. Chem. Phys. **116**, 6435 (2002).

[111] P. R. T. Schipper, O. V. Gritsenko, S. J. A. van Gisbergen, and E. J. Baerends, J. Chem. Phys. **112**, 1344 (2000).

[112] A. Facco Bonetti, E. Engel, R. N. Schmid, and R. M. Dreizler, Phys. Rev. Lett. **86**, 2241 (2001).

[113] O. V. Gritsenko and E. J. Baerends, Phys. Rev. A **54**, 1957 (1996).

[114] C.-O. Almbladh and U. von Barth, Phys. Rev. B **31**, 3231 (1985).

[115] F. Furche, Phys. Rev. B **64**, 195120 (2001).

[116] M. Fuchs and X. Gonze, Phys. Rev. B **65**, 235109 (2002).

[117] M. Fuchs, Y. M. Niquet, and X. Gonze, unpublished.

[118] G. Csanyi and T. A. Arias, Phys. Rev. B **61**, 7348 (2000).

[119] A. M. K. Müller, Phys. Lett. **105A**, 446 (1984).

[120] W. L. Luken and D. N. Beratan, Theor. Chim. Acta **61**, 265 (1982).

[121] W. L. Luken, Int. J. Quantum. Chem. **22**, 889 (1982).

[122] E. Engel, A. F. Bonetti, S. Keller, I. Andrejkovics, and R. M. Dreizler, Phys. Rev. A **58**, 964 (1998).

[123] R. van Leeuwen, personal communication.

[124] S. Goedecker and C. J. Umrigar, Phys. Rev. Lett. **81**, 866 (1998).

[125] E. Runge and E. K. U. Gross, Phys. Rev. Lett. **52**, 997 (1984).

[126] E. K. U. Gross and W. Kohn, in *Advances in Quantum Chemistry* (Academic Press, 1990), vol. 21, p. 255.

[127] E. K. U. Gross, C. A. Ullrich, and U. J. Gossman, in *Density Functional Theory*, edited by E. K. U. Gross and R. M. Dreizler (Plenum Press, New York, 1995), p. 149.

[128] M. E. Casida, in *Recent Advances in Density Functional Methods*, edited by D. P. Chong (World Scientific, Singapore, 1995), vol. 1.

[129] E. K. U. Gross, J. F. Dobson, and M. Petersilka, Top. Curr. Chem. **181**, 81 (1996).

[130] M. E. Casida, in *Recent Developments and Applications of Modern Density Theory*, edited by J. M. Seminario (Elsevier, Amsterdam, 1996).

[131] C. Filippi, C. Umrigar, and X. Gonze, J. Chem. Phys. **107**, 9994 (1997).

[132] S. J. A. van Gisbergen, F. Kootstra, P. R. T. Schipper, O. V. Gritsenko, J. G. Snijders, and E. J. Baerends, Phys. Rev. A **57**, 2556 (1998).

[133] M. Petersilka, U. J. Gossmann, and E. K. U. Gross, in *Electronic Density Functional Theory: Recent Progress and New Directions*, edited by J. F. Dobson, G. Vignale, and M. P. Das (Plenum, New York, 1998), pp. 177–197.

[134] A. Savin, C. J. Umrigar, and X. Gonze, Chem. Phys. Lett. **288**, 391 (1998).

[135] A. I. Al-Sharif, R. Resta, and C. J. Umrigar, Phys. Rev. A **57**, 2466 (1998).

[136] M. Petersilka, E. K. U. Gross, and K. Burke, Int. J. Quantum Chem. **80**, 534 (2000).

[137] H. Appel, E. K. U. Gross, and K. Burke, Phys. Rev. Lett. **90**, 43005 (2003).

[138] A. Görling, Phys. Rev. A **54**, 3912 (1996).

[139] A. Görling and M. Levy, Phys. Rev. A **45**, 1509 (1992).

[140] N. T. Maitra, K. Burke, E. K. U. Gross, and R. van Leeuwen, in *Reviews in modern quantum chemistry: a celebration of the contributions of R.G. Parr*, edited by K. D. Sen (World-Scientific, Singapore, 2002), vol. 2, pp. 1186–1225.

[141] S. Swain, Adv. At. Mol. Phys. **22**, 387 (1986).

[142] K. Burke, M. Petersilka, and E. K. U. Gross, in *Recent Advances in Density-Functionals Methods*, edited by P. Fantucci and A. Bencini (World Scientific, Singapore, 2002), vol. 3, pp. 67–79.

[143] O. V. Gritsenko, S. J. A. van Gisbergen, A. Görling, and E. J. Baerends, J. Chem. Phys. **113**, 8478 (2000).

[144] F. Aryasetiawan, O. Gunnarsson, and A. Rubio, Europhys. Lett. **57**, 683 (2002).

[145] M. E. Casida, F. Gutierrez, J. G. Guan, F. X. Gadea, D. Salahub, and J. P. Daudey, J. Chem. Phys. **113**, 7062 (2000).

[146] Z. L. Cai, K. Sendt, and J. R. Reimers, J. Chem. Phys. **117**, 5543 (2002).

[147] B. Champagne, E. A. Perpete, S. J. A. van Gisbergen, E. J. Baerends, J. G. Snijders, C. Soubra-Ghaoui, K. A. Robins, and B. Kirtman, J. Chem. Phys. **109**, 10489 (1998).

[148] S. J. A. van Gisbergen, P. R. T. Schipper, O. V. Gritsenko, E. J. Baerends, J. G. Snijders, B. Champagne, and B. Kirtman, Phys. Rev. Lett. **83**, 694 (1999).

[149] O. V. Gritsenko, S. J. A. van Gisbergen, P. R. T. Schipper, and E. J. Baerends, Phys. Rev. A **6201**, 12507 (2000).

[150] V. I. Gavrilenko and F. Bechstedt, Phys. Rev. B **55**, 4343 (1997).

[151] F. Kootstra, P. L. de Boeij, and J. G. Snijders, Phys. Rev. B **62**, 7071 (2000).

[152] Y. H. Kim, M. Stadele, and A. Görling, Int. J. Quantum Chem. **91**, 257 (2003).

[153] L. Reining, V. Olevano, A. Rubio, and G. Onida, Phys. Rev. Lett. **88**, 66404 (2002).

[154] R. Del Sole, G. Adragna, V. Olevano, and L. Reining, Phys. Rev. B **67**, 45207 (2003).

[155] Y. H. Kim and A. Görling, Phys. Rev. Lett. **89**, 96402 (2002).

[156] E. K. U. Gross and W. Kohn, Phys. Rev. Lett. **55**, 2850 (1985), erratum: 57, 923.

[157] J. F. Dobson, Phys. Rev. Lett. **73**, 2244 (1994).

[158] G. Vignale and W. Kohn, Phys. Rev. Lett. **77**, 2037 (1996).

[159] G. Vignale, C. A. Ullrich, and S. Conti, Phys. Rev. Lett. **79**, 4878 (1997).

[160] M. van Faassen, P. L. de Boeij, R. van Leeuwen, J. A. Berger, and J. G. Snijders, Phys. Rev. Lett. **88**, 186401 (2002).

[161] M. van Faassen, P. L. de Boeij, R. van Leeuwen, J. A. Berger, and J. G. Snijders, J. Chem. Phys. **118**, 1044 (2003).

[162] P. L. de Boeij, F. Kootstra, J. A. Berger, R. van Leeuwen, and J. G. Snijders, J. Chem. Phys. **115**, 1995 (2001).

[163] M. Petersilka, U. J. Gossmann, and E. K. U. Gross, Phys. Rev. Lett. **76**, 1212 (1996).

[164] J. C. Slater, Phys. Rev. **81**, 385 (1951).

[165] A. Görling, Int. J. Quantum Chem. **69**, 265 (1998).

[166] Y. H. Kim and A. Görling, Phys. Rev. B **66**, 35114 (2002).

[167] G. Onida, L. Reining, and A. Rubio, Rev. Mod. Phys. **74**, 601 (2002).

[168] O. V. Gritsenko, R. van Leeuwen, and E. J. Baerends, J. Chem. Phys. **101**, 8955 (1994).

[169] G. Hunter, Int. J. Quantum Chem. **9**, 237 (1975).

[170] O. V. Gritsenko and E. J. Baerends, Theor. Chem. Acc. **96**, 44 (1997).

[171] E. Engel, J. A. Chevary, L. D. MacDonald, and S. H. Vosko, Z. Phys. D **23**, 7 (1992).

[172] J. C. Slater, *Quantum Theory of Molecules and Solids*, vol. 4 (McGraw-Hill, New York, 1974).

[173] O. Gritsenko, R. van Leeuwen, E. van Lenthe, and E. J. Baerends, Phys. Rev. A **51**, 1944 (1995).

[174] O. V. Gritsenko, P. R. T. Schipper, and E. J. Baerends, Chem. Phys. Lett. **302**, 199 (1999).

[175] O. V. Gritsenko, P. R. T. Schipper, and E. J. Baerends, Int. J. Quantum Chem. **76**, 407 (2000).

[176] D. J. Tozer and N. C. Handy, J. Chem. Phys. **109**, 10180 (1998).

[177] M. E. Casida, C. Jamorski, K. C. Casida, and D. R. Salahub, J. Chem. Phys. **108**, 4439 (1998).

[178] M. E. Casida, K. C. Casida, and D. R. Salahub, Int. J. Quantum Chem. **70**, 933 (1998).

[179] I. Vasiliev, S. Ögüt, and J. R. Chelikowsky, Phys. Rev. Lett. **82**, 1919 (1999).

[180] S. J. A. van Gisbergen, J. G. Snijders, and E. J. Baerends, Comput. Phys. Commun. **118**, 119 (1999).

[181] E. J. Baerends, D. E. Ellis, and P. Ros, Chem. Phys **2**, 41 (1973).

[182] L. Versluis and T. Ziegler, J. Chem. Phys. **88**, 322 (1988).

[183] G. te Velde and E. J. Baerends, J. Comput. Phys **99**, 84 (1992).

[184] N. C. Handy and D. J. Tozer, J. Comput. Chem. **20**, 106 (1999).

[185] J. B. Foresman, M. Headgordon, J. A. Pople, and M. J. Frisch, J. Phys. Chem. **96**, 135 (1992).

[186] C. Adamo, G. E. Scuseria, and V. Barone, J. Chem. Phys. **111**, 2889 (1999).

[187] J. Lorentzon, P. A. Malmqvist, M. Fulscher, and B. O. Roos, Theor. Chim. Acta **91**, 91 (1995).

[188] S. Grimme and M. Waletzke, J. Chem. Phys. **111**, 5645 (1999).

[189] G. Herzberg, *Spectra of Diatomic Molecules*, vol. 1 of *Molecular Spectra and molecular structure* (Krieger, Malabar, Fla., 1991).

[190] R. Antoine, D. Rayane, A. R. Allouche, M. A. Frecon, E. Benichou, F. W. Dalby, P. Dugourd, M. Broyer, and C. Guet, J. Chem. Phys. **110**, 5568 (1999).

[191] W. Muller and W. Meyer, J. Chem. Phys. **85**, 953 (1986).

[192] S. J. A. van Gisbergen, V. P. Osinga, O. V. Gritsenko, R. van Leeuwen, J. G. Snijders, and E. J. Baerends, J. Chem. Phys. **105**, 3142 (1996).

[193] M. E. Casida and D. R. Salahub, J. Chem. Phys. **113**, 8918 (2000).

[194] R. C. Raffenetti, J. Chem. Phys. **59**, 5936 (1973).

[195] J. Kobus, D. Moncrieff, and S. Wilson, J. Phys. B-At. Mol. Opt. Phys. **34**, 5127 (2001).

[196] D. P. Chong, O. V. Gritsenko, and E. J. Baerends, J. Chem. Phys. **116**, 1760 (2002).

[197] H. H. Landolt, R. Börstein, and K.-H. Hellwege, *Numerical data and functional relationships in science and technology. Group II, Atomic and molecular physics* (Springer, Berlin, 1967).

[198] T. N. Olney, N. M. Cann, G. Cooper, and C. E. Brion, Chem. Phys. **223**, 59 (1997).

[199] G. D. Zeiss and W. J. Meath, Mol. Phys. **33**, 1155 (1977).

[200] B. L. Jhanwar, W. J. Meath, and J. C. F. McDonald, Can. J. Phys. **59**, 185 (1981).

[201] M. A. Spackman, J. Chem. Phys. **94**, 1288 (1991).

[202] A. J. Russell and M. A. Spackman, Mol. Phys. **90**, 251 (1997).

[203] A. J. Russell and M. A. Spackman, Mol. Phys. **98**, 633 (2000).

[204] J. Dougherty and M. A. Spackman, Mol. Phys. **82**, 193 (1994).

[205] H. Sekino and R. J. Bartlett, J. Chem. Phys. **98**, 3022 (1993).

[206] J. Geiger and B. Schröder, J. Chem. Phys. **50**, 7 (1969).

[207] W. F. Chan, G. Cooper, R. N. S. Sodhi, and C. E. Brion, Chem. Phys. **170**, 81 (1993).

[208] D. C. Comeau and R. J. Bartlett, Chem. Phys. Lett. **207**, 414 (1993).

[209] J. Pitarch-Ruiz, J. Sanchez-Marin, I. Nebot-Gil, and N. Ben Amor, Chem. Phys. Lett. **291**, 407 (1998).

[210] S. J. A. van Gisbergen, J. G. Snijders, and E. J. Baerends, J. Chem. Phys. **103**, 9347 (1995).

[211] R. Bauernschmitt and R. Ahlrichs, Chem. Phys. Lett. **256**, 454 (1996).

[212] R. E. Stratmann, G. E. Scuseria, and M. J. Frisch, J. Chem. Phys. **109**, 8218 (1998).

[213] S. Hirata and M. Head-Gordon, Chem. Phys. Lett. **302**, 375 (1999).

[214] S. J. A. van Gisbergen, J. M. Pacheco, and E. J. Baerends, Phys. Rev. A **6306**, 63201 (2001).

[215] S. J. A. van Gisbergen, J. A. Groeneveld, A. Rosa, J. Snijders, and E. J. Baerends, J. Chem. Phys. A **103**, 7835 (1999).

[216] A. Rosa, E. J. Baerends, S. J. A. van Gisbergen, E. van Lenthe, J. A. Groeneveld, and J. G. Snijders, J. Am. Chem. Soc. **121**, 10356 (1999).

[217] A. Rosa, G. Ricciardi, E. J. Baerends, and S. J. A. van Gisbergen, J. Phys. Chem. A **105**, 3311 (2001).

[218] R. T. Sharp and G. K. Horton, Phys. Rev. **90**, 317 (1953).

[219] A. Unsöld, Z. Phys. **43**, 563 (1927).

[220] J. O. Hirshfelder, W. Byers Brown, and S. T. Epstein, Adv. Quantum Chem **1**, 255 (1964).

[221] B. H. Brandow, Rev. Mod. Phys. **39**, 771 (1967).

[222] K. F. Freed, Annu. Rev. Phys. Chem. **22**, 313 (1971).

[223] P. Baltzer, M. Larsson, L. Karlsson, B. Wannberg, and M. C. Gothe, Phys. Rev. A **46**, 5545 (1992).

[224] D. W. Turner, C. Baker, A. D. Baker, and C. R. Brundle, *Molecular Photoelectron Spectroscopy* (Wiley-Interscience, New York, 1971).

[225] C. R. Brundle, M. B. Robin, N. A. Kuebler, and H. J. Basch, J. Am. Chem. Soc. **94**, 1451 (1972).

[226] S. Hirata, S. Ivanov, I. Grabowski, R. J. Bartlett, K. Burke, and J. D. Talman, J. Chem. Phys. **115**, 1635 (2001).

[227] T. Koopmans, Physica (Amsterdam) **1**, 104 (1933).

[228] B. Champagne, D. H. Mosley, M. Vracko, and J. M. Andre, Phys. Rev. A **52**, 178 (1995).

[229] B. Champagne and D. H. Mosley, J. Chem. Phys. **105**, 3592 (1996).